Solar Powered Desalination

By
Abdulkarim Mayere, BEng, PgDip

Thesis submitted to the University of Nottingham for the degree of Doctor of Philosophy

August, 2011

Contents

CONTENTS 1
ABSTRACT 5
ACKNOWLEDGMENT 6
LIST OF FIGURES 7
LIST OF TABLES 13
SYMBOLS AND UNITS 15
ABBREVIATIONS 16

CHAPTER 1: INTRODUCTION 17
1.0 BACKGROUND 18
1.1 AIMS AND OBJECTIVES 20
1.2 RESEARCH METHODOLOGY 21
1.3 NOVELTY OF RESEARCH 22
1.4 RESEARCH BENEFIT AND ITS IMPACT 23
1.5 SUMMARY AND OVERVIEW OF THESIS 24

CHAPTER 2: LITERATURE REVIEW 27
2.0 INTRODUCTION 28
2.1 THE GLOBAL WATER RESOURCES 28
2.1.1 WATER SHORTAGE AND CONSUMPTION 29
2.1.2 MEASURING WATER AVAILABILITY 31
2.2 DESALINATION AS A SOLUTION TO WATER PROBLEM 33
2.2.1 EXISTING DESALINATION TECHNOLOGIES 34
2.2.1.1 REVERSE OSMOSIS (RO) 37
2.2.1.2 ELECTRODIALYSIS (ED) 37
2.2.1.3 MULTI-STAGE FLASH DISTILLATION (MSF) 38
2.2.1.4 MULTIPLE EFFECT DISTILLATION (MED) 39
2.2.2 DESALINATION AND CLIMATE CHANGE 40
2.3 DESALINATION AND RENEWABLE ENERGY 42
2.3.1 PARABOLIC TROUGH 44
2.3.2 HELIOSTATS FIELD 45
2.3.3 LINEAR FRESNEL 46
2.3.4 PARABOLIC DISH 47

2.4 DESALINATION ECONOMICS AND INDUSTRY ANALYSIS 48
2.4.1 DESALINATION COSTS 49
2.4.2 MARKET OPPORTUNITIES 50
2.5 CONCLUSION 53

CHAPTER 3: DESIGN AND TEST OF DESALINATION UNIT 55
3.0 INTRODUCTION 56
3.1 HUMIDIFICATION DEHUMIDIFICATION DESALINATION 56
3.1.1 CLASSIFICATION OF HDD SYSTEMS 60
3.1.2 HUMIDIFIERS FOR WATER DESALINATION 62
3.1.3 DEHUMIDIFIERS FOR WATER DESALINATION 64
3.2 PSYCHROMETRIC ANALYSIS OF THE DESALINATION SYSTEM 65
3.2.1 FACTORS AFFECTING THE DESALINATION SYSTEM 65
3.2.2 BASIC PSYCHROMETRIC PROPERTIES MODELS 67
3.2.3 THEORETICAL PERFORMANCE OF THE SYSTEM 69
3.3 DESIGN OF THE DESALINATION SYSTEM 73
3.3.1 THE DEHUMIDIFICATION CHAMBER 74
3.3.2 THE HUMIDIFICATION CHAMBER 77
3.4 PRELIMINARY TEST OF THE DESALINATION SYSTEM 79
3.4.1 EXPERIMENTAL SET-UP 79
3.4.2 RESULTS AND DISCUSSION 80
3.4.2.1 EFFECT OF AIR AND WATER FLOW RATE 80
3.4.2.2 EFFECT OF AIR AND WATER TEMPERATURE 81
3.4.2.3 EFFECT OF ENERGY INPUT AND WATER PRODUCTION 82
3.4.2.4 SYSTEM COP AND ABSORPTION RATIO 83
3.5 SYSTEM OPTIMISATION 85
3.6 CONCLUSION 87

CHAPTER 4: DESIGN AND TEST OF SOLAR COLLECTOR 89
4.0 INTRODUCTION 90
4.1 CONCENTRATED SOLAR COLLECTORS FOR WATER DESALINATION 90
4.2 V-TROUGH CONCENTRATING SOLAR COLLECTOR 92
4.3 EXPERIMENTAL TEST OF THE SOLAR COLLECTOR 96
4.3.1 INDOOR TEST 99

4.3.2 OUTDOOR TEST 107
4.4 MODELLING OF SOLAR COLLECTOR FOR THE HDD UNIT 109
4.5 CONCLUSION 116

CHAPTER 5: SOLAR DESALINATION EXPERIMENTAL FACILITY 117
5.0 INTRODUCTION 118
5.1 EXPERIMENTAL SET-UP 118
5.2 EXPERIMENTAL SYSTEM DESIGN 119
5.2.1 SOLAR SIMULATOR 120
5.2.2 SOLAR COLLECTOR 120
5.2.2.1 HIGH TEMPERATURE RECEIVER 120
5.2.2.2 SOLAR CONCENTRATOR 121
5.2.3 HUMIDIFICATION DEHUMIDIFICATION DESALINATION UNIT 122
5.2.3.1 HUMIDIFICATION CHAMBER 122
5.2.3.2 DEHUMIDIFICATION CHAMBER 123
5.2.4 HOT WATER TANK 123
5.2.5 AUXILIARY COMPONENTS 124
5.3 SYSTEM CONSTRUCTION AND OPERATION 127
5.4 INSTRUMENTS AND MEASUREMENT 131
5.4.1 MEASUREMENT OF LIGHT INTENSITY 131
5.4.2 TEMPERATURE MEASUREMENT 131
5.4.3 MEASUREMENT OF LIQUID FLOW RATE 133
5.4.4 MEASUREMENT OF AIR FLOW RATE 134
5.4.5 MEASUREMENT OF HOT WATER LEVEL IN TANK 134
5.4.6 MEASUREMENT OF SALT CONCENTRATION, WATER PRODUCTION AND RECOVERY RATE 135
5.5 TEST PROCEDURE 136
5.6 CONCLUSION 137

CHAPTER 6: EXPERIMENTAL RESULTS AND DISCUSSION 138
6.0 INTRODUCTION 139
6.1 EXPERIMENTAL RESULTS 139
6.1.1 RESULT FOR SOLAR-ONLY OPERATION 139
6.1.2 RESULT FOR ELECTRIC HEATER-ONLY OPERATION 143
6.1.3 RESULT FOR HYBRID SOLAR/ELECTRIC OPERATION 150

6.1.4 SUMMARY OF RESULTS 151
6.2 DISCUSSION OF THE RESULTS 152
6.2.1 EFFECT OF WATER FLOW RATE 152
6.2.2 EFFECT OF OPERATING TEMPERATURES 153
6.2.3 EFFECT OF TEMPERATURE ON AIR FLOW RATE 154
6.2.4 WATER RECOVERY RATE 155
6.2.5 SYSTEM PERFORMANCE AT HIGH TEMPERATURE 155
6.3 CONCLUSION 158

CHAPTER 7: ECONOMIC AND ENVIRONMENTAL ANALYSIS 160
7.0 INTRODUCTION 161
7.1 SYSTEM SPECIFICATION AND ECONOMIC CONSIDERATIONS 161
7.2 COST ANALYSIS 162
7.3 CARBON SAVINGS 164
7.4 WATER COST 165
7.5 CONCLUSION 166

CHAPTER 8: CONCLUSION AND FURTHER WORK 167
8.1 CONCLUSION 168
8.2 FURTHER WORK 170
8.2.1 LARGE-SCALE/FIELD TRIALS 170
8.2.2 TURBINE COGENERATION 173

REFERENCES 174

APPENDIX A 180
APPENDIX B 181
APPENDIX C 185
APPENDIX D 187
APPENDIX E 188
APPENDIX F 189
APPENDIX G 193

PUBLICATIONS 199

Abstract

Despite water being apparently abundant, up to half of the world's population is faced with water crises which is growing at an alarming rate most especially in developing countries such as African countries where both physical and economic water scarcities prevail. Thus with the abundant salty water and solar intensity in the regions or seasons when water is mostly scarce, solar powered desalination presents an attractive and promising solution towards availability of clean water.

A unique and simple solar desalination system has been developed. The system which based on humidification/dehumidification process is a low cost solution and very competitive with conventional desalination systems. It can be used to provide clean water to the over one billion population who have no access or have water shortages which threaten their health and economies. The developed solar desalination system consists of a purposely designed concentrating solar collector and the desalination core which consist of the humidification and dehumidification chambers. The novel concentrating v-trough solar collector which has its focal point at the bottom of the concentrator provides enough thermal energy required to heat up seawater which is then pumped and sprayed to humidify the incoming air in the humidification chamber. The humidified air enters the dehumidification chamber and is cooled by the incoming cold seawater. The moisture is condensed out and the pure water is accumulated at the base of the chamber, and the dehumidified air is discharged to the outside. The key point is the psychrometric energy re-use, most of the energy is from the condensing of the moisture in the carrier gas.

Both theoretical analysis and experimental tests were carried out and good water output up to 20kg/h and COP around 3 was obtained. This would require $8m^2$ of the newly designed v-trough collector operating at 100°C at $1000W/m^2$ solar intensity. And economic and environmental analysis showed that the solar powered desalination system can achieve a 6 year payback period when compared with when driven by electricity and also a saving of up to 4730 $kgCO_2$ per year. The system can be manufactured from inexpensive plastics rather than exotic and expensive metals. It can easily be sized and scaled to location's needs, can be operated in diverse geographies unattended on a continuous basis and require minimal maintenance.

Acknowledgment

Special thanks to my supervisor Professor Saffa Riffat to whom I am indebted for his unlimited technical support and dedicated involvement throughout my research work. I would like to thank my parents for making my research work possible and their continued prayers, moral and financial support. I should also thank the Petroleum Technology Development Fund (PTDF) for their sponsorship.

I am also grateful to my colleagues and working partners, especially Dr Yuehong Su, Prof. Hongfei Zheng, Mr Yijun Yuan and Dr G. Q. Qiu for their continued support. I would like to thank the technicians of the School for their tolerance and co-operation.

List of Figures

Chapter 1

Figure 1-1: Humidification-Dehumidification process 19

Chapter 2

Figure 2-1: Distribution of earth's water 27
Figure 2-2: Projected freshwater demand by region 28
Figure 2-3: Distribution of water use by sector 29
Figure 2-4: Distribution of water availability across the world . . . 31
Figure 2-5: Global installed capacities of desalination 32
Figure 2-6: Total desalination capacity by country 33
Figure2-7: Total installed capacity by technology 35
Figure 2-8: Principle of reverse osmosis process 36
Figure 2-9: Principle of electrodialysis process 37
Figure 2-10: An illustration typical MSF plant 37
Figure 2-11: An illustration of MED plant 38
Figure 2-12: Projection of world CO_2 emissions and percentage by sector . . 39
Figure 2-13: Sources of water use globally and for major sectors . . . 40
Figure 2-14: World distribution of desalination capacity by major RES . . 41
Figure 2-15: Distribution of solar intensity around the world . . . 41
Figure 2-16: The Andasol Parabolic Trough Power Plant Spain . . . 44
Figure 2-17: The decommissioned Solar Two Heliostats Field . . . 45
Figure 2-18: PS10 Solar Plant Developed by Abengoa 45
Figure 2-19: Linear Fresnel Collectors by Ausra Inc 46
Figure 2-20: The Parabolic Dish Collector 47
Figure 2-21: Major cost of desalination plants 48
Figure 2-22: Unit water cost comparison of major desalination technologies . 49
Figure 2-23: Projected growth of global installed capacities of desalination . 50
Figure 2-24: Desalination market share 51

Chapter 3

Figure 3-1: Natural hydrological cycle 55
Figure 3-2: Illustration of HDD system 56

Figure 3-3: Classification of HD system 59
Figure 3-4: Materials for pad humidifier 61
Figure 3-5: Coil in tube condensing heat exchanger 62
Figure 3-6: Psychrometric chart 63
Figure 3-7: Variation of moisture content with temperature for different relative humidity 66
Figure 3-8: Variation of enthalpy with temperature for different relative humidity . 66
Figure 3-9 Schematic of HD process showing the basic parameters . . . 67
Figure 3-10: Humidification dehumidification process on psychrometric chart . 70
Figure 3-11: One stage solar HDD system 71
Figure 3-12: Principle of the PEPD membrane E/C-Core 72
Figure 3-13: Reduction of energy consumption for the E/C-Core . . . 73
Figure 3-14: Comparison of cooling water requirement for condensation and E/C-Core 74
Figure 3-15: Honeycomb cellulose paper 74
Figure 3-16: Variation of energy requirement with temperature over different air flow 75
Figure 3-17: Variation of water evaporation with temperature over different air flow 75
Fig 3-18: Side view of the desalination unit 76
Figure 13-19: view of the inner core (membrane) of the desalination system showing fresh water condensation 77
Figure 3-20: Measuring instruments 77
Figure 3-21: Amount of fresh water produced as function of cooling water temperature78
Figure 3-22: Amount of water produced as function of temperature at inlet of the humidification chamber for two different weather conditions . . . 78
Figure 3-23: Amount of water produced as function of feed water temperature at inlet of the humidification for different water flow rates at both the dehumidification and humidification chamber inlets 79
Figure 3-24: Amount of fresh water produced as function of temperature at the inlet of the humidification chamber for two different air mass flow rates . . . 79
Figure 3-25: Experimental amount of fresh water produced as function of temperature at inlet of humidification chamber for two different energy inputs at a constant flow rate 80
Figure 3-26: Amount of fresh water produced as function of temperature at inlet of the humidification chamber 81
Figure 3-27: Variation of heat input and COP with water production . . 81

Figure 3-28: Variation of absorption ratio and temperature with rate of water evaporation 82
Figure 3-29: Variation of water production rate with temperature . . . 83
Figure 3-30: Variation of water production with COP 84
Figure 3-31: Two stage solar HDD system 84

Chapter 4

Figure 4-1: Schematic of the new v-trough solar collector 90
Figure 4-2: Schematic of experimental set-up of the new trough solar collector system 92
Figure 4-3: Calibration of thermocouples 93
Figure 4-4: Tungsten lamp used for solar simulator 94
Figure 4-5: Light intensity along reviver tube surface 94
Figure 4-6: Measurement of light intensity along the surface of the receiver tube . 94
Figure 4-7: Tube I-Double layer coated glass vacuum tube with U-shape pipe . 95
Figure 4-8: Tube II-Double layer coated glass vacuum tube with concentric pipe . 95
Figure 4-9: Tube III-Double layer uncoated glass vacuum tube with U-shape pipe . 95
Figure 4-10: Tube IV-Single layer uncoated glass vacuum tube with coated finned U-pipe 95
Figure 4-11: Aluminium fins 96
Figure: 4-12: Schematic of the solar concentrator 96
Figure 4-13: Complete indoor experimental rig 97
Figure 4-14: Solar collector with various receiver tubes 97
Figure 4-15: Variation of time with temperatures for Tube I without fins . . 98
Figure 4-16: Variation of time with temperatures for Tube I with fins . . 98
Figure 4-17: Variation of time with temperatures for Tube II with fins . . 99
Figure 4-18: Variation of time with temperatures for Tube III with fins . . 100
Figure 4-19: Variation of time with temperatures for Tube IV with oil as HTF . 101
Figure 4-20: Variation of time with temperatures for Tube IV with water as HTF . 101
Figure 4-21: Comparison of combine collector efficiency for different receiver tubes 103
Figure 4-22: Complete outdoor experimental rig showing receiver tube . . 104
Figure 4-23: Complete outdoor experimental rig 105
Figure 4-24: Manual solar tracking of the collector 105
Figure 4-25: Variation of various temperature and solar irradiation with time . 106

Figure 4-26: Variation of water temperature in storage tank with time . . 106
Figure 4-27: Efficiency of the solar collector system. 107
Figure 4-28: Typical collector performance compares with the new V-Trough collector 108
Figure 4-29: Variation of water production with collector area for different types of solar collectors 111
Figure 4-30: Variation of solar collector area and water production with operating temperature for different types of solar collectors 112
Figure 4-31: Variation of v-trough with water production for different amount of solar intensities 113
Figure 4-32: Variation of water production with collector area for different temperature difference at inlet/outlet of humidification chamber 113

Chapter 5

Figure 5-1: Schematic of desalination unit integrated with solar collector . . 116
Figure 5-2: Structural dimension of the solar simulator 118
Figure 5-3: The V-trough solar collector 118
Figure 5-4: The high temperature receiver tube 119
Figure 5-5: The V-trough solar collector 119
Figure 5-6: Desalination unit 120
Figure 5-7: The humidification chamber 120
Figure 5-8: The dehumidification chamber 121
Figure 5-9: Insulated water tank 121
Figure 5-10: Electric Immersion Heater 122
Figure 5-11: Axial fan 122
Figure 5-12: Heat transfer oil tank 123
Figure 5-13: Cold water tank 123
Figure 5-14: System pumps 124
Figure 5-15: Solar collector system set-up 127
Figure 5-16: Integration of solar collector with oil and water tank . . . 127
Figure 5-17: Complete system schematic 128
Figure 5-18: Complete solar desalination system set-up 128

Figure 5-19: Measurement of distribution of light intensity on the high temperature receiver 129
Figure 5-20: CMP 3 Pyranometer 129
Figure 5-21: Types of thermometers used for calibration 130
Figure 5-22: An in-line flow meter and a control valve supplied by RS Components 131
Figure 5-23: Hot wire anemometer 132
Figure 5-24: Log-linear transverse for round ducts, two-diameter approach . . 132
Figure 5-25: Calibrated water tank 133
Figure 5-26: Soy sauce 133
Figure 5-27: Measuring cup 133

Chapter 6

Figure 6-1: Thermal efficiency of solar collector for different oil flow rates . 138
Figure 6-2: Temperature variation of solar collector over period of time . . 138
Figure 6-3: Variation of energy and COP with water produced for solar-only operation 139
Figure 6-4: Variation of amount of fresh water production with solar collector area 140
Figure 6-5: Variation of energy and COP with water produced for electric-only operation and high flow rate unsaturated cooling water 142
Figure 6-6: Variation of energy and COP with water produced for electric-only operation and high flow rate saturated cooling water 143
Figure 6-7: Variation of energy and COP with water produced for electric-only operation and medium flow rate unsaturated cooling water 144
Figure 6-8: Variation of energy and COP with water produced for electric-only operation and low flow rate unsaturated cooling water 145
Figure 6-9: Variation of energy and COP with water produced for electric-only operation and low flow rate saturated cooling water 146
Figure 6-10: Variation of energy and COP with water produced for electric-only operation and equal flow rate unsaturated cooling water 147
Figure 6-11: Variation of energy and COP with water produced for electric-only operation and equal flow rate saturated cooling water 148
Figure 6-12: Variation of energy and COP with water produced for hybrid system operation and saturated cooling water 149

Figure 6-13: Variation of energy input from solar collector and electric heater with time 149
Figure 6-14: Effect of cooling water flow rate on the amount of freshwater produced 151
Figure 6-15: Effect of hot water mass flow rate on the amount of fresh water produced 152
Figure 6-16: Variation of system operating temperatures and amount of fresh water produced with time 153
Figure 6-17: Variation of air velocity with air temperature at outlet of the dehumidification chamber and temperature of water at inlet of humidification chamber 154
Figure 6-18: Operation of the desalination system showing operating temperatures and amount of water produced with time 155
Figure 6-19: Hot water tank with wrap around heater at the bottom . . . 156
Figure 6-20: Operation of the desalination system without drum heater showing operating temperatures and amount of water produced with time for 430kg/h hot flow and 240kg/h cold flow 156
Figure 6-21: Operation of the desalination system with drum heater showing operating temperatures and amount of water produced with time for 120kg/h hot water flow and 30kg/h cold water flow 156
Figure 6-22: Variation of energy and COP with water produced for high temperature operation 157
Figure 6-23: Damaged water tank due to high temperature 158

Chapter 7
Figure 7-1: Net present value analysis 164

Chapter 8
Figure 8-1: Schematic of the solar-driven micro turbine system . . . 172
Figure 8-2: A simple Rankine cycle 173
Figure 8-3: Proposed combined water and power system 174
Figure 8-4: Proposed large scale application 176
Figure 8-5: Overview of the proposed large scale application . . . 176

List of Tables

Chapter 2

Table 2-1: Water per capita index 30

Table 2-2: Solar Collectors 42

Table 2-3: Main items of cost of construction and cost of water . . . 48

Chapter 3

Table 3-1: Comparison of "SODESA System" and "Oman System" . . 58

Table 3-2: Theoretical calculations of the performance of the HDD system . . 69

Chapter 4

Table 4-1: All measured parameters and measuring devices 93

Table 4-2: Specification of receiver tubes 96

Table 4-3: Measured and calculated experimental data 102

Table 4-4: Solar collector performance curve equations 109

Chapter 5

Table 5-1: Description of calibrated thermocouples and their data logger channels . 130

Chapter 6

Table 6-1: Summary of result for solar only operation with cooling water saturated 139

Table 6-2: Summary of result for electric-only operation with cooling water unsaturated for high flow rate 141

Table 6-3: Summary of result for electric-only operation with cooling water saturated for high flow rate 142

Table 6- 4: Summary of result for electric-only operation with cooling water unsaturated for medium flow rate 143

Table 6-5: Summary of result for electric-only operation with cooling water unsaturated for low flow rate 144

Table 6-6: Summary of result for electric-only operation with cooling water saturated for low flow rate 145

Table 6-7: Summary of result for electric-only operation with cooling water unsaturated for equal flow rate 146

Table 6-8: Summary of result for electric-only operation with cooling water saturated for equal flow rate. 147
Table 6-9: Summary of result for hybrid system operation with cooling water saturated 148
Table 6-10: Summary of experimental test results 150
Table 6-11: Summary of result for high temperature test 157

Chapter 7
Table 7-1: Key considerations 162
Table 7-2: Capital cost for solar system 162
Table 7-3: Capital cost for prototype desalination system 163
Table 7-4: Running costs of the desalination unit for both solar and electric . 163
Table 7-5: Carbon emissions 165
Table 7-6: Water cost 165

Chapter 8
Table 8-1: Performance data for micro turbine systems 171
Table 8-2: Specification for large scale application 175
Table 8-3: Total cost of installation 175
Table 8-4: Cost of a proposed 1000m³/d system 177

Symbols and Units

ω	Moisture content	Kg/kg
p_{vs}	Partial pressure	Pa
T	Temperature	°C
p	Total pressure	Pa
h	Enthalpy	kJ/kg
ϕ	Relative humidity	%
c_p	Specific heat capacity	kJ/kgK
Q	Energy	kW
w_p	Water production	Kg/h
h_l	Latent heat of condensation	kJ
m	Mass flow rate	Kg/h
Q	Heat	kW
L	Length of the collector	m
d	Diameter of receiver tube	m
u	Flow rate of the liquid	m/s;
ρ	Density of the liquid	kg/m^3;
μ	Viscosity of the liquid	kg/(m·s)
x_c	Max. light inlet half-width	m
L	Length of the collector	m
η	System efficiency	%
I	Solar Intensity	W/m^2
η_o	Optical efficiency	%
A	Collector area	m²

Subscripts

1	State 1
2	State 2
3	State 3
4	State 4
Δ	Differential
E/C	Evaporation/condensation
evp	Evaporation
C	Cold/cooling
cond	Condensation
ε	Absorption ratio
ab/abs	Absorber
U_L	Heat loss factor
C	Concentration ratio
F_R	heat removal factor
I_n	Intercept
S	Slope
r	Receiver tube
min	Minimum
s	Surface
cyc	Cycle
FW	Freah water
EA	Exhaust air
amb	Ambient
Cumm.	Cumulative
I_o	Capital cost
F_t	Running cost
i	Interest rate
t	Time in years

Abbreviations

WHO	World Health Organisation
ASHRAE	American Society of Heating, Refrigerating and Air Conditioning Engineers
CAOW	Close Air Open Water
CFM	Cubic foot per minute
COP	Coefficient of Performance
CWOA	Close Water Open Air
ED	Electrodialysis
EDI	Electrodeionisation
EDR	Electrodialysis Reversial
EES	Engineering Equation Solver
FAO	Food and Agricultural Organisation of United Nations
GDP	Gross Domestic Product
GDP	Gross Domestic Product
HD	Humidification Dehumidification
HFC	Heliostat Field Collector
HTF	Heat Transfer Fluid
HX	Heat Exchanger
IDA	International Desalination Association
IEA	International Energy Agency
IPCC	Intergovernmental Panel on Climate Change
MD	Membrane Distillation
MED	Multi Effect Distillation
MENA	Middle East and North Africa
MSF	Multi Stage Flash
NPV	Net Present Value
PDC	Parabolic Dish Collector
PEPD	Psychometric Energy Process Desalination
PV	Photovoltaic
RES	Renewable Energy Sources
RO	Reverse Osmosis
SD	Solar Desalination
SEGS	Solar Energy Generating Systems
SNL	Sandia National Laboratory
TDS	Total Dissolved Solids
UNESCO	United Nations Educational, Scientific and cultural organisation
VC	Vapour Compression
VTC	V-Trough Collector
WRR	Water Recovery Rate

Chapter 1: Introduction

1.0 Background

Water scarcity has become a fast growing major global challenge which is linked to climate change**.** One third of the world's population already live in areas of moderate to high water stress; some 1.5 billion people lack ready access to drinking water, with some 80 countries suffering from water scarcity**.** Even in UK where water is apparently abundant, the industry is struggling to keep up with demand from rising population while maintaining stringent standards on water quality and the environment. Water use has yet to adapt to the realities of scarcity, with much action that can be taken in water conservation and water re-use; furthermore water effectively is being exported from water-scarce countries to water-rich countries in the form of 'virtual water' (the water embodied in food and clothing)**.** In much of the world, the health of river systems is threatened by overuse and pollution; rivers are often no longer able to provide and purify the volumes of water needed, while the impact of pests and diseases is increasing**.** With the introduction of powerful pumping (from deep underground) and piping (across long distances), groundwater aquifers are increasingly being depleted well beyond sustainable recovery levels; this also leads in many cases to brackish water with high concentrations of dangerous minerals and to resulting health problems.

Desalination has become a major new source of fresh water tapping into the vast reserves of seawater and brackish water. It is especially useful where (cheaper) water conservation and water re-use either have limited potential or face major problems of implementation
It is increasingly recognised that desalination should not detract from such demand-side action and the use of cheaper water sources. Desalination technology is now mature, with two alternate processes dominating the market; namely thermal and membrane processes. The technologies for thermal process include mainly Multiple Effect Distillation (MED) or Multi Stage Flash (MSF). They generally have higher capital costs and extremely energy intensive. However, they are mostly attractive situations of high water salinity. They are most used in the Arabian Gulf where co-location with power plants means that waste heat can be utilised effectively and where the economies of scale are attractive. The membrane process has a single technology which is largely dominating. It is called the Reverse Osmosis (RO). The technology is less suitable for high salinity or poor water quality. It has lower capital but higher maintenance costs (pre-treatment costs and

membrane replacement requiring partial plant shut down). Furthermore requires less land area (some 25% less than MED) and ease of scaling up.

In general, the current desalination technologies are expensive, sensitive to increases in energy prices and highly carbon intensive. The challenge is to design a low cost and low carbon desalination system which can be easily scaled up to any size and attractive to both developing countries with low GDP/capita, already facing massive water deficits (and indeed increasing internal conflict), but unable to afford the conventional technology and developed countries with high GDP/capita, again facing water challenges, but wishing to diversify their economies from oil/gas driven technology.

There are various emerging technologies for water desalination. These include technologies such as capacitive deionisation (CDI), membrane distillation (MD) and humidification dehumidification (HD) process. The HD technique is a thermal process that is promising due to high efficiency and possibility of directly integrating it with renewable energy source [79]. The HD process is illustrated in Figure 1-1. In this air is humidified by mixing with hot water in the humidification chamber to form vapour. The vapour is transported to the dehumidification chamber though either natural or forced convection where it is condensed and obtained as fresh water. The humidification dehumidification desalination process will be investigated in this research work.

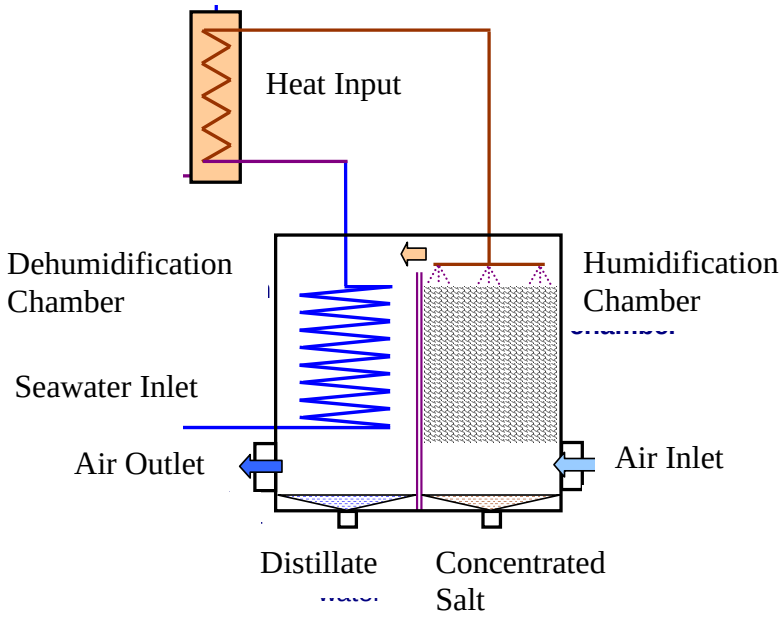

Figure 1-1: Humidification-Dehumidification process

In the proposed system as illustrated in Figure 1-1, the solar collector will be used as energy source to heat up the seawater. The hot seawater is then sprayed to humidify the incoming air in the humidification chamber. The humidified air enters the dehumidification chamber and is cooled by the incoming seawater. In the meantime the seawater is pre-heated to recover heat. The moisture is condensed out and the pure water is accumulated at the base of the chamber, and the dehumidified air is discharged to the outside.

1.1 Aims and Objectives

The proposed project aims to investigate the performance of a novel HD system driven by a concentrated solar absorber. The HD system utilises novel and integrated design concept for optimising system performance, size, reliability and costs. It is based on psychrometric energy process using a special membrane. It is aimed to also investigate the performance of a suitable solar collector to be integrated with the HD system. In the proposed system, the solar collector will be used to heat up salty water. The hot salty water is then sprayed to humidify the incoming air in the humidification chamber. The humidified air enters the dehumidification chamber and is cooled by the incoming salty water. The moisture is condensed out and the pure water is accumulated at the base of the chamber, and the dehumidified air is discharged to the outside or re-circulated.

Another aim of the research is to increase the awareness of water scarcity and its relationship with climate change with the need to shift from non-renewable energy conventional desalination systems to a more clean and affordable systems driven by solar energy by using disruptive technologies such as solar humidification dehumidification technology.

The overall objective of this research is to develop a very simple technology with a reasonable efficiency to provide clean and affordable fresh water most especially in developing countries where there is very low infrastructure and unskilled manpower, but with high abundance of solar energy. Such system would result in significantly reduced CO_2 emissions to the environment. And the anticipated cost of production is low since inexpensive materials could be used. Specific objectives are as follows:

- To review the extent of water scarcity, market potential and past work on desalination and solar technologies.
- Analysis of the thermal performance and operating characteristics of humidification dehumidification desalination (HDD) system by theoretical/experimental methods.
- Theoretical and experimental investigation of the performance of solar collectors suitable for water desalination.
- Theoretical and experimental investigation of the performance of the combined solar collector and HDD system.

1.2 Research Methodology

In order to achieve the aims and objectives of the research project, literature review was carried out. And then later theoretical and experimental investigations were carried out. These were conducted in the following ways;

Review of global water resources and also major desalination and concentrating solar technologies was carried out in order to understand the advantage and disadvantages of the systems. The impact of desalination and climate change was analysed and then general industry analysis was carried out. This helped the research project by understanding most potential regions with high water demand; thereby increase awareness and develop an optimised system for such regions. It also helped to understand the existing market and industry where by a disruptive technology can be developed so as it can benefit the quality of life of millions of people. It generally helps create the balance between the trade-off of efficiency and cost towards commercialization.

Desalination based on humidification/dehumidification process has been previously reviewed and all the aspects related to design parameters and system configurations have been looked at and these include both the closed and opens systems. The review also covered factors affecting evaporation rate, materials, the psychometric properties and energy recycling. Different suitable solar technologies and their design parameters reported by other researchers have been reviewed.

For the theoretical investigation, psychrometric analysis was conducted to estimate the performance of the system, potential for energy recovery and cooling water requirement.

This helped to come up with a design base on psychrometric energy process. The sizing of the required solar collector was theoretically investigated. And the design of more appropriate collector system was carried out to suit the overall objective of the project.

Series of experimental tests were carried out on both the novel desalination and solar unit independently to investigate the performance of the systems. Initial experimental test on the HDD unit helped to determine the actual amount of solar collector area required and an appropriate way of integrating the HDD unit with the solar unit. It also enables further estimation of the performance of the HDD unit theoretically. Test on the solar unit was mainly to establish efficiency of the solar collector for integration with the HDD unit. Then a final test was carried out on the combined solar HDD unit to establish the performance of the integrated system and also the effect of amount of hot water flow rate that can be potentially supplied by the solar collector on the output of the HDD unit.

1.3 Novelty of Research

The innovative aspect of the current research work project includes the following;

- The core of the desalination unit is made of a new membrane. The membrane has a wavy structure with one side having a hydrophobic surface and the other side having a hydrophilic surface. The design of the membrane allows for simple cycle to be used for the water separation process with evaporation and condensation taking place simultaneously at the core, and thus regarded as the evaporation/condensation core (E/C-Core). Other technologies such as vacuum compression have complex cycles and thus making them expensive. The system utilizes the solar thermal energy multiple times based on the psychrometric energy process to provide an extremely high quality treated water. So the thermal energy requirement is much lower than the conventional HDD system. It is suitable for high concentration salty water with no fouling or scaling and no membranes to change when compared to reverse osmosis based systems.

- The E/C-Core forms two channels with one channel as the evaporative channel where cooling water and outside fresh air at atmospheric temperature mix in a cross flow direction, and then the air and water mixture gets humidified to form vapour. The

vapour is transported to the humidification chamber to get further humidified. The second channel is the condensing channel where the hot and humidified vapour from the humidification chamber get condensed and transfer its latent heat to the cooling water in the evaporation channel through the membrane. Thus there is heat and mass exchange mechanism between the hot humid vapour and cooling water, and then between the warmed cooling water and fresh air.

- The new E/C-Core requires low temperature difference across the hot and cold channels for evaporation of water by mixing with air flow to form vapour and then condensation of water from the vapour. The hydrophilic channel acts as a wetted media in order to aid evaporation of the warmed cooling water by the latent heat of condensation. And the hydrophobic channel aids condensation by ensuring all condensed water droplets are repelled and efficiently accumulated as fresh water. .Design of a counter-cross flow arrangement of the E/C-Core for both evaporation and condensation process significantly reduce the requirement for feed water with high water recovery rate.

1.4 Research Benefit and its Impact

This research work has great benefit to the scientific community and researchers. The testing and selection of suitable configuration of a novel solar collector leads to an efficient integration of solar thermal collectors for water desalination. This shows potential for the need of more specifically designed and optimized solar collectors for water desalination within the research field. This will lead to rapid commercialization of solar powered desalination systems.

And in terms of new knowledge, a whole new concept of desalination is introduced which provides more efficient processes of desalination. The thermal energy required for evaporation is decreased significantly by recycling the heat of condensation of the distillate (i.e. vapour). The application of the research will lead to increase in the maximum water production currently achieved by other conventional humidification/dehumidification systems

The impact of the current research is rather wide. One of the challenges within the industry is to develop a competitive system that can be scaled to any size. Smaller modules give greater flexibility to size. Hence the HDD unit can benefit from small scale

domestic application to large scale community or village based installations. The modular structure of the new HDD system allows it to be easily combined with other industries such as power plants to utilise waste heat when compared with conventional technologies.

Desalination offers the potential for taking pressure off freshwater resources that are of vital importance to the environment. It also provides an opportunity to diversify sources of water supply and to make use of resources that otherwise would not be usable most especially in developed countries of regions that are less water stressed. As the availability of fresh water is related to healthy economies, this research will create a great impact by improving the economies of many nations. It will have impact on agriculture and food security, health and industries.

A further benefit comes from making economic use of the waste brine stream, for example by co-locating with a chemical works needing salt solution (e.g. for soaps and detergent, dyes, paper and glass production), or domestic salt production. In the case of some solar systems, there may be an opportunity for improved economics by using the shaded space below the solar collectors for horticulture. Solar greenhouses, with a focus on agricultural production in desert conditions, have been pursued with trials now underway. Alternatively solar systems may be combined with forestry or date palms, making a convenient wind break reducing dust and sand.

1.5 Summary and Overview of Thesis

The research was carried out in different stages and covered a number of tasks as reported in different chapters and sections of this thesis. The thesis report comprises of eight chapters. A brief outline of these is given below:

Chapter one gives a background information which introduces the proposed research. It describes the aims and objectives of the research, and further breaks down the objectives into overall and specific objectives. The research methodology was presented detailing methods used to achieve the aims and objectives of the research. It describes the novelty of the research and the potential benefit and impact presented by the technology. The chapter concludes with the complete outline of the thesis report.

Chapter two presents literature review on global water resources in order to understand water availability, consumption and shortage. Major desalination technologies were reviewed. And the relationship between water scarcity and climate change was analysed with carbon emissions from conventional technologies and potential carbon savings renewable energy presents. It further reviews the solar thermal collector technology as the most prospective renewable energy technology and its suitability for desalination. Market potential and industry analysis was also presented with focus on Africa and Middle East region where most countries almost completely depend on desalination.
Chapter three describes technical literature review of previous work on HDD system. And then psychrometric analysis carried out to determine the performance of the desalination system theoretically. Thus this enables the design of a prototype system which was later tested to determine the actual output and overall efficiency of the system. Based on the tests carried out, a further psychrometric analysis was carried out in order to determine the performance of the system at high temperatures.

Chapter four discusses suitable solar collectors for water desalination. A modelling was carried out to determine the size of concentrating and non concentrating collector area required based on the experimental test of the HDD unit carried out in chapter three. It further discusses the use of concentrating solar collectors for water desalination and its many advantages. Hence a more suitable concentrating solar collector was designed and experimentally tested both indoors and outdoors in order to determine its efficiency.

Chapter five explains the experimental set up of the combined solar water desalination unit. It describes the individual components of the system, system instrumentation and measuring devices with their accuracies, measurement and calibration. It describes the difficulties faced during construction and initial operation of the system. And then it finally gives a simple layout of the experimental procedure.

Chapter six describe the results and discussion of the experimental test carried out.

Chapter seven explains the economics of the desalination unit in terms of costs and environmental carbon savings. A comparative analysis using the net present value

method was carried out for when the system is operated using solar energy and electricity from fossil fuels.

Chapter eight concludes and presents further work that needs to be done associated with the desalination system. It draws conclusion from the literature review, theoretical, experimental and economic analysis carried out. With regards to further work, the need for large scale and field trials of the desalination system is highlighted. Furthermore, the possibility of combining a turbine with the desalination unit in order to produce electricity and water at the same time was presented.

Chapter 2: Literature Review

2.0 Introduction

The literature associated with water desalination is presented here. An assessment of the global water crises was carried out base on the availability and consumption of water, water scarcity and possible solutions. Hence the review of desalination as one possible solution to the growing crises due to scarcity of nature's most abundant resource. This includes a review of growing trend in adopting desalination for fresh water supply. Various technologies for water desalination are presented. The suitability of integrating renewable energy sources to desalination is explored. And finally the cost of desalination and market opportunities are analysed.

2.1 The Global Water Resources

Water is the essence of life and a fundamental need for human existence. About 70% of the surface of the earth is covered with water. However, up to 97% of earth's water is salt water from the oceans with salinity up to 30,000 parts per million of total dissolved solids (ppm TDS). Only 3% of the earth's water is fresh water. A Freshwater body contains low concentrations of dissolved salts and other total dissolved solids. Freshwater according to the World Health Organisation (WHO) can be defined as water with less than 500ppm TDS. Most of the fresh water comes from ground water sources such as wells, or from surface waters such as rivers, lakes and reservoirs. The distribution of earth's water is shown in Figure 2-1. The ultimate source of fresh water is the precipitation of atmosphere in the form of rain and snow. This indicated as "other" in the figure below.

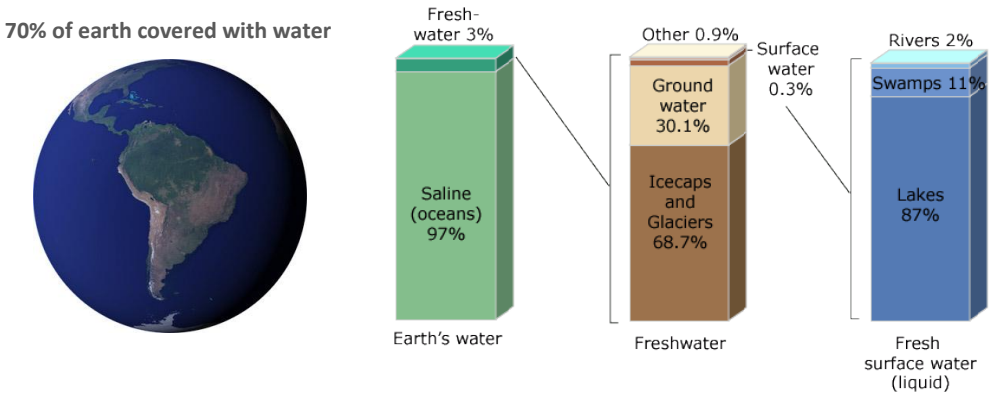

Figure 2-1: Distribution of earth's water (US Geological Survey) [78]

The current global water demand is above 4 x 10^{12} m^3 per year. The annual global water withdrawal is expected to grow by about 10-12% every ten years to more than 5 x 10^{12}

m³ per year by 2050 (UNESCO, 1999). Figure 2-2 shows projected global and regional demand for fresh water.

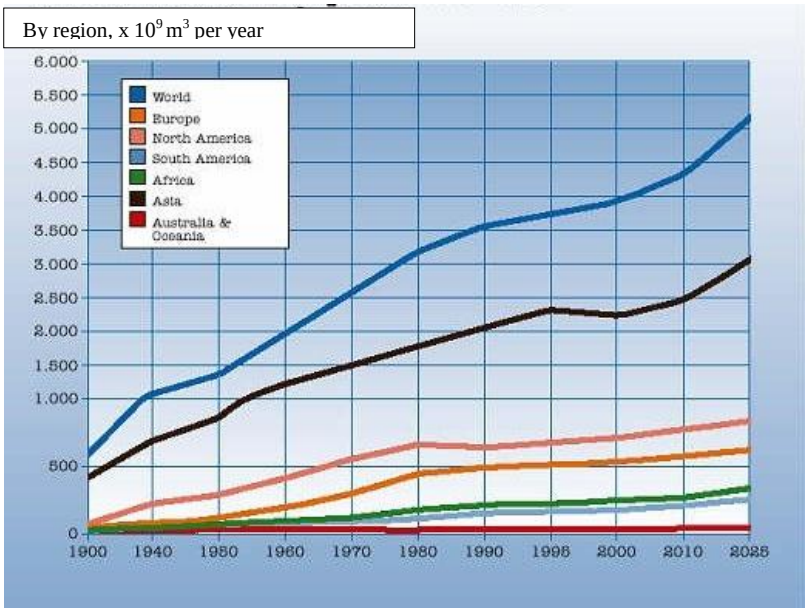

Figure 2-2: Projected freshwater demand by region [1]

There have been various estimates of the global water resource base on different calculation methods [2]. Shiklomanov in Gleick (1993) calculated the total volume of water in the world to be approximately 1.4 x 10^{18} m^3. Surface freshwater is 1.05 x 10^{14} m^3 or 0.3% of the world's freshwater [3]. Niemczynowicz (2000) estimated more than 50% of the surface freshwater as non renewable water [4]. The amount of renewable water is therefore around 4.2 x 10^{13} m^3 per year which replenishes groundwater source or returns to the oceans by rivers. Most of it (around 3 x 10^{13} m^3 per year) is in flush flows that are not captured by man. It is assumed that the available renewable freshwater resource is between 9 x 10^{12} and 14 x 10^{12} m^3 per year. However around 70% of is required for the ecosystem and thus only 30% or 4.2 x 10^{12} m^3 per year is available for human consumption [5]. The balance between availability of fresh water and demand has reached critical level. If the world is to depend only on freshwater source, soon any form of life will face extinction.

2.1.1 Water Shortage and Consumption

Despite huge water resources, many countries and regions do not have enough fresh water. Global water problems are attracting interesting attention. Water shortages are

mainly as a result of rapid increase in world population. According to World Bank, about 80 countries now have water shortages that threaten health and economies while 40 percent of the world population mostly located in arid, remote areas and islands have no access to clean water [6].

According to International Desalination Association (IDA), humans use as little as $0.02m^3$ (20 litres) of water a day for domestic use in the developing countries to as high as $0.2m^3$ (200 litres) in the developed countries. And although a lot of water is consumed by industry, the largest use of water is for producing the products we eat and wear. Consider these facts [77]; it takes $0.245m^3$ (245 litres) of water to produce 0.25kg of wheat. It takes $2.7m^3$ (2700 litres) of water to produce an average size cotton shirt. Around $1.23m^3$ (1230 litres) are required to produce 0.25kg of cheese. And $13m^3$ (13000 litres) of water are needed to produce 1kg of beef. Agriculture uses up to 70 times more water to produce food than is used in drinking and other domestic purposes, including cooking, washing and bathing. Figure 2-3 shows distribution of water consumption in three major sectors.

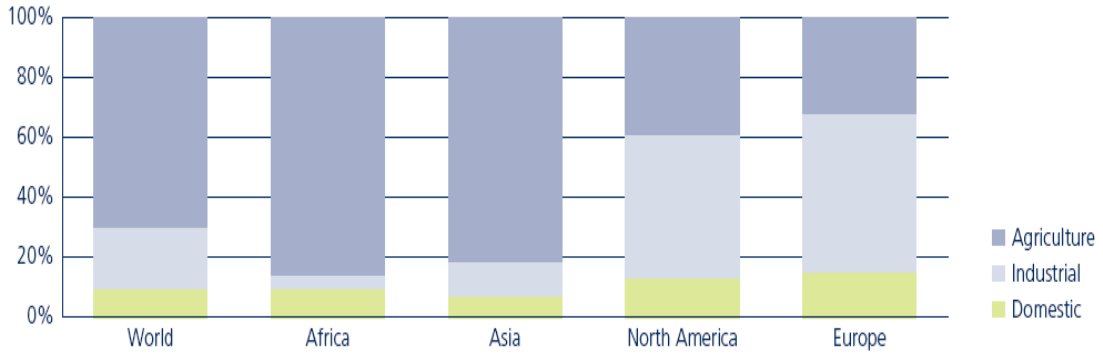

Figure 2-3: Distribution of water use by sector (source: fao-aquastat)

If the estimated 4×10^{12} m^3 per year available freshwater is divided by the current world population of 6.8 billion people, there will be only around 600 m^3 per person per year. Base on the world distribution in Figure 2-3, there will be around $430m^3$ (70%) per person per year for agriculture. There will be around $120m^3$ (20%) and $60m^3$ (10%) per person per year for industrial and domestic consumption respectively. The world population is projected to reach 9 billion by 2050 (see population projection in Appendix A). This will further reduce the available freshwater to around $450m^3$ per person per year.

2.1.2 Measuring Water Availability

There are several methods of measuring water availability. The most widely used is Falkenmark's per capita index. This is the relationship between the available water resource and the population. Falkenmark projected about $0.1m^3$ (100 litres) per person per day is the rough minimum required for domestic needs. And 5 to 20 times of the domestic need is required to meet the demands of the agricultural and industrial sectors [7]. Hence a benchmark which indicates water stress and water scarcity was established. A country is said to be water stressed when availability per capita is between 1000 to 1700m³ per year. And anything below 1000m³ per year per capita is regarded as water scarcity. The benchmark was further divided into four main categories by Schram (1999) as shown in Table 2-1 [5]. It should be noted that the Falkenmark's concept do not account for other factors which include non renewable water sources and virtual water. It only accounts for renewable water from rainfall or snow. Bearing in mind the world major rivers drying up, depletion of groundwater level and melting glaciers, it can be concluded that the approximation is generous. One advantage of the approximation is that data is widely available. And hence the concept is widely accepted by big organizations such as United Nations.

Table 2-1: Water per capita index

Renewable fresh water per capita [m³ per year]	Effects
>1700	Limited stress
1700-1000	Water stressed
1000-500	Water scarce
<500	Absolute scarcity

A detailed breakdown of annual renewable fresh water by country is attached in Appendix B. Figure 2-4 shows the alarming extent of water scarcity across the world. The map shows the projected number of countries that will need to import 10% or more of their water by no later than 2025 [8]. It shows two key types of scarcity; water is said to be either physically scarce or economically scarce. Economic water scarcity occurs due to a lack of investment and is characterised by poor infrastructure and unequal distribution of water. Physical scarcity occurs when the water resources cannot meet the demands of the population. Arid regions are most associated with physical water scarcity.

However, there is an alarming trend in artificially created scarcity even in areas where water is apparently abundant.

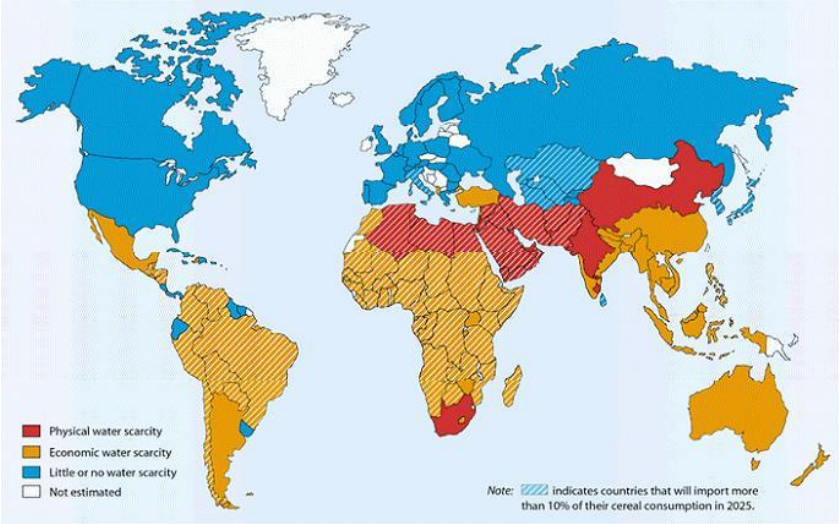

Figure 2-4: Distribution of water availability across the world

As the world's population is expected to grow every year as much as 40 to 50% over the next 50 years and with it the demand for water will also rise. But there are other issues with our existing water sources from pollution to climate changes and water mismanagement that are literary drying out our resources.

Having seen the growing demand for water and very soon demand will be higher than supply. If the whole world were to depend of available freshwater sources only, it cannot meet the demand. Measures are taken for water recycling and proper management, but are expensive. Even if it were possible to correct this problem with traditional methods such as dams, canals, reservoirs and deep wells, it would require an annual investment of approximately $180 billion on top of the $30 billion already spent each year [9].

And the fact that water withdrawal is higher than consumption, water management could play a vital role. However, it could be more costly than seeking out alternative source of water. For example in the UK alone, there is leakage of up to 3 billion litres of water per year [10]. And to repair all the leakage will cost more than seeking alternative source. And this is said to be the water has reached the economic leakage level. Reducing leakage level down to zero is virtually impossible and enormously expensive [11].

2.2 Desalination as a Solution to Water Problem

Water conservation is really a very crucial part of the overall water strategy. Every drop of water that is used is another drop in supply. It is very much encouraged to strengthen conservation efforts before turning to desalination. But in many communities additional water supply is needed even after they have fully considered the conservation measures. There are in fact communities around the world that rely 100% on desalinated water for their supply (communities listed in Appendix B). Hence desalination technique is the most promising solution to supply some remote regions with fresh water.

Desalination is the process of removing salt from water. Over the past decade, the number of desalination plants and their total capacity has almost doubled [6]. As shown in Figure 2-5, the current production capacity exceeds 65 million m³ per day and the number of plants has increased to more than 14,000 units [12].

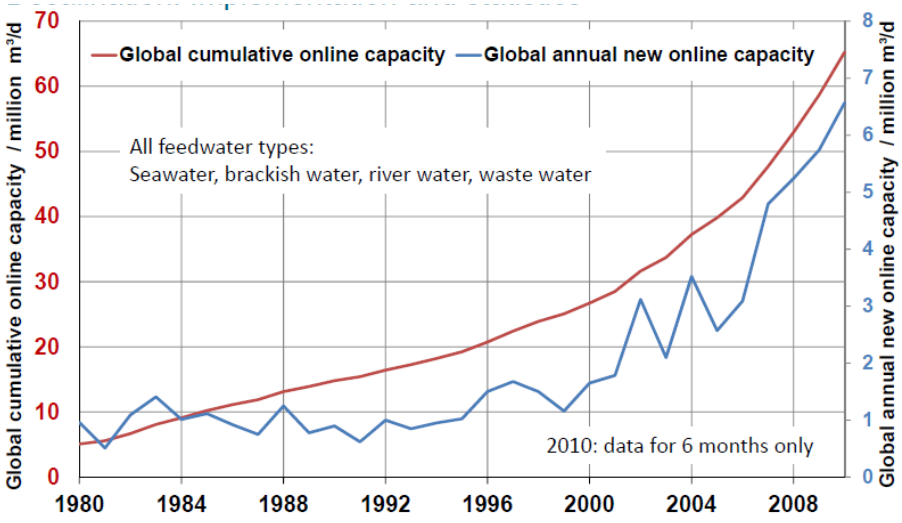

Figure 2-5: Global installed capacities of desalination (IDA Year Book 2010-2011)

The global installed capacity of desalination is shown in Figure 2-6 (see complete list in Appendix C). Saudi Arabia in Middle East has the largest installed capacity, and then followed by Spain in Europe and then USA in North America. All other top ten capacities are within the Middle East with Qatar and Kuwait depending 100% on desalination except Algeria and Libya in North Africa and then China in Asia [13].

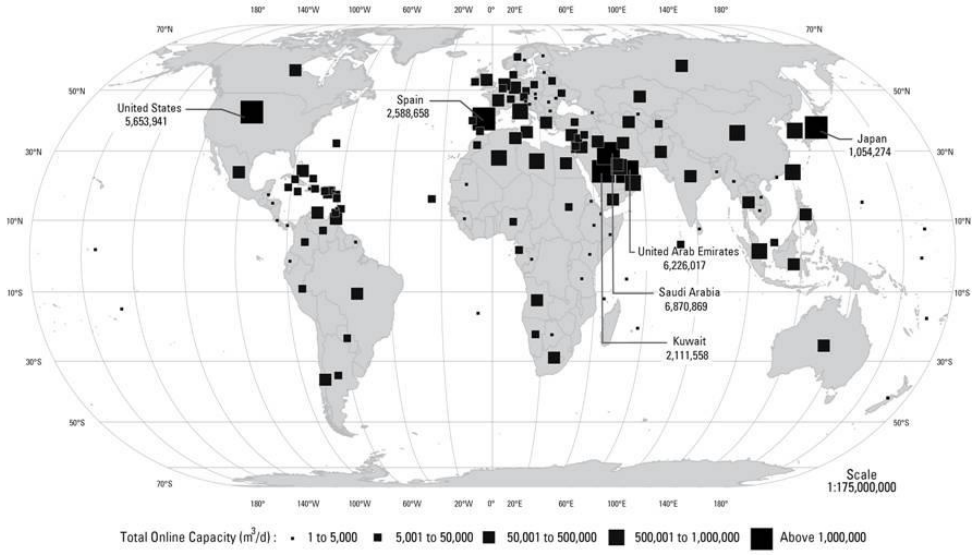

Figure 2-6: Total desalination capacity by country [14]

2.2.1 Existing Desalination Technologies

There are several desalination processes and most of them are reliable and in commercial use. The most important processes are divided into two classes; the thermal and the membrane processes. The thermal process is based on natural processes of distillation and usually involves heat transfer. Main thermal technologies are the multi-effect distillation (MED) and multi-stage flash (MSF). The membrane process is base on filtration through a membrane and usually driven by electricity. Major membrane technologies are electrodialysis (ED) and reverse osmosis (RO). Thermal processes produce water around 20 ppm TDS and membrane processes are usually designed to produce water of 100-500 ppm TDS while 1000 ppm TDS is the maximum limit for drinking water [5]. Other desalination technologies which are either not very common or are currently under research includes processes such as the membrane distillation, vapour compression and electrodeionization.

Membrane distillation (MD) combines the use of both thermal distillation and membranes. The process was introduced commercially on a small scale in 1980s. It primarily depends upon thermal evaporation and the use of membranes to pass vapour, which is then condensed to produce fresh water. In the process, saline water is warmed to enhance vapour production. This vapour is then exposed to a membrane that can pass water vapour but not liquid water. After the vapour passes through the membrane, it is condensed on a cooler surface to produce fresh water. In the liquid form, the fresh water

cannot pass back through the membrane, so it is trapped and collected as the output of the plant [19].

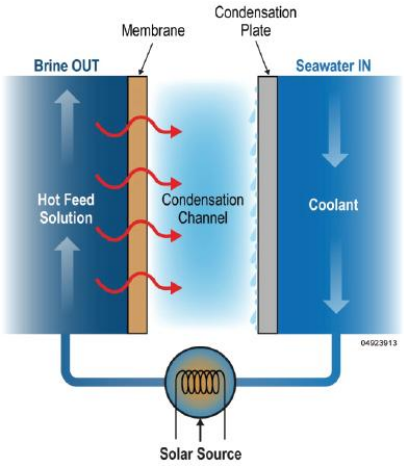

Figure2-7: Principle of membrane distillation [23]

MD has been used only in a few facilities, since it requires more space, more pumping energy per unit of fresh water produced, and more money and other approaches. The main advantages of MD lie in its simplicity and the need for only small temperature differentials to operate. Commercially it is of little significance.

In Vapour Compression (VC) technique, the mechanism is similar to MED except that the heat for evaporating the water comes from the compression of vapour rather than the direct exchange of heat from vapour produced in a boiler. They are usually built in relatively small units ranging from a few litres up to 3000m³ per day [15]. It has high energy requirement and capital cost compared to other technologies.

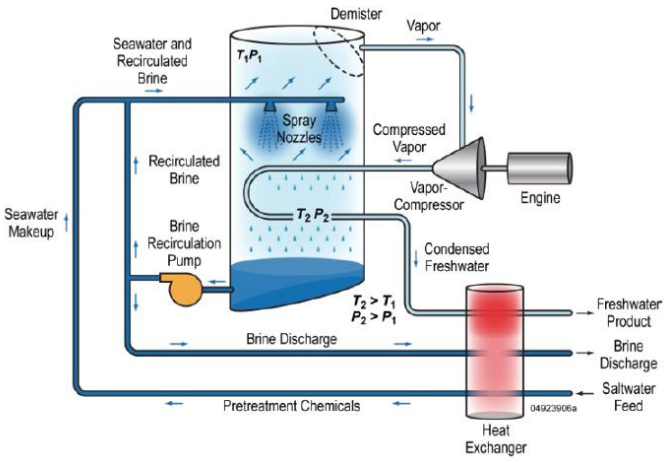

Figure 2-8: Vapour compression desalination system [23]

Electrodeionisation (EDI) is a modification of electrodialysis that combines ion exchange and membrane filtration. In this process, ions are removed using conventional ion exchange resin. However, an electric current allows the continuous regeneration of the resin eliminating the elution stage which induces addition of chemical reagents [16]. The main advantages of the EDI process include continuous operation, stable product quality, and the ability to produce high purity water without the need of chemical regeneration [17]. However, the principal application of EDI is limited to the further purification of water obtained from reverse osmosis.

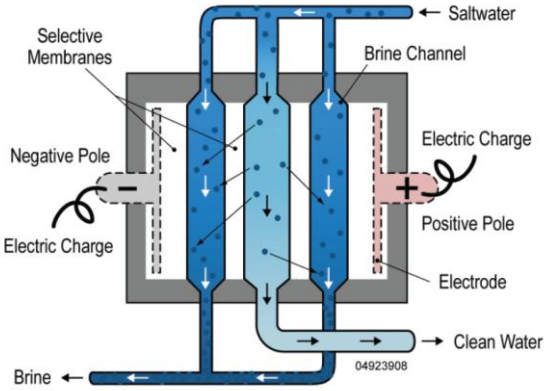

Figure 2-9: Principle of Electrodeionisation [23]

Figure 2-10 shows distribution of total worldwide installed capacity of desalination by technology. Each of the desalination technologies has its own unique advantage. However all desalination technologies are known to be highly energy intensive. The investment and operation costs are also very high. And finally the discharge of large amount of high concentration salt known as brine can have effect on the environment.

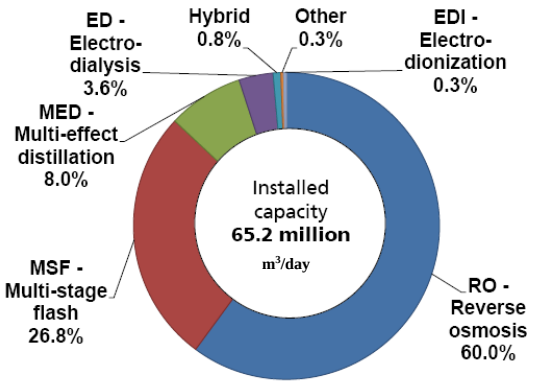

Figure2-10: Total installed capacity by technology [IDA Year Book]

2.2.1.1 Reverse Osmosis (RO)

Membrane processes represents the fastest growing process. In the reverse osmosis process, pressure is used for separation by forcing seawater to move through a membrane from a solution of saltwater to obtain fresh water. A diagram of RO process is illustrated in Figure 2-11. In RO process, there is no need for heating or phase change. The major energy requirement is for pressurising the feed water. This pressure ranges from 10 to 25 bars for brackish water. Due to higher concentration of seawater, it requires pressure from 50 to 80 bars. A turbine could be used to recover most of the energy consumed. Hence the RO process consumes 3kWh/m³ energy for brackish water and 5kWh/m³ consumption for seawater [20].

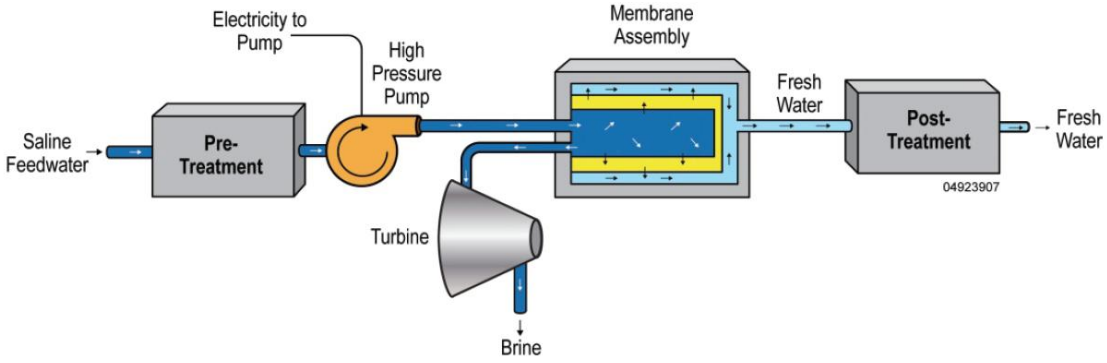

Figure 2-11: Principle of reverse osmosis process [23]

RO plants have low capital cost and high maintenance and running cost due to the high cost of the membrane replacement and the cost of the energy used to drive the plant. The process also requires intensive pre/post-treatment. The RO system has range from as little as 0.5m³ per day, the largest RO plant (Ashkelon Plant) is located in Israel with capacity of 330,000m³ per day which contribute 5-6% water needs. The plant cost $212m with water cost $0.52/m³. It occupies 75,000m³ of land, and it consists of four 5.5MW high pressure pump and 40,000 membrane modules.

2.2.1.2 Electrodialysis (ED)

Electrodialysis was commercially introduced in the early 1950s, about 10 years before RO [15]. In the 1960s, Electrodialysis Reversal (EDR) was introduced, to avoid organic fouling problems. Electrodialysis uses an electrical potential to move salts selectively through a membrane and leaving fresh water as product water. The amount of electricity

required for ED and its costs increase with increasing salinity of feed water. The total energy consumption under ambient temperature conditions and assuming product water of 500 ppm TDS would be about 1.5 to 4 kWh/m³ for a feed water of 1500 to 3500 ppm TDS respectively [21]. The ED process is illustrated in Figure 2-12. ED/EDR is not always a cost effective option for seawater desalination and does not have a barrier effect against microbiological contamination. Hence it is more suitable for brackish water and used in conjunction with conventional water treatment plants.

Like RO, ED/EDR can have capacity from 1m³ per day. The largest EDR plant is located in Abrera with a capacity of treatment of 220.000 m³ per day (576 stacks in two stages, provided by GE Water & Process) and it is related with desalting brackish water to improve the quality of the produced drinking water. The cost of the plant is €61 million with operation and maintenance cost of $25 million over two years.

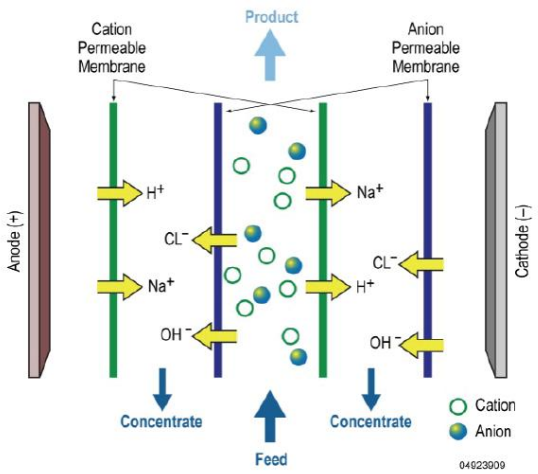

Figure 2-12: Ion exchange in electrodialysis process [23]

2.2.1.3 Multi-Stage Flash Distillation (MSF)

Multi-Stage flash is currently the most common technique used in thermally driven desalination. Seawater is heated and pressurised in the brine heater and then flows into chambers or stages. A fraction of it flashes into vapour due to lower pressure in the chamber and the brine passes from one stage to another and flashes repeatedly without adding more heat. The vapour produced by flashing is converted to fresh water by being condensed on tubes of heat exchangers that run through each stage. The feed water going

to the heater cools the tubes and in turn gets heated, so a reduced amount of thermal energy is required in the heater. A typical MSF unit is shown in Figure 2-13.

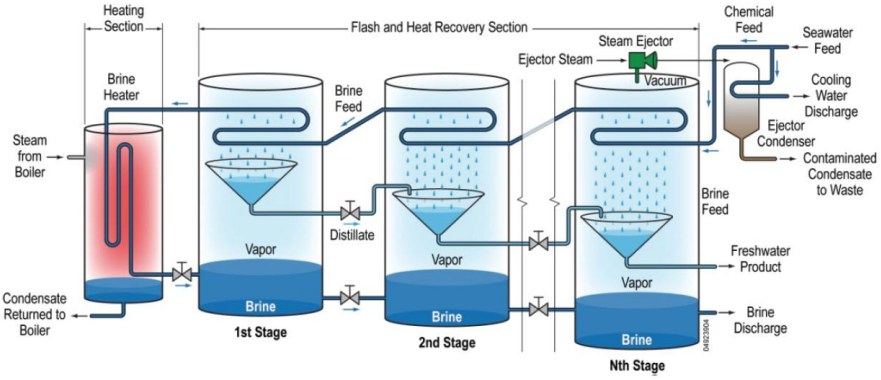

Figure 2-13: An illustration typical MSF plant [23]

A MSF plant can contain from 4 to about 40 stages, and usually operate at temperatures of 100 - 110 °C to produce 6-11kg of distillate per kg of steam applied [22]. Performance ratio can be as high as 12 and a 40 year life span [21]. A plant with performance ration greater than 7 could consume thermal energy of 290kJ/kg and the electricity used to drive auxiliary components is only 4 to 6 kWh/m³. However the overall capital and energy cost are very high. The largest MSF plant is Shoaiba Desalination Plant, Saudi Arabia. It was completed in 2003 with total capacity of 450,000m³ per day at an estimated total project cost of $1.06 billion.

2.2.1.4 Multiple Effect Distillation (MED)

The MED process uses same principle of evaporation and condensation at various stages known as effects. Each effect has reduced pressure than the previous effect. Hence the seawater goes through multiple boiling without the need to supplying additional heat. Preheated steam from boiler is fed into a series of tubes. It then heats the tube and act as heat exchanger to evaporate incoming seawater from another channel. The evaporated seawater becomes less salty and is fed into the next effects which are lower in pressure. The vapour condenses into fresh water. This is illustrated in Figure 2-11.

The MED has performance ratio up to 15 for 8 to 16 effects [20]. It has maximum operating temperature of 80°C and energy consumption of 290kJ/kg (thermal) and 2.5 to

3kWh/m³ (electrical). The largest MED plant is to be completed by 2012 with capacity of 68,000m³ per day at the cost of $124 million in Yanbu Saudi Arabia.

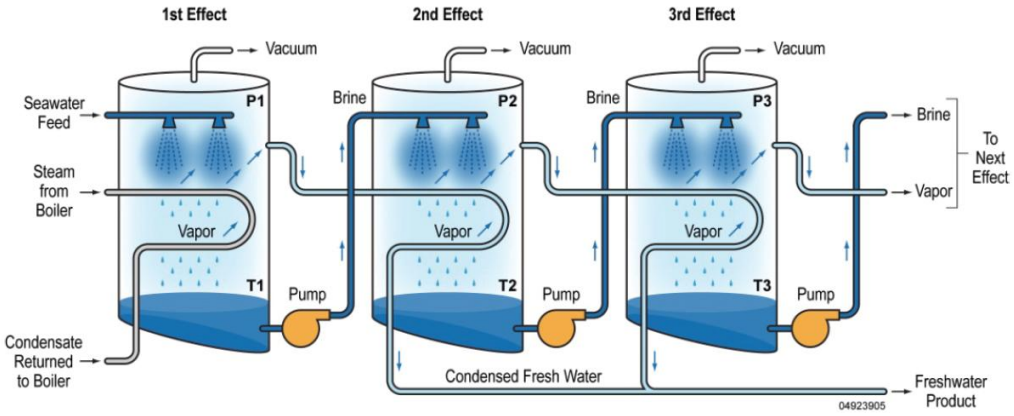

Figure 2-14: An illustration of MED plant [23]

2.2.2 Desalination and Climate Change

Climate change is caused by the emission of greenhouse gases. About 72% of the totally emitted greenhouse gases is carbon dioxide (CO_2), 18% Methane and 9% Nitrous oxide (NOx). Carbon dioxide emissions therefore are the most important cause of climate change. CO_2 is inevitably created by burning fuels like e.g. oil, natural gas, diesel, organic-diesel, petrol, organic-petrol, and ethanol. Energy is the major source of climate change. Over 80% of the world energy is from fossil fuel. The emissions of CO_2 have been dramatically increased within the last 50 years and are still increasing by almost 3% each year. The current emission is 29 billion tCO_2 and is projected to reach 58 billion tCO_2 by 2050 if action is not taken [23] as shown in Figure 2-15.

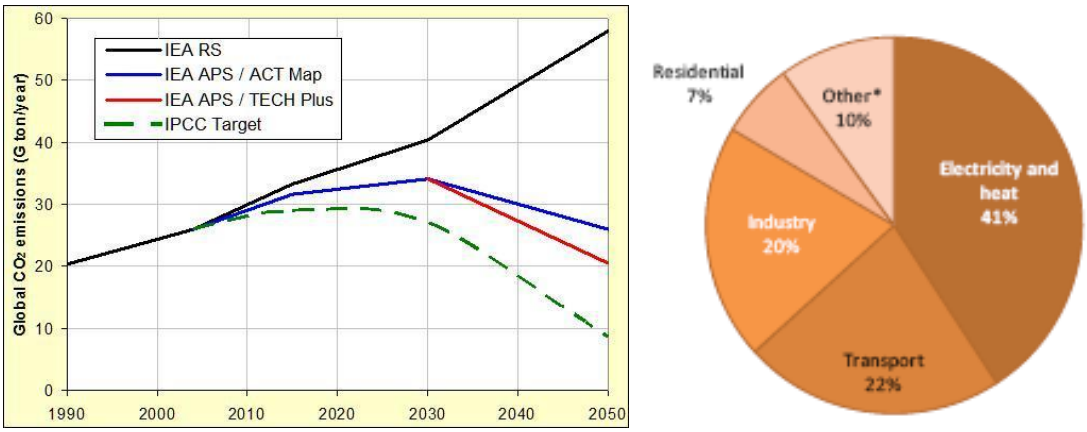

Figure 2-15: Projection of world CO_2 emissions and percentage by sector [24]

As shown in Figure 2-15, the electricity and heat generation sector accounts for major emission at 41%. Then followed by transport, industry and residential with 22%, 20% and 7% respectively. The other remaining 10% includes commercial/public service, agriculture/forestry, fishing, energy industries other than electricity generation, and other emissions not specified elsewhere.

The effect of climate change is posing threat to the whole world with global disasters, and most importantly drought which generally affects the availability of fresh water. Desalination which is seen as the best alternative to supply freshwater is very energy intensive. The use of desalination process will add to the already growing carbon emissions. And thus it can be seen that desalination alone without considering energy will not mitigate the growing water shortage but rather make it worse.

The global sources of freshwater are shown in Figure 2-16. Going by current estimate of water demand and the current installed capacity of desalination, it can be seen that desalination contributes to only 0.34% of global water supply. This contributes 0.7% of carbon emission to the electricity and heat generation sector, and contributes 0.3% to the global carbon emission from all sectors. If by 2050 up 10% of global water supply is from desalination driven by fossil, water desalination will contribute 33% to emissions from electricity and heat generation, and 14% to global carbon emission. A detailed breakdown of the analysis can be found in Appendix D. Hence this makes it a paramount priority to drive water desalination using alternative renewable energy sources.

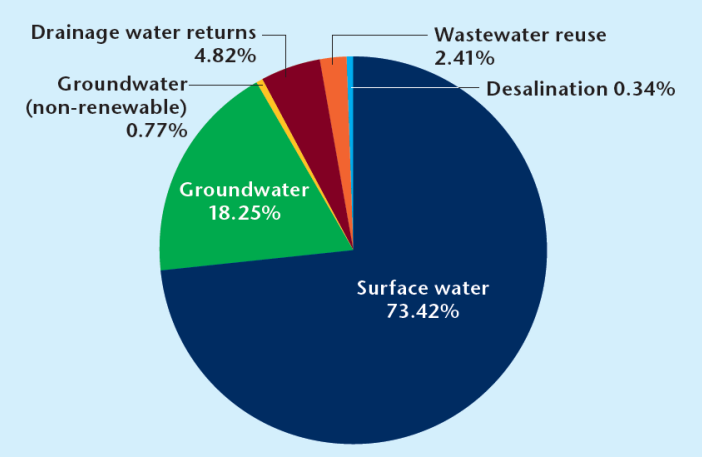

Figure 2-16: Global water withdrawal by source [12]

2.3 Desalination and Renewable Energy

Due to the large energy consumption in the major commercial desalination processes, along with the growing concern about carbon emissions, there is a strong interest in desalination units driven by alternate sources of energy, and in particular, renewable energy sources (RES) such as solar, wind, geothermal and biomass energy. While majority of desalination systems driven by RES are currently under research, the current installed capacity is more than 9,000m³ per day. The distribution of installed capacity of desalination by major RES is given in Figure 2-17. And list of countries by capacity of desalination and renewable energy source is given in Appendix E.

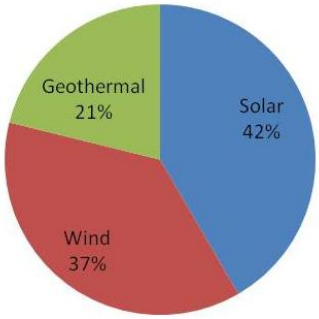

Figure 2-17: World distribution of desalination capacity by major RES [25]

It can be seen that solar energy dominates as renewable energy source for desalination. Figure 2-18 shows distribution of solar intensity around the world. It can be seen that regions with higher water scarcity have the most abundant solar energy. Hence the solar desalination process might be the answer for the optimum choice of water desalination. A 6kWh/m²/d of solar energy is equivalent to 0.6 litre/m²/d of oil [12].

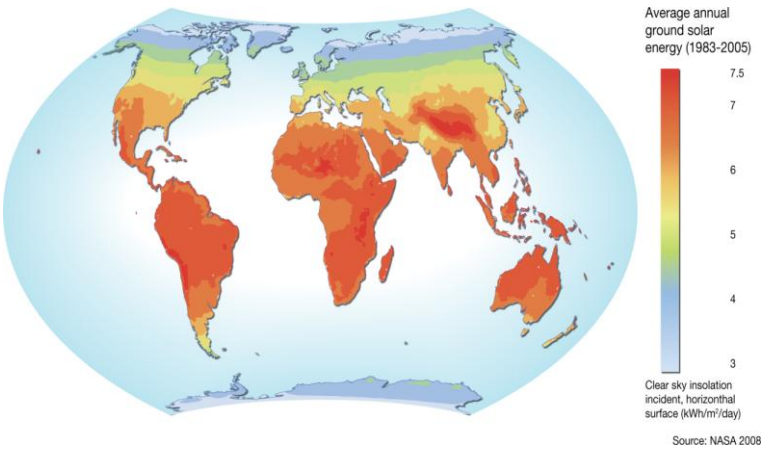

Figure 2-18: Distribution of solar intensity around the world

Solar energy systems are now proven technologies and economically promising. There are two main types of solar energy systems. There is the photovoltaic (PV) system which converts solar radiation directly into electricity, and the solar thermal system which converts solar radiation into useful heat. The PV systems are characterised with high cost and lower efficiency when compared to the solar thermal systems. In solar thermal systems, solar collectors are used to harness the energy from the sun. The solar collector is a device that basically absorbs solar energy in form of heat through a heat transfer medium and converts it into useful energy. The useful heat/energy collected can then be used for various applications. It can be used for electric power generation using an expander or turbine, for hot water supply, for cooling, industrial process heat and most importantly for desalination.

Solar collectors are divided into two. They are the concentrating and non-concentrating solar collectors. The concentrating solar collector uses reflectors to focus and concentrate the solar radiation onto and absorber. While the non-concentrating solar collector do not focus the solar radiation but only uses flat surface absorbers to capture the solar energy. The types of major concentrating solar collectors and their characteristics are given in Table 2-2.

Table 2-2: Major concentrating solar collectors [26]

Collector Type	Absorber Type	Concentration Ratio	Indicative Temperature Range (°C)
Linear Fresnel	Line	10-40	60-250
Parabolic trough	Line	10-50	60-300
Parabolic dish	Point	100-1000	100-500
Heliostat field	Point	100-1500	150-2000

The non-concentrating collectors can provide the energy required for desalination. However, they are characterised with low efficiency. They are more suitable for domestic application as they are generally inexpensive and widely used for domestic hot water systems. A large area of non-concentrating solar collector is required for small to large scale community based desalination systems. And this generally increases cost and land footprint. Concentrating solar collectors coupled with desalination systems have more

potential compared to non-concentrating solar collectors. They are more suitable for non domestic application. The systems are complex and require large infrastructures. There are four major types of concentrating solar collectors which have been implemented with primary aim of generating electricity. These systems can be adapted for desalination and most especially thermal desalination process. They are described as follows.

2.3.1 Parabolic Trough

Parabolic trough collector is a type of concentrating solar collector that uses the mirrored surface of a linear parabolic concentrator to concentrate direct solar radiation to an absorber tube running along the focal line of the parabola. The collector consists of long parallel rows of reflectors that are curved to form a parabolic trough with its receiver (absorber tube) placed at the focal point of the reflector. The receiver of a collector is linear [26]. The absorber is often a metallic tube covered by a glass tube in order to reduce heat loss. The parabolic trough can collect up to 60% of the incident solar radiation and has achieved a peak electrical conversion efficiency of 20% [27].

The first parabolic power plant was built in Egypt by Frank Shuman (1912) with a total capacity of 55kW [28]. The parabolic trough collector is already a rather matured technology due to many years of designing and operating experience. Parabolic trough collectors have been previously used mainly for large scale grid application. Commercial parabolic trough plants have been operation for more than 15 years [29]. Solar Energy Generating Systems (SEGS) is the largest solar energy generating facility in the world. It consists of nine plants with a total of 354 MW connected to the Californian electric grid. The plants have proven a maximum efficiency of 21 % for the conversion of direct solar radiation into grid electricity.

Another important application of this type of collector is the first commercial parabolic trough power plant in Europe known as the Andasol developed by Solar Millennium AG (Figure 2-19). The plant is located in Spain with total capacity of 50 MW and operates with thermal storage. The collector has surface area of over 510,000m^2 which is equivalent to 70 soccer pitches. There are two more plants currently under construction. The Andasol 2 to be commissioned later this year and the Andasol 3 slated for 2011 [30].

Figure 2-19: The Andasol Parabolic Trough Power Plant Spain (Source: Solar Millennium AG)

2.3.2 Heliostats Field

The heliostat field solar thermal plant as shown in Figure 2-20 consists of a central receiver known as power tower which is surrounded by a large array of heliostats field collector. The heliostats are flat mirrors that track the sun and reflect the solar energy onto a central point receiver. The energy is transferred to a fluid (water, air, liquid metal and molten salt have all been used) which is then pumped to a heat exchanger or directly to a turbine generator. The systems are generally known as power tower or central receiver systems. The heliostats and the receiver can be put into different configurations depending on geographic location.

Central receivers with concentration ratios up to 800 can achieve high temperatures up to 500 °C. The solar collection efficiency is approximately 46% and the peak electrical conversion efficiency (i.e., conversion from solar radiation to electricity) is 23% [26].

Figure 2-20: The decommissioned Solar Two Heliostats Field (Source: SNL)

The heliostat system was built in the U.S. called the Solar One plant located in California. And later after certain changes were made to the plant, it was called Solar Two. It

consists of 1926 individually oriented heliostats with a total area of 40 m^2 for a total array of 82750 m^2. The plant was a success and demonstrated the ability of solar molten salt technology to provide long-term, cost effective thermal energy storage for electricity generation [31]. It provided 10 MW of power and was decommissioned in 1999.

Abengoa Solar has developed the first commercial heliostat system in Europe. The system known as the PS10 uses 624 units of heliostat collectors to generate 11 MW of electrical power (Figure 2-21). Each of the heliostat has total surface area of 120m^2 which concentrate solar energy to the top of a 115 meter (equivalent to 40-storey building) solar receiver. The heliostats do not surround the tower but rather use a north-side field which is believed to be more efficient for its geographical location [32]. There is the PS20 currently under construction. It is said to be double the capacity of PS10.

Figure 2-21: PS10 Solar Plant Developed by Abengoa (Source: solarpaces.org)

2.3.3 Linear Fresnel

The linear Fresnel collector system consist of set of parallel array of linear mirrors which concentrate light on to a fixed receiver mounted on a linear tower. The system operates base on principles of Fresnel. The system is similar to parabolic trough but instead it is not parabolic in shape. It is also similar to the heliostat system, but the receiver is a linear tube mounted on a tower not very high above the collector. D. R. Mills et al (1997) recorded a maximum 38.5% thermal efficiency using compact linear Fresnel reflectors technology developed by Ausra Power [31]. The plant is said to be operating with near perfect reflection and near zero thermal losses.

The first to apply this principle in a real system for solar collection was Francia (1968) who developed both linear and two axis tracking Fresnel collectors systems. The system

has been faced with several difficulties [33]. One difficulty with the linear Fresnel technology is that avoidance of shading and blocking between adjacent reflectors leads to increased spacing between reflectors. Blocking can be reduced by increasing the height of the absorber towers, but this increases cost. There is currently no commercial system of such that exist. However Ausra Power has plans to commercialise such system after a demonstration of their 5 MW pilot plant (Figure 2-22) located in California.

Figure 2-22: Linear Fresnel Collectors by Ausra Inc (Source: solarpaces.org)

2.3.4 Parabolic Dish

A parabolic dish collector is a point-focus collector that tracks the sun and concentrates its energy onto a receiver located at the focal point of the dish. The dish structure must track fully the sun to reflect the beam into the thermal receiver. The receiver absorbs the solar energy and converts it to thermal energy in a circulating fluid. A low molecular fluid is mostly preferred because of its good heat transfer characteristics of and low-pressure drop behaviour. Thus hydrogen or helium is usually used as working fluids [32]. Concentration ratios usually range from 100 to 1000, and they can achieve temperatures in excess of 500 °C. The main use of this type of concentrator is for parabolic dish-engines for electricity generation. The parabolic dish system does not have thermal storage capabilities, however, it can be hybridised to run on fossil fuel or other alternative renewable energy source during periods without sunshine.

Several dish-engine prototypes have successfully operated over the last 10 years. The systems range between 10kW to the 400m^2 100kW of the Australian National University. They are particularly well suited for decentralised power supply and remote, stand-alone systems [34]. The Stirling Energy Systems (SES) demonstrated the dish-engine system in a 150kW plant which has 6 units of the dish collectors each providing 25kW of electrical

power (Figure 2-23). A comprehensive report titled: A compendium of Solar Dish Stirling Technology, prepared by SNL gives details of different types of systems around the world.

Figure 2-23: The Parabolic Dish Collector (Source: SES)

2.4 Desalination Economics and Industry Analysis

The relatively high financial costs of desalination prevented the application and commercialisation of desalination technologies in most areas. However, desalination cost is changing with improved and less expensive technologies. Cost of desalination is already low enough to make desalination an attractive option for some communities when the benefits of desalination are considered, such as providing a drought resistant supply and providing a means to diversify a large community's water supply portfolio. The cost of water desalination varies with technology used. It depends mainly on size, location and environment conditions, quality of feed water, labour, operation and maintenance, and life span of the system. Although desalination plants have longer life, it is recommended for a plant to have 20 years life span [35]. A breakdown of cost of desalination system is adapted from Delyannis (1985) and given in Table 2-3 below.

Table 2-3: Main items of cost of construction and cost of water

COST OF CONSTRUCTION
1. Construction of desalination unit
2. Land and site preparation
3. Auxiliaries include:
Pipe and pumps of salt water and distillate
Storage for salt water and distillate
Any other items of investment costs

Total investment cost should be reported per m³ of system capacity

COST OF PRODUCT WATER

1. Energy and power for pumping, kg fuel or kWh
2. Cost of raw water, if purchased or transported
3. Cost of water treatment, if necessary
4. Cost of maintenance and material replacement
5. Labour for operation and maintenance
6. Amortization of capital cost
7. Taxes, insurance and subsidies, where applicable

Annual operating charges should be computed per m³ of product water.

2.4.1 Desalination Costs

The cost of building a desalination unit and cost of fresh water produced are very crucial to designing a desalination system. The costs of energy and carbon emissions from a desalination plant are generally very high regardless of the type of technology used. Figure 2-24 shows percentage cost of major desalination systems and that driven by RES.

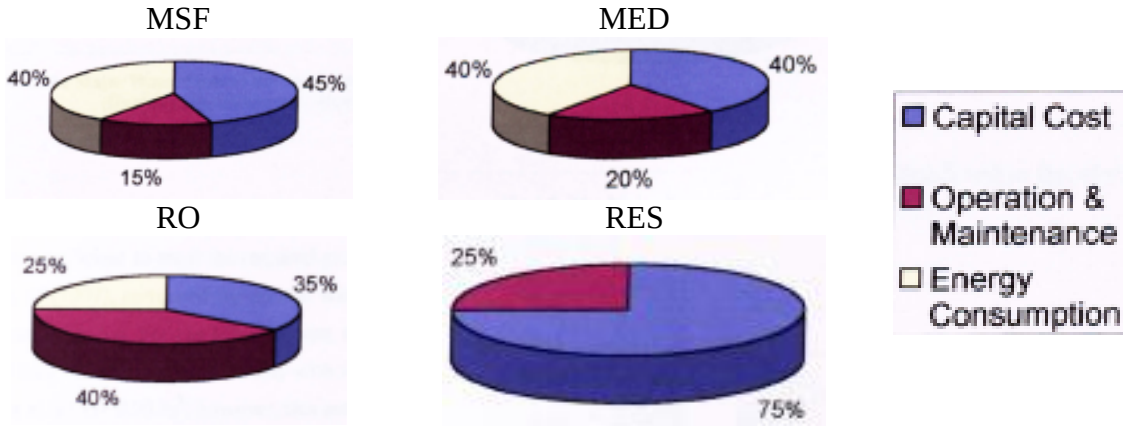

Figure 2-24: Major cost of desalination plants [36].

Not-with-standing the anticipated cost reduction offered by new emerging desalination technologies, the conventional desalination process remains expensive and unfeasible in many countries around the world. The limited means of financial resources of many countries are insufficient to meet the required process capital and operation expenses. Bednarski et al. (1997) compared the current water production cost of the MSF, RO, MED processes [37]. Figure 2-25 shows comparison of the major desalination technologies. For the MSF process, with a 27,000m³ per day plant, the unit cost \$0.8/m³.

This is almost equivalent to that of the RO process at an average of 0.93 per m^3. However, the value presented is not the real final value and mostly scientific and not based on a commercial plant. The actual value is highly dependent on the feed water source and the treatment cost of the feed water. So also with the MED, despite the fact that a lower unit cost is documented at \$0.45 per m^3, this method has only been utilised commercially by the desalination industry to a very limited scale. Both the values from MSF and MED do not include thermal energy cost of the systems. Assuming utilising solar energy to provide the thermal which can be considered free of charge, the cost of solar desalination SD will be \$1.03 per m^3. This indicates solar energy as very competitive when compared to fossil fuel driven desalination system. More about economics of water desalination can be found in chapter 7.

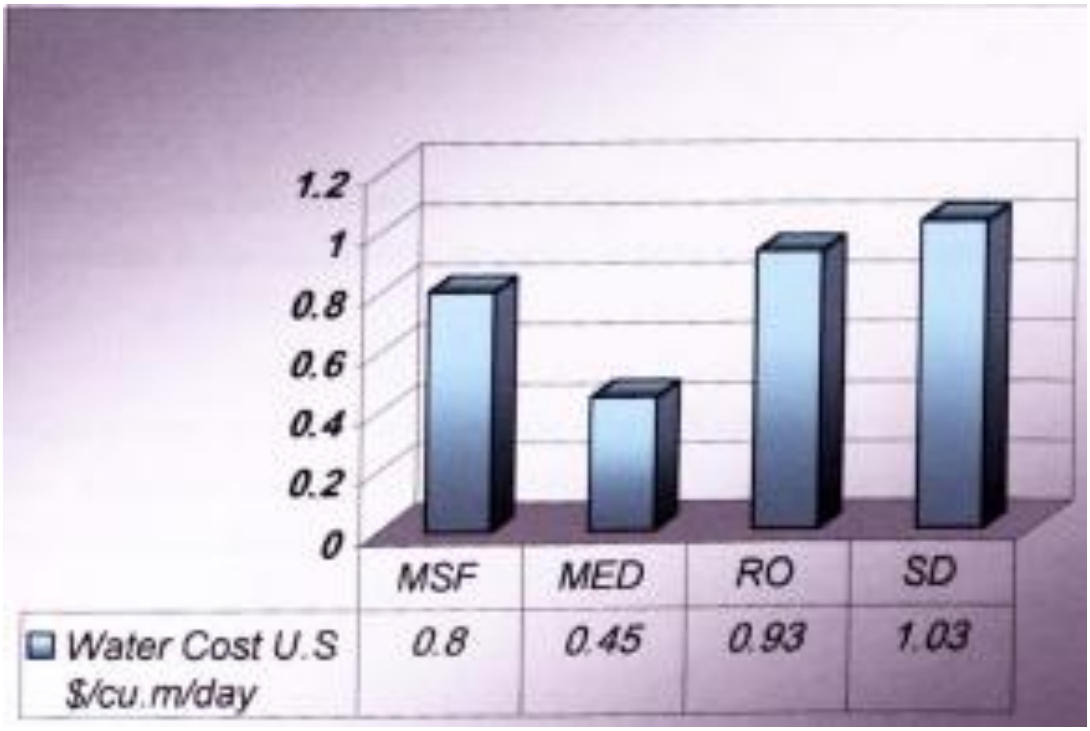

Figure 2-25: Unit water cost comparison of major desalination technologies

2.4.2 Market Opportunities

Worldwide, less 1% of drinking water is produced by desalination which is supplied by more than 14000 plants in more than 120 countries. Considering that almost one quarter of the world's population lives less than 25 km from the coast, seawater could become one of the main sources of freshwater in the near future. The market volume has soared from \$2.5 billion in 2002 to \$3.8 billion in 2005 with a growth rate of over 15% per

annum (estimated value is only for plant and equipment, and not considering the whole value chain). The market worldwide is estimated to reach nearly $30 billion with installed capacity of more than 4.38 x 10^{10} per year (1.2 x 10^{8} m³ per day) by 2015 (Figure 2-26). A dramatic increase is expected in new technologies and small systems applications in Asia and in particular in India and China [38].

Current desalination plants are large installations. Their size and capital cost mean that only very large companies can engineer and install them. Their complexity means that local municipalities are often unable or unwilling to operate them. Modular size solar driven systems can be the ultimate solution for these local municipalities. This also creates a huge new opportunity for those firms able to integrate the design, building and operation of these plants

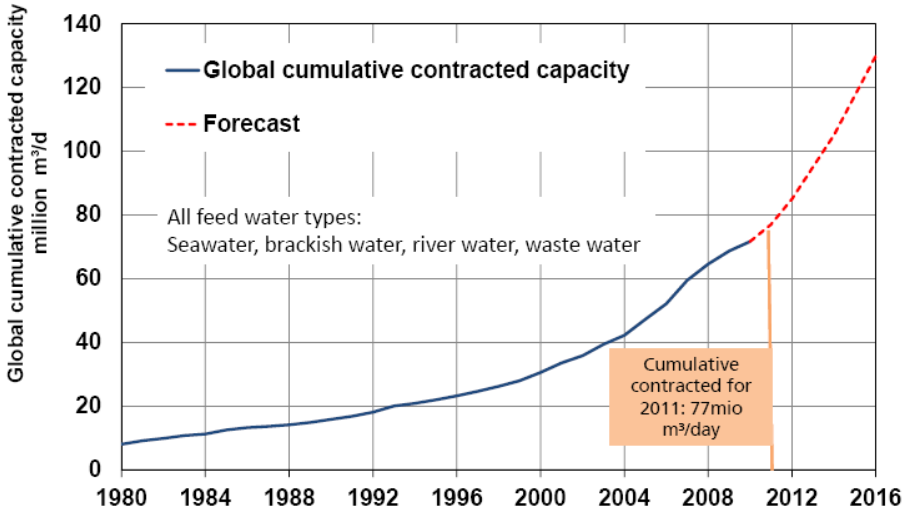

Figure 2-26: Projected growth of global installed capacities of desalination (IDA Year Book 2010-2011)

In terms of the geographical breakdown of the market, the regions of the Middle East and North Africa (MENA) clearly dominate the demand (over 50% of the market share), followed by America, Europe, Asia Africa and Australia that share about 50% of the market respectively (Figure 2-27). Although desalination is currently not a commonly used technology in Africa and the Caribbean where water supply is not only scarce and unreliable, but often not potable even when accessible, governments and private organisations are strongly considering desalination as a way to meet the growing demand

for potable and industry-quality water in these regions. In fact, in many of these countries, water distribution infrastructure is poorly developed and the few pipes that are laid often have leakages. This creates a whole new opportunity for decentralised non large scale distributed water supply.

Urban end users that have the financial resources and require good quality water are turning to reverse osmosis RO desalination rather than rely on local water services. Industrial end users are also using RO to pre-treat municipal water before it is used as process water. Rural and remotely located end users such as tourist lodges and commercial farmers are also using desalination. The tourism industry in Southern and East Africa is booming and with island-based tourist lodges often having limited or no sources of fresh water, they therefore have to desalinate seawater. Desalinated brackish groundwater can be a good source of water for commercial farmers. Other key sector is the oil/gas sector and general energy sector which require large amount of process water.

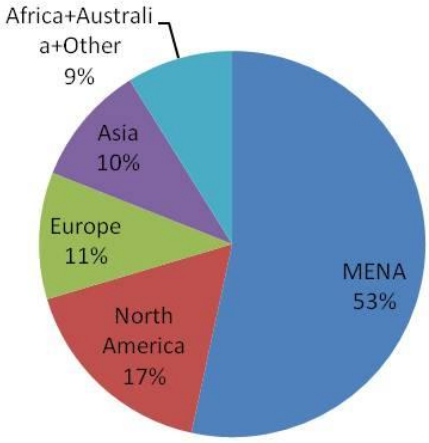

Figure 2-27: Desalination market share [13]

The most attractive markets for desalinated water are within the MENA region which constitute over 50% market share. However, there are other potential regions where the price of public water is already comparatively high, and also a region where the climate is arid and regions where the population is rapidly growing. The future water demand in the MENA region was assessed by an analysis of FutureWater (Immerzeel et al. 2011), which included effects of climate change on the future availability of natural surface and groundwater resources. The analysis suggests that there will be a significant reduction of

available surface and groundwater in the medium and long-term future, from 2.25 x 10^{11} m³ per year (6.16 x 10^{8} m³ per day) in the year 2000 to less than 1.9 x 10^{11} m³ per year (5.2 x 10^{8} m³ per day) in 2050. At the same time, water demand will grow from 2.55 x 10^{11} m³ per year (7 x 10^{8} m³ per day) in the year 2000 to 4.5 x 10^{11} m³ per year (1.2 x 10^{10} m³ per day) in 2050, opening a very dangerous gap of supply that will affect the whole region from now on [39].

Taking into consideration the severity of the water gap projected in the MENA region the need for sustainable energy alternatives other than fossil fuel has never been more urgent. For being sun-rich and water-scarce region, the MENA region is one of the most suitable regions in the world to start implementing desalination plants sourced by solar thermal energy. According to scenarios generated within a study carried out by Fichtner (2011) for The World Bank, solar desalination is likely to become predominant starting from 2020 to 2030 when oil and gas sources are expected to be decreasing. The study identified huge solar desalination potential corresponding to 5.5 10^{10} m³ per year in 2030 and 9.8 x 10^{10} m³ per year by 2050. Until then the key challenge is to take measures through research to bring solar desalination to its desired well-engineered level, achieving highest efficiency gains most especially using technologies such as membrane distillation and humidification dehumidification which are currently the most promising for solar thermal desalination. This potential transition from conventional desalination to solar desalination would further contribute to the climate protection. In the MENA region alone, there is potential to reduce the emissions of carbon dioxide from fossil fuel from 570 million tCO_2 in 2010 to 270 million tCO_2 in 2050. This can be achieved in spite of a significant growth of population and economy expected in the region that would lead to emissions of over 1.5 billion tCO_2 following a business as usual strategy if no action is taken [39].

2.5 Conclusion

There is no doubt humanity is faced with growing scarcity of fresh water despite huge abundance on the planet. Demand exceeds supply with consumption only around 50% of withdrawal due to mismanagement. It will cost more to manage water resource only and not seek for alternative source. Water desalination has huge potential as a solution to global water shortage as larger population of the world live along coastlines. However,

desalination technologies are energy intensive. Combing desalination with RES is promising solution.

Although the strong potential of solar thermal energy to seawater desalination is well recognized, the process is not yet developed at the commercial level. The main reason is that the existing technology, although demonstrated as technically feasible, cannot presently compete on the basis of produced water cost with conventional distillation and RO technologies. However, it is also recognized that there is still potential to improve desalination systems based on solar thermal energy. Conventional desalination benefits from considerable economies of scale, hence a trend in recent years to ever larger plants. Solar desalination capital costs are less dependent on scale and this raises the prospect of increased competitive margin for systems supplying smaller communities or small towns. Potential integration with other industries and projects, such as using the waste brine solution for salt production, or growing crops in and around the solar collector area, may further enhance local economic attractiveness.

The Middle East and North Africa is an attractive region for low cost solar systems – enjoying high levels of solar irradiance with limited seasonal fluctuation, and in many cases a largely uninhabited desert coastal strip with land either owned by the government or having low commercial value. Two potential MENA markets have been identified. The first is oil and gas exporting countries with high government revenues, already dependent on desalinated water but wishing to diversify their oil-intensive economies. The second is developing countries with low GDP per capita (such as Yemen, Sudan, Djibouti and Eritrea), now facing massive water deficits often leading to increasing internal conflict, but unable to afford conventional desalination technology. In these cases there is likely to be both private industry and public sector interest, and potentially donor funding for pilot schemes.

Chapter 3: Design and Test of Desalination Unit

3.0 Introduction

This chapter describes various types and classification of humidification dehumidification desalination systems. It presents psychrometric analysis carried out in order to predict the performance of the desalination system under different operating conditions. This using the psychrometric property models enables the design of the desalination system. Hence system energy requirement and water flow rates were estimated. After system design the operation strategy has to be adapted to the local conditions. Thus a preliminary test was carried out to understand the practical behaviour of the system. Various operating parameters which include temperatures and flow rates were measured and the overall system performance was obtained based on the measured parameters. And it was seen that the system output can be greatly improved by operating at higher temperatures.

3.1 Humidification Dehumidification Desalination

The humidification dehumidification process is similar the natural hydrological process whereby the sun heats the ocean. And then the water in the ocean evaporates through natural convection to form cloud. The cloud is condensed and water is obtained as rainfall. The process is illustrated in Figure 3-1. The HD process tends to replicate this natural hydrological cycle but instead in a box where evaporation takes place by hot water mixing with dry air in the humidification chamber and then passed to the dehumidification chamber where a condenser is used to obtain fresh water.

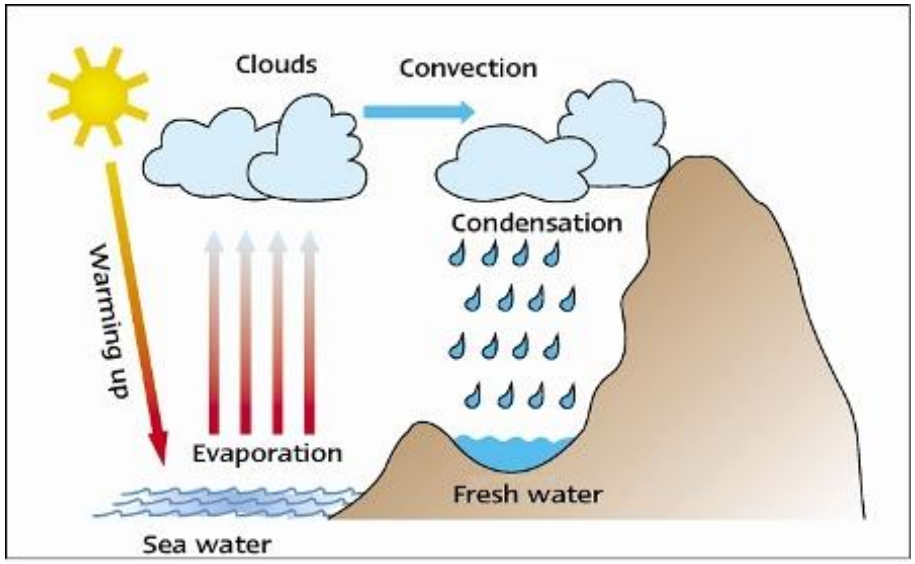

Figure 3-1: Natural hydrological cycle

One advantage of the HDD process is that it is seen as the most promising desalination technology compatible with renewable energy application most especially solar energy. In the HDD system, the humidified air flows in a circuit driven by natural or forced convection between dehumidification chamber and the humidification chamber. The air is sprayed or distributed on a wetted media and then moves in either co-current or counter-current flow to the hot feed (seawater) through the humidification chamber and becomes saturated. In the dehumidification chamber, water vapour from the humid air condenses on a heat exchanger. The distillate runs down the heat exchanger and collected in a basin. The heat of condensation is mainly transferred to the cold seawater feed flowing through the heat exchanger. Thus the temperature of the feed in the condenser rises. This feed can be discharged or further heated in a solar collector or by waste heat. The principle of a desalination system developed by Muller et al. [41] is illustrated in Figure 3-2. The system regarded as multi effect humidification (MEH) is based on concept of humidification dehumidification desalination (HDD) process where the humid air flows in a circuit driven by natural or forced convection between condenser and evaporator.

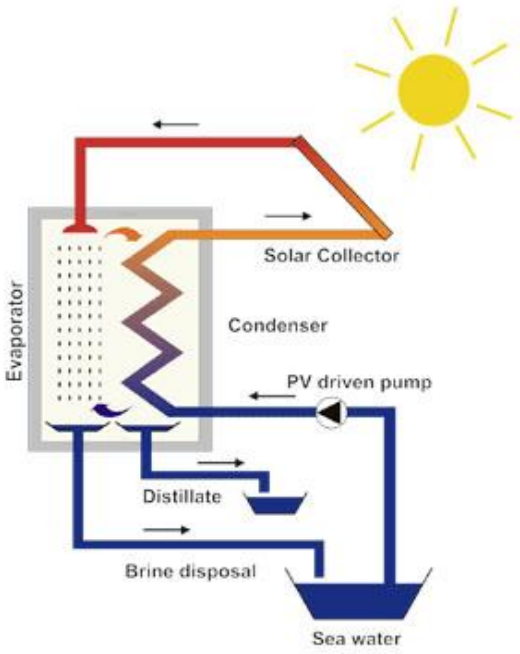

Figure 3-2: Illustration of HDD system [41].

In the evaporator the hot feed (seawater) heated in a solar collector, is distributed onto vertically hanging fleeces and it slowly trickles downwards. The air moves in countercurrent flow to the hot feed through the evaporator and becomes saturated. Partial

evaporation cools the brine and brine leaves the evaporation as concentrated brine with higher salt content and temperature of approximately 45ºC.

In the condenser water vapor from the humid air condenses on a flat plate heat exchanger. The distillate runs down the plates and collected in a basin. The heat of condensation is mainly transferred to the cold seawater feed flowing upwards inside the flat plate heat exchanger. Thus the temperature of the feed in the condenser rises from 40ºC to approximately 75ºC. This feed is further heated from 80 to 90ºC in a solar collector or by waste heat. Salt content of the feed as well as its temperature increases by partial reflux of the evaporator outlet brine to feed.

During last decade a number of HDD units have been developed and tested [40-44]. Detailed investigation of desalination unit based on HDD process is presented in [40]. In this unit the air is circulated by natural or forced convection and it is heated and humidified by the hot water obtained either from a flat-plate solar collector or using an electrical heater. The latent heat of condensation is recovered in the condenser to preheat the saline feed water. Investigations showed that no significant improvement in the performance would be achieved by using forced air circulation at high temperature. But at low temperatures it is significant. A strong effect of feed water flow rate on unit production was also observed. Production rate increased by increasing the feed flow rate up to a certain value and decreased beyond that value.

Dependence of the HDD system performance on the feed water and airflow rates was also studied in [43] and the optimum values were determined. They concluded that system with forced air circulation is suitable for small-scale solar desalination. Their system achieved productivity of 12 l/m^2d, which is three times more than that of a conventional system.

Testing and evaluation of series of the HDD based plants were described in [41, 42 and 44]. In [41], pumping energy was supplied by PV-modules and thermal energy from solar collectors. An average daily distillate production was 100 litres with 8.5 m^2 collector area without thermal storage. The process heat requirement was 150 to 180 kWh per m^3 of distillate at a temperature of 80ºC. The daily average GOR-factor (heat recovery factor

equivalent to COP) was between 3.0 and 4.5. They concluded that the system efficiency could improve by continuous operation with hot water storage. Solar MEH-desalination system studied in [41 and 42] used 2 m^3 hot water storage tank which increased the production rate to 500 l/d with 38 m^2 collector area (about 13 l/m^2).

Two different desalination units were tested in [42]. Table 3-1 presents the comparison of designed parameters of the two systems. The first one ("SODESA system") consisted of a thermal storage tank at ambient pressure and a collector field. The feed water was heated by direct circulation through the collector. The system efficiency was high due to elimination of heat exchangers, but costly materials to resist seawater corrosion at 100ºC were required for the collector and the heat storage tank.

Table 3-1: Comparison of "SODESA System" and "Oman System".

	SODESA System	Oman System
Characteristic	Completely seawater filled system: Everywhere corrosion resistant components needed. No heat exchangers required	Divided System: Heat Supply contains fresh water: standard collector / storage technique. Titan Heat exchanger separates heat supply and distillation unit
Collectors	Seawater proof special collectors made from silicon / glass pipes (ISE Freiburg scg)	Standard Evacuated Flat Plate Collector thermoSolar 400 V
Collector Aperture Area	47.2 m^2	40 m^2
Max. Storage Temperature	99°C	120°C
Storage Tank Size	6,3 m^3 (Ambient Pressure)	3,2 m^3 (Pressurized)
Designed Prod.	550 - 850 litres per day	650 - 900 litres per day

The second unit tested in Oman consisted of a standard evacuated flat plate collectors and a pressurized storage tank with a closed fresh water loop at 2.5bar for heat supply. The storage tank was made with mild steel and all piping with standard copper. The feed was

heated by a titanium heat exchanger. The required electrical power was supplied by PV-cells. Daily production rates are 11.7 to 18 l/m^{2}d and 16.3 to 22.5 l/m^{2}d. It can be seen that the system operating at higher temperature required less amount of solar collector area and at the same time producing higher amount of fresh water.

The efficiency of the HDD system is much higher than that of the conventional systems. However, they retain some weak points such as the usage of relatively high quantity of feed water. Estimation based on the data presented in [41] shows that the feed water flow rate is around 20 times the distillate production rate without brine recirculation. On the other hand if the HDD system works with brine circulation, the quantity of cooling water will be 6 to 10 times larger than the distillate produced. These circumstances are crucial when the units are operated in the arid areas having limited water sources. Heating up to 80-85ºC is not sufficient for water disinfections, thus HDD desalination systems need chemical pre/post treatment of product water. Operation personnel are needed for running the systems. It will be shown that the water requirement of the HDD system can be reduced through energy recycling while increasing the amount of fresh water production.

3.1.1 Classification of HDD Systems

The HD process can be classified according to cycle configuration, flow mechanism and heat transfer medium. They are generally classified into the closed water open air (CWOA) and closed air open water (CAOW) as illustrated in Figure 3-3.

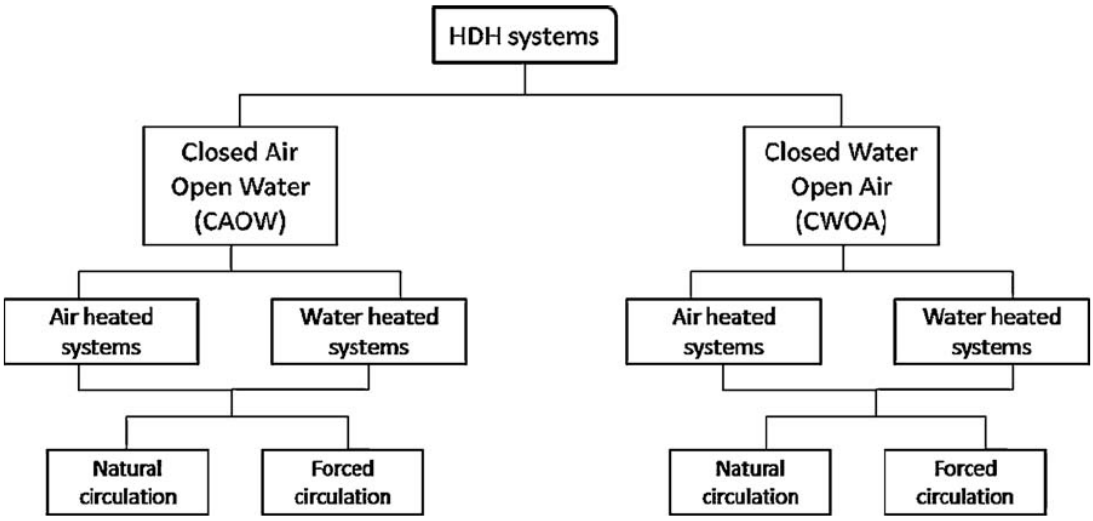

Figure 3-3: Classification of HD system

In CAOW, the air is circulated between the humidification chamber and the dehumidification chamber in a closed loop while the water is not re-circulated through the dehumidification chamber but rather discharged or partially re-circulated in the humidification chamber to recover heat. Thus this cycle configuration is associated with requirement of large amount of cooling water which at same time serve as the hot feed. Almost all research works reported in literature are CAOW configuration. Saadawy et al. (2008) and Narayan et al. (2010) reported in great details research activities on HDD over the past three decades [45 and 46]. Narayan et al. (2010) pointed out that almost all the investigators have observed that the performance is maximized at a particular value of the water flow rate. And also natural circulation of air yields better efficiency than forced circulation of air. However, it was not possible to report on the exact advantage from the data available in literature. It was found water production was between 4 and 12 kg/m²/day and the COP varied between 1.2 and 4.5. COP indicates thermal performance of the system. The low COP was mainly due to non recovery of the latent heat of condensation, while the high was due to high heat recovery. Thus this shows the importance of recovery of latent heat of condensation in order to reduce the energy consumption of the system.

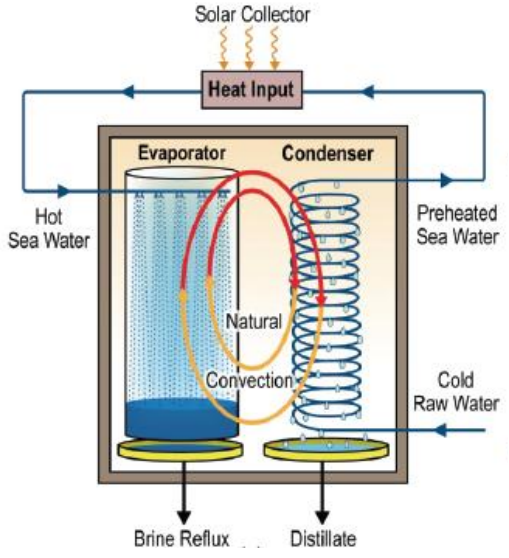

Figure 3-4: Closed air open water HDD system with natural convection

In CWOA, the water is circulated in a closed loop and only make up water is added while the air is discharged to the ambient. The water is usually heated is such systems. It is used to emphasize recycling the brine through the system to ensure a high utilization of the salt

water for freshwater production. Thus the system requires less cooling water. Very few literature based on this cycle configuration have been reported. One disadvantage of the CWOA is that the temperature of cooling water at the dehumidification chamber rapidly increases. This limits the dehumidification of the humid air resulting in a reduced water production compared to the CAOW system.

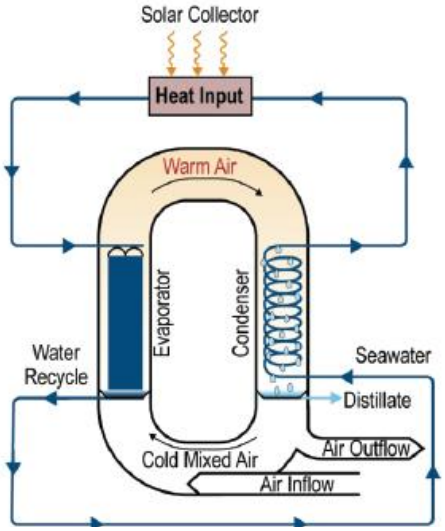

Figure 3-5: Closed water open air HDD system

In both the CAOW and CWOA configuration, it was reported that the mode of air flow at the humidification chamber can either be in counter-current or co-current flow mode. And the latter lead to more efficient humidification. Most previous work performed the HDD process in two separate columns, which increases the complexity of the system and limits the humidification effect of the carrier gas as well as the thermal efficiency of the process [47].

3.1.2 Humidifiers for Water Desalination

The humidifiers are an important part of the HHD process. Together with the solar collectors, they are the main items that determine the efficiency and the cost of the whole system. There are two main types of humidifiers; the steam humidifiers and adiabatic humidifiers. In the steam humidifiers, the introduction of steam into a stream of air will cause it to be humidified. The change in state from liquid to gas has already taken place with necessary enthalpy. Adiabatic humidifiers bring about the direct evaporation of water into the air. The heat of vaporisation is removed from the air, and thus negligible

external energy is required. Saturated vapour forms with a partial pressure equal to the saturation pressure at the temperature of the liquid.

Within the adiabatic humidifiers are the spray humidifiers and pad humidifiers. In the spray humidifiers liquid is sprayed into the gas stream usually by means of a nozzle, which disperses the liquid into a fine spray of drops. Pad humidifiers uses contact surfaces where water and air mix for evaporation. They are commonly used in greenhouses, poultry and livestock houses, painting rooms etc. The contact surface is made of sheets of rigid and porous/corrugated material, which is saturated with water supplied by a pump. Materials in the construction of the pad include cellulose, fibreglass and porous ceramics that have been treated with anti-rot, rigidifying resins and other chemicals to give high absorbency. Some of the materials used in pad humidifiers are illustrated in Figure 3-6. Because the water circulation rate and its head are low, pumping power is low when compared to spray humidifiers with equivalent evaporative effectiveness.

(a) Rigid media (b) Aspen pad (c) Porous ceramic

Figure 3-6: Materials for pad humidifier

Yanniotis and Xerodemas (2003) compared the performance of spray and pad humidifiers for water desalination [48]. It was reported that the pad humidifier is generally more efficient than the spray humidifiers. Furthermore, the quality of water was very high in the case of the pad humidifier (around 1-20ppm for air speed up to 2m/s). However, with the spray humidifier the water quality was much lower (200- 500ppm). The value is not high when compared to the standard required for drinking water.

Nevertheless this means that the air carries some seawater droplets from the spray humidifier to the dehumidifier. This on a long term basis will significantly reduce the quality of fresh water and may eventually cause corrosion on the dehumidifier.

3.1.3 Dehumidifiers for Water Desalination

The dehumidifiers are generally made of condensing heat exchangers. Different air-liquid heat exchangers can be used. Most researchers use the coil or finned tube heat exchangers [45] (Figure 3-7). Not much work has been done on improving the condensation side of the desalination systems. However, Beckman et al. (2001) proposed an interesting desalination process known as dewvaporation, in which the humidification and dehumidification process were simultaneously performed in one continuous contact tower [49]. The tower was made up of multiple, flat, vertical chambers in which the humidification and dehumidification processes were performed alternately. Xiong et al. (2005) worked on a baffled shell and tube desalination unit. It was built to perform humidification and dehumidification simultaneously at the tube and shell side of the column, respectively [47]. It was reported that the productivity and thermal efficiency of the process both increase with increasing inlet water temperature. And external steam flow rate increased the productivity but decreased thermal efficiency of the process. A design of new and improved compact condenser with large surface area, small in size, lower cooling water requirement which results to lower pumping power requirement and high thermal efficiency through energy recycle is presented in current research work.

Figure 3-7: Coil in tube condensing heat exchanger

3.2 Psychrometric Analysis of the Desalination System

Psychrometric process is the process which relates the interaction between dry air and water vapour. The mixture of dry air and water vapour is called moist air. The interaction can be analysed using thermo physical properties which are dry-bulb temperature, wet-bulb temperature, humidity ratio or moisture content, enthalpy, specific volume and percentage saturation which is known as relative humidity. A psychrometric chart is a tool which represents the physical properties of moist air at a constant pressure. It graphically show how various properties relate to each other. Figure 3-8 presents the thermo physical properties found on the psychrometric charts. Only two properties are needed to characterize air because the point of intersection of any two property lines defines the state-point of air on a psychometric chart. Once this point is located on the chart, the other air properties can be obtained directly.

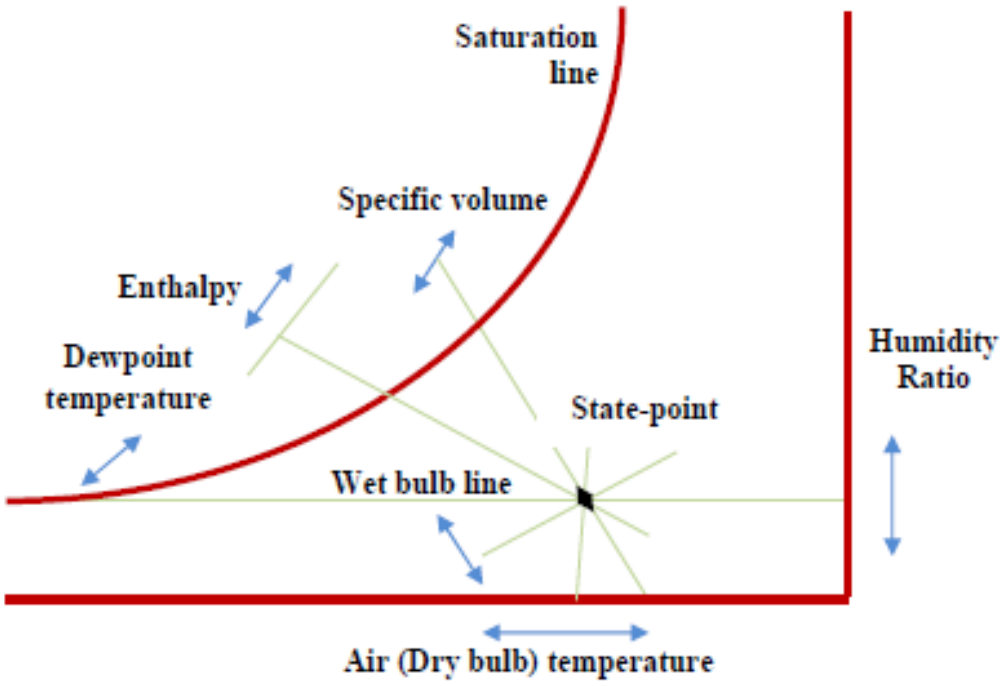

Figure 3-8 Psychrometric chart

3.2.1 Factors Affecting the Desalination System

The performance of the desalination system is mainly affected by relative humidity, temperature, surface area and pressure. They affect the rate of humidification (evaporation) and the rate of dehumidification (condensation). They are described as follows:

Relative humidity

This is the amount of the water vapour in the air as a percentage of the maximum quantity of water vapour that the air would be capable of holding at a specific temperature. Air with low relative humidity holds only a small percentage of the total possible quantity of water vapour that it is capable of holding at the same temperature. In this case the potential of evaporating an extra amount of water is very high. When air reaches 100% humidity, it is said to have reached saturation and hence referred to as dew point. There is a clear relationship between relative humidity and temperature.

Temperatures

The evaporation process requires heat, while the condensation process requires cooling. The ability of air to hold water vapour increases with the increase of its temperature. Therefore with heating, the air would be close to saturation and have a higher relative humidity. At temperature lower than the dew point, water vapour condense out of the air onto the cooler surfaces. Therefore the higher the temperature the higher the rate of evaporation, and the lower the temperature results in higher rate of condensation.

Surface area

Both the rate of evaporation and condensation increases with the increase of surface area. This is because a larger surface area allows more molecules or atoms to leave the liquid, and evaporation occurs more quickly. For example, the same amount of water will evaporate faster if spilled on a table than if it is left in a cup, the greater surface area can get the wetted surface to interact more fully with the incoming air.

Pressure

Air pressure determines how fast the water molecules will diffuse away from the water surface. Higher air pressure will slow down the diffusion process while low air pressure will speed up the diffusion process. Air pressure below the vapour pressure of water at the same temperature will make the water boil. As the atmospheric pressure compresses the water molecules near the surface, more energy is required under higher pressures to speed up the water molecules in order to escape. For example, water molecules need more energy at sea level in order to evaporate than at higher altitudes under the same temperature and relative humidity.

3.2.2 Basic Psychrometric Properties Models

Regardless of the type of humidification dehumidification system, the following mathematical model can be used to evaluate the basic properties required for the analysis of the desalination unit.

- Specific humidity, ω

This is also referred to humidity ratio. It is the moisture content of water vapour in dry air. The specific humidity can also be expressed in terms of partial pressure p_{vs}

$$\omega = 0.622 \frac{p_{vs}}{p - p_{vs}} \quad (1)$$

$$p_{vs} = \exp(23.5771 - \frac{4042.9}{T - 37.58}) \quad (2)$$

Relative humidity is given by;

$$\phi = \frac{p_{vs}}{p} \quad (3)$$

- Enthalpy of moist air, h

This is the specific enthalpy of dry air summed with specific enthalpy of water vapour multiplied by the corresponding moisture content.

$$h = h_a + \omega h_v \quad (4)$$

$$h = c_{pa} T + \omega(2501 + 1.9T) \quad (5)$$

The properties of moist air and liquid water are obtained from Engineering Equation Solver (EES). Dry air properties are evaluated using the ideal gas formulations presented by Lemmon [50]. Moist air properties are evaluated using the formulations presented by Hyland and Wexler [51] which are in close agreement with the data presented in ASHRAE Fundamentals [52]. EES calculates water properties using the IAPWS (International Association for Properties of Water and Steam) 1995 Formulation [53].

The EES (see appendix F for calculation procedure) was used to calculate psychrometric properties (water content as humidity ratio and enthalpy) of moist air for temperature up to 90°C and 10-100% relative humidity. Figure 3-9 and 3-10 shows variation of moisture content in one kilogram of dry with temperature for different relative humidity. The maximum achievable moisture content is 1.4 kg/kg at 90°C and 100% relative humidity. There is general increase of amount of water content with temperature and relative humidity. The enthalpy also increases with increase in temperature and relative humidity.

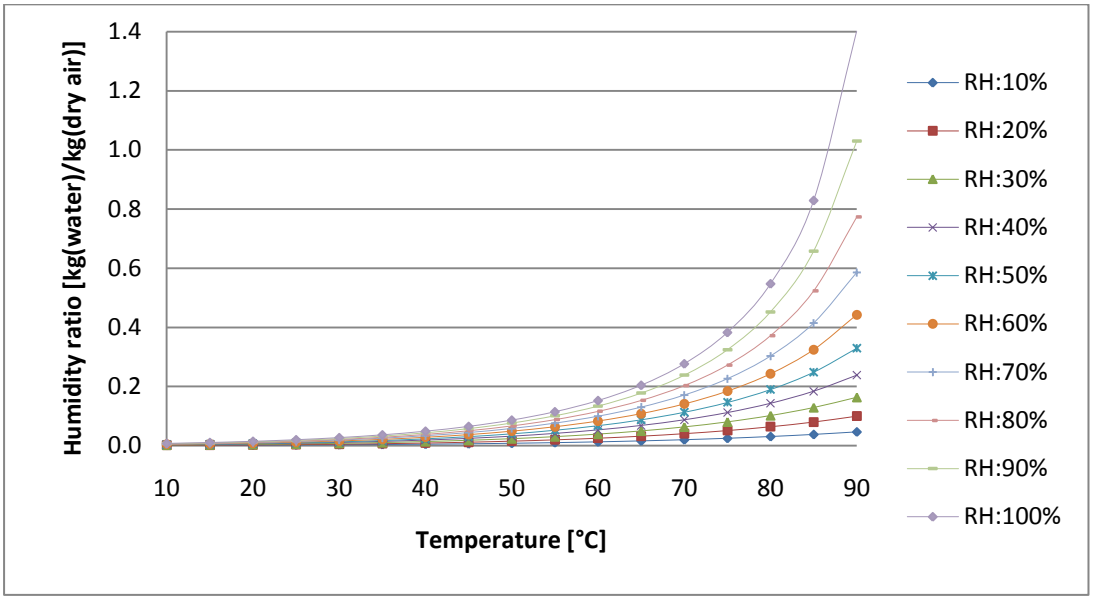

Figure 3-9: Variation of moisture content with temperature for different relative humidity

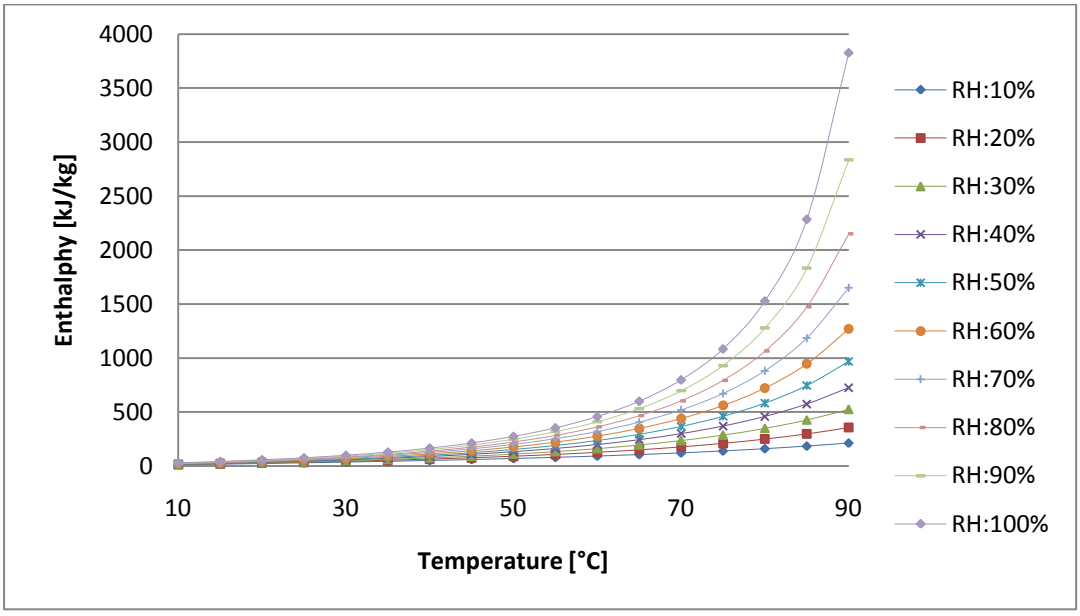

Figure 3-10: Variation of enthalpy with temperature for different relative humidity

3.2.3 Theoretical Performance of the System

In order to investigate the theoretical performance of the HDD system, a mathematical model was used. The mathematical model includes energy and mass balances for the humidification chamber and dehumidification chamber. Figure 3-11 shows a schematic of the humidification and dehumidification process. Water evaporates from the water stream into the air during humidification process. The removal of the latent heat for evaporation from the water stream as well as the transfer of sensible heat from the water to the air stream occurs. During the dehumidification process, the heat and mass transfer processes are reversed, where water condenses from the air stream. Also, latent and sensible heats are transferred from the air stream to the cooling water stream.

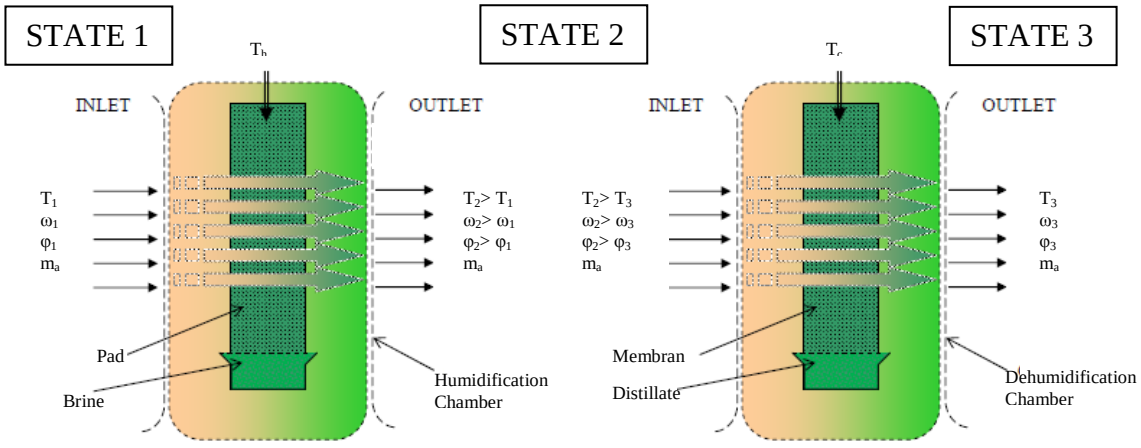

Figure 3-11 Schematic of HD process showing the basic parameters

The total energy Q_{input} consumed by the system is the combination of heat input (from solar collector and/or electric heater) and energy consumed by auxiliary components (pumps and fan). This is given by;

$$Q_{input} = Q_{aux} + Q_{hum} \quad (6)$$

Where Q_{hum} is the energy input at the humidification chamber. This is calculated as follows:

$$Q_{hum} = m_{w,h} c_p (T_{h,i} - T_{h,o}) = Q_{sol} + Q_{heater} \quad (7)$$

Where $m_{w,h}$ is mass flow rate of hot water in the humidification chamber, c_p is specific heat capacity of water, $T_{h,i}$ and $T_{h,o}$ are temperatures at the inlet and outlet of the humidification chamber.

The condensation energy Q_{output} is the energy given up in order to obtain fresh water.

$$Q_{output} = h_l \text{ x } W_p \quad (8)$$

Where h_l (=2400 kJ/kg) is the latent heat of condensation and W_p is the amount of fresh water produced. This is given by;

$$W_p = m_a(\omega_2 + \omega_3) \quad (9)$$

Where m_a is mass flow rate of air and ω_2 and ω_3 are water specific humidity at inlet and outlet of the dehumidification chamber.

The coefficient of performance (COP) of the system indicates how efficient the system operates. This is the energy given up for condensation (latent heat of condensation) divided by the overall energy input in the system. If the energy input is greater than the latent heat of condensation, then the COP is less than one. Hence a very high COP means the system is highly efficient. The COP is calculated as follows;

$$COP = \frac{Q_{output}}{Q_{input}} \quad (10)$$

Mathematical analysis based on equations 6-10 has been performed. In performing the analysis the following assumptions have been made;

- The processes involved operate at steady-state conditions.
- There is no heat loss from the humidifier or the dehumidifier to the ambient.
- Pumping and fan power is negligible compared to the energy input to the heater.
- It was assumed that the system is a control volume, thus air mass flow rate is constant.
- The conditions at state one is always less than conditions at state two and three.
- Conditions at state two reaches full saturation.
- Condition at state three is less than state two.
- Temperature difference $(\Delta T = T_{h,i} - T_{h,o})$ at inlet and outlet of the humidifier is 5°C.

The spreadsheet software was used to carry the mathematical analysis using mathematical psychrometric models in section 3.2.2. The calculated psychrometric properties were compared with that of the EES and another commercial psychrometric

software called CYTSoft. The model was in agreement for both enthalpy of moist air and specific humidity (humidity ratio) with that obtained using the software as shown in Figure 3-12. There was a 0.01% deviation compared to ESS and 0.84% compared to CYTSoft.

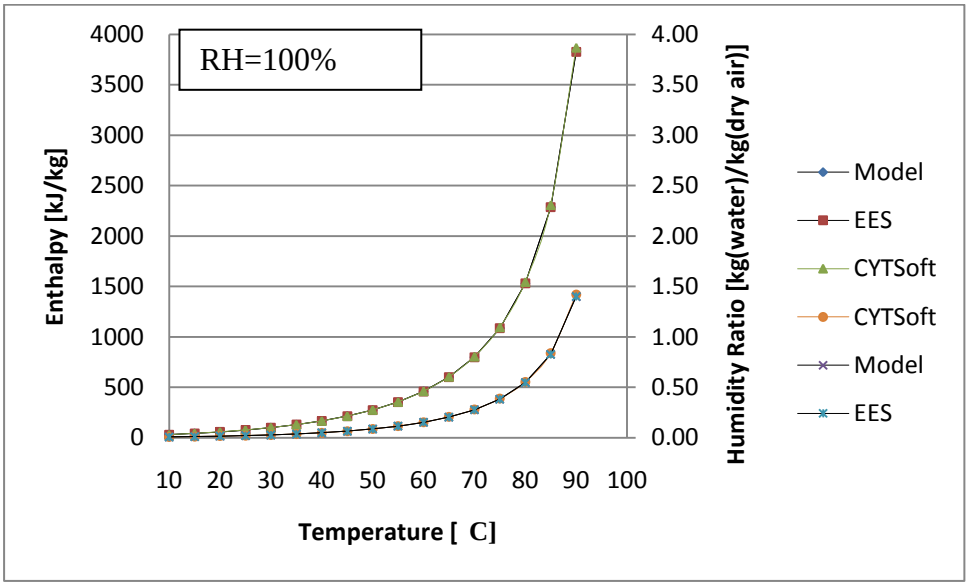

Figure 3-12: Calculated pyschrometric models using spreadsheet compared to ESS and CYTSoft

Thus the model was used to carry out the mathematical analysis using Microsoft Excel spreadsheet for the range of given temperatures (10-90°C) at 5°C interval and relative humidity (10-100%) at 10% interval. The selection of the temperature interval for the simulation is based on assumption that temperature variations in the humidifier are small. This assumption was validated through experimental measurements which indicate the temperature differences between the inlet and outlet of the humidification chamber averages 5°C.

The maximum COP obtained was 3.4 and it corresponds to only 0.14kg/kg water content (moisture content). This is ten times lower than the maximum achievable water content obtained per kg of dry air obtained in section 3.2.2. On the other hand the maximum achievable water content can be obtained at higher temperatures with COP at 0.9 which is just below one. Thus the higher the temperature, the higher the possible amount of fresh water that can be obtained and the lower the COP of the system. The optimum operating

conditions was selected for when maximum water production occurs at COP is greater than one. Such condition exists at 80-90% relative humidity state one.

However, higher COP can be obtained at less than 5°C ΔT (temperature difference between state one and state two). Consider the following case calculations in Table 3-2. Here also the psychrometric properties at state two are greater than that at state one and three. And condition at state three was considered in worst case scenario at full saturation. It can be seen in case one that even though the ΔT is high at 10°C, a reasonable COP greater than one was obtained. And when ΔT was below 5°C there was general increase in COP for both case two and case three. It can be seen as the COP increase from 4 to 7, there was only a tiny fraction of increase in water content.

Table 3-2: Theoretical calculations of the performance of the HDD system

	STATE 1				STATE 2				STATE 3				CALCULATED				
Case	T_1	Φ	Ω	h	T_2	φ	Ω	h	T_3	φ	ω	H	ΔT	Qi	Wp	Qo	COP
1	60	85	0.13	386	70	70	0.17	519	25	100	0.02	76	10	133	0.15	362	2.7
2	67	93	0.21	612	70	95	0.26	752	25	100	0.02	76	3	140	0.24	574	4.1
3	68	100	0.25	715	70	100	0.28	804	25	100	0.02	76	2	88	0.26	622	7.0
T = [°c], φ = [%], ω = [kg/kg], h = [kJ/kg], Q = [kJ], Wp = [kg]																	

While amount of water that can be condensed has limit, the COP of the system is theoretically infinite. And so a good optimisation technique is to achieve the maximum achievable fresh water production first and then recover the energy used to produce the water which can then be used for reheating, thus allowing energy re-use. Hence the COP of the system can be drastically improved. Base on the analysis carried out it is evident that there is potential for energy re-use in order to achieve high energy efficiency for fresh water production.

The process of energy recycling in humidification-dehumidification processes could be illustrated on a psychrometric chart, see Figure 3-13. The line '1-3' represents humidification while the line '3-4' represents dehumidification. As the heat discharge in the process '3-4' is recovered by the seawater to meet most of the heat demand in the process '1-3', the additional heat input from the heat sources is small and may be denoted by the line '2-3'.

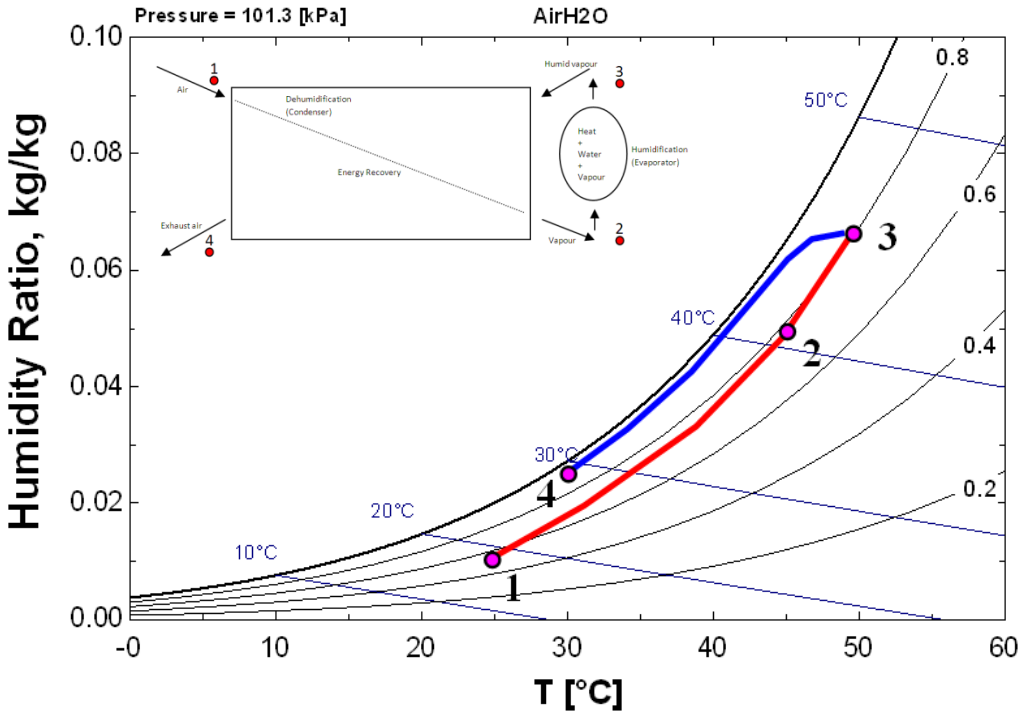

Figure 3-13: Humidification dehumidification process on psychrometric chart

3.3 Design of the Desalination System

A novel water desalination system was designed. The system employs the concept of humidification dehumidification based on psychrometric energy process using a special membrane. It consist of the humidification chamber which contains an evaporation core (E-core) where evaporation takes place and dehumidification chamber which contain an evaporation-condensation core (E/C-Core) where both evaporation and condensation takes place for energy recycling and water production respectively.

The key point is the psychrometric energy "re-use", a little thermal energy is put into the humidification and dehumidification process. Most of the energy is from the psychrometric energy from the condensing of the moisture in the carrier gas. The HDD system could be one stage, or multiple stages such as two stages. The schematic of one stage solar HDD process is shown in Fig.3-11. The system is featured with high efficiency and low cost Evaporation/Condensation core (E/C core) and Evaporation Core (E-Core). The E/C core contains a special membrane with two channels, the evaporation channels with hydrophilic surface and condensation with hydrophobic surface. This makes the condensation and evaporation process in the E/C core very efficient.

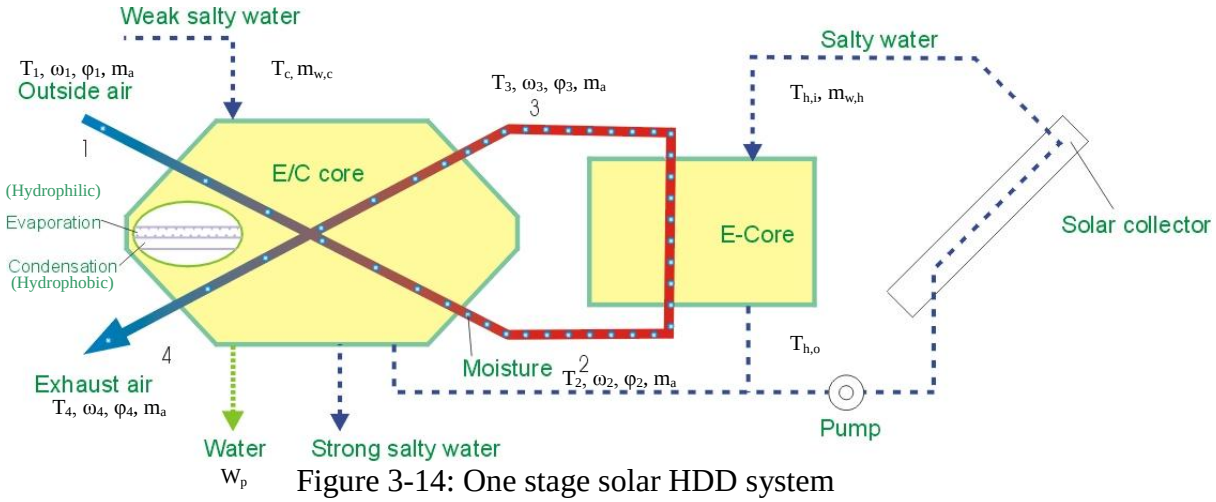

Figure 3-14: One stage solar HDD system

As shown in Fig. 3-11, the outside air at point 1 gets humidified in evaporation channel of E/C core to become point 2, and the energy required is from the condensation channel of the water condensation, so most of the energy for desalination is reused. Air at point 2 then pass E-core to get humidified further from solar energy input to become point 3, then air at point 3 pass the condensing channel of the E/C core to get dehumidified and at last discharged as exhaust air.

3.3.1 The Dehumidification Chamber

The dehumidification chamber is an important part of the desalination unit. It is designed to utilise all energy that can be re-used thus increasing efficiency and enhancing the amount of fresh water that can be produced. The dehumidification chamber consists of E/C-core which is made of special membrane for both evaporation and condensation processes. It consists of two channels as shown in Figure 3-; the evaporation (hydrophilic) and condensation (hydrophobic) channels.

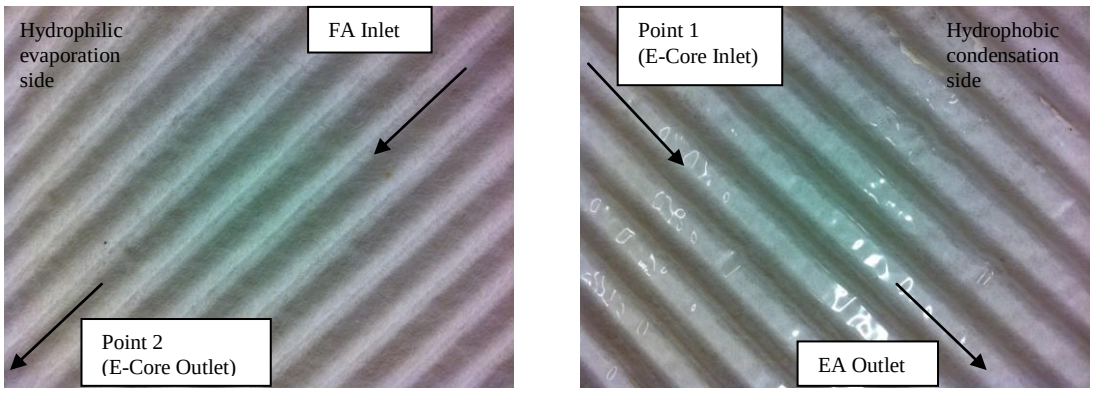

Figure 3-15: Polymer membrane with condensation channel laminated with plastic

The special membrane serves as heat exchanger where heat of condensation is transferred and utilised in the evaporation channel. Cooling seawater or brackish water and fresh air are mix in the evaporation channel in order to aid evaporation. At the same time they aid in condensation process by extracting the heat from the vapour in the condensation channel. The principle of the psychrometric energy process desalination (PEPD) is illustrated in Figure 3-16.

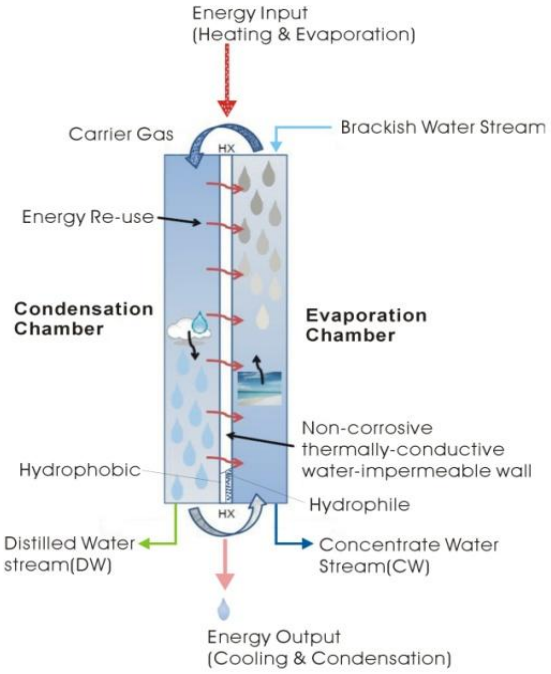

Figure 3-16: Principle of the PEPD membrane E/C-Core

The following equations where used to illustrate the possibility of reduction in both energy and cooling requirement of E/C-Core. A comparison was made for when condensation only occurs at the Core without evaporation.

$$q_{cond} = m_a(h_3 - h_4) = q_{latent} \quad (11)$$

$$q_{evp} = m_a(h_2 - h_1) \quad (12)$$

$$q_{E/C} = (q_{cond} - q_{evp}) \quad (13)$$

$$m_{w,c} = \frac{q_{E/C}}{c_p(T_{c,o} - T_{c,i})} \quad (14)$$

Having known or assumed the initial operating conditions, all other system parameters such as energy requirement, cooling water requirement and fresh water production rate can be obtained using equations 11 to 14 and equation 9. The analysis was carried out for individual processes namely, the condensing process, the evaporation process and the combined simultaneous evaporation/condensation process.

As seen in all cases in Figure 3-17, energy is directly proportional to amount of fresh water production. The higher the water produced, the higher the energy required. The calculated energy given up during condensation is approximately equal to the latent heat based on amount of fresh water production. The difference between the two values is substantially due to the approximations used in the calculation, given that the heating of air is in fact due to the condensation of water. Around 70% of the heat of condensation which is the amount required for evaporation can be re-used. And thus only 30% energy input is required for further evaporation at the humidification chamber. It can be seen that the energy requirement of the E/C-core is significantly reduced when compared to if the dehumidification chamber where to contain condensation process only

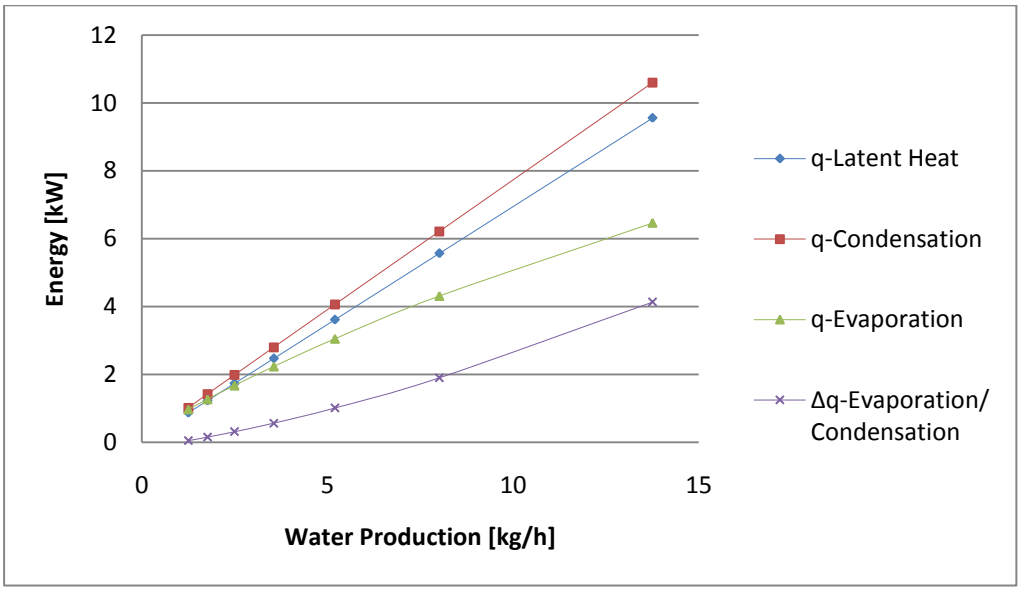

Figure 3-17: Reduction of energy consumption for the E/C-Core

Another important parameter is the amount of cooling water requirement in the dehumidification chamber. This was calculated using equation 14. And the amount of cooling water is dependent on the energy at the E/C-core. The variation of cooling water

with fresh water production is shown in Figure 3-18. The amount of cooling water increases with increase in fresh water production. It was found out that the amount of cooling water requirement could be reduced by up to 80% if the E/C-Core is used in the dehumidification chamber.

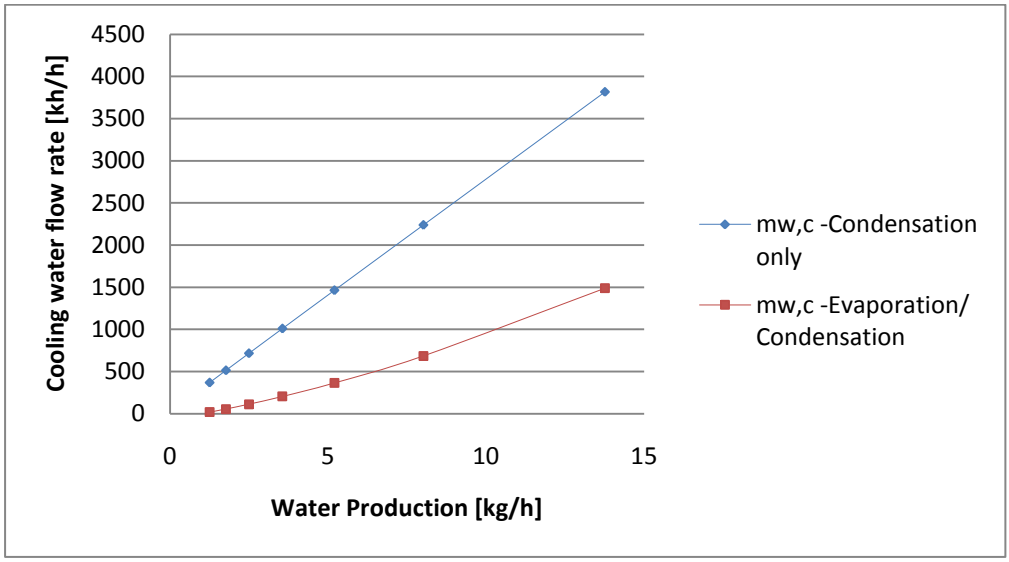

Figure 3-18: Comparison of cooling water requirement for condensation and E/C-Core

3.3.2 The Humidification Chamber

It is intended to use honeycomb arrangement of cellulose papers as the contact surface in the E-Core. The commercial honeycomb celluloses as evaporative pads are widely available (Figure 3-19). The cellulose material is impregnated with decay-resisting chemicals to give good durability, self-supporting and also to provide efficient wetting.

Figure 3-19: Honeycomb cellulose paper

The humidification chamber was designed based on minimum amount of water that can be evaporated using the specified initial conditions. This is highly dependent on the outside temperature and relative humidity, air flow rate and hot water temperature difference between the inlet and outlet of the humidification chamber ΔT.

Figure 3-20 and 3-21 shows variation of energy water evaporation rate with air flow. It can be seen that air flow rate is directly proportional to both the energy and water evaporation rate.

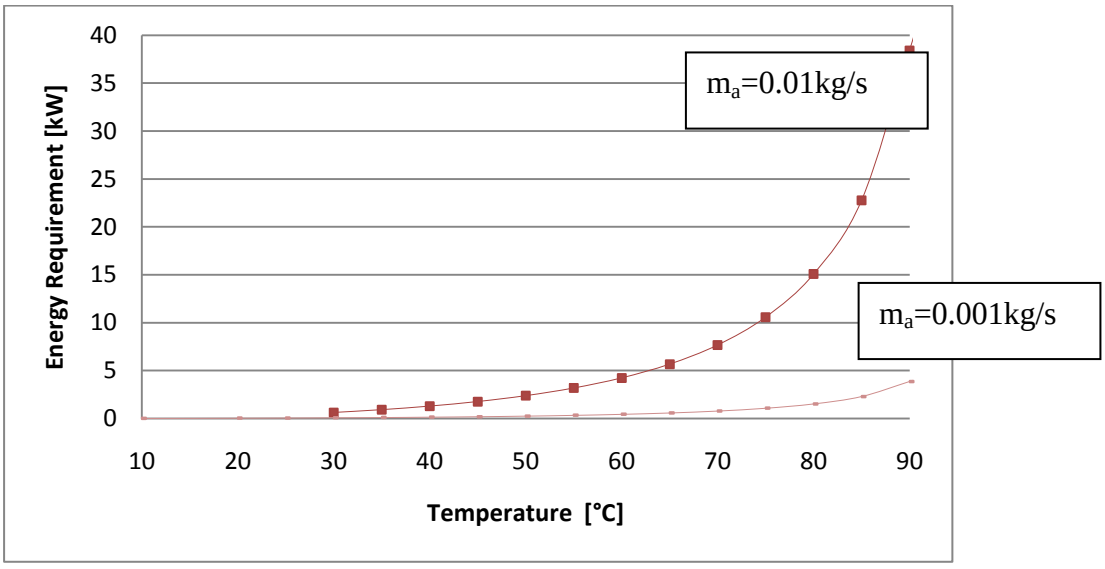

Figure 3-20: Variation of energy requirement with temperature over different air flow

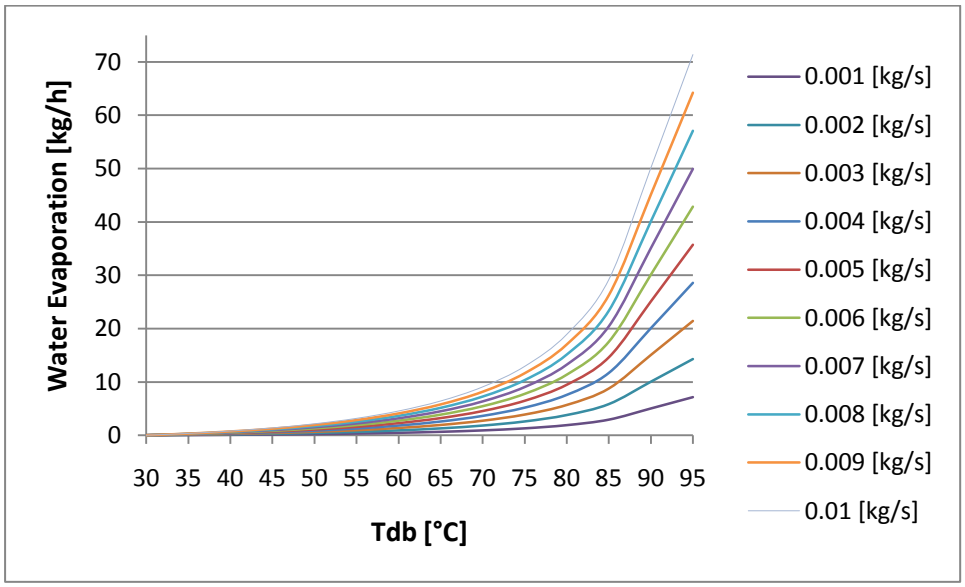

Figure 3-21: Variation of water evaporation with temperature over different air flow

3.4 Preliminary Test of the Desalination System

The experimental investigation of the desalination system shows that the amount of fresh water and thermal performance depends on three main parameters. These are the energy input, the mass flow rates and working temperature of the system. Several experiments were carried out under different operating conditions. These are described in the next following sections.

3.4.1 Experimental Set-Up

The experimental set up as shown in Figure 3-22 consists of the desalination unit with dimension of 1.5m x 0.5m x 0.8m. The unit incorporates the humidification and dehumidification chambers and also a fan to blow air into the system. An electric heater of 2.4kW heat capacity was used to supply the energy required. Two pumps were used to circulate the feed water in the system; one pump circulates the feed water through the dehumidification chamber and the other pump circulates the feed water through the electric heater to the humidification chamber.

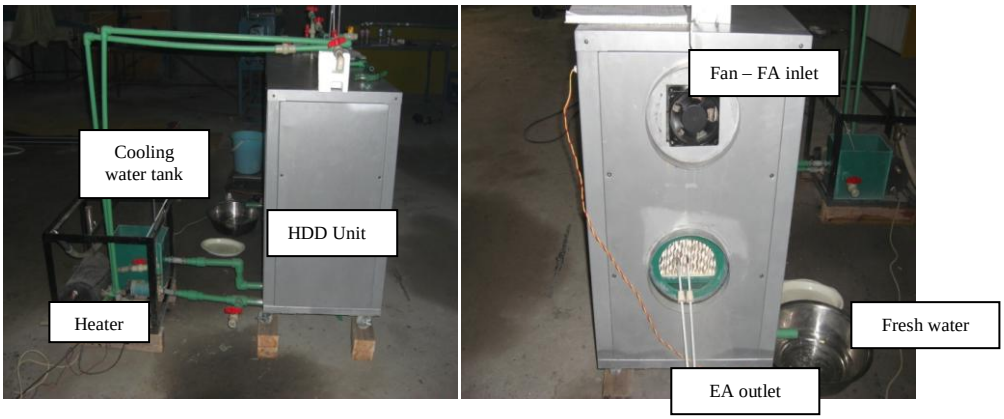

Fig 3-22: Side view of the desalination unit

Figure 3-23: Membrane of the desalination system showing fresh water condensation

The measuring instruments are mainly dry and wet bulb thermometers which are used as probes at different points of the system to measure temperatures. An air flow meter for measuring the velocity of air flow in the system, and a scale for measuring the amount of fresh water produced. It was ensured that both thermocouples and airflow meter were calibrated.

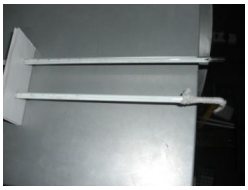

Dry/Wet bulb thermometer

Air flow meter

Scale

Figure 3-24: Measuring instruments

3.4.2 Results and Discussion

3.4.2.1 Effect of Air and Water Flow Rate

The system was tested using two different air mass flow of 100CFM and 120CFM rated maximum flow. It can be seen as shown in Figure 3-25 there was no any significant change in the amount fresh water produced at the same temperature around 80°C. The measured air flow rate using the air flow meter was around 0.6m/s (15CFM) or 30kg/h.

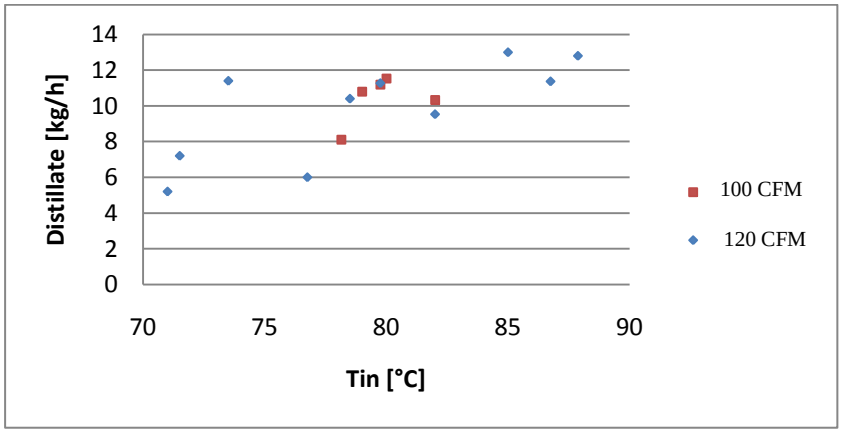

Figure 3-25: Amount of fresh water produced as function of temperature at the inlet of the humidification chamber for two different air mass flow rates

The system uses two different feed water flow rates. The hot feed at inlet of the humidification chamber and the cold feed at inlet of the dehumidification chamber. As

illustrated in Figure 3-26, while keeping the flow rate at the inlet of the dehumidification chamber low (30kg/h), the amount of fresh water production increases with increase in temperature and feed water flow rate at the inlet of the humidification chamber. The optimum operating flow rate is 120kg/h at the humidification chamber and 30kg/h at the dehumidification chamber.

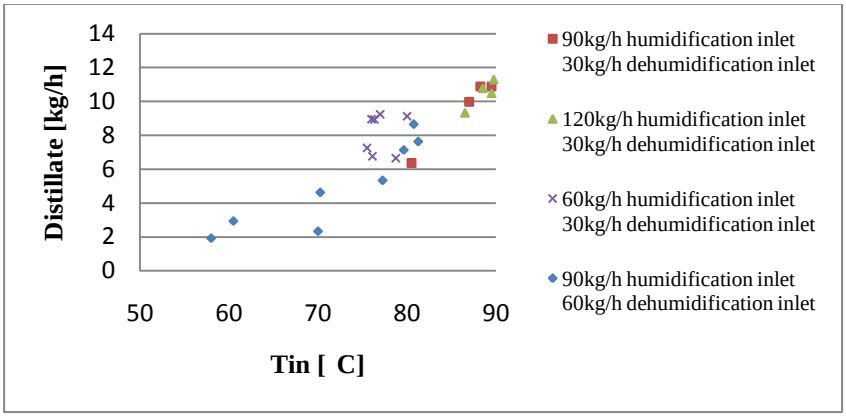

Figure 3-26: Amount of water produced as function of feed water temperature at inlet of the humidification for different water flow rates at both the dehumidification and humidification chamber inlets

3.4.2.2 Effect of Air and Water Temperature

Experimental result was compared for two different days. The amount of fresh water produced for two different weather conditions of 21°C and 16°C atmospheric weather condition at the same energy inputs and flow rates is shown in Figure 3-27. The water production rate was 3.3% less for the lower temperature compared to higher temperature.

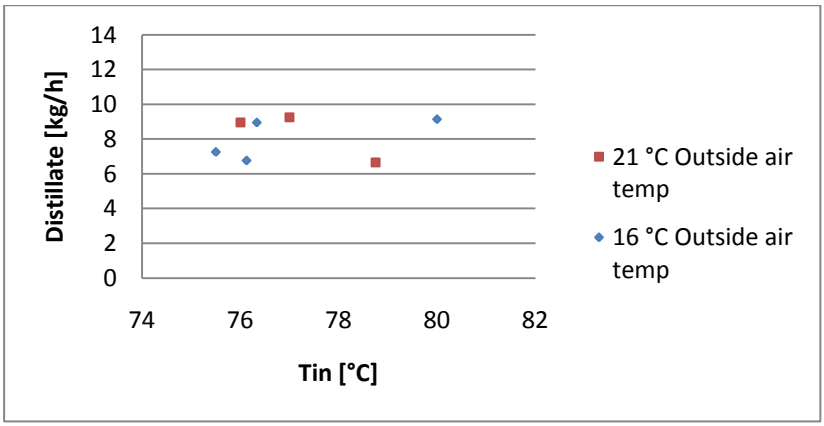

Figure 3-27: Amount of water produced as function of temperature at inlet of the humidification chamber for two different weather conditions

The system depends on temperature of hot feed into the humidification chamber for evaporation and also temperature of cold feed into the dehumidification chamber for condensation. As seen from previous section in all cases of flow rates, the higher the temperature of the hot feed, the higher the rate of evaporation and thus possible fresh water output. Experimental results indicate an optimum temperature of the cold feed (i.e. cooling water). As illustrated in Figure 3-28, the optimum cooling water temperature was 40-50°C. The highest fresh water production was obtained at this temperature range.

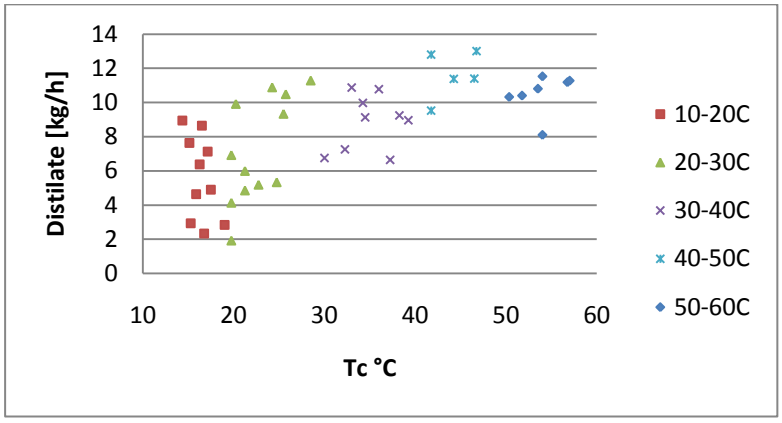

Figure 3-28: Amount of fresh water produced as function of cooling water temperature

3.4.2.3 Effect of Energy Input and Water Production

The system was tested using two different heat inputs of 1.2 kW and 2.4 kW. Figure 3-29 indicates that the amount of fresh water produced is a direct function of feed water temperature. The increase in temperature depends on the energy input and the feed water flow rate of the system. A low energy input limits the temperature and flow rate of hot feed. And this subsequently limits the amount of fresh water production.

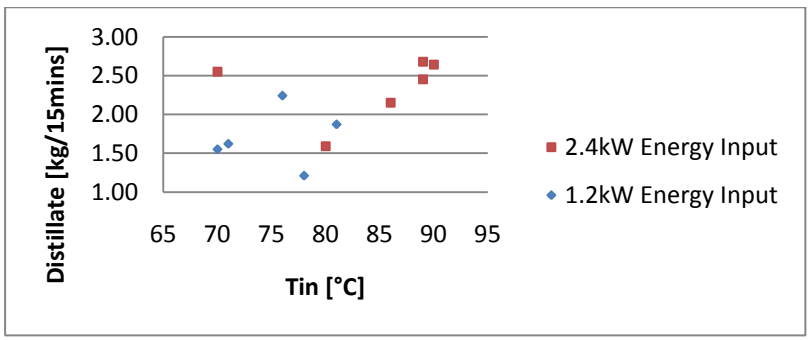

Figure 3-29: Experimental amount of fresh water produced as function of temperature at inlet of humidification chamber for two different energy inputs at a constant flow rate

As shown in Figure 3-30, the highest amount of fresh water was obtained at higher temperatures at the inlet of the humidification chamber. The figure shows a representation of about 20 different experiments carried out under different conditions which were carried out at 15 minutes intervals. The maximum amount of fresh water produced is about 13 kg/h with 2.4kW energy input.

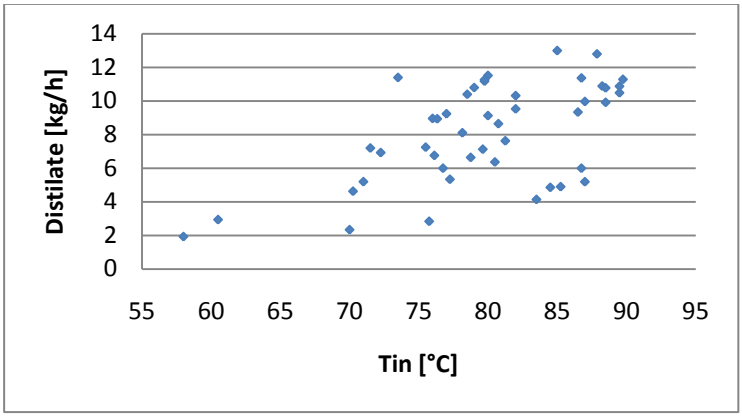

Figure 3-30: Amount of fresh water produced as function of temperature at inlet of the humidification chamber

3.4.2.4 System COP and Absorption Ratio

The COP of the system was calculated using equation 10 base on the data obtained. It was found that the system had a maximum fresh water production of 13kg/h and a COP of 3.6 was calculated. The initial test shows that the system has great potential with room for improvements and further optimisation.

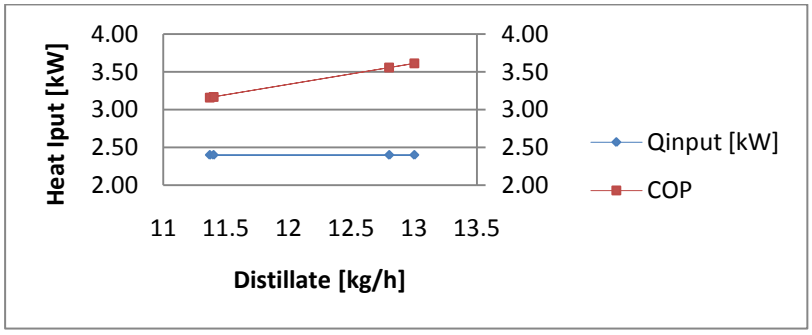

Figure 3-31: Variation of heat input and COP with water production

Another important parameter to investigate the performance of the system is the absorption ratio ε. This is used to evaluate the characteristics of the adiabatic humidifier.

Only part of the water introduced into the humidifier is evaporated. Hence the absorption ratio is the ratio between flow rate mw,h of the water effectively absorbed by the air stream, and the flow rate of water introduced. This is given by;

$$\varepsilon = \frac{m_a(\omega_2 - \omega_1)}{m_{w,h}} \qquad (15)$$

Where m_a is the mass flow rate of air obtained using the air flow meter. ω_1 and ω_2 are moisture content at the inlet and outlet of the humidifier, these are obtained using the EES software with the measured the dry bulb and wet bulb temperatures at the inlet and outlet of the humidification chamber as inputs. And $m_{w,h}$ is mass flow rate of hot water into the humidification chamber. This also can be calculated if energy input is known and by measuring the temperatures of water at inlet and outlet of the humidification chamber.

The absorption ratio parameter is logically equal to one (ε=1) when all the water introduced into the humidifier is absorbed by the air being humidified. This parameter is particularly important in determining the amount of solar collector area required (see Chapter 4). From the experimental result as shown in Figure 3-32, the absorption ratio increase with increasing water flow rate and temperature into the humidification chamber.

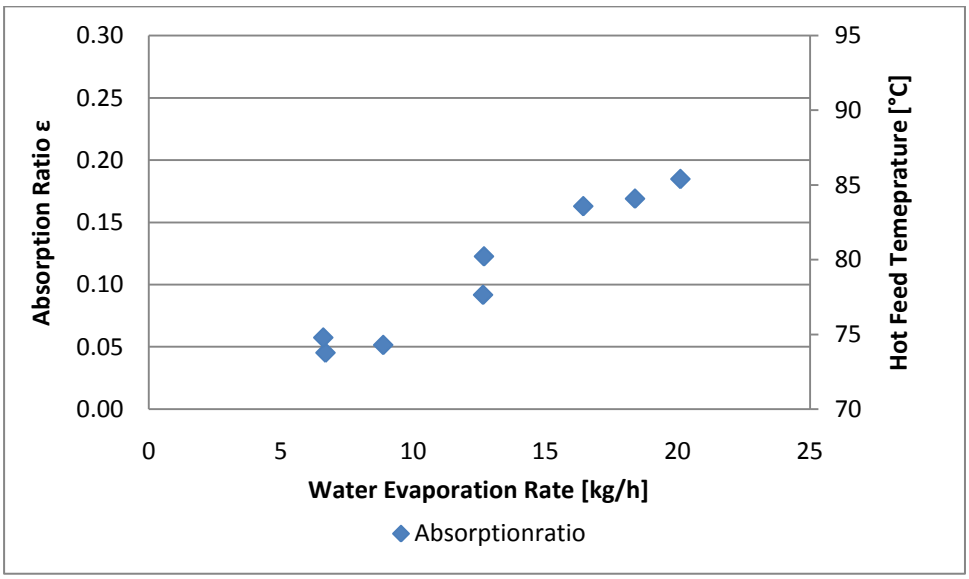

Figure 3-32: Variation of absorption ratio and temperature with rate of water evaporation

3.5 System Optimisation

The performance of the system can be improved by increasing the operating temperature of the system. The psychometric properties of moist air at temperatures above 90°C are highly dependent on the pressure of the system since it does not operate at atmospheric pressure. For any given absolute pressure, the highest temperature cannot exceed that temperature at which the saturation vapor pressure equals the absolute pressure. In other words, moist air properties are valid for any dry bulb temperatures below or equal to the saturation temperature of water at the same given absolute pressure, above that limit saturated moist air cannot exist. CYTSoft psychrometric software was used to calculate psychrometric properties of moist air at estimate higher operating temperatures. The software is based on formulations by Hyland and Wexler. The upper limit of the absolute pressure is set at 5 MPa, which restricts the temperature range to 200°C. The performance of the system was estimated based operating conditions used in the experimental test.

Figure 3-33 shows maximum amount of water that can be produced at 30°C and 100% relative humidity exhaust air conditions. And the air mass flow rate is 20kg/h. The maximum fresh water that can be obtained at 200°C is 260kg/h. It can be seen there is significant increase in fresh water production at high temperatures. Water production was constant for temperatures 95-150°C with around 0.4kg/h per degree rise in temperature.

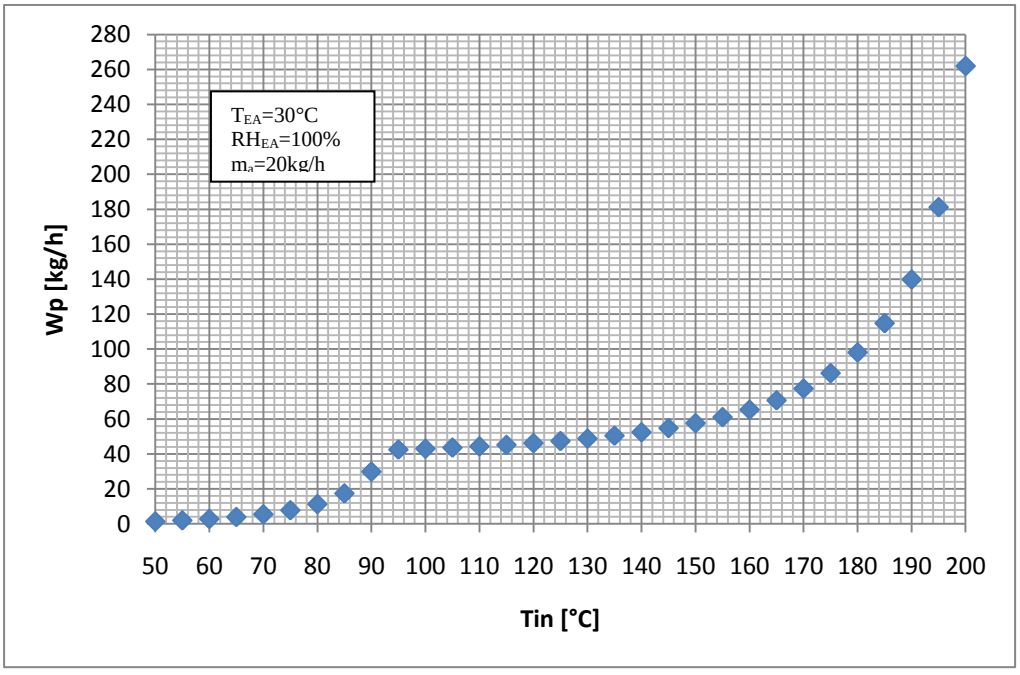

Figure 3-33: Variation of water production rate with temperature

Figure 3-34 shows variation of COP with water production assuming 2.4kW energy input. It can be seen that the COP is a direct function of water production. A COP above 70 was obtained for maximum water production. However, operating the system at such higher temperature results in high heat loss and thus requires system design optimization.

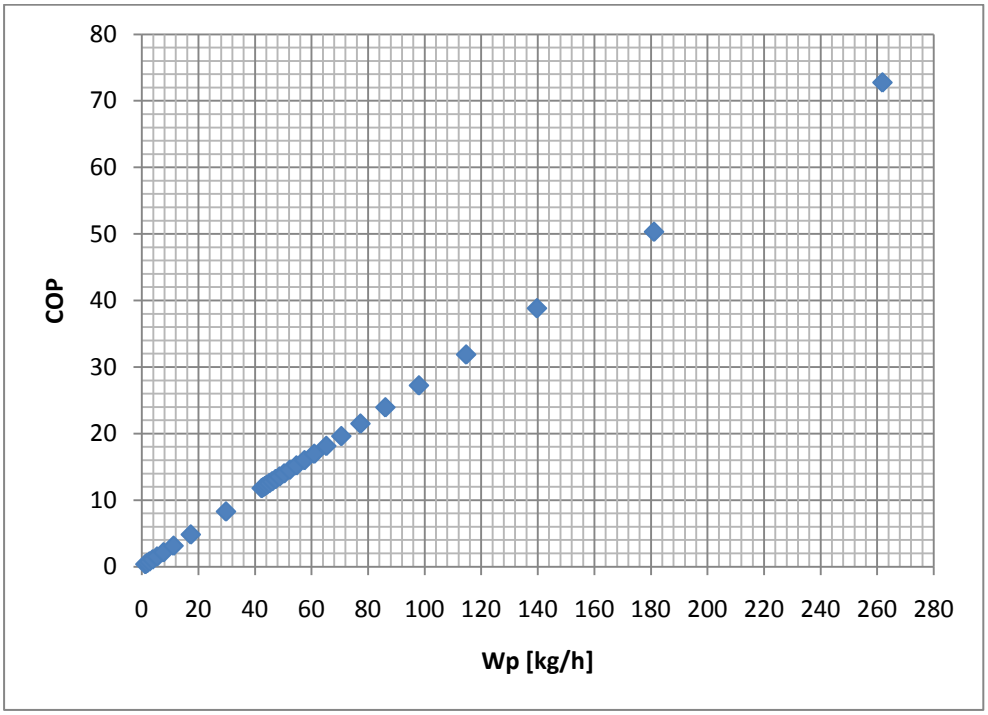

Figure 3-34: Variation of water production with COP

The HDD system can be further optimized by designing a two stage configuration as shown in Figure 3-35. The system is a combination CWOA and CAOW configurations. The first stage heat sink act as the second stage heat source, hence heat loss reduced.

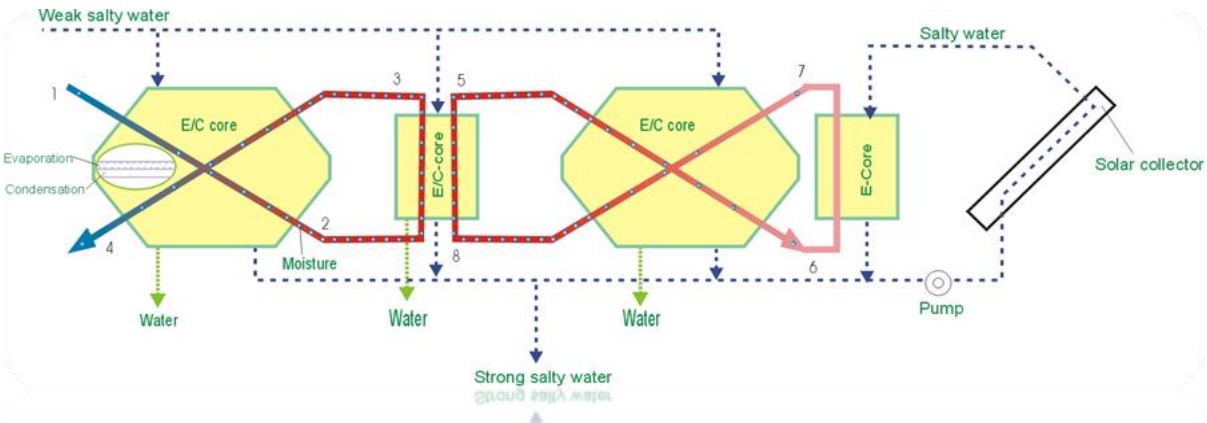

Figure 3-35: Two stage solar HDD system.

3.6 Conclusion

A novel HDD unit was proposed. The system use pad type adiabatic humidification process for water evaporation with water and air flow mixing in counter-current flow mode. And the dehumidification process uses a two channel heat exchanger made of a special membrane for condensation and evaporation process. The hot seawater is sprayed to humidify the incoming air in the humidification chamber. The humidified air enters the dehumidification chamber through a forced convection using a fan and is cooled by the incoming seawater. Cold seawater is circulated through the condenser, hence the moisture is condensed out and the pure water is accumulated at the base of the chamber while the dehumidified air is discharged to the outside. In the meantime the heat of condensation is recovered using the cold seawater and partially evaporated through the hydrophilic channel of the condenser.

A theoretical analysis was carried out to investigate the characteristics and performance of the proposed system. Psychrometric analysis indicates an increase in moisture content and enthalpy with increase in temperature and relative humidity. Mathematical models for calculating the performance of the system were given. Based on the models it was found that the COP generally decrease with increase in water production and hot feed temperature, and the water production rate decrease with increase in COP. The design of the system presents great potential for reduction in energy consumption and cooling water requirement through energy recycling.

A prototype system was constructed. Several experiments were carried out on the water desalination unit under different conditions. The effect of heat input, temperature and flow rates on the amount of fresh water produced were examined. The experimental result showed that:

- The amount of energy supplied to the system is a direct function of amount of fresh water produced.
- The temperature of feed water at the inlet of the humidification chamber is a direct function of the amount of fresh water produced.

- While the temperature of cold feed varies with amount of fresh water production, the experimental result suggests a temperature of around 40-50°C for the optimum operation of the system.
- A ±5°C temperature of the environment does not affect the performance of the system.
- The mass flow rate of air (±10kg/h) into the system does not affect the amount of fresh water produced. And only a fraction of the supplied air was utilized for fresh water production (only 30kg/h was utilised for rated fans of 200kg/h and 240kg/h).
- The optimum water flow at humidification chamber was 120kg/h for 30kg/h dehumidification chamber cooling water.
- A maximum 3.6 COP and 13kg/h fresh water were obtained at around 80-90°C operating temperature. And the average ratio of actual water flow to evaporated water (absorption ratio ε) is 0.1.

It was seen that the performance of the system can be greatly improved by operating the system at higher temperatures. For given certain conditions, water production was around 1kg/h per degree rise in temperature between temperature range 50-90°C, and 0.4kg/h per degrees for range 90-150°C. And there was significant increase to 4kg/h per degree for temperature range 150-200°C. System operation at such higher temperature will lead to large amount of heat loss. Hence the system can be designed in two stages to recover most of the heat used.

Chapter 4: Design and Test of Solar Collector

4.0 Introduction

This chapter reports on the design and experimental test of solar collector for water desalination. The chapter is divided into three sections. Design and performance analysis of the solar collector is presented. The performance of the solar collector was investigated through experimental testing. Both indoor and outdoor tests were carried out. The indoor test was mainly to establish the efficiency of the collector while the outdoor test was carried out in order to determine the combined efficiency of the solar collector with heat exchange water storage tank under real weather condition so as to enable the modelling of the solar collector for the water desalination unit. The last section of the chapter reports on the mathematical modelling carried out to determine the area of solar collector required to drive the water desalination unit.

4.1 Concentrated Solar Collectors for Water Desalination

There are different types of solar collectors which can be used to convert solar energy into thermal energy. This is generally done by using a heat transfer medium; usually a fluid (water, synthetic fluids or oil) in a receiver tube (absorber) absorbs the solar radiation in form of heat energy while it is circulated through the collector. The heat energy is then utilised into useful application. As earlier seen in Chapter 2, solar collectors are classified into concentrating and non-concentrating collectors. They can be static or sun tracking on single axis or two axis tracking system. Different solar collectors have already been commercialised, yet there are enormous research and development being carried out in the field in order to improve the performance of the collector systems.

Solar concentrators have been used with different designs of solar collectors such as vacuum tube collector and even in improving the performance of a PV cell. The optical and thermal analyses of this type of concentrator together with geometries and designs have studied by several researchers. Concentrating collectors generally perform better than the non-concentrating collectors. Their main advantages are as follows;

- A high concentration can be achieved with these collectors and hence the heat transfer fluid can achieve higher temperatures when compared with the non-concentrating collectors.

- Higher thermodynamic efficiency due to small heat loss area relative to the receiver area can be achieved to provide the operating temperatures in various tasks such as desalination or power generation.

In the field of concentrating solar collectors, the conventional parabolic trough collector (PTC) is one of the most matured technologies [54]. It has been successfully used in many large scale high-temperature solar plants [55, 56]. It can collect the solar energy up to 400°C under the accurate control of a solar tracking system. However, this type of solar collector has disadvantages. Main disadvantages include;

- The focus line of the concentrator is over the concentrating surface. So, the high temperature solar receiver in the focus line can cast its shadow on the concentrating surface which affects the concentration ratio. The concentrator collects little diffuse radiation, the rate depending on the concentration ratio.

- Because the high temperature solar receiver is installed over the concentrating surface, heat loss environment is very high which is very important to the heat preservation of the receiver.

- There is requirement high solar tracking precision. Once the solar radiation cannot be reflected to the solar receiver, then the reflector of the concentrator becomes less effective which is the case with many large scale units.

In this research, a new imaging compound parabolic v-trough solar concentrator is constructed and tested. The most important feature of the new concentrator is that the single curved focusing surface in the conventional concentrator is replaced with a multiple curved focusing surface. This enables the high temperature solar receiver to be synchronously heated by the upper and lower surfaces of the concentrator. This generally helps to improve the efficiency of the receiver. Because the focus line of the concentrator is positioned at the bottom of the unit, it helps to capture both the diffuse and direct beam solar radiation. This helps to the heat preservation of the receiver. At the same time, it also avoids the shadow of the receiver on the concentrating surface.

4.2 V-Trough Concentrating Solar Collector

The new solar concentrator designed in this work is shown in Fig. 4-1. It consists of the new compound parabolic concentrator, secondary reflection plane mirror, lower parabolic trough concentrator and high-temperature solar receiver. Its operating principle is described as follows. The light '4' at a direction parallel with the symmetry axis '5' enters the trough. The surface '1' of the new compound parabolic trough concentrator reflects the light '4' to the secondary plane mirror '2'. The light is then reflected by the secondary plane mirror '2' to concentrate at a mirror image focus line. The centre line of the high-temperature solar receiver '8' just superposes with the mirror image focus line. A vacuum glass tube '7' is positioned outside the receiver '8' to reduce heat loss. The new trough solar concentrator also has a lower parabolic concentrator '3' connected with the secondary plane mirror '2' by the flange '9', which allows the lower parabolic concentrator to be removed easily to provide access to the receiver for cleaning or maintenance. The focus line of the surface '3' also superposes with the centre line of the receiver '8'of the solar collector. The solar energy radiated onto the lower trough parabolic concentrator '3' is reflected to the receiver '8'. Therefore, the receiver '8' can accept the reflected solar radiation from both top-side and bottom-side of the concentrator so that the receiving efficiency is enhanced. The reflected solar radiation is absorbed on the receiver to heat the HTF inside. Finally, the high-temperature thermal energy is utilised through the HTF. Detailed design of the collector can be found in Appendix H.

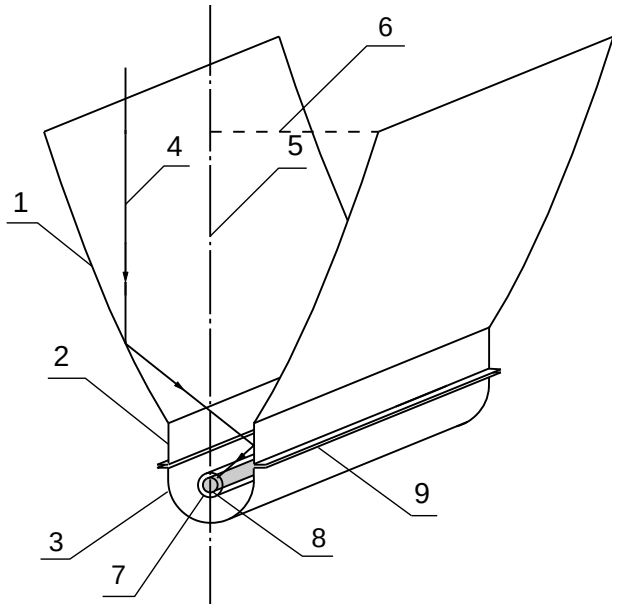

Figure 4-1: Schematic of the new v-trough solar collector

The v-trough collector (VTC) is a solar tracking collector. In order to track the sun throughout the day for every day of the year, the geometric relationship between the system and the sun need to be known. Thus the knowledge of solar geometry is of vital importance for any solar driven application. The angular position of the sun as seen from a particular place on the surface of the earth varies from hour to hour and from season to season. The basic position of the sun in the sky at any instant can be described by two angles as shown in Figure 4-2; t he altitude angle γ of the sun above the ground or horizon plane and the azimuth angle z which is compass direction of the sun on the ground plane. The reference plane for the solar altitude is the horizontal plane. The altitude is the angle between the line to the centre of the sun and the horizontal plane. When the sun is on the horizon, the solar altitude is 0°; when directly overhead 90°. The reference plane for the solar azimuth is the vertical plane running north-south through the poles. The azimuth is the angle between true south and the point on the horizon directly below the sun. By convention, it is negative before noon and positive after noon. The azimuth is referenced to due south in the Northern hemisphere. The Azimuth may be given in two ways; either East or West of South, or clockwise from North. That determines the direction of solar tracking depending on different geographic locations.

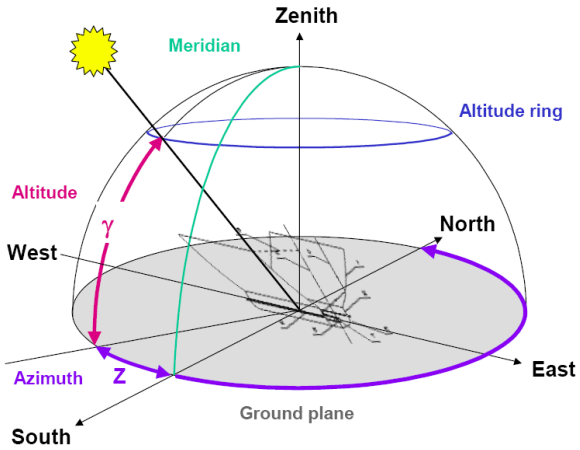

Figure 4-2: Solar geometry [80]

Other related solar angles include declination angle, hour angle and incidence angle. The declination angle is the angle between the equatorial plane and a line joining the centres of the sun and the earth. The declination angle changes as the earth orbits the sun, and is

also the same for the whole globe on any given day. It changes from day to day while altitude and azimuth angles change with time throughout the day. The hour angle of a point is the angle between two planes: one containing the Earth's axis and the zenith, and the other containing the Earth's axis and the given point. The hour angle is negative during the morning, reduces to zero at solar noon and becomes increasingly positive as the afternoon progresses. The hour angle is paired with the declination to fully specify the position of a point on the surface of the earth. The angle of incidence is the angle in which solar energy is received at the solar collector.

The solar altitude and azimuth over the year can be plotted on a solar chart. There are many different ways of graphically displaying the relative position of the sun at different times of the day and year. The most widely used is the sun path diagram. On the sun path diagram, the altitude scale is shown on a series of concentric circles. The azimuth scale is set around the perimeter of the chart. The azimuth angle is read by setting a straight edge from the centre of the chart to the intersection of the required hour and date path lines and noting where it cuts the chart perimeter. Different charts are required for different latitudes. The Ecotect software was used to obtain the sun path diagram of Liuzhou in China as illustrated in Figure 4-3. It is expected to carry out outdoor test of the solar collector in Lizhou.

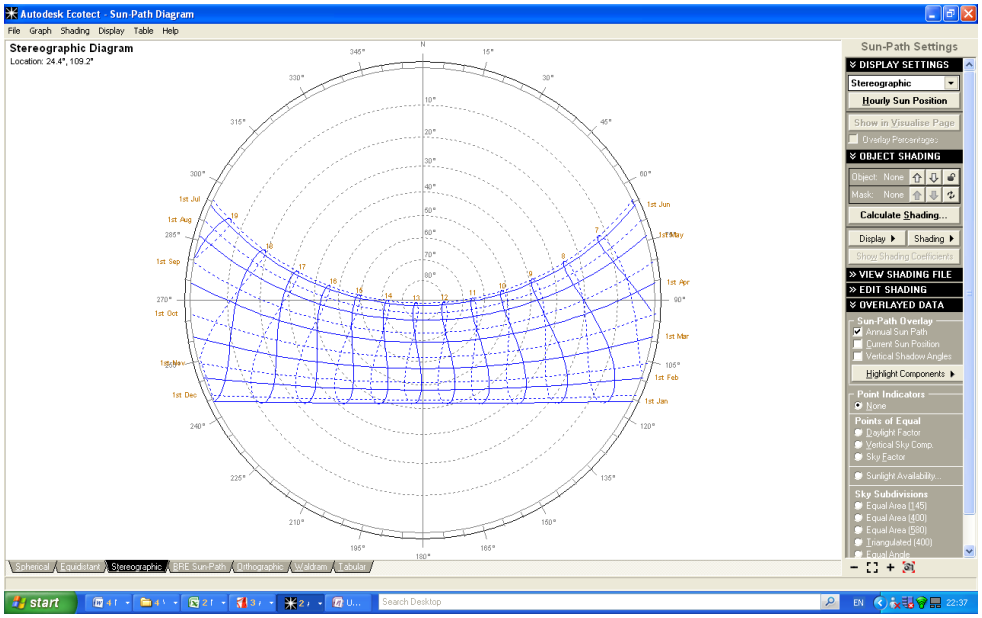

Figure 4-3: Sun path diagram for Liuzhou

In order to investigate the performance of the proposed solar collector, it may be assumed that the length of the collector is L, the tube diameter of the receiver is *d*, the outlet and inlet temperature in the receiver is T_{out} and T_{in}, respectively. In order to effectively utilize the solar energy by the receiver, the fluid in the tube is required to have a turbulence flow. Based on the condition, Reynolds number of the flow in the tube must be bigger than 10^4 [57]. This is defined as follows;

$$\frac{ud\rho}{\mu} \geq 10^4 \tag{16}$$

Where, u is the flow rate of the liquid, m/s; ρ is the density of the liquid, kg/m^3; μ is the viscidity of the liquid, kg/(m·s). And then, for the certain heat transfer liquid, its flow rate must be,

$$u \geq \frac{\mu \times 10^4}{d\rho} \tag{17}$$

Hence, the minimum mass flow rate in the tube is;

$$m = \frac{\pi}{4} d^2 \cdot \rho \cdot u \tag{18}$$

Therefore, the thermal energy carried out the receiver by the liquid in unit time is,

$$Q_L = mc_p(T_{out} - T_{in}) = \frac{\pi}{4} d^2 \rho u c_p (T_{out} - T_{in}) \tag{19}$$

For the system with maximum light inlet half-width x_C and length L, the total solar energy irradiating into system in unit time is $2Lx_C I$ .Where, I is solar intensity and $2Lx_C$ is the area of the collector. If the efficiency of the system is η, the total energy irradiating on the receiver tube and absorbed by the liquid in tube is;

$$Q_I = 2Lx_C I\eta \tag{20}$$

According to conservation of energy, $Q_L = Q_I$. Hence;

$$x_C = \frac{\pi d^2 \rho c_p u(T_{out} - T_{in})}{8LI\eta} \tag{21}$$

In order to satisfy the turbulence flow in tube, it requires the minimum collector half-width as follows,

$$\eta = \frac{\pi d c_p \mu (T_{out} - T_{in}) \times 10^4}{8x_{C\min} LI} = \frac{Q_L}{2Lx_{C\min} I} \tag{22}$$

It can be seen that the efficiency is dependent upon c_p and μ of the liquid in receiver tube and as well the size of the system and receiver. The longer the length of the system, the less the minimum collector width is required. The stronger solar radiation received, the higher the efficiency of the system and hence the less the minimum collector width is required. At the same time, in order to reduce the size of the concentrator, it must be noticed that *d* should be taken relatively small value because it is proportional to $x_{C\min}$. A more precise tracking unit will be required if *d* takes a relatively small value. Therefore, in order to retain the small inner diameter, *d*, of the tube a finned tube is frequently used in practical applications.

4.3 Experimental Test of the Solar Collector

The experimental set up as shown in Figure 4-4 consists of the solar collector which includes the multi-curved surface concentrator and the high temperature receiver tube. It also consists of a solar tracking device (for outdoor test) which is mounted on the collector, receiver fluid (HTF) circulation tank measuring 0.15m height by 0.22m diameter, pump (pump flow rate range between 3-8L/min, 4 bar max pressure and 150°C maximum temperature) and a water storage tank for heat exchange with 80L capacity (for outdoor test only).

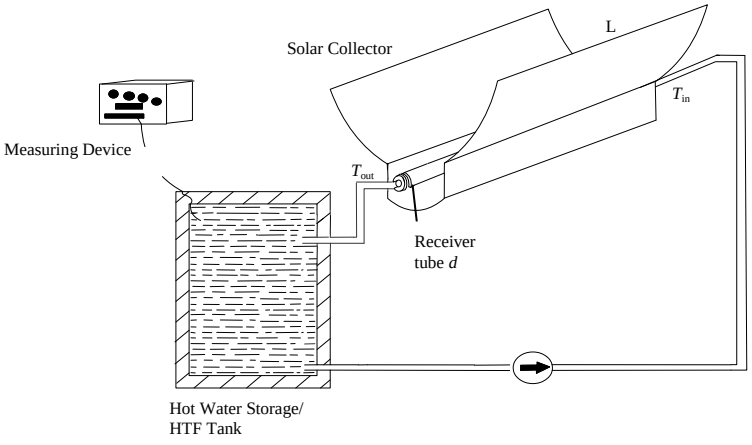

Figure 4-4: Schematic of experimental set-up of the new trough solar collector system

The measuring devices include a Pyranometer which is mounted on the solar collector to measure the intensity of solar irradiation. The device has measuring accuracy of ±5%.

And set of thermocouple used to measure the surface temperature of the concentrator, the surface and inside of the receiver tube, the inlet and outlet temperatures of the HTF and finally the ambient temperature. All thermocouples used are K-type sensors supplied by RS components with an accuracy of 0.1°C. Table 4-1 lists all the measured parameters and the thermocouple calibration shown in Figure 4-5.

Table 4-1: All measured parameters and measuring devices

Parameter	Symbol	Unit	Measuring Device
Solar Intensity	I	W/m^2	CMP3 Pyranometer
Collector Surface Temp	$T_{c,s}$	°C	K-Type thermocouple
Receiver Surface Temp	$T_{r,s}$	°C	K-Type thermocouple
Receiver Inside Temp	$T_{r,i}$	°C	K-Type thermocouple
HTF Inlet Temp	$T_{HTF,i}$	°C	K-Type thermocouple
HTF Outlet Temp	$T_{HTF,o}$	°C	K-Type thermocouple
Ambient Temp	T_a	°C	K-Type thermocouple

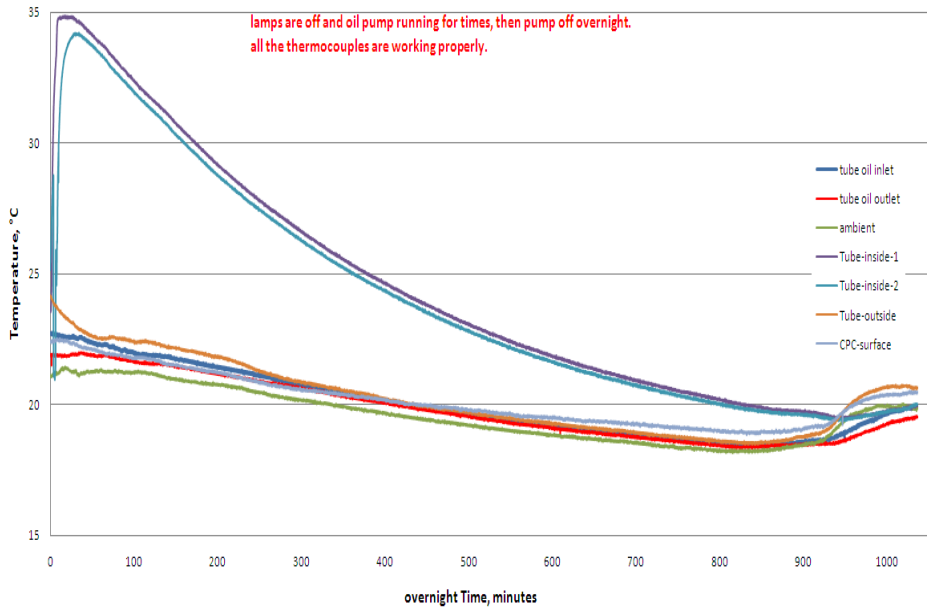

Figure 4-5: Calibration of thermocouples

The tungsten lamps as shown in Figure 4-6 are widely used in the SBE as solar simulator. The lamp is similar to sunlight must especially in terms of thermal radiation. A 12 x 400W lamp simulator was used for the experiment with a light control dimmer to control

the intensity of the light in order to obtain the required irradiation. The intensity was measured using the CMP 3 pyranometer with sensitivity of 17.99 x 10^{-6} V/Wm^{-2}. The light intensity was measured at nine different points along the receiver tube as shown in Figure 4-7 and 4-8. The average solar intensity measure was 18.86mV which is around 1046W/m^2.

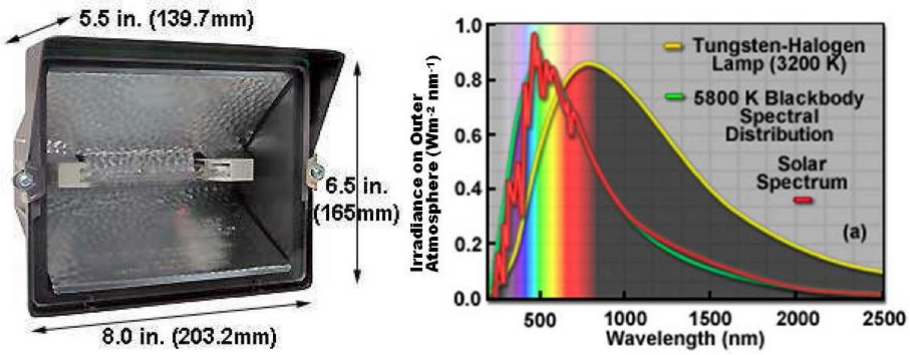

Figure 4-6: Tungsten lamp used for solar simulator

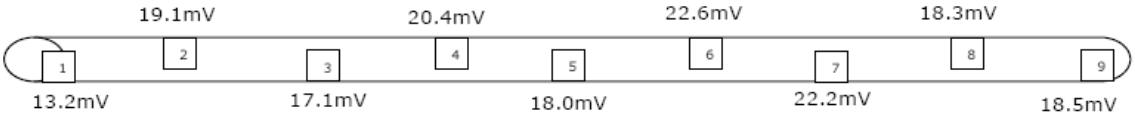

Figure 4-7: Light intensity along reviver tube surface

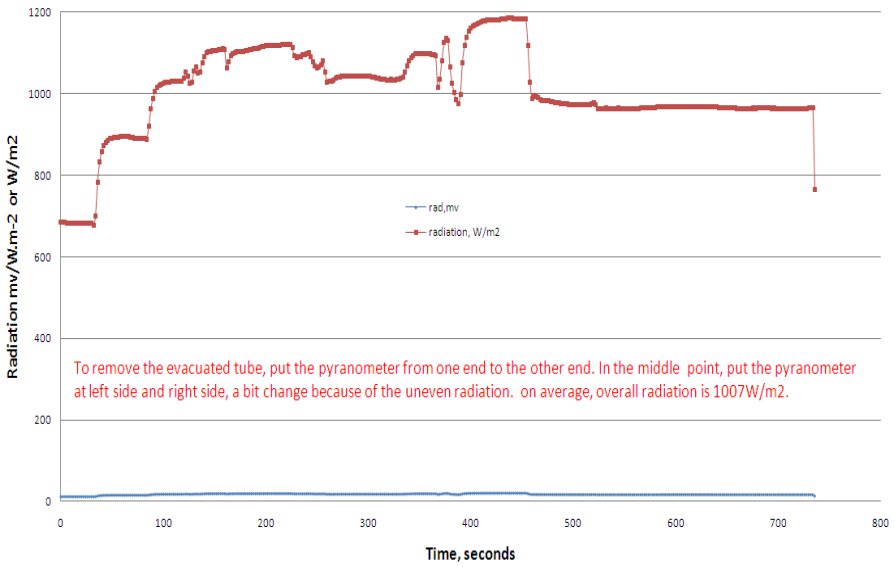

Figure 4-8: Measurement of light intensity along the surface of the receiver tube

4.3.1 Indoor Test

The experimental test for the solar collector was carried out indoors at the University of Nottingham. The performance of the system was tested using four different types of receiver tubes as shown in Figure 4-9 to 4-12. All the receiver glass tubes used are vacuum tubes. Tube I is a double layer glass tube with selective absorber coating in between the two layers of the glass. It is combined with a U-shaped pipe for circulating the heat transfer fluid. Tube II is the same as Tube I but only uses a different type of pipe. It uses the concentric (pipe-in-pipe) type pipe. Tube III is also the same with Tube I. However, it is a double layer glass but do not have selective coating. Tube IV is a single layer glass tube with no coating on the glass tube but rather it has a coated finned U-shaped pipe. Initial test was carried out with oil as working fluid and later with water as working fluid. Operation of the collector system with water at high temperature would produce high pressure and thus increase overall cost. And in order to increase heat transfer between the glass vacuum tube and the receiver pipe, aluminum fins were inserted into the glass tube to create a direct contact between the glass and the pipe, therefore heat transfer through conduction. Hence tests were also carried out to compare the receiver tube with and without fins. The specification of the receiver tubes used is given in Table 4-2.

Figure 4-9: Tube I-Double layer coated glass vacuum tube with U-shape pipe

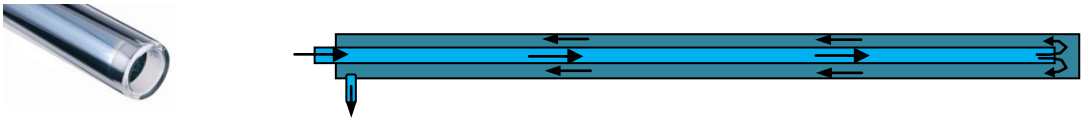

Figure 4-10: Tube II-Double layer coated glass vacuum tube with concentric pipe

Figure 4-11: Tube III-Double layer uncoated glass vacuum tube with U-shape pipe

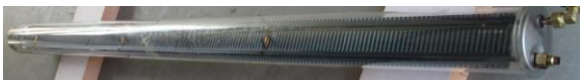

Figure 4-12: Tube IV-Single layer uncoated glass vacuum tube with coated finned U-pipe

Table 4-2: Specification of receiver tubes

Parameters	**Tube I**	**Tube II**	**Tube III**	**Tube IV**
Aperture area, m^2	1.4 (2mx0.7m)	1.4 (2mx0.7m)	1.4 (2mx0.7m)	1.4 (2mx0.7m)
Absorber area, m^2	0.209(1.8m×ø37mm)	0.209(1.8m×ø37mm)	0.377(2m× ø60mm)	0.528(2m×ø84mm)
Absorptivity, α	0.93	0.93	0.90	0.93
Emissivity, ε	0.035	0.035		0.05
Transmittance, τ	0.90	0.90		
Reflectivity, ρ	0.84	0.84	0.84	0.84
Absorber eff. η_{ab}	52.4%	52.4%	66.7%	51.8%
Irradiance I, W/m^2	1000	1000	1000	1000
Absorber heatflux ($Q=I\times A_{ab}\times\eta_{ab}$), W	110	110	252	274
Type of pipe	U-shape	Concentric	U-shape	Finned U-Shape

In order to increase heat transfer between the glass vacuum tube and the receiver pipe, aluminium fins were inserted into the glass tube to create a direct contact between the glass and the pipe, therefore heat transfer through conduction. Hence tests were carried out and compared for receiver tubes with fins and without fins.

Figure 4-13: Aluminium fins

Figure 4-14 shows schematic of the solar concentrator. It measures 2m x 0.7m giving a total surface area of $1.4m^2$

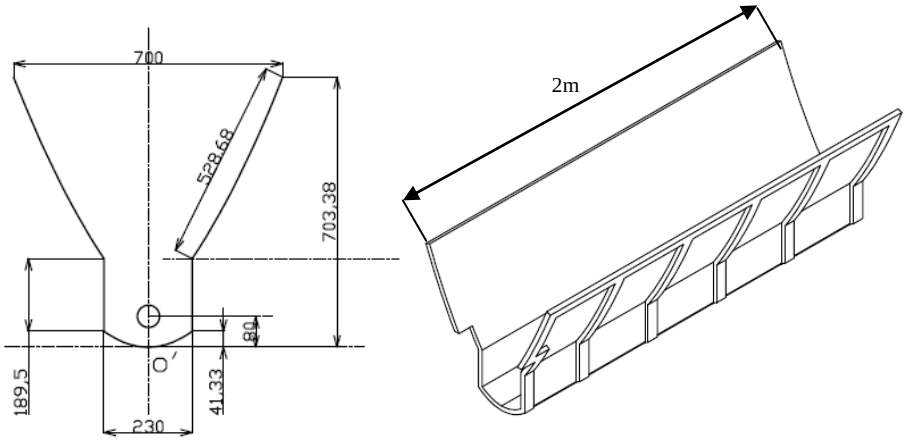

Figure: 4-14: Schematic of the solar concentrator

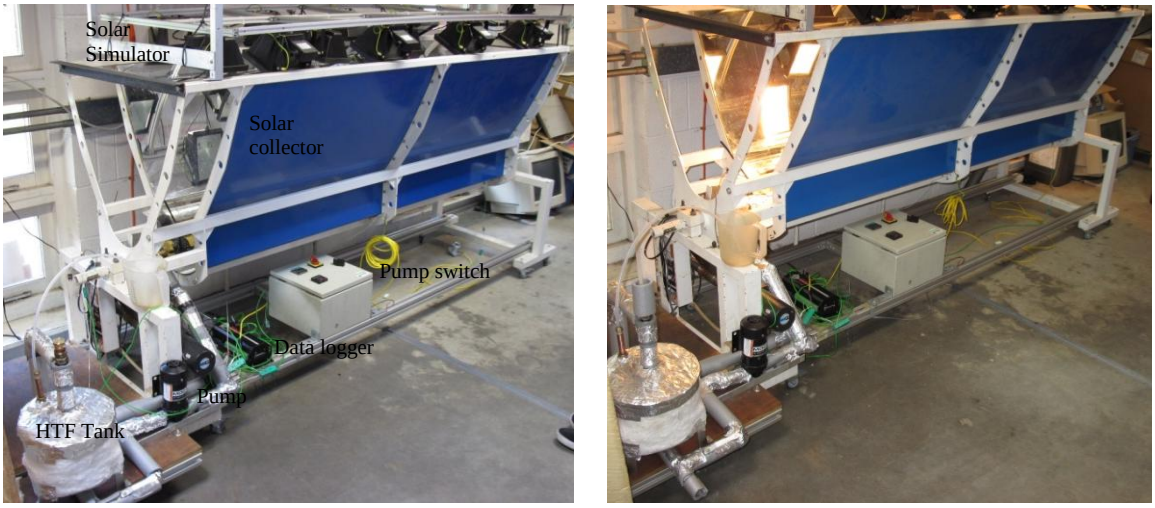

(a) Solar simulator off (b) Solar simulator on

Figure 4-15: Complete indoor experimental rig

(a) Solar collector with Tube I receiver (b) Solar collector with Tube II receiver

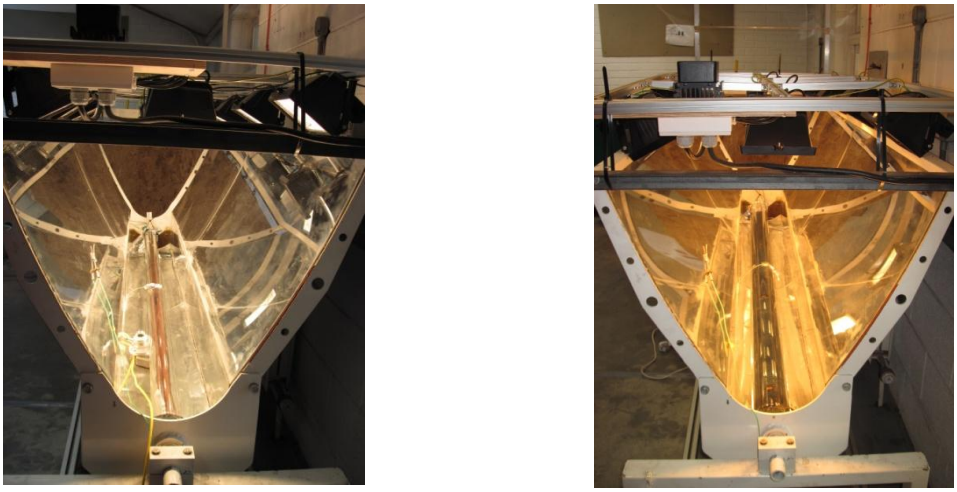

(c) Solar collector with Tube III receiver (d) Solar collector with Tube IV receiver

Figure 4-16: Solar collector with various receiver tubes

Tube I: u-piped double layer coated vacuum tube

Experimental test was carried out using Tube I. Tests were carried out using fins and without fins in the receiver tube and the results are presented in Figure 4-17 and 4-18. The HTF was heat transfer oil. The mass of the oil circulated is 5.86kg. The oil temperature ΔT for the Tube I without fins rise to 35°C while that with fins rise to 38°C from the initial temperature.

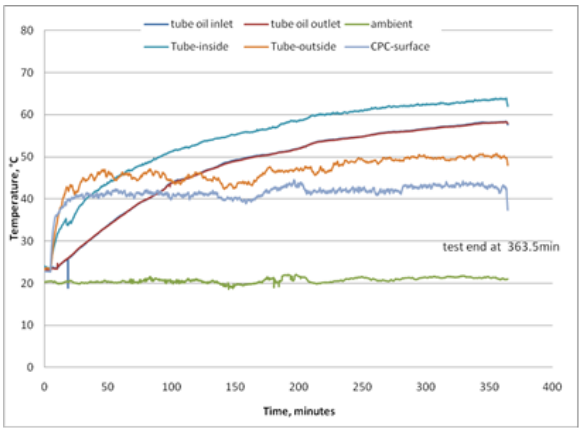

Figure 4-17: Variation of time with temperatures for Tube I without fins

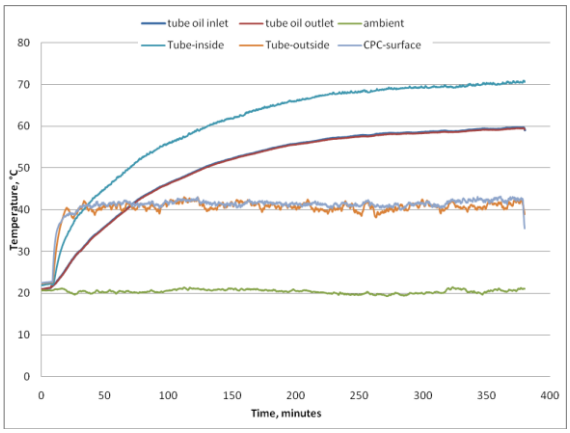

Figure 4-18: Variation of time with temperatures for Tube I with fins

Tube II: concentric piped double layer coated vacuum

Experimental test was carried out using Tube II. Tests were carried out with fins inserted into the receiver tube and the results are presented in Figure 4-19. The HTF was water. And mass of the water circulated is 6.68kg. The water temperature ΔT was raised to 33°C from the initial temperature. It can be seen the rate temperature increase for water as HTF was low compared to when using the oil as the HTF. However, the concentric pipe which is a double pipe counter flow heat exchanger improves the heat transfer rate. Coulson et al. (1999) mentioned that one of the advantages of the concentric tube is that they produce turbulent flows at low flow rates which increase heat transfer coefficient and hence the heat transfer rate [58].

The temperature rise in Tube II is generally lower than that of Tube I because water was used as heat transfer fluid in larger volume than that of Tube I which uses a smaller volume of oil as heat transfer fluid. However, the overall performance of the Tube II is higher than Tube I (see performance comparison below).

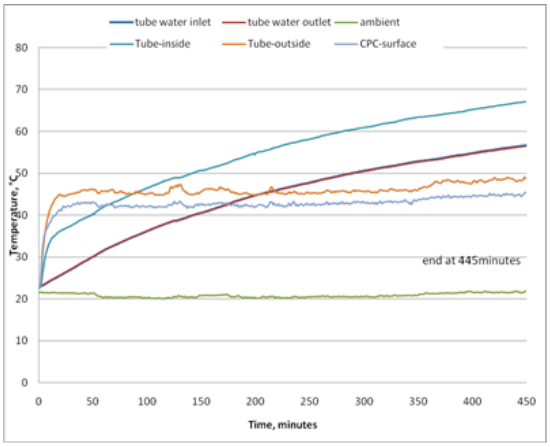

Figure 4-19: Variation of time with temperatures for Tube II with fins

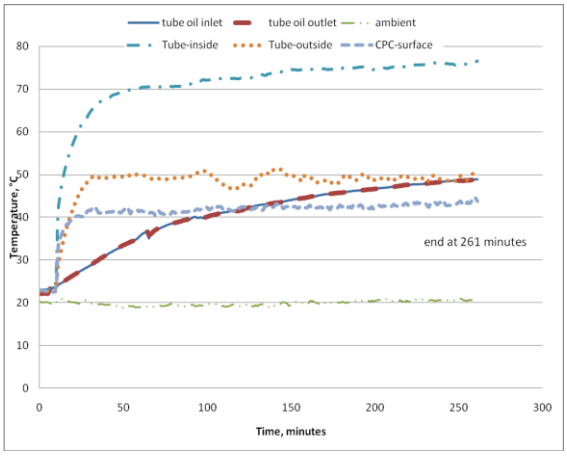

Figure 4-20: Variation of time with temperatures for Tube III with fins

Tube III: u-piped double layer uncoated vacuum tube

Experimental test was carried out using Tube III. Tests were carried out with fins inserted into the bottom of the receiver tube and the results are presented in Figure 4-20. The HTF was oil. And mass of the water circulated is 5.86kg. The oil temperature ΔT was raised to 25°C from the initial temperature. It was noticed that surface temperature and the inside temperature raised shapely compared to Tube I and II. This was due to the vacuum glass being clear glass with no coating and thus higher transmittance. However due to the receiver tube not having selective coating, much of the heat received was emitted and reflected to the environment. This results in very high heat loss. It was suspected that the aluminium fins which were meant to increase heat transfer instead further reflected to the environment much of the incident thermal radiation. Nevertheless the results show that the rate of rise in temperature for the clear receiver tube is faster when compared to the coated glass tube. Thus this type of glass vacuum tube can be useful in reducing the much long time required to obtain the required water temperature level for water desalination. Nafey et al. (2004) carried out experimental investigation of desalination based on humidification/dehumidification process. It was reported that a delay time was noticed between the start of a run and the start of fresh water production [59]. Yet in another research of similar system, Al-Hallaj et al. mentioned a 3 hour delay was noticed between sunrise and start of water production [60]. Both authors agreed that most of the energy received in the early hours is used as sensible heat to warm the large water mass to be desalinated.

Tube IV: coated finned u-pipe single later vacuum tube

Experimental test was carried out using Tube IV. Tube IV is a clear single glazed vacuum glass with selective coating on the finned receiver pipe. Thus it is expected to have high transmittance and very low emittance due to the selective coating, and hence low heat loss. Two different tests were carried out using oil and then water as the HTF. The mass of the circulated oil and water are 5.48kg and 6.29kg respectively. The results are plotted in Figure 4-21 and 4-22. The oil temperature ΔT was raised to 47°C while that of water was raised to 40°C from the initial temperature. The rise in temperature of oil was faster compared to that of water due to different heat capacities.

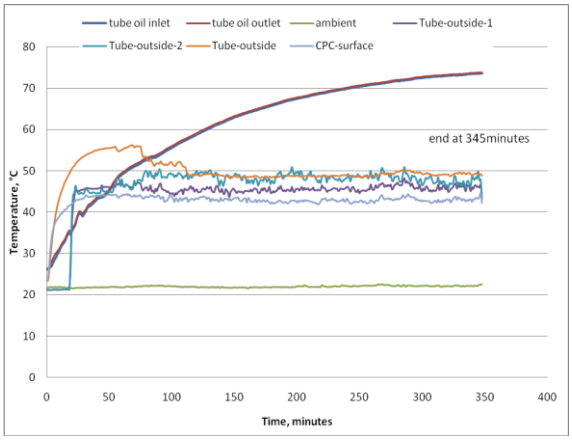

Figure 4-21: Variation of time with temperatures for Tube IV with oil as HTF

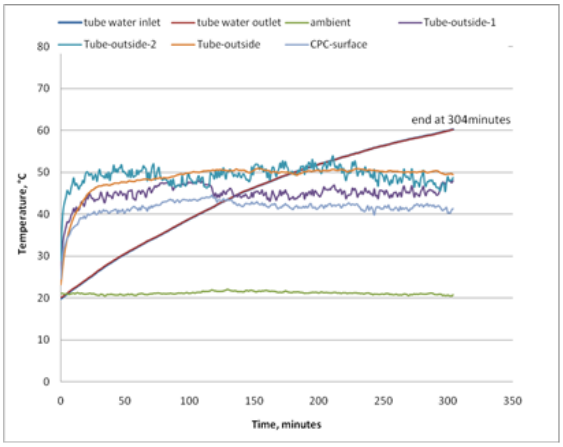

Figure 4-22: Variation of time with temperatures for Tube IV with water as HTF

It was not possible to measure the inside temperature of the tube because it is a sealed single glazed receiver tube. Nevertheless a sharp rise in surface temperature was noticed similar to that of Tube II. With a larger receiver surface area, the concentration ratio of the receiver tube is expected to be lower and hence limitation on the maximum achievable temperature. All tests carried out indicated that Tube IV performs better.

Comparison of Efficiencies

The efficiency of the solar collector for different receiver tubes was calculated. Because of difference in the sizes of the receiver tubes, Equation 22 was modified to calculate the efficiency based on the actual heat flux on the received on the receiver tube. This is dependent on the size and efficiency of the tubes. This is given by;

$$\eta = \frac{Q_L}{A_{abs} I_{abs} \eta_{abs}} = \frac{Q_L}{Q_{ideal}} \quad (23)$$

Where Q_L is the actual measured energy absorbed by the HTF, this can be calculated using Equation 4. And A_{abs} is area of the receiver tube (absorber), η_{abs} is efficiency of the absorber (obtained from manufacturers data) and I_{abs} is solar intensity received directly at the surface of the receiver tube measured using the CMP3 Pyranometer.

Table 4-3: Measured and calculated experimental data

Receiver Type	A_{abs} [m^2]	I_{abs} [W/m^2]	η_{abs} [%]	Q_{ideal} [W]	m_{HTF} [kg]	C_p [J/kg.K]	Time [min]	ΔT [°C]	Q_L [W]	η [%]	HTF
Tube I (fins)	0.209	1000	52.4	110	5.86	1860	370	38	18.7	17	Oil
Tube I (no fins)	0.209	1000	52.4	110	5.86	1860	359	35	17.7	16.1	Oil
Tube II (fins)	0.209	1000	52.4	110	6.68	4178	439	33	35	31.8	Water
Tube III (fins)	0.377	1000	66.7	252	5.86	1860	251	25	18.1	7.1	Oil
Tube IV	0.528	1000	51.8	274	5.48	1860	342	47	23.4	8.5	Oil
Tube IV	0.528	1000	51.8	274	6.29	4178	304	40	57.6	21	Water

Table 4-3 shows breakdown of calculated efficiencies based on the experimental data obtained. It can be seen that Tube II with the concentric receiver with water as HTF has the highest efficiency with water as HTF. And Tube IV shows great potential with also. However, it can be seen from the change in temperature ΔT that the sensible heat transfer to the oil is higher than of water most especially when the results of Tube I and Tube II are compared. This is mainly as a result of different heat capacities of the fluids where oil has a lower specific heat capacity than water.

The instantaneous efficiency of the receiver tube was calculated and compared with the ideal efficiency reported by Brunold et al. (1994) [61]. The efficiency is shown in Figure 4-23. It can be seen that the efficiency drastically drop with increasing temperature. And there is big difference between the ideal efficiency of Tube IV with the real efficiency. It was suspected that the poor performance was due to the receiver tube not in vacuum. This is a common problem with sealed single glazed vacuum tube glasses. And hence that is why double glazed tubes as the most widely used and cheaply available in the market.

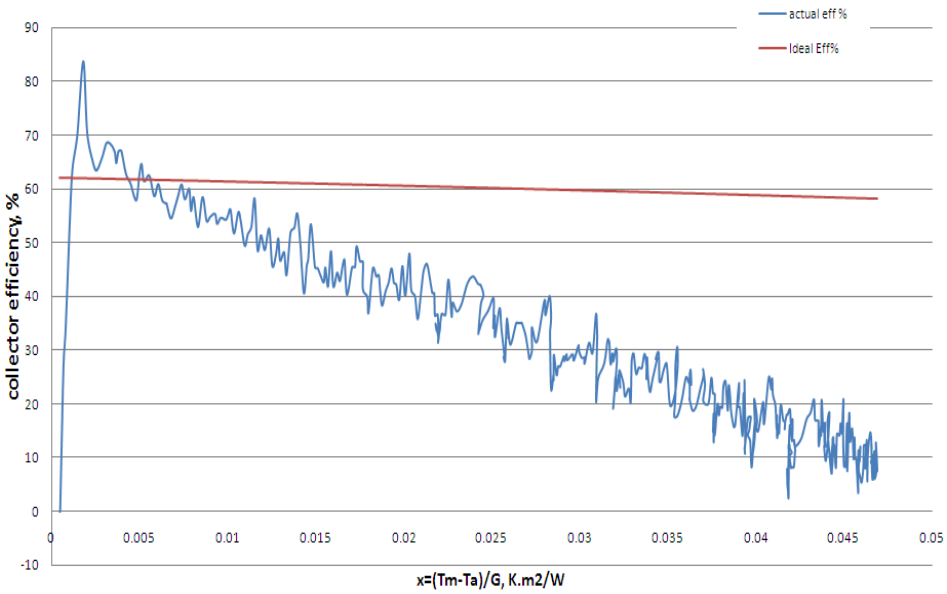

Figure 4-23: Comparison of combine collector efficiency for different receiver tubes

The selection of an optimum solar collector configuration to power the water desalination unit is very critical. The main criteria for selecting the optimum configuration include quick solar collector start up time to fresh water production. This can be achieved by both Tube III and Tube IV due to high transmittance through the vacuum tube. Secondly, it is essential to keep heat loss down to the minimum. This can be achieved through increasing the absorptivity of the receiver tube and at the same time decreasing the emissivity of the receiver tube. Base on the experimental results obtained it is evident that receiver tubes with selective coating perform better than the receiver without the coating (i.e. Tube III). Even though fins were used in the Tube III in order to increase heat transfer by direct contact (conduction), results from Tube I (no fins) indicate a better performance. This shows how important it is to have the selective coating on the receiver tube of the collector. Experimental results show that Tubes II and IV can achieve this criterion. It was expected that Tube IV with oil as HTF should have a much higher efficiency when compared to Tube III which has no selective coating. It was found that the poor performance was due to the receiver tube not in vacuum (i.e. the vacuum tube has leakage). This is a common problem with sealed single glazed vacuum tube glasses. And hence that is the reason why coated double layer vacuum tubes as the most widely used and cheaply available in the market. Therefore Tube II configuration was selected for outdoor test of the collector.

4.3.2 Outdoor Test

An outdoor test of the solar collector was carried out in order to determine the efficiency of the solar collector combined with water storage tank using real weather conditions. The experimental testing of the unit was carried out in Liuzhou city China. The experimental is shown in Figure 4-24 and 4-25.

Figure 4-24: Complete outdoor experimental rig showing receiver tube

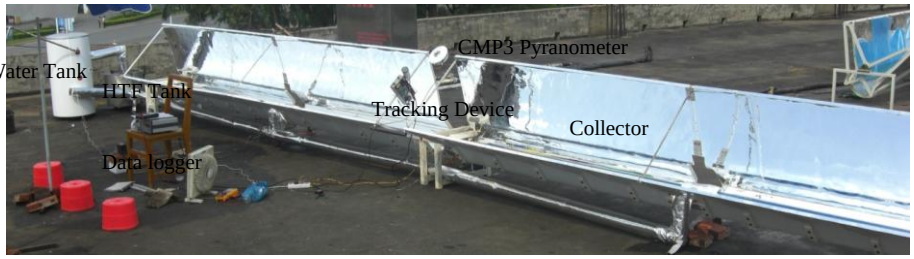

Figure 4-25: Complete outdoor experimental rig

The test was carried out using 8m by 0.7m solar collector with total area of 5.6m^2. And the selected receiver tube was Tube II but using a different oil as HTF with 2186J/kg.K specific heat capacity. The oil is supplied by Feira Lubricant. It has higher specific heat capacity and thermal conductivity than that of the previous oil used (HT5 Perfecto supplied by Castrol). The choice of using oil as HTF was mainly because the aim of the test was to achieve temperatures above 100°C. And oil is potentially lower risk than water in terms of boiling and pressure.

The tracking device is constructed locally in laboratory at the university. It was set to track the sun from east to west direction. However, the failure of the tracking device during the experiment left no choice but to track sun manually. A white paper (for easy visibility) was used at the bottom of the collector in order to observe and shadow casted by the receiver tube on the collector. If there is shadow, the collector is tilted until the shadow disappears.

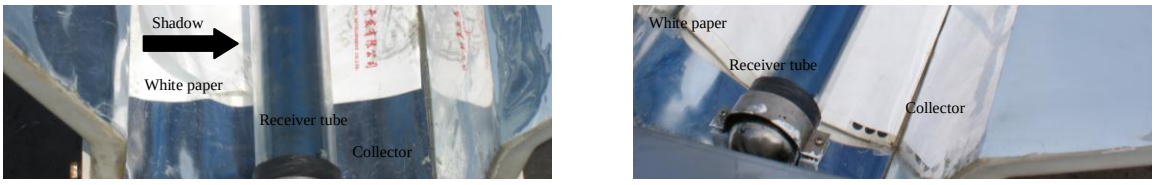

(a) Visible shadow before adjustment (b) No visible shadow after adjustment

Figure 4-26: Manual solar tracking of the collector

Figure 4-27 present experimental data solar intensity, receiver outlet temperature, receiver inside temperature. An average of approximately 700W/m^2 was measured between 08:00 to 18:00 hours. The maximum receiver tube surface temperature measured was around 150 °C. The oil temperature raised to more than 120°C. It can be seen from Figure 4-28 the water temperature reached 100°C in approximately 4 hours.

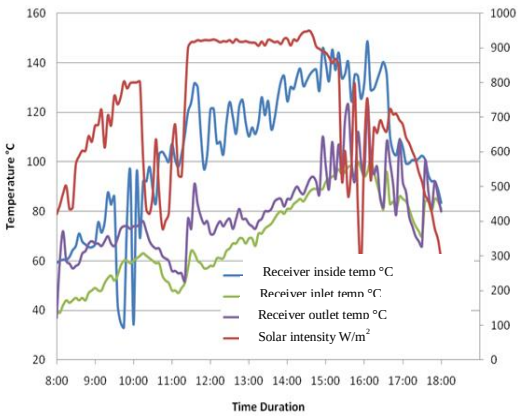

Figure 4-27: Variation of various temperature and solar irradiation with time

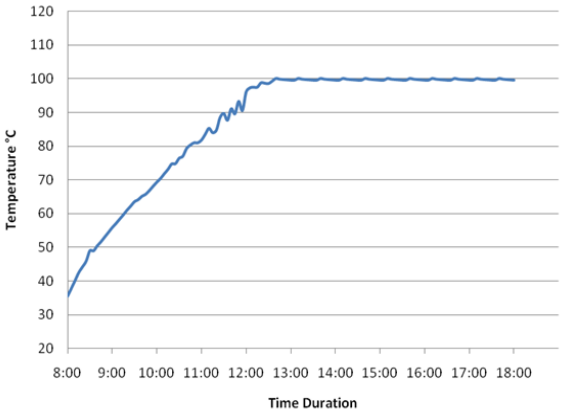

Figure 4-28: Variation of water temperature in storage tank with time

After the useful data was extracted, the thermal energy and efficiency of the system were calculated using Equation 19 and 22 using the experimental results obtained. It was found

that the thermal energy delivered by the solar collector in order to raise water temperature from 35 to 100 100°C was around 1.5 kW. The thermal efficiency of the combined system (both collector and water tank) was found to be 38%. The plot of the efficiency of the system is presented in Figure 4-29.

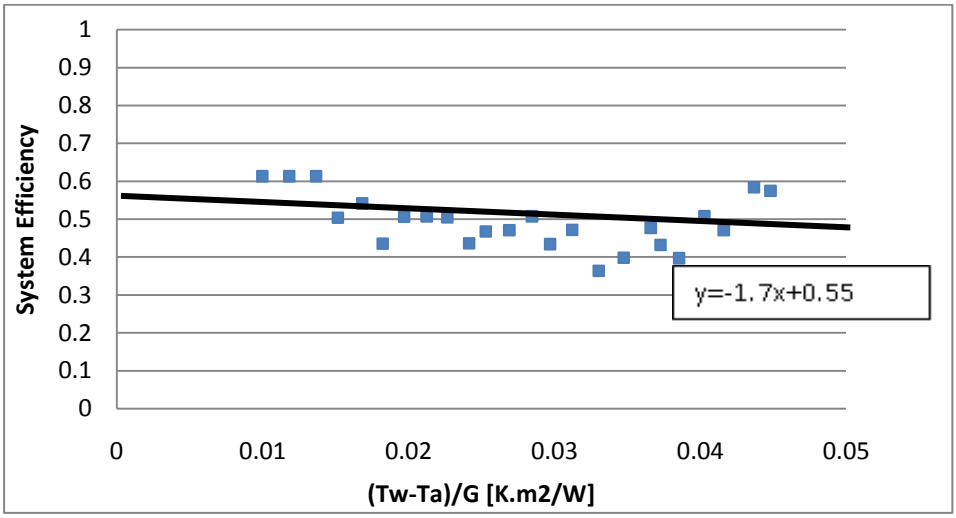

Figure 4-29: Efficiency of the solar collector system

4.4 Modelling of Solar Collector for the HDD Unit

The efficiency of a solar collector is very important in order to determine the area of collector required for water desalination. The efficiency varies with types of collectors used which depend on optical efficiency, heat loss, concentration ratio and perhaps the environmental conditions. The thermal efficiency of a concentrating solar collector is designed as the ratio of the useful energy delivered to the energy incident at the concentrator aperture. This may be calculated from an energy balance on the receiver [62, 63] which is given by:

$$\eta = \eta_o - \frac{U_L(T_r - T_a)}{IC} \qquad (24)$$

Where η_o is optical efficiency of the concentrator which depends on material used in construction of the solar collector and also the geometry of the collector. U_L is the heat loss factor. T_r and T_a are the receiver and the ambient temperatures respectively. I is the solar intensity and C is the concentration ratio of the collector. (see Appendix H).

Equation 24 can be expressed in terms of heat removal factor F_R [64]. This is given by;

$$\eta = F_R\eta_o - \frac{F_R U_L (T_r - T_a)}{IC} \qquad (25)$$

The advantage of concentrating collectors is that the heat losses are inversely proportional to the concentration ratio. The standard performance of both concentrated and non-concentrated collectors can be related to straight line equation with slope of the line related to the heat loss and the intercept related to the optical efficiency. The equation is given as follows;

$$\eta = I_n - S\left(\frac{\Delta T}{I}\right) \qquad (26)$$

Where I_n = Intercept = $F_R\eta_o$ and S = Slope = $(F_R U_L)/C$

The standard performance of various collectors reported by different researchers is compared with the performance of current V-Trough. The typical collector performance curves are reported by Kalogirou (2004) and are related to the straight line equation [26]. This is shown in Figure 4-30.

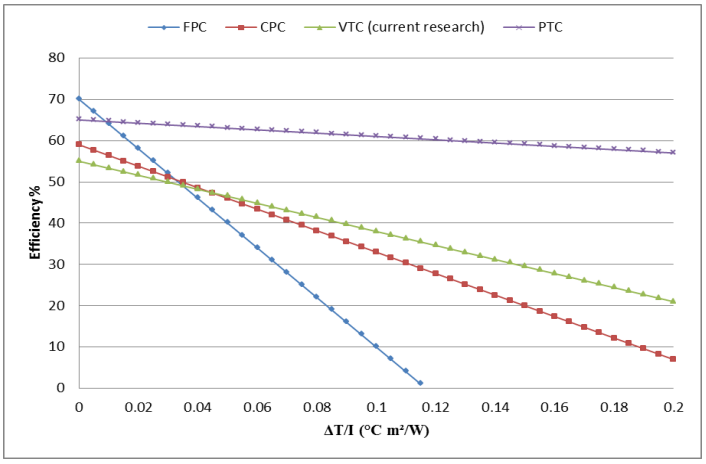

Figure 4-30: Typical collector performance compares with the new V-Trough collector

It can be seen from the figure that at lower temperatures the non-concentrating flat plate collector (FPC) is more efficient compared to the three other concentrating collectors.

The concentrating collectors tend to perform better at higher temperatures. For example, at 100°C which corresponds to 0.1; the PTC works at 61% efficiency, the new VTC works at 38% efficiency, the CPC works at 33% efficiency and the FPC works at 10% efficiency. The performance curve equations obtained from Figure 4-30 are given in Table 4-4. These equations are used to model the amount of solar collector required for water desalination for each type of the collector.

Table 4-4: Solar collector performance curve equations

Collector	Concentration Ratio	Temperature [°C]	Equation
FPC	1	30-80	η=0.7-6(ΔT/I)
CPC	1-5	60-240	η=0.59-2.6(ΔT/I)
VTC	5-15	60-300	η=0.55-1.7(ΔT/I)
PTC	15-45	60-400	η=0.65-0.4(ΔT/I)

In order to model the size of solar collector required to provide energy for the water desalination system based experimental work carried out in Chapter 3, there is need to know the actual amount of hot water required for the evaporation process. The actual amount of water required depends on the absorption ratio of the humidification chamber. Many literatures mention in order to ensure effective humidification, there is need for an abundant supply of hot water into the humidification chamber [65]. But none of the literature mentioned the actual amount of the water that is needed with respect to size and material used in the humidification chamber.

The amount of water supplied and evaporated depends on the mass flow rate of air through the humidification chamber and also temperature and flow rate of water which in turn depends on energy input. The amount of evaporated water can be calculated as follows;

$$m_v = m_a(\omega_{out} - \omega_{in}) \qquad (27)$$

Where m_v is mass of water vapour (i.e. amount of water that is evaporated), m_a is mass flow rate of air, ω is the amount of water content per kg of dry air at the inlet and outlet of the humidification chamber.

The water content and other psychrometric properties can be obtained using the psychrometric chart or software once the temperature and relative humidity of air are known. The water flow rate into the humidification chamber in any case is always much greater than the amount of water that gets evaporated;

$$m_{w,h} >> m_v \tag{28}$$

Thus minimum water flow rate into the humidification chamber is equal to the mass of evaporated water.

$$m_{w,h(\min)} = m_v \tag{29}$$

From Equation 15, the absorption ratio of the humidification chamber is given as;

$$\varepsilon = \frac{m_v}{m_{w,h}} \tag{30}$$

The minimum energy required to evaporate the water greatly depends on the temperature difference ΔT at the inlet and outlet of the humidification chamber. This can be calculated as follows;

$$Q_{\min)} = m_{w,h(\min)} c_p (\Delta T) = AI\eta \tag{31}$$

And finally the total area of solar collector required depends on the amount of energy required for evaporation. This depends on the amount of solar intensity and also efficiency of the solar collector in converting the solar intensity into useful energy. This can be calculated as follows;

$$A_{(\min)} = \frac{m_a c_p \Delta\omega \Delta T}{I\varepsilon\eta} \tag{32}$$

The modeling of the solar collector for water desalination was carried out using Microsoft Excel Spreadsheet. The calculation was carried out for three different solar collectors using the performance curve equations in Table 4-4. And the solar collector area for the VTC was calculated over three different solar intensities. The following initial conditions were used for the modelling. They are based on preliminary experiment of the HDD unit carried out in Chapter 3. However, some other parameters were assumed in order to predict the system under conditions not considered in the experimental work.

- The initial environmental condition measured was 20°C average temperature and 80% relative humidity.
- The absorption ratio varied with temperature and flow rate, and hence minimum ratio (ε=0.04) was considered in order to create an optimum model.
- The average measured ΔT at the humidification chamber was 20°C, and an assumed 5°C ΔT was also considered. Temperature range was up to 200°C and the air fully saturated (relative humidity =100% at humidification chamber).
- The exhaust condition was 30°C and 100% relative humidity as worst case scenario.
- Air mass flow rate was considered at 10kg/h which is slightly lower than the measured air flow rate.

Figure 4-31 shows the variation of water production and solar collector required for four different solar collectors. The water production rate is presented for up to 20kg/h. It can be seen for water production up to 2-3kg/h, there is no much difference in the amount of collector required. Hence the best choice of collector is the FPC which less complex and more economically affordable. It can be seen that the 2m^2 of the CPC and the new VTC could produce up to 6kg/h of fresh water. However when water production is above 6kg/h, the new VTC performs better than the CPC.

In terms of operating temperature (i.e. required temperature of hot water), the FTC can work with the desalination system up to 80°C. The efficiency of the FTC drastically drops at temperatures above 80°C and hence larger collector area requirement which is not economically viable compared to other collectors. The temperature limitation of the FTC at around 130°C as shown in Figure 16 indicates the theoretical limit of the FTC to water production of around 20kg/h. On the other hand, the required amount of the CPC

and the new VTC are the same for up to 120°C. The VTC becomes more competitive at temperatures above 120°C.

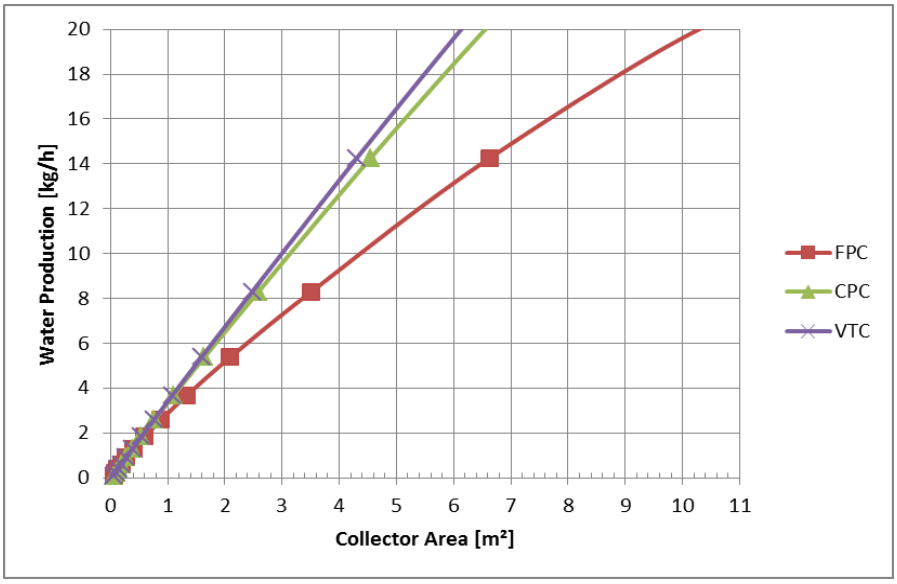

Figure 4-31: Variation of water production with collector area different types of solar collectors

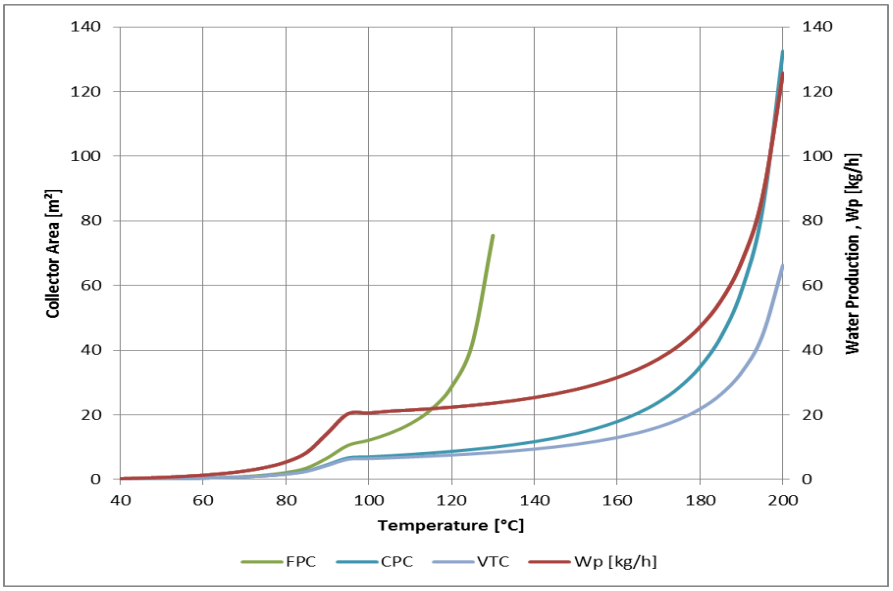

Figure 4-32: Variation of collector area and water production with operating temperature for different types of solar collectors

The variation of the required VTC area with water production for three different solar intensities is shown in Figure 32. In order to produce up to 120kg/h of fresh water, at

least 60m² collector area is required at 1000W/m^2 solar intensity. It shows that it is possible to produce 2kg/m²/h.

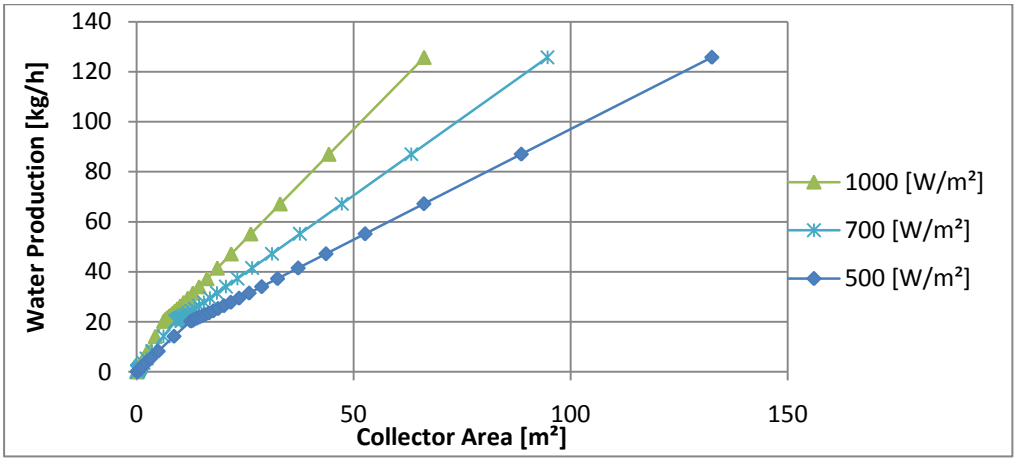

Figure 4-33: Variation of v-trough collector area with water production for different amount of solar intensities

Figure 4-34 shows water production and collector area for two different inlet/outlet temperatures of the humidification chamber. Higher water production and lower collector area can be achieved at lower ΔT. Base on previous experimental test of the desalination system using an electric heater, low ΔT at 5°C is achieved at high hot water flow rates for operating temperatures below 80°C. Above that operating temperature, the desalination system operates at around 20°C ΔT.

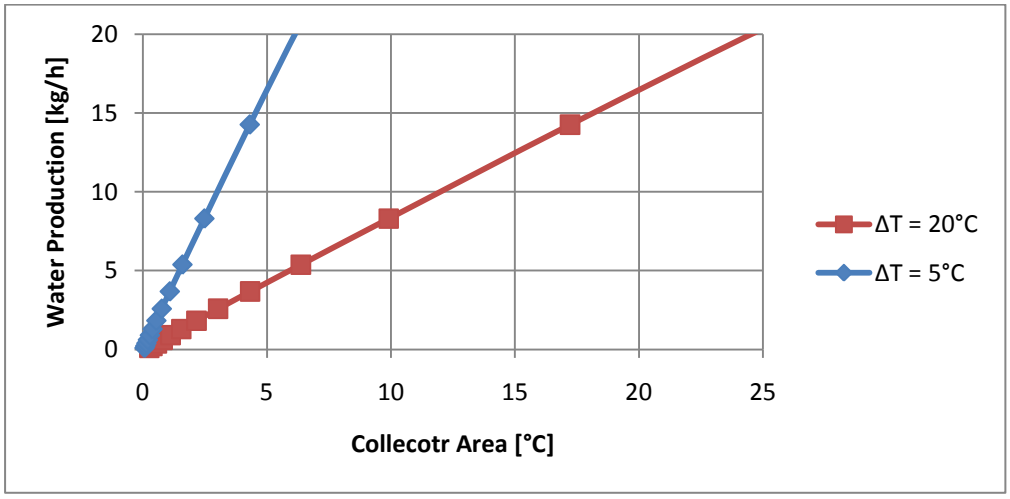

Figure 4-34: Variation of water production with collector area for different temperature difference at inlet/outlet of the humidification chamber

4.5 Conclusion

The types of solar collectors and their suitability to drive the newly designed HDD unit were reviewed. And it was found there is need to design a new solar collect to mitigate the current challenges presented by conventional systems. The design of new V-Trough solar collector was presented. Performance analysis of the solar collector was carried out through experimental work. Various receiver tubes have been tested and the best was selected which fits the requirement of operating a desalination system. The selection of the most suitable collector for a given application (i.e. small scale or large scale) should take into account; the required operation temperature, the solar intensity and environmental temperatures and other technical and economic factors. In addition, to determine the size of solar collector, the efficiency of both the humidification chamber and that of solar collector are very crucial.

Potential solar collectors for water desalination are the flat plate collectors (FPC), evacuated tube collectors (ETC) for non-concentrating collectors. For the concentrating collectors, linear focusing collectors which include compound parabolic collectors (CPC) and parabolic trough collectors (PTC) have more potential than point focusing collectors. However the PTC and the point focusing parabolic dish collector (PDC) and heliostat field collector (HFC) are seen as more suitable for large scale power generation and other high temperature applications. Thus the only choice left is the CPC which very expensive for small scale desalination application most especially in the developing countries. And at the same time it is not economically viable for large scale application. The modelling work carried out suggests that the new VTC has more potential for water desalination compared to other collectors at certain operating conditions.

Hence there is need to carry out further experimental tests to combine the solar collector and the water desalination unit and validate the modelling work compared with the experimental data. There is need to operate the system at lower ΔT in order to achieve higher water production with lower collector area. This will require operating the system at higher flow rate. And hence focus on flow rate will be given in next experimental test which can be found in chapter 6. Furthermore, in order to take best advantage the desalination unit needs to be operated at higher temperatures at least above 100°C so as to determine the real performance of the system under such conditions.

Chapter 5: Solar Desalination Experimental Facility

5.0 Introduction

Having established the need for a water desalination system driven by renewable energy source from literature review in Chapter 2, a desalination unit and solar collector were designed and pre-tested separately in Chapters 3 and 4. Hence a combined solar desalination unit need to be tested in order to assess the combined system performance under different operating conditions. The experimental facility is presented in five sections of the chapter. It describes the experimental set-up which covers summary of the test rig and the components/measuring devices required, and then the experimental design which detailed construction of all the components of the system, and another section which describe difficult challenges experienced and how they were overcome. The other key and important section describes measuring instruments used, their specification, accuracy and calibration. And the final section describes the experimental test procedure of the system.

5.1 Experimental Set-Up

The experimental set up consists of five main components as illustrated in Figure 5-1. These are the solar simulator located directly above the solar collector, novel v-trough concentrating solar collector, the heat transfer oil tank, the coil heat exchanger water tank, the humidification dehumidification desalination /(HDD) unit and cooling water tank. Other auxiliary components include electric heater, pumps and valves.

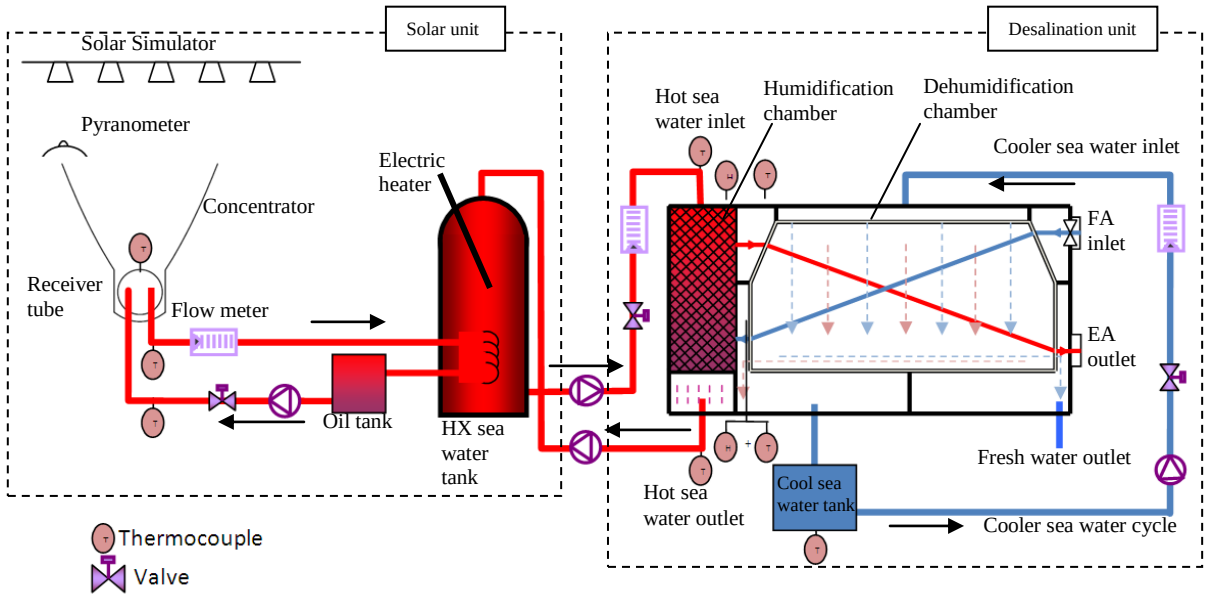

Figure 5-1: Schematic of desalination unit integrated with solar collector

The measuring instruments required are thermocouples, fluid flow meters, air flow meter (hot wire anemometer), light meter (Pyranometer), humidity sensors for measuring relative humidity and a digital metric scale with calibrated measuring cup to measure the amount of fresh water produced. Fig. 5-1 illustrates a schematic of the experimental rig showing location of measuring instruments.

There should be nine temperature sensors. One thermocouple, T_s is required to measure the surface temperature of the receiver tube of the solar collector. Two thermocouples T_{in} and T_{out} at inlet and outlet of the receiver tube are required to measure the temperature of heat transfer oil. Another two thermocouples $T_{h,i}$ and $T_{h,o}$ are required to measure the temperature of hot sea water cycle in and out of the humidification chamber from the heat exchange (HX) tank. One other thermocouple T_{cyc} is required to measure temperature of cooling water cycle for condensation in the dehumidification chamber. Finally three sensors to measure the temperature of the exhaust air $T_{EA,}$ temperature of fresh water produced T_{FW} and a temperature sensor T_{amb} to measure the ambient temperature.

One flow meter m_o is required to measure the mass flow rate of heat transfer oil round the solar collector. And two other flow meters $m_{w,h}$ and $m_{w,c}$ are required to measure water mass flow rate round the humidification and dehumidification chambers respectively. An air flow meter is necessary to measure the air flow rate in the desalination unit. A computer and data logger are required to monitor and record the data readings from the measuring instruments while the amount of fresh water produced is measure manually using the digital scale and calibrated measuring cup.

5.2 Experimental System Design

The experimental system design includes the sizing and selection of main system components. The capacity and size of the system was determined in the section of theoretical work carried out. It was designed regardless of specific heat input but rather base on the amount of fresh water that can be obtained over different range of heat input. The selection of system components and equipments are based on heat input and flow rate parameters and as well other assumptions carried out during numerical analysis.

5.2.1 Solar Simulator

The solar simulator is used to simulate the sun. As shown in Figure 5-2, it consists of 12 x 400W metal halide lamps supplied by Screwfix. Each of the lamps has dimension of 210 x 185mm. There is also dimmer switch to control the light intensity.

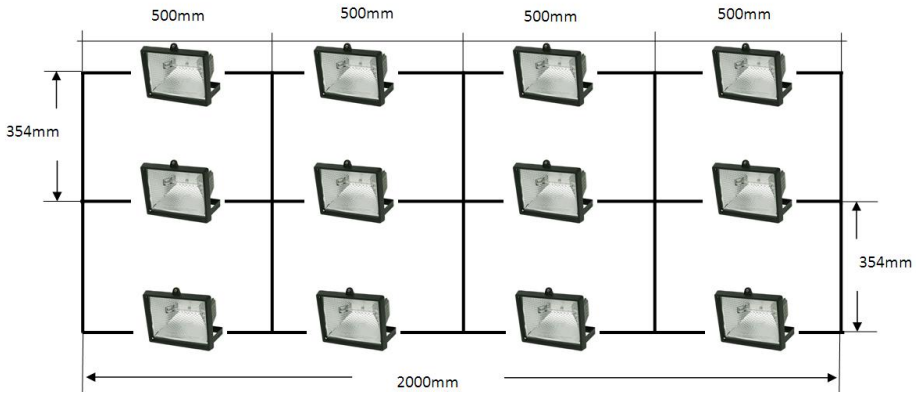

Figure 5-2: Structural dimension of the solar simulator

5.2.2 Solar Collector

The solar collector as illustrated in Figure 5-3 is a combination of a novel v-trough concentrator and a high temperature absorber tube as the receiver.

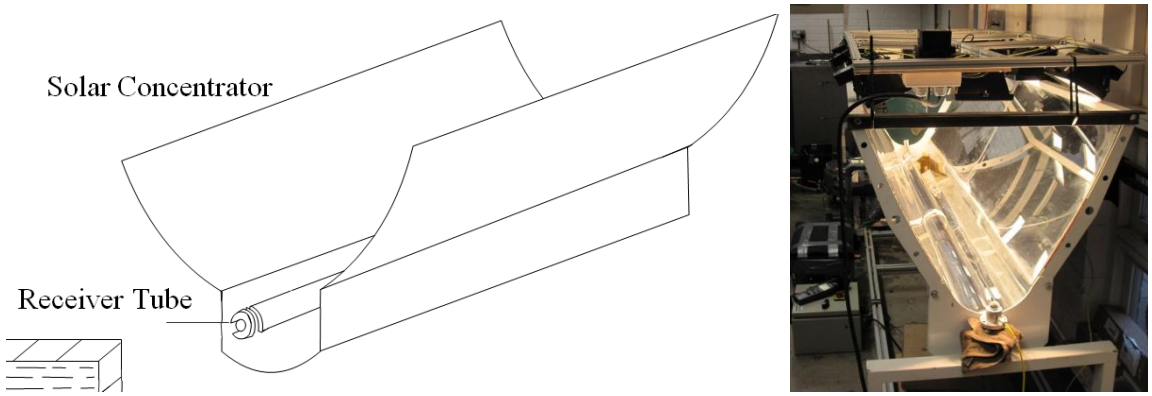

Figure 5-3: The V-trough solar collector

5.2.2.1 High Temperature Receiver

The high temperature receiver has total length of 2m and 12cm in diameter. It consists of an evacuated glass tube with up to 90% transmittance and vacuum pressure $\leq 5x10^{-3}$Pa. Inside the glass tube is a U copper pipe with 12mm diameter. The pipe is attached to a plate fin (1.8m x 0.84m) which has a coating with selective absorbing surface. The

selective coating has 90% absorptance and 6% emittance. The receiver tube is shown in Figure 5-4 below.

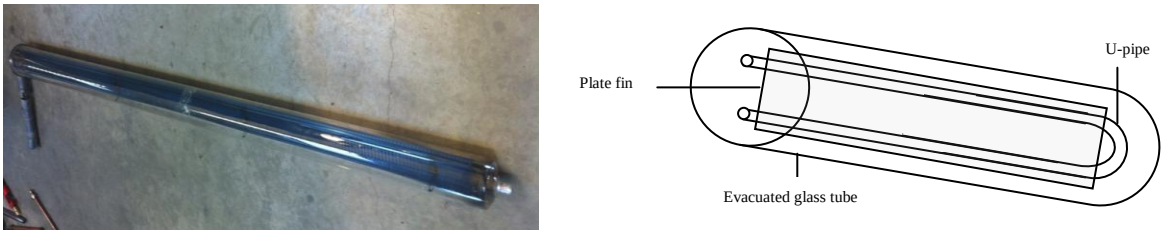

Figure 5-4: The high temperature receiver tube

5.2.2.2 Solar Concentrator

The solar concentrator uses mirror as its reflector with 90% reflectivity. The dimension of the solar concentrator and the position of the receiver tube in the concentrator are shown below in Figure 5-5.

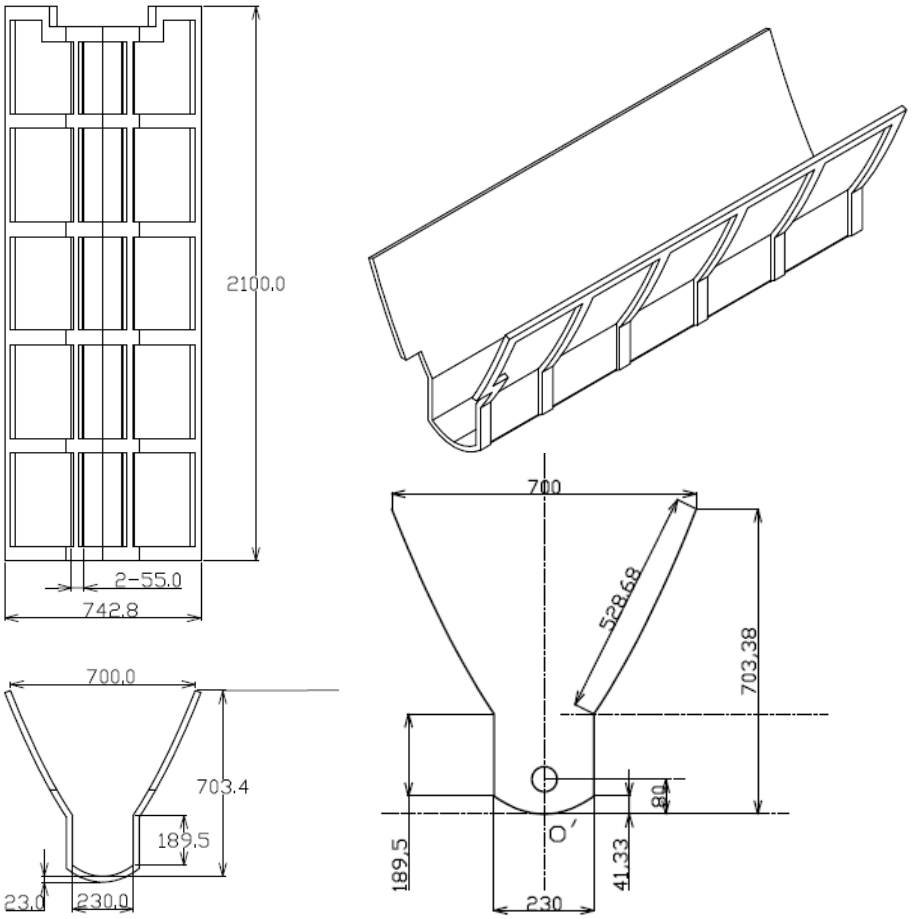

Figure 5-5: The V-trough solar collector

5.2.3 Humidification Dehumidification Desalination Unit

The desalination unit consists of the humidification chamber which is regarded as the evaporation core (E-Core), and the dehumidification chamber which is regarded as the evaporation/condensation core (E/C-Core).

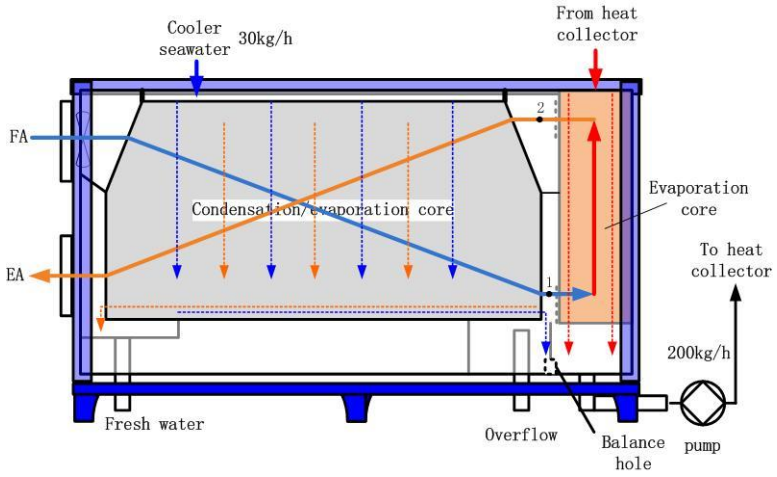

Figure 5-6: Desalination unit

5.2.3.1 Humidification Chamber

The humidification chamber consists of porous media made of cellulose material and a single tube water sprayer. It has a dimension of 0.7x0.5x0.2 meters.

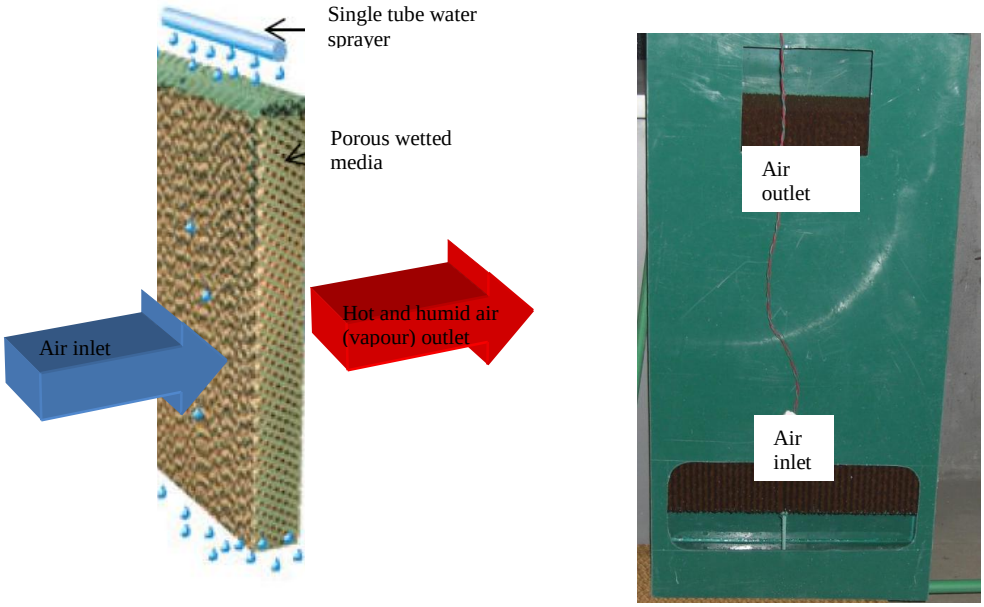

Figure 5-7: The humidification chamber

5.2.3.2 Dehumidification Chamber

The dehumidification chamber is a multi-pass heat exchanger made of a specially designed membrane. It has the wet channel made of hydrophobic material while the dry channel made of hydrophilic material. It has a total dimension of 0.7x1.25x0.5.

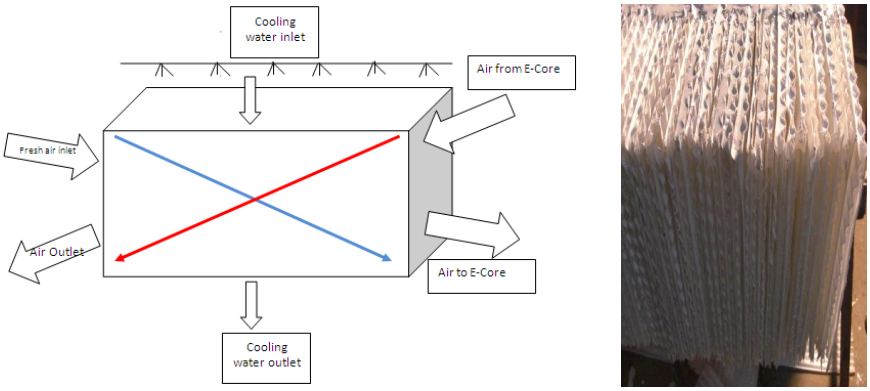

Figure 5-8: The dehumidification chamber

5.2.4 Hot Water Tank

A water tank was used to store pre-heated sea water which is circulated through the humidification chamber for evaporation. The tank as shown in Figure 5-9 is incorporated with and electric immersion heater at the top and a coil heat exchanger at the bottom for the solar collector. The tank has a total capacity of 140L. Up to 30% of the volume is dedicated to solar capacity, and 70% can be heated via an electric immersion heater or through the primary coil using fossil fuel or biomass. A 30mm thickness of insulation material was used to insulate the tank.

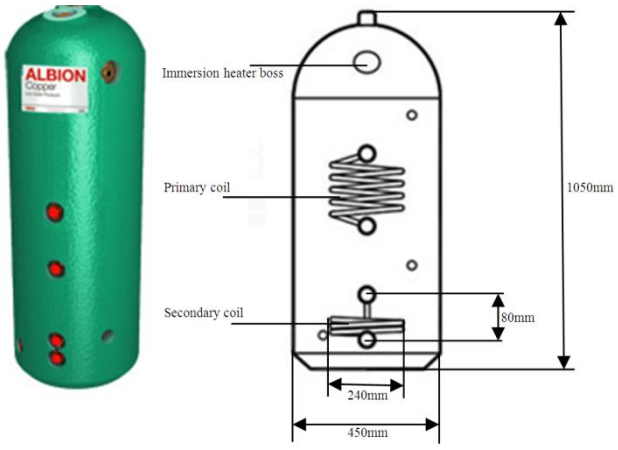

Figure 5-9: Insulated water tank

5.2.5 Auxiliary Components

The auxiliary components are equipments that are necessary for integration and operation of the entire system. They include the electric heater, fan and pumps. Total energy consumption excluding the electric heater is under 1kW. Other components are the heat transfer oil tank and cooling water tank.

Electric Immersion Heater

A 3kW electric immersion heater was used to provide heat energy required to raise the temperature of water to be desalinated. The electric heater as shown in Figure 5-10 has a total length of 27 inches.

Figure 5-10: Electric Immersion Heater

Fan

An axial fan was used to supply the air required for humidification and transport of vapour through the system. The fan has energy consumption of 22W with a maximum flow of 80 cubic feet per minute (CFM). This is equivalent to mass flow rate of 164kg/h.

Figure 5-11: Axial fan

Heat Transfer Oil and Tank

And industrial heat transfer oil supplied by Castrol was used. It has specific heat of 1.86kJ/kg °C. Full technical data of the oil can be found in Appendix F. The heat transfer oil tank was locally constructed in the laboratory by the technicians. The tank is constructed base on the size of the receiver tube and the heat exchange coil inside the hot water tank so that it can accommodate enough oil to be circulated round the system. It has dimension of 22cm diameter by 15cm height and a total capacity of 7 litres.

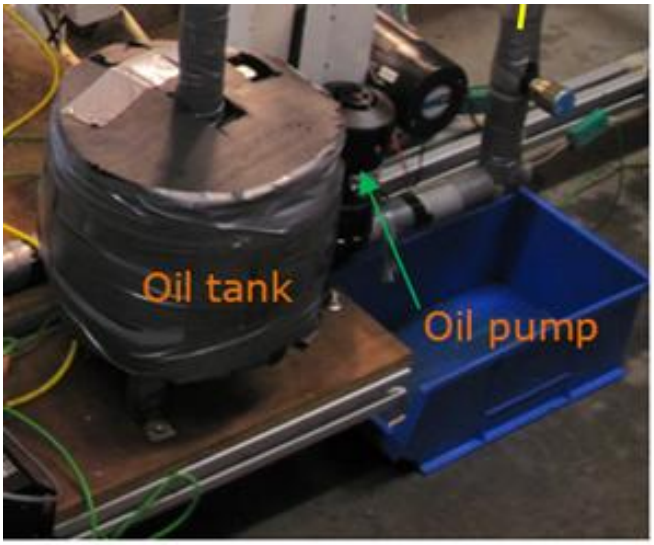

Figure 5-12: Heat transfer oil tank

Cold Water Tank

The cold water tank stores the cooling water that is circulated through the E/C-Core for condensation process to occur. It has a capacity of 20 litres.

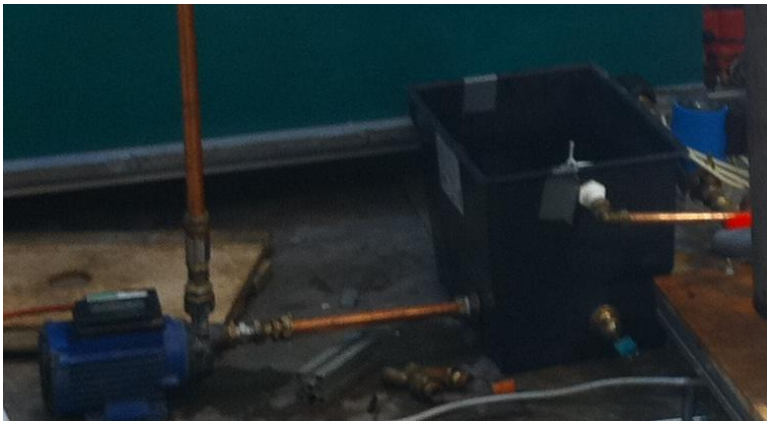

Figure 5-13: Cold water tank

Pumps

It was difficult to find pump that matches the exact requirement of power consumption, flow rate and operating temperature. Four different pumps have been used in the complete system which includes the solar collector. The pump in Figure 5-14(a) is used to circulate heat transfer oil in the solar collector system. It is supplied by Mocal Pumps. It has maximum flow rate of 10L/min and maximum operating temperature of 130°C. The E-core uses two pumps. One pump supplied by Grundfos (Fig. 5-14b) circulates hot sea water into to chamber. Its maximum temperature and flow rate are 110°C and 3m³/min respectively. The second pump which is which is supplied by Flojet as shown in Fig 11c circulates the sea water out of the E-Core to the hot water tank. It has maximum flow rate of 10L/min and operating temperature 60°C. And finally the pump in Fig. 5-14(d) circulates the cooling water round the E/C-Core for condensation process. It is supplied by Clarke and has 10L/min flow rate and 40°C operating temperature. The total power consumption of all the pumps is less than 1000W.

(a) Heat transfer oil pump

(b) Hot water circulating pump (inlet)

(c) Hot water circulating pump (outlet)

(d) Cold water circulating pump

Figure 5-14: System pumps

5.3 System Construction and Operation

In the proposed system, concentrating solar collector and electric heater will be used to heat up the sea water in an insulated tank. The hot sea water is then sprayed to humidify the incoming air in the humidification chamber. The humidified air enters the dehumidification chamber and is cooled by the incoming sea water. In the meantime the cool sea water is pre-heated to recover heat from the condensation process. The moisture is condensed out and the pure water is accumulated at the base of the chamber, and the dehumidified air is discharged to the outside.

The system was constructed according to design as illustrated in the schematic of Figure 5-1. The system was constructed and pre-tested in two steps. First the solar collector was connected to the coil heat exchanger in the hot water tank and also connected to the heat transfer oil tank as shown in Fig. 5-16. The solar simulator was positioned directly above the solar collector. Secondly the outlet of the hot water tank was connected to the inlet of the E-Core of the desalination unit, while the outlet of the E-core was connected to the inlet of the hot water thank. A cold water tank was connected between the outlet and inlet of the E/C-Core. During the system preliminary test, a number of key issues affecting the operation of the system were noticed and rectified.

After positioning the solar simulator 300mm above the solar collector (Fig. 5-18), there was no enough light intensity to simulate up to 1000W/m² even when the dimmer is switched to maximum. So the distance of the solar simulator was reduced by placing it directly on top of the solar collector as illustrated in Fig. 5-15.

The system was initially designed to operate with solar collector only. And hence the solar collector was connected to both the upper and lower coils of the water tank. It was designed to operate with both coils simultaneously in order to have large heat exchange surface area. Despite such configuration, it took very long time (almost 24hrs) to raise the temperature of water in the tank from around 20°C to 50°C. As a result, it was suggested to make the system hybrid to use an electric heater and solar collector for energy source required for heating the water. It was also noticed as the water level goes below the upper coil, there was no contact between the coil and water and hence no heat transfer takes

place but rather heat loss. Therefore the system was changed to operate using the lower coil only.

Since the solar collector uses only one heat exchanger coil, the size of the heat transfer oil tank was reduced. Previously with the larger oil tank (Fig. 5-18), the quantity of the heat transfer oil was large that even without heat exchange it took long time for the solar collector to heat up the heat transfer oil. And hence by reducing the size of the oil tank means improving the performance of the system and reducing heat loss (Fig. 5-16).

After all the improvements on the solar collector system, there was a poor performance when the system was tested with small amount of water in the tank (45L). So the receiver tube was suspected to have no vacuum. And there was no convenient way of checking if there was leakage on the glass tube. The glass tube was sealed and the inner temperature could not be measured also. But it was noticed that the heat transfer oil never exceeds the outer surface temperature of the glass tube. This shows that the outer surface temperature of the tube is the same with the inner temperature. If vacuum was present, more heat will be trapped and hence inner temperature can be higher than outer temperature. This suggests it was necessary to change the receiver tube in order to improve the performance of the solar collector.

One pump was used to circulate water in the E-Core through the water tank. However, the circulation was inconsistent and water flow rate was unstable and largely depended on amount of water in the tank. Hence it was required to use two pumps instead. One pump transport the water from the bottom of the E-Core to the water tank through the top while the other pump transport the hot water from the bottom of the water tank to the top of the E-Core.

Another problem was the electric heater position at the top of the tank. Whenever the water level in the tank drops, the level of the heater immersed in the water reduces. This means energy input is not uniform. Hence the hot water tank was always topped up via the cool water tank. This was done by connecting the hot water cycle was connected to the cold water cycle.

Figure 5-15: Solar collector system set-up

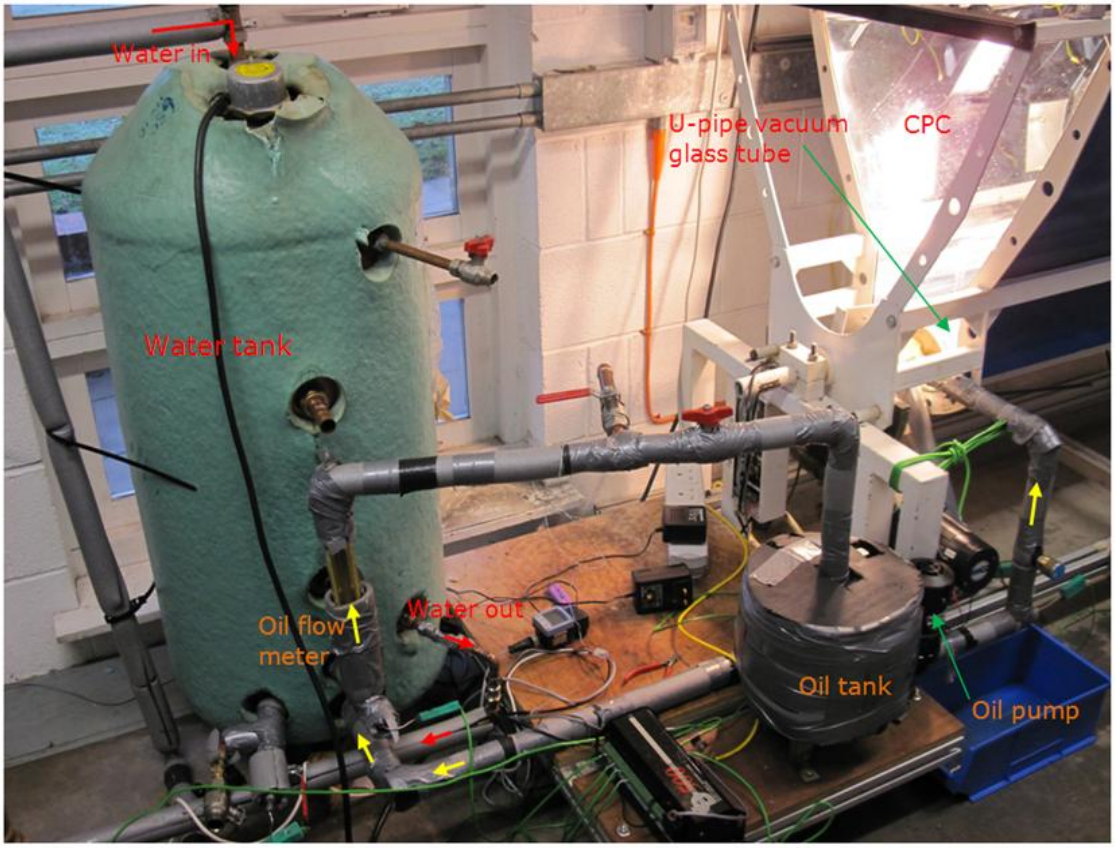

Figure 5-16: Integration of solar collector with oil and water tank

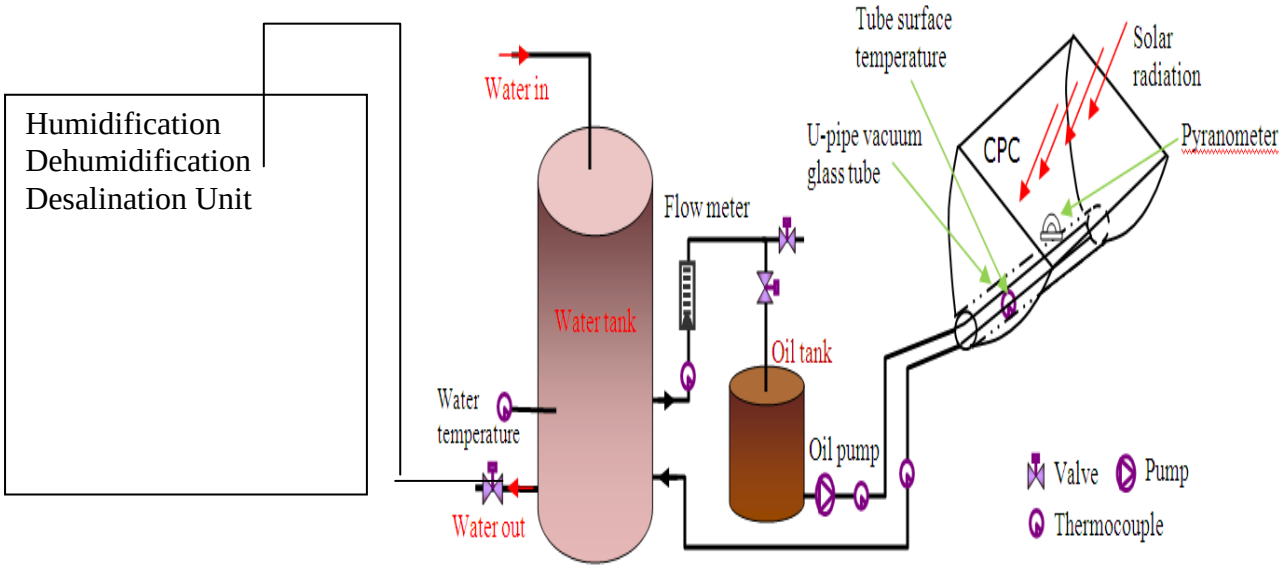

Figure 5-17: Complete system schematic

Figure 5-18: Complete solar desalination system set-up

5.4 Instruments and Measurement

The performance of the system depends greatly on accuracy of instruments used and also methods of measurement. Operating temperatures and flow rates of system parameters are the main key performance indicators.

5.4.1 Measurement of Light Intensity

The light intensity was measured using a Pyranometer CMP 3 supplied by Kipp & Zonen. It has sensitivity of 17.99mV/W.m^{-2}. An even distribution of the light intensity from the simulator is ensured by measuring the light intensity at nine different points along the focus of the solar collector as illustrated below.

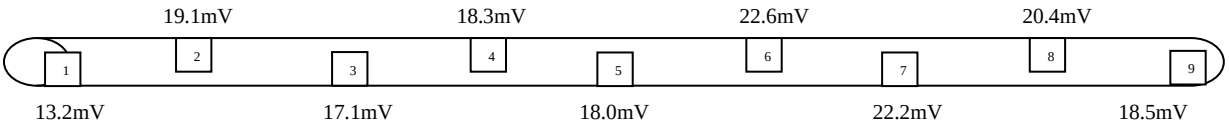

Figure 5-19: Measurement of distribution of light intensity on the high temperature receiver

Average measured output = 18.82mV

Hence equivalent solar irradiance = device sensitivity x measured output

= 17.99 x 18.82 = 1046W/m²

Figure 5-20: CMP 3 Pyranometer

5.4.2 Temperature Measurement

In order to achieve accuracy in temperature measurements, all temperature sensors used in the experiment were of the same type (K-type) and connected to the data logger

(DT500) using the same type of wire. Table 5-1 shows list of all temperature sensors used and their corresponding channel on the DT500.

Table 5-1: Description of calibrated thermocouples and their data logger channels

Data Logger Channel	Sensor Type	Channel/Parameter Description
1*	K-Type	Receiver Surface Temp
1+		Receiver Inlet Temp
1-		Receiver Outlet Temp
2*		Oil Tank Inlet Temp
2+		Hot Water Tank
2-		Cool water tank
3*		Humidification Chamber Inlet
3+		Humidification Chamber Inlet
3-		Exhaust air temperature
3*		Fresh water temperature
3+		Fresh air temperature

It was ensured that all sensors where initially tested and calibrated to provide approximately the same reading by exposing them to the ambient temperature and compare them to a mercury-in-glass thermometer with ±1 division accuracy (Fig. 5-21a). The sensors were later immersed into hot water bath and same readings were obtained. The accuracy of the thermometer was checked with a handheld digital thermometer which has 0.1°C accuracy (Fig. 5-21b).

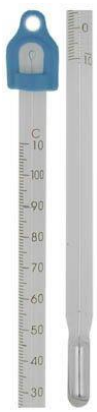

(a) General purpose mercury thermometer

(b) Handheld digital thermometer

Figure 5-21: Types of thermometers used for calibration

5.4.3 Measurement of Liquid Flow Rate

Variable flow indicators with a float inside an outer graduated flow scale on the viewing sleeve were used as shown in Figure 5-22(a) to measure the flow rate of hot water, cooling water and heat transfer oil. All flow meters used utilise the technique of differential pressure across a piston which, as the flow increases, moves the piston against a calibrated spring. The flow meters have accuracy ±2%, repeatability of ±1%, 10 bar operating pressure and 60°C maximum operating temperature. Three sets of the flow meters where used. Two meters have flow range of 0.2-2L/min and the other one has flow range of 1.5-10L/min. Control valves as shown in Figure 5-22(b) were used to manually adjust the flow rates during experiment. All flow meters where calibrated to ensure they have the same and accurate readings using a stop watch and calibrated measuring can (in litres). And later the fluid flow rate was converted from litres to kilograms. The accuracy of the calibrated measuring can is validated using a digital scale. The flow meters are designed for measuring water flow rate. In order to measure oil flow, a conversion factor was determined using the timer and measuring can method. And it was calibrated as 1L/min flow indicated on the flow meter is equivalent to 0.2L/min actual oil flow.

(a) In-line flow indicator (b) Control valve

Figure 5-22: An in-line flow meter and a control valve supplied by RS Components

5.4.4 Measurement of Air Flow Rate

The air flow was measured using a hot wire anemometer as shown in Figure 5-23. The device has a velocity range of 0.2 to 20m/s with 0.1m/s resolution. It has accuracy of ±5%. The log-linear method in accordance with Ashrae standard was used to obtain an accurate air flow rate. The log-linear method provides high accuracy (±3%) in flow totalization. The two diameter method is shown in Figure 5-24. This method consists of taking two sets of maximum ten readings depending on the area of the air passage and 90° apart. Airflow is obtained by multiplying average velocities measured at all points within the area.

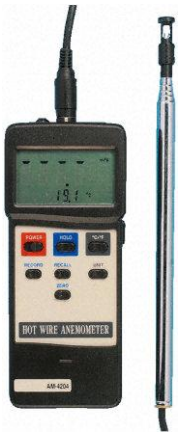

Figure 5-23: Hot wire anemometer

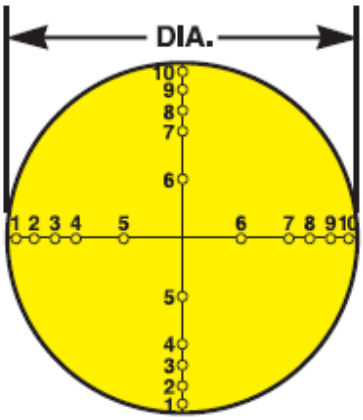

Figure 5-24: Log-linear transverse for round ducts, two-diameter approach.

It is also possible to take a single reading to measure air velocity or air volume flow in a duct, measuring in the centre of the duct and multiplying the reading by 0.9 to correct for the higher velocity at the centre of the duct. If conditions are very good an accuracy of ±5 or ±10 percent may be obtained this way. This method is not reliable, however, and should only be used where small duct size

5.4.5 Measurement of Hot Water Level in Tank

It was possible to measure the amount and level of water inside the hot water tank by attaching a clear transparent tube to the top and bottom of the tank as illustrated in Figure 5-25. The tank was calibrated using a calibrated measuring cup by putting water into the tank one litre at a time. Then as the water level in the tank rises, it shows on the clear tube which is then marked. The range of calibration is 45-140L at 5L interval.

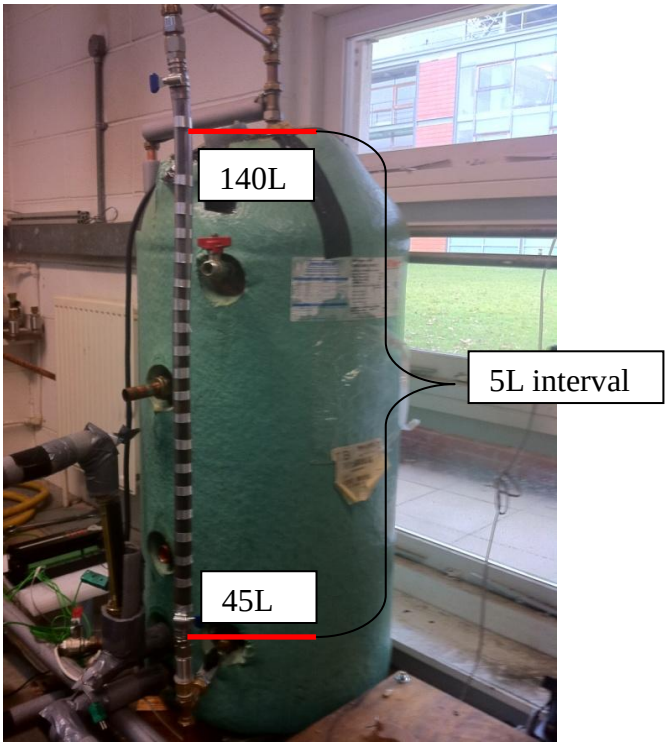

Figure 5-25: Calibrated water tank

5.4.6 Measurement of Salt Concentration, Water Production and Recovery Rate

Concentration of Soy sauce produced by Sanchi was used to add salt and coloration to water in order to simulate seawater and brackish water. Up to 1L of the solution was added to 140L of water in the hot water tank. This equates to around 7g/L or 7000ppm salt content. It recommended to have 100ppm for drinking water and most standards allow maximum of 500ppm. In any case water obviously looks and tastes different at 2000ppm. Hence final concentration of fresh water produced is measured by physical observation of clarity and taste of the water. The amount of fresh water produced is measured using the calibrated measuring can. And the fresh water recovery is measured by dividing water input to the system by water output.

Figure 5-26: Soy sauce

Figure 5-27: Measuring cup

5.5 Test Procedure

The system was assembled and measuring devices were positioned and connected to a data logger as described in the experimental set-up above. The flow circuit was tested for possible leaks by flowing fluid at maximum flow rate through the circuit. Any leakage found was completely eliminated. The system was completely insulated to minimise heat loss. The start up procedure listed below was followed every time the experimental rig was started to collect experimental data. Experimental data was collected at 15min interval and later at 5mins interval.

- Solar intensity is adjusted to desired level intensity.
- The water level in both hot water tank and cooling water tank are measured prior to start of the experiment. It was ensure there was maximum contact between the electric heater and water in hot water tank.
- Electric heater was activated to bring the water in the storage tank to a desired operating temperature.
- The pumps circulating water from the water tank to the humidification chamber of the desalination unit and back to the tank were switched on and the control valve was adjusted to desired flow rate. The flow rate is monitored until when stable and throughout the experimental period in order to maintain constant flow.
- The solar simulator and oil pump was switched on.
- Then the fan was switched on to circulate vapour to the dehumidification chamber.
- The pump circulating cooling water in the dehumidification chamber was switched on and control valve adjusted to desired flow rate.
- The amount of fresh water produced is collected and measure using the measuring cup at regular intervals. At the same time the clarity of the water is monitored. If the water output contains some colouration due to the soy sauce, it indicates an overflow of the salt water into the condensation channel. In his case the pump circulating water into the humidification chamber is stopped while the one taking the water out of the humidification chamber is left running in order to drain the water out of the desalination unit back to the hot water tank.
- The amount of water in both the hot water and cooling water tank is measured at the end of every one during the experiment by topping up the tanks. This is mainly to calculate the percentage rate of fresh water recovery and to ensure maximum effective contact between the water in the tank and the electric heater.

5.6 Conclusion

The experimental system was set up according to design specification. Both the solar collector and desalination unit where fabricated in China. Other system components where ordered from different companies within the UK. Due to space constraint in the lab, it permits only 2m² solar collector to be installed. And several challenges were encountered most especially with the solar collector not providing enough heat as anticipated due to leakage in the vacuum receiver tube. Other experimental problems such as leakages were also encountered. However, different measures were taken to minimise these problems and obtain reading as accurate as possible. Nevertheless, the system operated successfully. The system operation and test procedure were outlined. Measuring devices were installed and calibrated. The system was commissioned and ready to obtain accurate readings.

Chapter 6: Experimental Results and Discussion

6.0 Introduction

Previously, a preliminary outdoor test of the solar collect unit and the desalination unit were carried out separately. The thermal performance of both units was evaluated. Now the objective here is to carry out similar experiments under laboratory conditions. The main aim is as follows:

- To integrate solar collector to the desalination unit and investigates its operation.
- To repeat and revalidate previous experiments carried out.
- Investigate fresh water recovery rate.
- The effect of hot water temperature on air flow rate was investigated.
- And system operation at high temperature.

A water desalination unit powered by solar energy has been tested. However, due to the solar collector not supplying enough energy to run the desalination system, an electric heater was used as supplement to carry out tests for high temperature operation. The chapter is divided in to two sections. One section covers the experimental result section while the second section covers the discussion of the results. The experimental result section describes results obtained from three different operating conditions, namely; solar only, electric only and hybrid operation. The discussion of the results was also carried out where effect of various operating parameters and conditions were described.

6.1 Experimental Results

The experimental tests were carried out for the system and the performance was assessed by measuring temperatures and flow rates. More than ten different tests were carried out. The data presented here is for steady state operation of the system over one hour experimental duration at 15mins interval with instantaneous COP was calculated.

6.1.1 Result for Solar-Only Operation

Result from test of solar collector only

The desalination system was first tested using solar collector only as energy source. The amount of useful energy from the collector and also the thermal efficiency of the collector were experimentally evaluated. The maximum efficiency obtained was 20% and useful energy was around 0.3kW. The heat transfer oil flow rate was 0.2L/min and quantity of water to be heated was 40L. The efficiency was calculated using equation 3 and plotted in Figure 6-1. When the oil flow rate was increased to 0.4L/min the efficiency

dropped to 7% with maximum oil temperature at 54°C. So clearly the optimum oil flow rate is 0.2L/min.

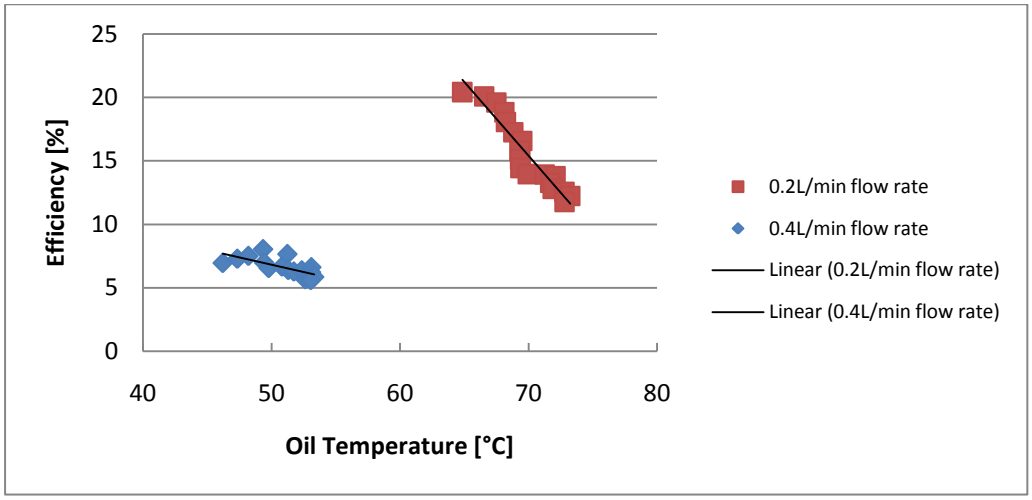

Figure 6-1: Thermal efficiency of solar collector for different oil flow rates

The variation of system operating temperature is shown in Figure 6-2. It can be seen that the oil temperature is directly proportional to water temperature with 10°C increase over the experimental period. Meanwhile, the ambient temperature strongly affect the surface temperature of the receiver tube which in turn affects the oil temperature. Thus the environmental condition is a key determinant for the performance of the solar collector.

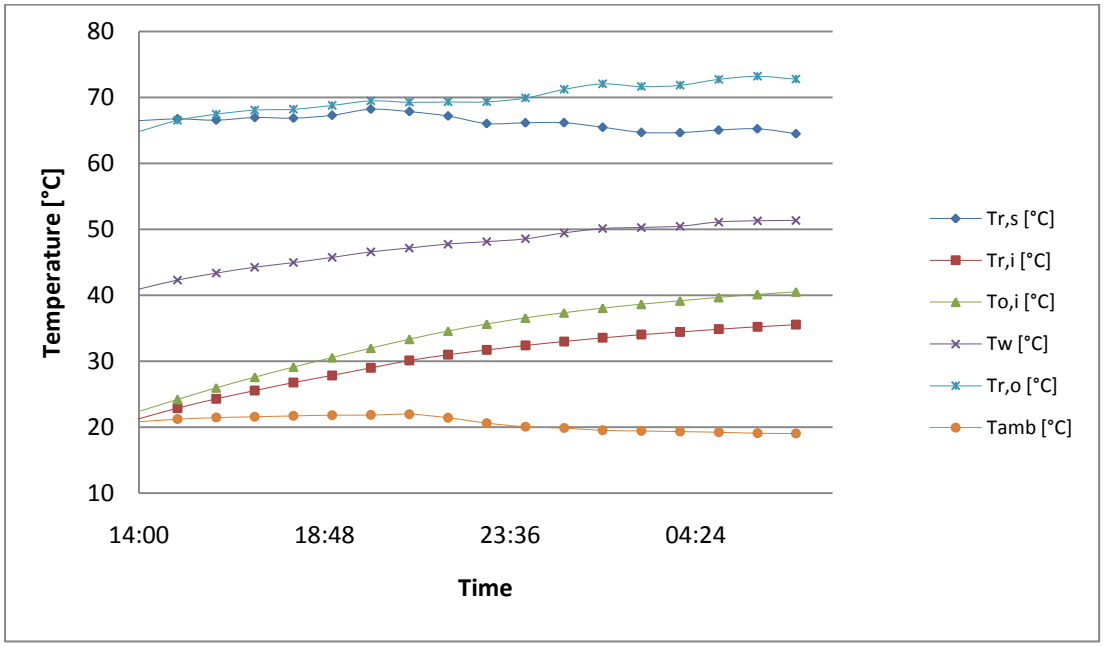

Figure 6-2: Temperature variation of solar collector over period of time

Result from test of combined solar desalination system

The hot water flow rate into the humidification chamber was set to 30kg/h based on the amount of energy provided by the solar collector. The cooling water flow rate was set to 120kg/h. The average hot water temperature was around 62°C with around 9°C temperature difference between the inlet and outlet of the humidification chamber. There was only 2°C rise in temperature of the cooling water which indicated the cooling water had reached saturation basically due to high flow rate of the cooling water (four times higher that rate of evaporation in the humidification chamber). The results were calculated as shown in Table 6-1. The average heat energy consumed by the system was 0.3kW. The amount of fresh water production was up to 4kg/h and the COP of the system was approximately 2 over the one hour steady state operation of the system. The result is illustrated in Figure 6-3.

Table 6-1: Summary of result for solar only operation with cooling water saturated

Hot/cold water flow rate = 30/120 [kg/h]							Results				
Time	$T_{h,i}$ [°C]	$T_{h,o}$ [°C]	T_{cyc} [°C]	W_p [kg]	Q_{source} [kW]	Q_{aux} [kW]	$W_{p(Cumm.)}$ [kg]	Q_{hum} [kW]	Q_{input} [kWh]	Q_{output} [kWh]	COP
12:15	65.1	53.5	38	0.97	1.4	1	0.97	0.40	1264	2338	1.85
12:30	62.5	54.4	39	0.93	1.4	1	1.91	0.28	2309	4574	1.98
12:45	61.7	54.1	39	1.36	1.4	1	3.27	0.27	3416	7843	2.30
13:00	60	53	40	1.10	1.4	1	4.37	0.24	4480	10488	2.34

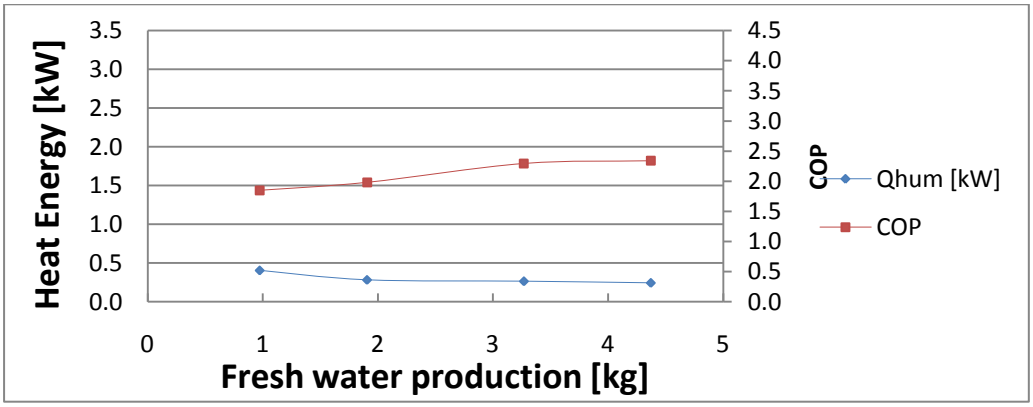

Figure 6-3: Variation of energy and COP with water produced for solar-only operation

It should be noted that the hot water was pre-heated using electric heater to bring it to a steady state operation. This is because of the limitation by the size of the solar collector used as a result it takes long period of time to heat the water. Increasing the number size

of solar collector used will water production, heat and overall efficiency. An outdoor experiment of a larger solar collector with an area of 5.6m² was carried out. It was found the collector had average optimum 38% efficiency for 700W/m² solar irradiation. The feed water input to evaporated water ratio, absorption ratio is 0.04. This was obtained base on the optimum operating conditions for maximum water produced. Hence the variation of water production with area of solar collector required was calculated using experimental results obtained for both the outdoor test of solar collector and the desalination unit.

Measuring specific air flow was difficult, thus the calculation is based on the possible range of air flow that can be supplied from the fan in the desalination unit with range of 5-160kg/h. As shown in Figure 6-4 the calculation was carried out for three different solar intensities of 500W/m², 700W/m² and 1000W/m². As expected larger collector area is required for lower solar irradiation. And there is increase in water production with area of the solar collector.

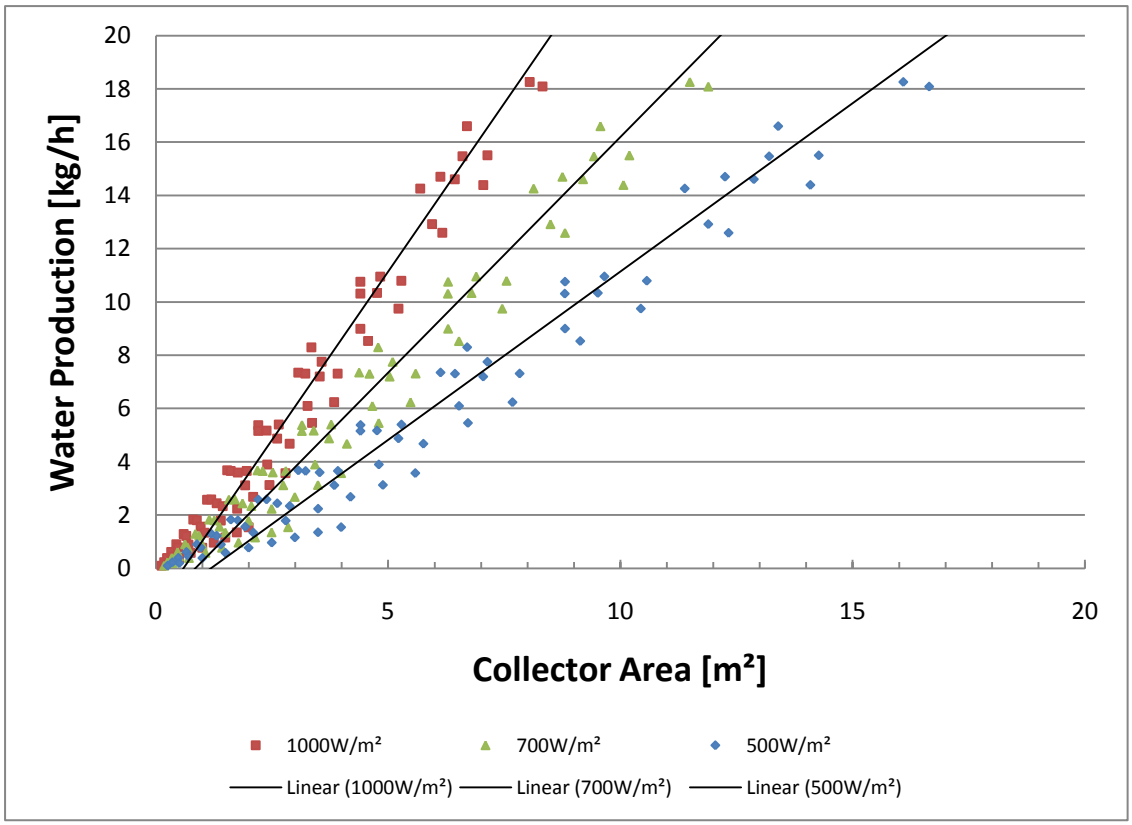

Figure 6-4: Variation of amount of fresh water production with solar collector area.

6.1.2 Result for Electric Heater-Only Operation

One way of achieving effective humidification is if there is abundant flow of water through the wetted media in the humidification chamber. More energy is required to provide an abundant high hot water flow rate in the humidification chamber. As a result the size of the solar collector used could not provide the required energy for effective humidification. Hence and electric heater was used to provide the required energy in order to supply abundant hot water flow in the humidification chamber. Thus the water flow rate was set to maximum at 432kg/h. However, the flow rate of cooling water in the dehumidification chamber strongly affects the water separation process i.e. condensation process. If the cooling water flow rate is high, heat exchange occur quickly and the cold water temperature increases sharply. Once the cold water temperature is high, the rate of condensation decreases. And if the cooling water flow rate is low, it implies low condensation process. Hence the system was tested in four different states of flow rates.

State 1: High Flow Rate

Abundant hot water supply was ensured in the humidification chamber by setting the flow rate to 432kg/h. And the cold water flow rate was set to 240kg/h through the dehumidification chamber. The temperature of the hot water ranges between 66-68°C with an average 5.1°C difference between the inlet and outlet of the humidification chamber. And there was 9°C increase in temperature of the cooling water in one hour. The results were calculated using equations 4 and 8 as shown in Table 6-2. The average heat energy consumed by the system was 2.6kW and up to 17kg/h of fresh water was produced and the COP of the system was approximately 3 over the one hour steady state operation of the system. The result is illustrated in Figure 6-5.

Table 6-2: Summary of result for electric-only operation with cooling water unsaturated for high flow rate

Hot/cold water flow rate = 432/240 [kg/h]							Results				
Time	$T_{h,i}$ [°C]	$T_{h,o}$ [°C]	T_{cyc} [°C]	W_p [kg]	Q_{source} [kW]	Q_{aux} [kW]	$W_{p(Cumm.)}$ [kg]	Q_{hum} [kW]	Q_{input} [kWh]	Q_{output} [kWh]	COP
15:45	66.7	61.3	40	3.4	3	1	3.4	2.72	3344	8160	2.44
16:00	66.9	61.4	43	4.7	3	1	8.1	2.77	6778	19440	2.87
16:15	67.6	62.6	47	4	3	1	12.1	2.51	9488	29040	3.06
16:30	68.1	63.6	49	4.9	3	1	17	2.26	11745	40800	3.47

The system COP over one hour was 4.4 and energy consumption was 2.6kW. However when the flow rate of cooling water is high, the temperature increased rapidly to saturation. Meanwhile there was a slight drop in energy input (Figure 6-7) due to the high flow rate at the inlet of the humidification chamber, and as a result there was increase in COP. The increase in temperature indicates good latent heat transfer. However this latent heat was not fully recovered through the evaporation channel of the E/C-Core.

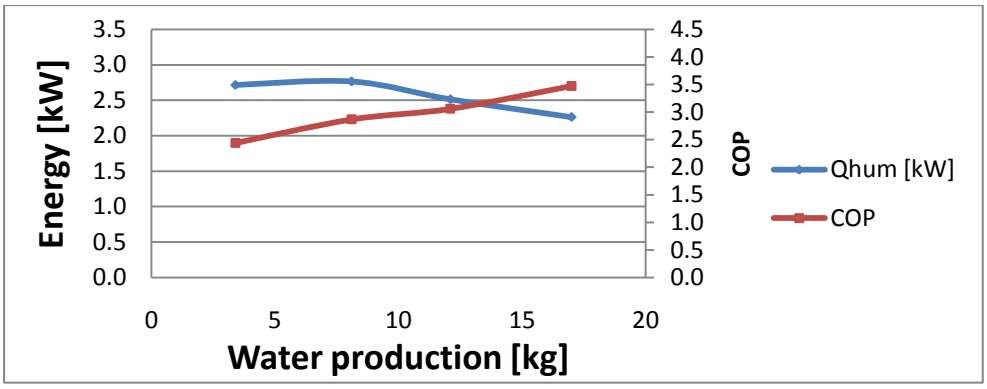

Figure 6-5: Variation of energy and COP with water produced for electric-only operation and high flow rate unsaturated cooling water

In table 6-3 the temperature of the hot water in the humidification chamber increased to an average of 73°C while the temperature difference between the inlet and out of the humidification chamber remain the same at 5.4°C. And energy consumption was around 2.7kW. As the cooling water temperature gets saturated, there was only 2°C increase in temperature in one hour operation of the system. As a result fresh water production was reduced to 14kg/h and hence the COP of the system reduced to 2.5. Results of energy consumption, fresh water production and COP are plotted in Figure 6-6.

Table 6-3: Summary of result for electric-only operation with cooling water saturated for high flow rate

Hot/cold water flow rate = 432/240 [kg/h]							Results				
Time	$T_{h,i}$ [°C]	$T_{h,o}$ [°C]	T_{cyc} [°C]	W_p [kg]	Q_{source} [kW]	Q_{aux} [kW]	$W_{p(Cumm.)}$ [kg]	Q_{hum} [kW]	Q_{input} [kWh]	Q_{output} [kWh]	COP
11:15	72.6	67.4	52.3	3.48	3	1	3.48	2.61	3253	8352	2.57
11:30	72.8	67.4	53.8	3.5	3	1	6.98	2.72	6687	16752	2.51
11:45	72.8	67.4	54	3.7	3	1	10.68	2.72	10031	25632	2.56
12:00	72.9	67.5	54.3	3.4	3	1	14.08	2.72	13374	33792	2.53

When the temperature gets saturated and the temperature reaches its optimum, it indicates latent heat of condensation effectively utilised by the evaporation channel of the E/C-Core. Energy recovery indicate constant energy input and COP (Figure 6-6).

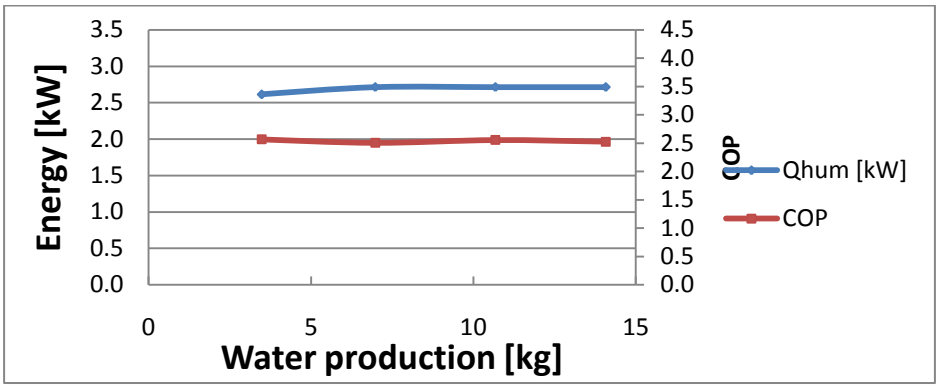

Figure 6-6: Variation of energy and COP with water produced for electric-only operation and high flow rate saturated cooling water

State 2: Medium Flow Rate

When the flow rate of the cooling water was reduced to 120kg/h while that of the hot water maintained at 432kg/h, the fresh water production rate was approximately 13kg/h. The hot water temperature was around 70°C with around 4.7°C temperature difference between the inlet and the outlet of the humidification chamber. Hence the energy consumption was 2.4kW. The COP of the system was approximately 2.4 as shown in Table 6-4. There was equally 9°C increase in temperature of the cooling water. This indicates that despite reducing the flow rate of the cooling water by half, there was the same rate of temperature increase of the cooling water when compared with higher flow rate. The results are calculated in Table 6-4 and plotted on a graph in Figure 6-7.

Table 6- 4: Summary of result for electric-only operation with cooling water unsaturated for medium flow rate

Hot/cold water flow rate = 432/120 [kg/h]							Results				
Time	$T_{h,i}$ [°C]	$T_{h,o}$ [°C]	T_{cyc} [°C]	W_p [kg]	Q_{source} [kW]	Q_{aux} [kW]	$W_{p(Cumm.)}$ [kg]	Q_{hum} [kW]	Q_{input} [kWh]	Q_{output} [kWh]	COP
11:15	69.3	65.0	44	2.7	3	1	2.7	2.16	2846	6480	2.28
11:30	69.9	65.5	48	3.3	3	1	6.0	2.21	5782	14400	2.49
11:45	69.8	64.6	51	3.5	3	1	9.5	2.61	9759	22800	2.34
12:00	69.7	64.5	53	3.4	3	1	12.9	2.61	13012	30960	2.38

Figure 6-7 shows steady operation until when the cooling water temperature reached above the optimum operating temperature. That indicated energy not recovered and thus resulted in energy loss.

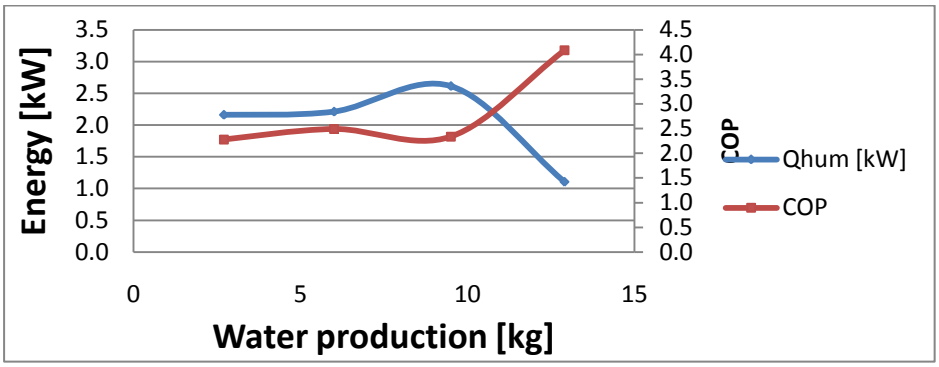

Figure 6-7: Variation of energy and COP with water produced for electric-only operation and medium flow rate unsaturated cooling water

State 3: Low Flow Rate

The flow rate of the cooling water was further reduced to 60kg/h which is three times lower than the higher flow rate. Meanwhile the flow rate of the hot water was still maintained at 432kg/h. The temperature of the hot water reached 60°C with 3°C temperature difference between the inlet and the outlet of the humidification chamber. Hence energy consumption by the system was around 1.7kW. The fresh water production was 8kg/h and system COP of 2 as shown in Figure 6-8. It can be seen from Table 6-5 the low flow rate of the cooling water shows slow increase in temperature at 7°C over one hour period. As it is obvious lower energy input means lower fresh water production, the low flow rate of the cooling water means low rate of heat transfer and consequently lower fresh water production.

Table 6-5: Summary of result for electric-only operation with cooling water unsaturated for low flow rate

Hot/cold water flow rate = 432/60 [kg/h]							Results				
Time	$T_{h,i}$ [°C]	$T_{h,o}$ [°C]	T_{cyc} [°C]	W_p [kg]	Q_{source} [kW]	Q_{aux} [kW]	$W_{p(Cumm.)}$ [kg]	Q_{hum} [kW]	Q_{input} [kWh]	Q_{output} [kWh]	COP
10:45	58.9	55.2	39	2	3	1	2	1.86	2574	4800	1.87
11:00	60.3	57.1	41	2	3	1	4	1.61	4696	9600	2.04
11:15	60.25	57.1	44	2	3	1	6	1.58	6976	14400	2.06
11:30	60.2	57.1	46	2	3	1	8	1.56	9211	19200	2.08

Figure 6-8 indicate a good heat recovery at low flow rates for the unsaturated cooling water. However, low flow rate results in lower fresh water production. So therefore, there is a trade-off between fresh water production, energy consumption/recovery rate and cooling water requirement.

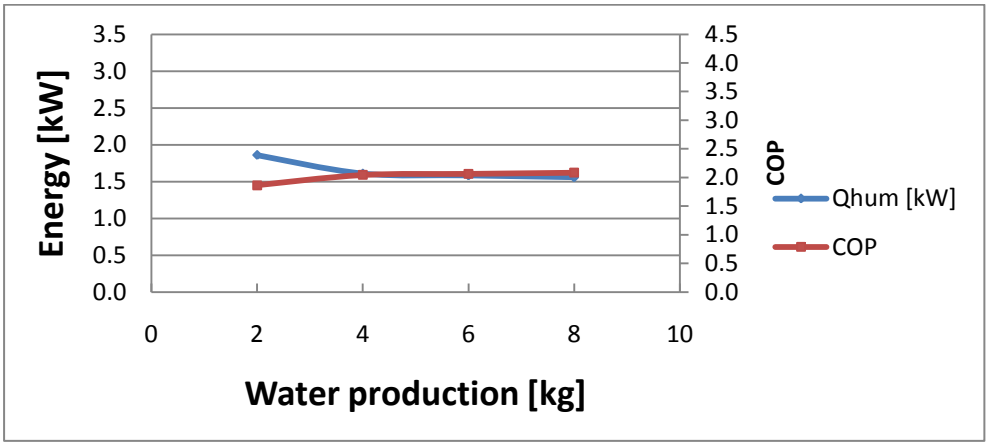

Figure 6-8: Variation of energy and COP with water produced for electric-only operation and low flow rate unsaturated cooling water

When the temperature of the hot water reached 70°C with 6°C temperature difference between the inlet and the outlet of the humidification chamber as illustrated in Table 6-6, the energy consumption by the system was around 3kW. And the fresh water production was increased to 11kg/h while flow rates of hot and cold water where maintained at 432kg/h and 72kg/h respectively. The COP of the system remained the same as there was increase in fresh water production with energy consumption of the system. The result is plotted in Figure 6-9.

Table 6-6: Summary of result for electric-only operation with cooling water saturated for low flow rate

Hot/cold water flow rate = 432/72 [kg/h]							Results				
Time	$T_{h,i}$ [°C]	$T_{h,o}$ [°C]	T_{cyc} [°C]	W_p [kg]	Q_{source} [kW]	Q_{aux} [kW]	$W_{p(Cumm.)}$ [kg]	Q_{hum} [kW]	Q_{input} [kWh]	Q_{output} [kWh]	COP
13:20	70.6	64.7	48	2.9	3	1	2.9	2.97	3570	6960	1.95
13:35	70.4	64.5	50.2	3.0	3	1	5.9	2.97	7140	14160	1.98
13:50	70.1	64.3	50.1	2.8	3	1	8.7	2.92	10574	20880	1.97
14:05	70.1	64.3	51.2	2.2	3	1	10.9	2.92	14098	26160	1.86

Figure 6-9 indicates further good energy recovery with overall energy input at 3kW while the COP was constant at 2.0. The COP was rather low due to lower fresh water production compared to energy input of system..

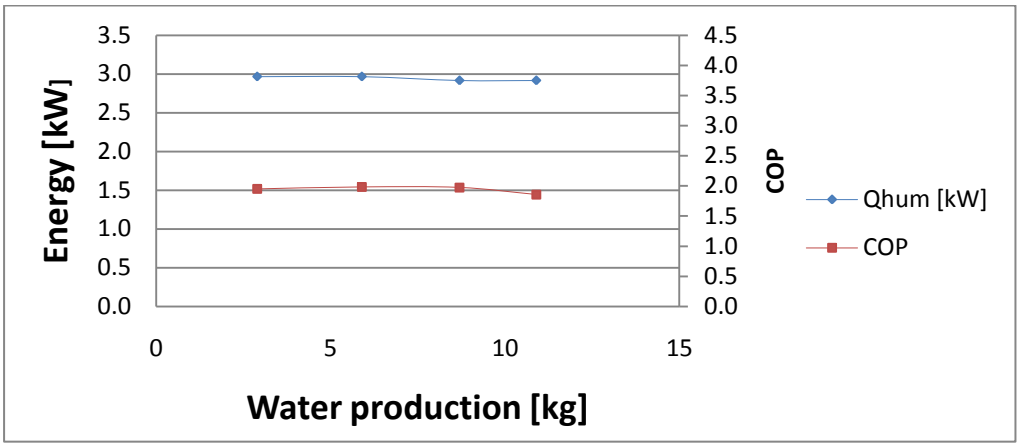

Figure 6-9: Variation of energy and COP with water produced for electric-only operation and low flow rate saturated cooling water

State 4: Equal Flow Rate

The hot water flow rate was reduce to four times lower than previous flow rate used, and that of the cooling water was set equal to the hot water flow rate. There was increase in temperature of hot water to an average of 79°C. And the cooling water temperature increased to 9°C over one hour period of operation. The temperature difference between the inlet and the outlet of the humidification chamber was 18°C, and hence energy consumption was 2.3kW. This resulted in fresh water production rate of 11kg/h and COP of 2 and shown in the table below.

Table 6-7: Summary of result for electric-only operation with cooling water unsaturated for equal flow rate

Hot/cold water flow rate = 108/108 [kg/h]							Results				
Time	$T_{h,i}$ [°C]	$T_{h,o}$ [°C]	T_{cyc} [°C]	W_p [kg]	Q_{source} [kW]	Q_{aux} [kW]	$W_{p(Cumm.)}$ [kg]	Q_{hum} [kW]	Q_{input} [kWh]	Q_{output} [kWh]	COP
09:30	81.4	58.9	39	2.01	3	1	2.0	2.83	3445	4824	1.40
09:45	78.4	61.2	42	2.625	3	1	4.6	2.16	5692	11124	1.95
10:00	77	59.3	48	3.4	3	1	8.0	2.22	8707	19284	2.21
10:15	77.6	62.6	48	3.4	3	1	11.4	1.89	10388	27444	2.64

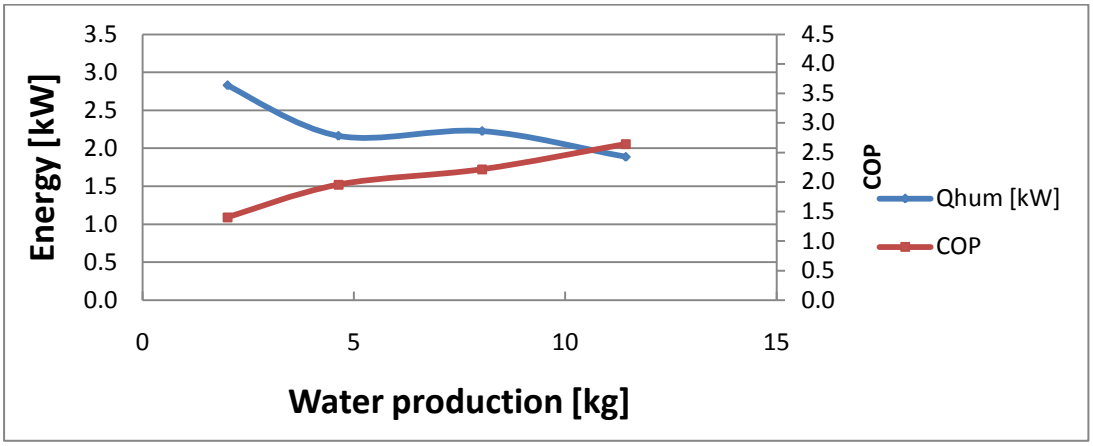

Figure 6-10: Variation of energy and COP with water produced for electric-only operation and equal flow rate unsaturated cooling water

There was a decrease in amount of fresh water production when the energy input was reduced to 1.2kW. The fresh water production was around 6kg/h and the COP of the system reduced to around 1.2. The result is shown in Table 9 and plotted in Figure 6-11.

Table 6-8: Summary of result for electric-only operation with cooling water saturated for equal flow rate

Hot/cold water flow rate = 120/120 [kg/h]							Results				
Time	$T_{h,i}$ [°C]	$T_{h,o}$ [°C]	T_{cyc} [°C]	W_p [kg]	Q_{source} [kW]	Q_{aux} [kW]	$W_{p(Cumm.)}$ [kg]	Q_{hum} [kW]	Q_{input} [kWh]	Q_{output} [kWh]	COP
12:15	66.1	54.5	38	0.3	3	1	0.3	1.6	2344	720	0.31
12:30	63.5	55.4	39	1.6	3	1	1.9	1.12	3816	4440	1.16
12:45	60.7	53.1	41	2.2	3	1	4.0	1.05	5537	9672	1.8
13:00	57	50	41	1.6	3	1	5.7	0.96	7084	13560	1.9

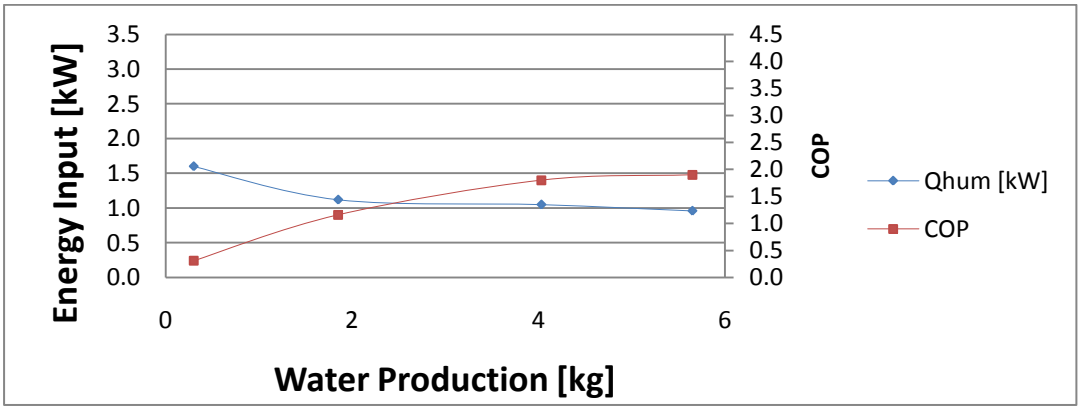

Figure 6-11: Variation of energy and COP with water produced for electric-only operation and equal flow rate saturated cooling water

6.1.3 Result for Hybrid Solar/Electric Operation

Both solar collector and electric heater were used as energy source. The hot water flow rate was 108kg/h while the cooling water flow rate was 240kg/h which was higher than that of the hot water. The temperature of the hot water was approximately 84°C over one hour of system operation. The temperature difference between the inlet and outlet of the humidification chamber was 26°C and total energy consumed was 3.3kW. The maximum energy that can be obtained from electric heater is 3kW and hence using equation 8 the energy from solar collector was calculated as approximately 0.3kW.

Table 6-9: Summary of result for hybrid system operation with cooling water saturated

Hot/cold water flow rate = 108/240 [kg/h]							Results				
Time	$T_{h,i}$ [°C]	$T_{h,o}$ [°C]	T_{cyc} [°C]	W_p [kg]	Q_{source} [kW]	Q_{aux} [kW]	$W_{p(Cumm.)}$ [kg]	Q_{hum} [kW]	Q_{input} [kWh]	Q_{output} [kWh]	COP
11:15	81.5	55.3	43.2	2.21	3	1	2.21	3.29	3864	5304	1.37
11:30	83	57.4	44.9	2.3	3	1	4.51	3.22	7592	10824	1.43
11:45	84.4	58.6	46.6	2.51	3	1	7.02	3.24	11456	16848	1.47
12:00	85.6	59.3	45.8	3.2	3	1	10.22	3.31	15501	24528	1.58

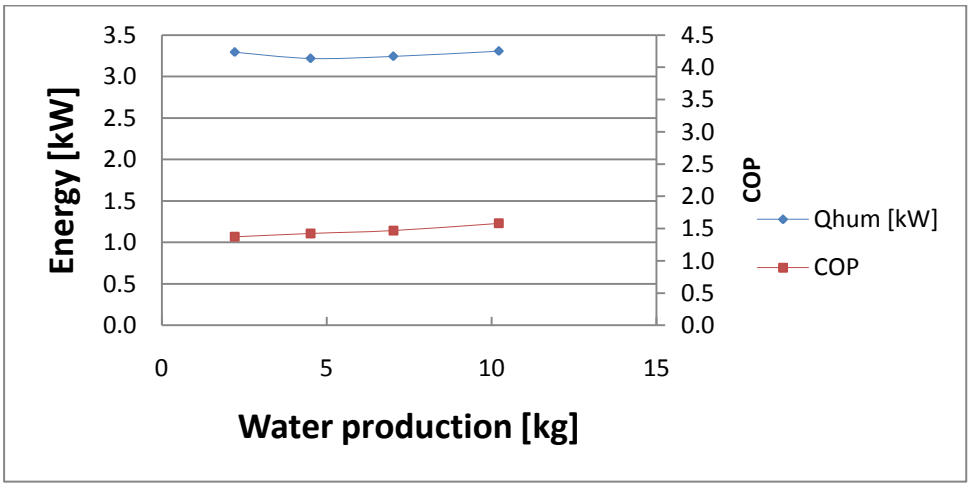

Figure 6-12: Variation of energy and COP with water produced for hybrid system operation and saturated cooling water

As heat from the solar collector is derived from a renewable energy which is free of charge, increasing the proportion of heat from this source would reduce the heat required from the electric heater, and consequently reduce the energy consumption from non-environmentally friendly energy source and thus overall running cost of the system. This would contribute to a reduction in CO, emission to the environment.

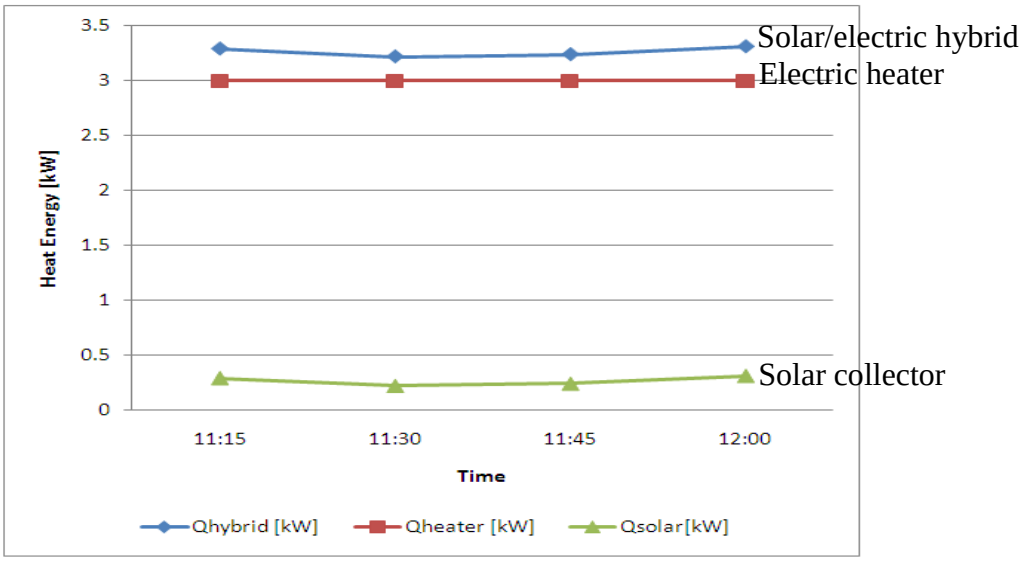

Figure 6-13: Variation of energy input from solar collector and electric heater with time

6.1.4 Summary of Results

The main criteria for optimum system performance are to have low energy input, high fresh water production and as a result high COP. The final COP was calculated over one hour operation. The summary of all the results of the experiment is presented in Table 6-10. The test results are arranged in order of water production. It can be seen that the highest fresh water production was 17kg/h for 2.6kW energy input and COP was 4.4. The lowest water production was 4kg/h for 0.3kW energy input and the COP was 8.9. This generally confirms the analysis in Chapter 3 which shows trade-off between water production and COP.

Table 6-10: Summary of experimental test results

Test	Q_{hum} [kW]	$T_{h,i}$ [°C]	ΔT_h [°C]	$m_{w,h}$ [kg/h]	T_{cyc} [°C]	ΔT_{cyc} [°C]	$m_{w,c}$ [kg/h]	W_p [kg/h]	COP
01	2.6	67	5	432	40	9	240	17	4.4
02	2.7	73	5	432	52	2	240	14	3.5
03	2.4	70	5	432	44	9	120	13	3.6
04	2.9	70	6	432	48	3	72	11	2.5
06	2.3	79	18	108	39	9	108	11	3.2
08	3.3	84	26	108	43	3	240	10	2.0
05	1.7	60	3	432	39	7	60	8	3.1
07	1.2	62	9	120	38	3	120	6	3.3
09	0.3	62	9	30	38	8	120	4	8.9

The energy input is directly proportional to amount of fresh water that can be produced. However, the temperature and flow rate of cooling water significantly affects the rate of condensation (fresh water production). Tests 02, 04 and 08 from Table 6-10 have higher energy input when compared with the energy input for maximum water produced in Test 01. This is as a result of recovery of latent heat of condensation. This is well indicated in Test 01 and 02 compared with the same flow rates. If energy the inputs are compared, it can be seen that up to 0.1kW was recovered. Yet the amount of water produced for Test 02 is lower than that of Test 01. This is because the cooling water temperature has reached above the optimum 40-50°C range identified from preliminary tests in Chapter 3.

The higher the energy input, the higher the feed temperature and consequently the higher the temperature of the cooling water. The flow rate of the cooling water determines the rate at which its temperature gets saturated. With a low cooling water flow rate, the rate of saturation is low but the effect is that the rate of water production is also low.

6.2 Discussion of the Results

6.2.1 Effect of Water Flow Rate

The effect of two different cooling water flow rates on amount of fresh water produced using the same amount of hot water flow rate at the humidification chamber is shown in Figure 6-14. The temperature of the cooling water was equally nearly the same. It was seen that the amount of fresh water production was higher at higher cooling water flow rates.

Figure 6-15 shows effect of different hot water flow rate on the amount of fresh water produced at the same cooling water temperature and flow rate. It was seen that the amount of fresh water production was higher for higher flow rate of water into the humidification chamber.

Therefore the best configuration for optimum water production it is best to keep the hot water temperature and flow rate as high as possible while the flow rate of the cooling water can also be high. However it is very important to keep the temperature unsaturated.

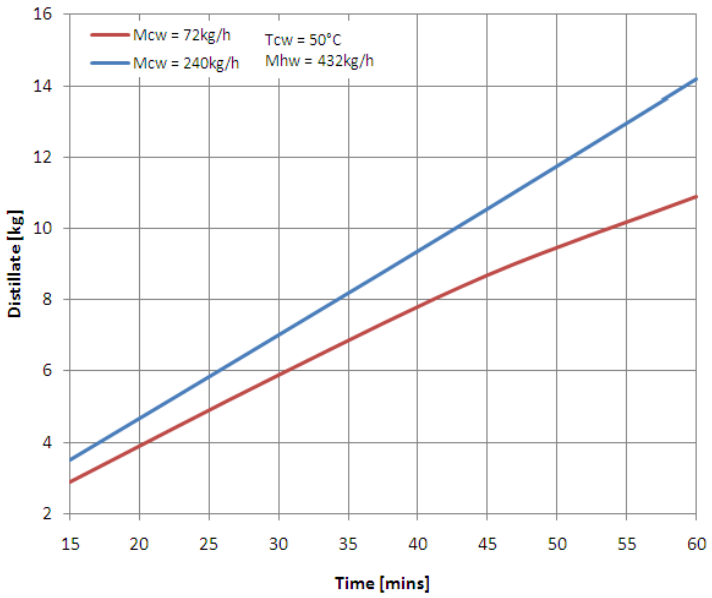

Figure 6-14: Effect of cooling water flow rate on the amount of freshwater produced

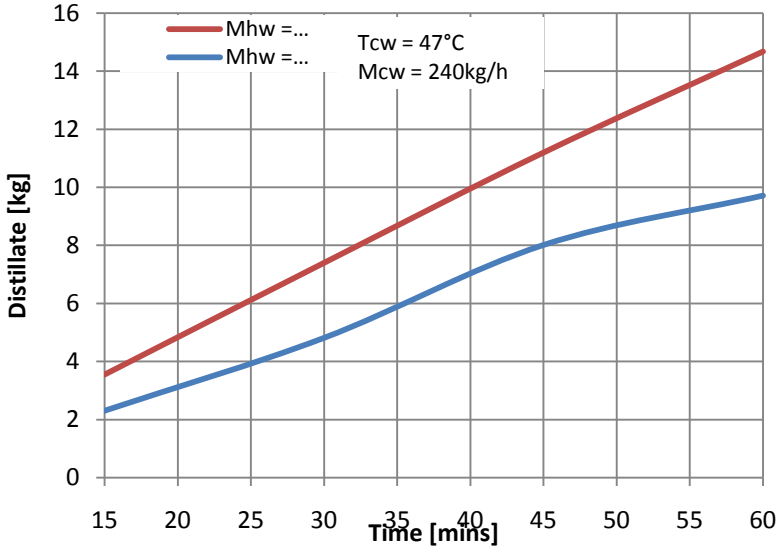

Figure 6-15: Effect of hot water mass flow rate on the amount of fresh water produced

6.2.2 Effect of Operating Temperatures

Figure 6-16 shows variation of system temperatures, namely; the inlet/outlet temperature of hot water at the humidification chamber, the temperature of cooling water, air inlet/outlet temperature. The exhaust air at the outlet of the humidification chamber was seen largely dependent on temperature of hot water in the humidification chamber. The cooling water reached a steady optimum temperature. Ideally the cooling water temperature should be rapidly increasing due to gain of latent heat of condensation, but it

remained steady. This indicates that the heat of condensation is effectively utilised through the evaporation channel of the E/C-Core.

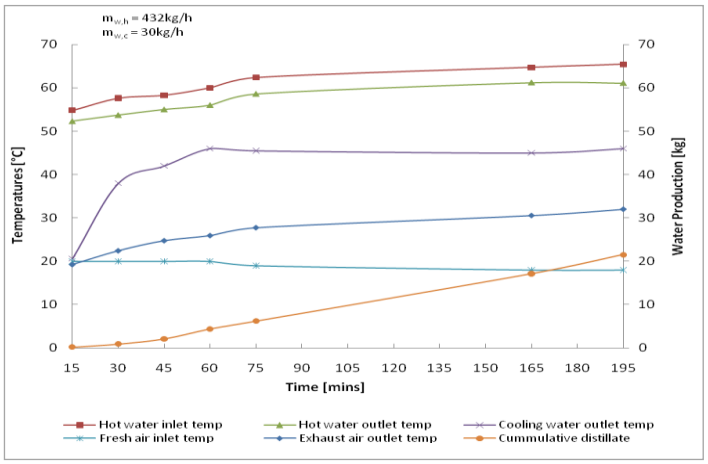

Figure 6-16: Variation of system operating temperatures and amount of fresh water produced with time

6.2.3 Effect of Temperature on Air Flow Rate

Figure 6-17 shows air velocity increasing with increase in hot water temperature at the humidification chamber and exhaust vapour at the dehumidification chamber. The fresh air goes through two processes of evaporation and condensation in the desalination unit. Normally less mass of air is transported from the fan (constant volume) as the air temperature increase the air becomes less dense (evaporation). But when the exhaust outlet temperature decrease, the air becomes denser and hence more mass is transported

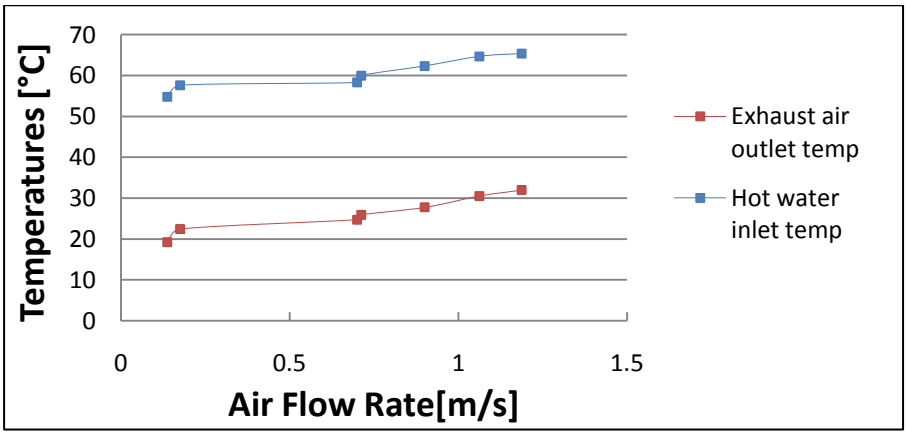

Figure 6-17: Variation of air velocity with air temperature at outlet of the dehumidification chamber and temperature of water at inlet of humidification chamber

6.2.4 Water Recovery Rate

The desalinated water recovery rate is the fresh water production relative to the feed water (seawater) input. There was up to 90% fresh water recovery rate. This is calculated as follows:

$$WRR = \frac{inital\ feedwater - final\ feedwater}{freshwater\ production} \tag{33}$$

$$WRR = \frac{140-121}{17.1} = 0.9$$

6.2.5 System Performance at High Temperature

The system was tested at high temperatures. And data was obtained at 10mins interval. The system was pre-heated at high temperature above 100°C. The energy input was 3kW and water was preheated in the hot water tank. The cooling water temperature reached 60°C. The maximum of 21kg/h of fresh water achieved. After sometime the electric heater was broken and so can notice a sudden temperature drop as shown in Figure 6-18.

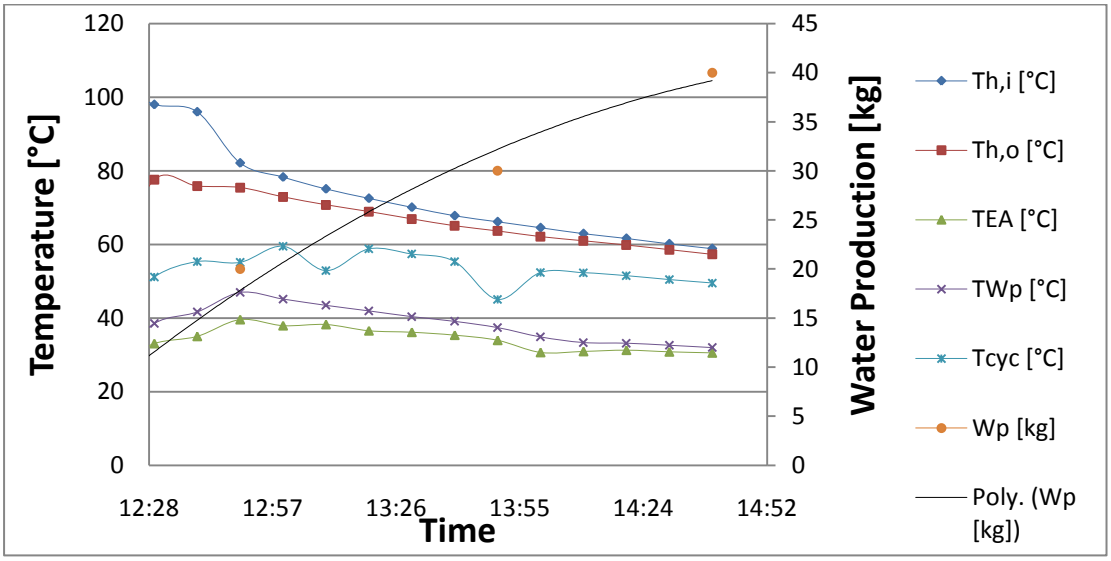

Figure 6-18: Operation of the desalination system showing operating temperatures and amount of water produced with time

The water desalination system was tested at high temperature at 100°C using an electric heater. In order to maintain water flow into the humidification chamber at high

temperature, a flexible wrap around drum heater was used as shown in Figure 6-19. However, the heater used was not sufficient to maintain the temperature as shown in Figure 6-20.

Figure 6-19: Hot water tank with wrap around heater at the bottom

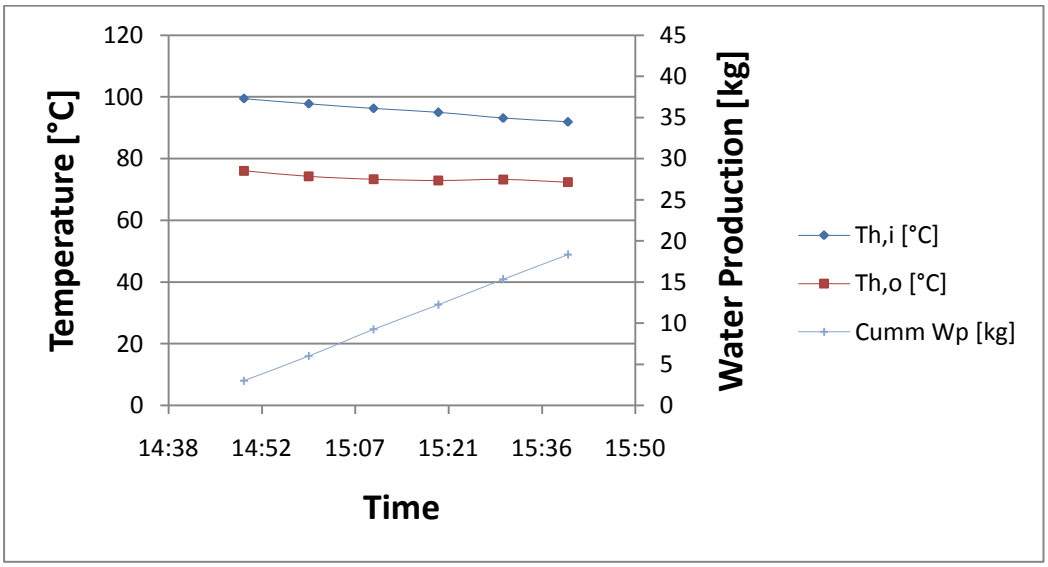

Figure 6-20: Operation of the desalination system with drum heater showing operating temperatures and amount of water produced with time for 120kg/h hot water flow and 30kg/h cold water flow

Conventionally, system operation at such high temperatures results in higher energy losses. However, with the newly designed desalination unit most of the energy is recovered.

The flow rate of the cooling water was set to 30kg/h while that of the hot water was at 120kg/h. The fresh water production rate was approximately 18kg/h. The hot water temperature was around 95°C with around 22°C temperature difference between the inlet and the outlet of the humidification chamber. Hence the energy consumption was 3.1kW. The final COP of the system over one hour was approximately 4.1 as shown in Table 6-11. There was 27°C increase in temperature of the cooling water. The COP and energy input with amount of water production is shown in Figure 6-21.

Table 6-11: Summary of result for high temperature test

Hot/cold water flow rate = 120/30 [kg/h]							Results				
Time	Th,i [°C]	Th,o [°C]	Tcyc [°C]	Wp [kg]	Qsource [kW]	Qaux [kW]	Wp (Cumm.) [kg]	Qhum [kW]	Qinput [kWh]	Qoutput [kWh]	COP
14:40	100.3	83.0	18.5	0	3.0	0.6	0	2.4			
14:50	99.4	76.1	19.7	3.0	3.0	0.6	3.0	3.3	2317.3	7200	3.1
15:00	97.8	74.2	24.7	3.0	3.0	0.6	6.0	3.3	5824.8	14400	2.5
15:10	96.2	73.3	35.5	3.3	3.0	0.6	9.3	3.2	9129.9	22200	2.4
15:20	95.0	72.9	39.9	3.0	3.0	0.6	12.3	3.1	12157.0	29400	2.4
15:30	93.1	73.3	43.1	3.1	3.0	0.6	15.4	2.8	14178.7	36840	2.6
15:40	91.9	72.3	45.6	3.0	3.0	0.6	18.4	2.7	17002.3	44040	2.6
Final Average	96.2	75.0	32.4	2.6	3.0	0.6	18.4	3.0	10697.1	44160	4.1

The constant COP indicated in Figure 6-21 shows good system performance despite higher energy input. This is mainly as a result of increased water production with increased energy input. Most of the additional energy is recovered as the cooling water temperature remains within the optimum operating temperature.

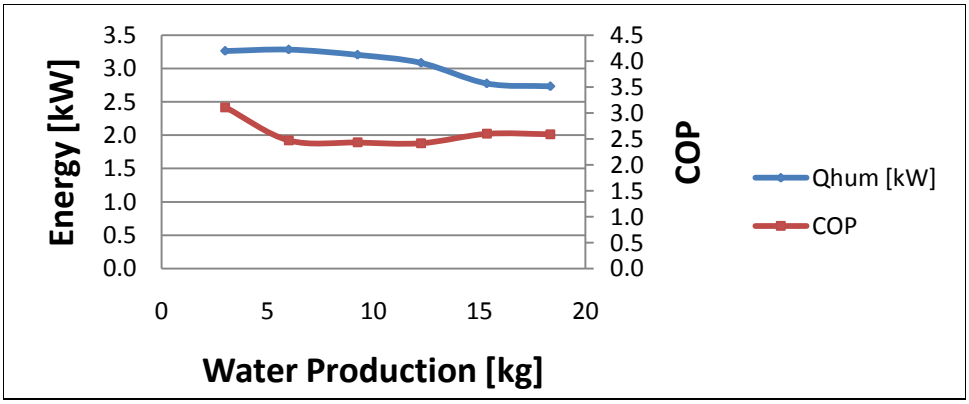

Figure 6-21: Variation of energy and COP with water produced for high temperature operation

It is worth to mention that during the experiment at high temperature, the desalination system suffered from high pressure. Though there was no any noticeable effect on the performance of the system, there might be internal damage to the system as it had a lot of vibration. Secondly operating the system at high temperature resulted in higher heat energy loss with a lot leakages and vapour escaping due to pressure. And finally the insulation on the hot water tank could not withstand the high temperature and as a result it was cracking and going off the tank as shown in the picture below.

Figure 6-22: Damaged water tank due to high temperature

6.3 Conclusion

The experimental investigation of the water desalination unit driven by solar collector and electric heater has been carried out. The system was constructed according to design specification. Tests were initially carried out separately on individual systems and later on the combined system to form hybrid solar electric desalination system.

The performance of the solar collector combined with the water heat exchange tank was around 20%. Previous indoor test of the collector did not incorporate the water tank and thus the efficiency was higher. However the collector could provide 0.3kW of energy which was used to power the desalination unit. A maximum of around 4kg/h of fresh water and COP around 8.9 was obtained using solar-only operation mode.

Experimental tests were carried out using electric heater as the only energy source. Different flow rate configurations for hot water in the humidification chamber and cooling water in the dehumidification chamber were set. It was found the system performed better at high flow rates. Maximum of 17kg/h of fresh water was obtained. The system COP was 4.4 and energy consumption was 2.6kW.

When the solar collector was used combined with the electric heater as hybrid (Test 07 and 08), the amount of water produced was 10kg/h. The system COP was 2.0 and energy consumption around 3.3kW. The low COP was clearly as a result of higher energy consumption and lower fresh water production. Due to the limit posed by the solar collector, the hot water flow rate into the humidification chamber was reduced. This limited the rate of evaporation and at the same time increased the temperature of the hot water. Hence with high temperature, the cooling water gets saturated and thus affected the output of the system. There is a trade-off between increasing the efficiency of the collector which results in decreasing the efficiency of the humidifier.

The system has a 90% fresh water recovery rate. And is a high prospect of better performance when the system was operated at high temperature above 100°C. Up to 20kg/h of fresh water was obtained base on the preliminary test carried out. Even though there is potential for high temperature operation, there was restriction in the lab to continue with the high temperature tests due to safety related issues. Furthermore, it will require most of the major components to be replaced as it was found out after the preliminary test most of the components do not conform with the manufacturers specification to withstand high temperatures.

Chapter 7: Economic and Environmental Analysis

7.0 Introduction

This chapter explains the economics of the desalination unit. A comparative analysis using the net present value method was carried out for when the system is operated using solar energy and electricity from fossil fuels. The system could provide different amount of fresh water depending on mode of operation. But for the purpose of comparison a standardised mode of operation was used for both the solar and electric operating conditions. The analysis also considers the amount of carbon savings that could be achieved and final cost of water produced per cubic meter.

The factors that influence the systems economic viability are the outputs and costs of the desalination unit and solar collector systems, the cost of alternative energy source, cost of operation and maintenance, and the geographic location of the system, i.e. solar intensity, environmental temperature and humidity.

7.1 System Specification and Economic Considerations

For cost effectiveness analysis, no consideration was made for certain costs such as packaging, transport and import taxes. Other costs such as that of raw water and concentrated salt disposal are not included. It should be noted the costs of the system is base on prototype. And there could be 50% reduction in cost when the system is mass produced.

The prototype desalination unit could produce up to 20L/h of fresh water per hour using 3kW heat input and 0.5kW electrical energy for auxiliary devices attached to the system. The operation time of the system was considered to be 8 hours per day. Hence annual fresh water production could be up to 58m³. As the system does not have any moving parts or excessive pressure, it is assumed the life time of the system is 20 years. Considering the system does not have fouling or scaling, no membranes to change and pre/post treatment of water, a modest 2% of the total cost of the system was assumed for operation and maintenance of the system over its life time. Table 7-1 shows the system specification and economical assumptions for the cost analysis.

Table 7-1: Key considerations

Water production	20L/h
COP	3
Heat input	3kW
Electrical input	0.5kW
Operation life span	20years
Interest rate	10%
Electricity cost	£0.07 per kWh
Maintenance	2%

7.2 Cost Analysis

The net present value method used for cost analysis is a comparison between the investments made at present using the present value of money considering interest rate over a period of time. The net present value analysis was made according to equation 34 [66]:

$$NPV = I_o + \frac{\sum_{j=1}^{t} F_t}{(1+i^t)} \qquad (34)$$

Where:

I_o = capital cost, F_t = running cost, i = interest rate, t = time in years

A cost breakdown of the capital cost of the solar collector unit is given in Table 7-2. The quantity of solar collector required to produce 20L/h of fresh was calculated as 7.5m² for 38% collector efficiency. The miscellaneous costs include costs such as piping and installation. This is considered at around 10% of the cost of the entire system.

Table 7-2: Capital cost for solar system

Item	Quantity	Unit Cost	Total Cost [£]
Solar collector	7.5 m²	£350 per m²	2625
Pump	1	£100	100
Miscellaneous	-	-	275
Total			3000

The capital cost of the desalination for the desalination unit is given in Table 7-3. The miscellaneous cost here is considered to be 15%. This includes insulation costs in addition to piping and installation.

Table 7-3: Capital cost for prototype desalination system

Item	Quantity	Unit Cost	Total Cost [£]
Desalination unit	1	£700	700
Pumps	3	£100	300
Water tank with coil HX	1 (140L)	£300	300
Miscellaneous	-	-	200
Total			1500

The running cost of the system is the cost of operating and maintaining the system over life of the system. The maintenance cost of the system is 2% of the total cost of the system. And then the energy cost base on the energy consumption of the system. For the solar driven system, the energy is said to be provided free from sun. However, there is still additional energy cost for the 0.5kW electricity used by the auxiliary components of the system. The cost of electricity is taken as £0.07 per kWh. The calculated running cost of the system is shown in Table 7-4.

Table 7-4: Running costs of the desalination unit for both solar and electric

Costs Items	Solar System	Electric System
Total capital cost (£)	4500	1500
O&M cost (£/yr)	90	30
Energy consumption (kWh/yr)	1460	10220
Energy cost (£/yr)	100	715
Total running cost (£/yr)	190	745

The results obtained from the net present value analysis are shown in Figure 7-1. It can be seen that by end of year six the investment for the solar system reaches breakeven when compared to the electric system. After this time the solar driven system will cost less than the electric driven system. This is mainly due to much less running cost of the solar system.

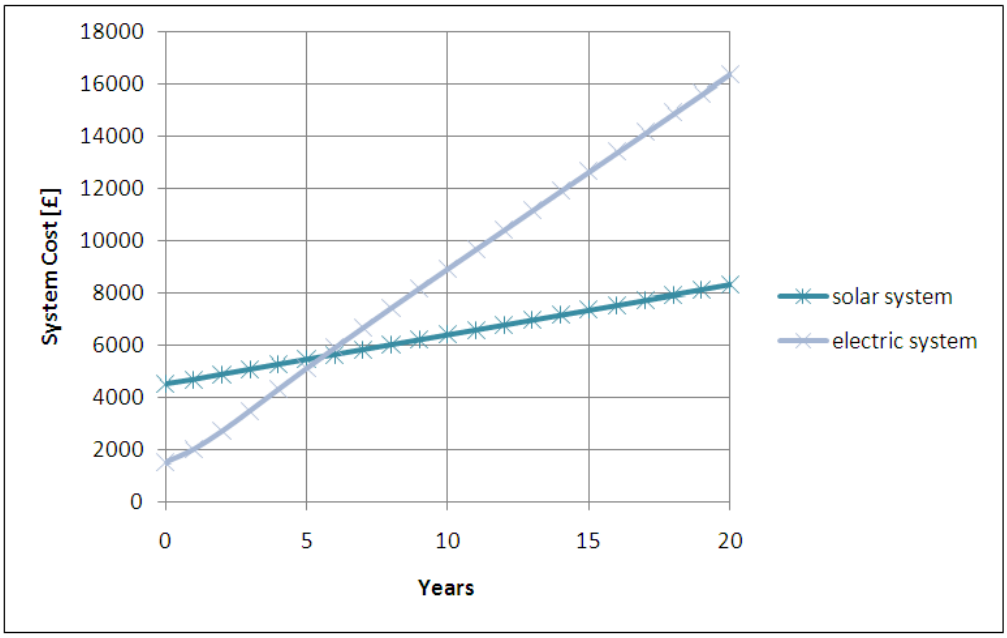

Figure 7-1: Net present value analysis

It can be seen that in year six of operation the investment comparison between the two systems is the same. And after the cost for the electric system increase sharply while that of the solar system is more steady and gradual. Hence the life cycle saving for using the solar system is around £8000 at the end of the 20 year period. And it is only around £3000 if 10 year operation period is considered.

7.3 Carbon Savings

To investigate the environmental benefit of utilizing solar energy instead of conventional source of energy, the different emission of $kgCO_2$ per unit energy resulting from the solar system operation are estimated and compared to those of a conventional electric system. The carbon emission is considered because it is reported as the emission which is responsible for the most important environmental problems. The analysis was carried out based on the UK guidelines for company reporting on greenhouse gas emissions. The equation for converting electricity to CO_2 is given as follows:

Carbon emission = electricity used per year (kWh) x 0.54 (CO_2 conversion factor)

The amount of carbon saving is amount of carbon from the solar system subtracted from that of the electric system. The amount of carbon emissions from both systems is

calculated and given in Table 7-5. If the solar system is considered, it will amount to saving up to 4730 $kgCO_2$ per year.

Table 7-5: Carbon emissions

	Solar System	Electric System
Energy consumption (kWh/yr)	1460	10220
Carbon emission ($kgCO_2$/yr)	788.4	5518.8

7.4 Water Cost

The cost of water produced is calculate by taking the net present value of the system as the life cycle cost (LCC) and divide it by the total amount of water produced over its life period.

$$\text{Water cost} = \frac{\text{LCC}}{\text{Water production}} \quad (35)$$

The cost of water produced is calculated as shown in Table 7-6. The water production cost was found to be 7 £/m^3. There is up 50% reduction in cost compared using electricity from the grid as main heat source. This is competitive to a 0.1m^3/day RO system reported in ref [76] with water production cost 14 \$/m^3.

Table 7-6: Water cost

Costs Items	Solar System	Electric System
LCC (£)	8000	16000
Water production (m^3)	1168	1168
Water cost (£/m^3)	7	14

The cost of the solar driven system is much cheaper than when driven by electricity from the grid with six years payback period. This can further be significantly reduced by up to 50% if the system is mass produced. The quantity of the fresh water can be also increased and its cost decreased if the system is optimised or operate for longer period of time using storage. This needs a cheaper collector with heat storage in large amounts. Such collector storage can be a solar pond. For a larger scale system (see section 8.2.1), the minimum cost of water production was estimated between £0.55-0.57 per m^3 for 20 years life cycle with running cost at 2% of total capital cost per annum, and interest rate at 10%. This is assuming the system operates 24 hours a day.

7.5 Conclusion

Up to 20kg/h of fresh water was obtained base on the test carried out. Cost analysis of the desalination system was carried out base on the preliminary result. The cost of the fresh water production is £7 per cubic meter which is 10 times higher than the tariff of conventional water. The energy requirement of the system constitutes about 58% of the system cost. When solar energy is used, there is about 34% reduction in energy cost of the system. The cost can be improved by improving the amount of water production and reducing the capital cost and energy consumption of the system.

Chapter 8: Conclusion and Further Work

8.1 Conclusion

Despite huge abundance of water resources, humanity is faced with growing challenge of access to fresh water for both domestic and industrial or agricultural needs most especially in the developing countries. Desalination has become a major new source of fresh water tapping into the vast reserves of seawater and brackish water. However, current desalination technologies are sensitive to increase in energy prices and highly carbon intensive. This makes them expensive and poorer countries cannot afford to desalinated water. Among emerging desalination technologies is the thermal process known as humidification dehumidification desalination (HDD) which is very promising.

A novel humidification dehumidification desalination system driven by concentrating solar collector was designed and developed. Theoretical analysis indicates possibility of reduction in energy consumption through energy recovery and at the same time reduction in requirement for cooling water. A prototype system was constructed. Several experiments were carried out initially on the water desalination unit only under different conditions. The effect of heat input, temperature and flow rates on the amount of fresh water produced were examined. The experimental result suggests a cooling water temperature of around 40-50°C for the optimum operation of the system. A maximum 3.6 COP and 13kg/h fresh water were obtained at around 80-90°C operating temperature. A further modelling was carried out at higher operating temperatures, it was seen that the performance of the system can be greatly improved. For given certain conditions, water production was around 1kg/h per degree rise in temperature between temperature range 50-90°C, and 0.4kg/h per degrees for range 90-150°C. And there was significant increase to 4kg/h per degree for temperature range 150-200°C.

The design of new V-Trough solar collector was presented. Performance analysis of the solar collector was carried out through experimental work. Various receiver tubes were tested indoors. And the double layer coated vacuum glass with concentric pipe has highest efficiency at 32% with water as HTF, and thus was selected for outdoor test. The outdoor test yielded 38% efficiency. The selection of the most suitable collector for a given desalination application (i.e. small scale or large scale) should take into account; the required operation temperature, the solar intensity and environmental temperatures and other technical and economic factors. In addition, to determine the size of solar

collector, the efficiency of both the humidification chamber and that of solar collector are very crucial. The modelling work carried out based on the efficiency performance of the solar collector suggests that the new VTC has more potential for water desalination compared to other collectors at certain operating conditions.

Further experimental tests were carried out on the combined solar collector and the water desalination unit and also to validate the modelling work by comparing with the experimental data. There is need to operate the system at lower ΔT in order to achieve higher water production with lower collector area. This will require operating the system at higher flow rate. And hence focus on flow rate was given. The experimental investigation of the water desalination unit driven by solar collector and electric heater has been carried out. The collector provided 0.3kW of energy which was used to power the desalination unit. A maximum of around 4kg/h of fresh water and COP around 2 was obtained using solar-only operation mode. Experimental tests were carried out using electric heater as the only energy source. Different flow rate configurations for hot water in the humidification chamber and cooling water in the dehumidification chamber were set. It was found the system performed better at high flow rates. Maximum of 17kg/h of fresh water was obtained. The system has a 90% fresh water recovery rate. And is a high prospect of better performance when the system was operated at high temperature above 100°C. Up to 20kg/h and a COP more than 4 were obtained. Thus it can e concluded the maximum capacity of the desalination unit is up to 20kg/h of fresh water at 100°C maximum operating temperature and 120kg/h hot water flow rate and 30kg/h cold water flow rate at the inlet of the humidification and that of the dehumidification chamber respectively. A fan with capacity of at least 80CFM is required to provide 10-30kg/h of fresh air.

The cost of the fresh water production is £7 per cubic meter which is currently competitive with a small scale reverse osmosis system but 10 times higher than the tariff of conventional water. This is rather currently expensive, and costs can be significantly reduced in the near future. Fresh water production cost of a large scale newly developed HDD system was estimated at £0.57 per cubic meter assuming 24hr operation. But as the sun is not available 24hrs, hence key challenge will be incorporate heat storage or alternative renewable energy technology. However, there is an annual carbon saving of

5000kgCO_2. The energy requirement of the system constitutes about 58% of the system cost. When solar energy is used, there is about 34% reduction in energy cost of the system. The cost of the system can be significantly reduced to up to 50% through mass production and as well further system optimisation/improvement. This can be achieved by improving the systems COP.

8.2 Further Work

There is a need to further optimise the E/C-Core membrane and its geometry. This requires the design theory of three-fluid heat exchanger with complex flow arrangements. The design of multifluid and multistream heat exchangers is algebraically complex and requires technique such as matrix formalism and chain rule methodology [67]. Further work can be carried out by testing of different construction materials such as the nano composite membranes and synthetic zeolites in order to obtain higher performance.

There is need to carry out field trials for the system under different climatic conditions and also large scale application of the technology in a village or town. This will help to further understand the behaviour of the system under practical conditions and also the performance of the system against contamination and other operational challenges over long period of time. Furthermore, a turbine technology could be incorporated for cogeneration of electricity and portable water. The feasibility of the cogeneration and field trials are further explained in the following subsequent sections of the chapter.

8.2.1 Large-Scale/Field Trials

Field testing can be carried out to ensure that the developed system operates satisfactorily under real life conditions and is suitable for commercial exploitation. A larger scale system can be designed for field trial based both theoretical and experimental research activity carried out in the laboratory. Having predicted maximum 8m^2 of v-trough collector required to drive the HDD unit with an optimum water production of 20L/h, it can be used to specify for larger scale systems ranging from domestic to town size application.

Typical numbers of dwellers in domestic, commercial, village and town categories are given in Table 8-2. The water needs is based on the requirement of 100litres/day per

person for household applications such as drinking, bathing and cooking. The industrial and agricultural applications are estimated to be 5-20 times more than that of household application. The equipment costs are 50% lower than those presented in Chapter 7 (assuming mass production). The land area requirement should be at least nothing less than an approximate of solar collector area required.

Table 8-2: Specification for large scale application

Scale	Population	Water Need [m^3/d]	HDD Unit	Cost [£'000]	VTC Area [m^2]	Cost [£'000]
Domestic	<10	1	2	0.7	16	2
Commercial	100	10	20	7	160	20
Village	2500	250	520	182	4160	520
Town	25000	2500	5208	1822	41664	5208

The total cost of the system is given in Table 8-3. Other associated costs are approximated at 20% of the cost of the desalination unit. However, there are costs such as that of land and labour which are depended on location and not included.

Table 8-3: Total cost of installation

Item	Domestic	Commercial	Village	Town
Solar Unit	2000	20000	520000	5208000
HDD Unit	700	7000	182000	1822800
Other	140	1400	36400	364560
Total	2840	28400	738400	7395360

It can be seen that the cost of solar collector constitute up to 70% of the cost of the system. If an alternative solar technology such as the solar pond which incorporates storage is considered, there can be a significant capital cost reduction.

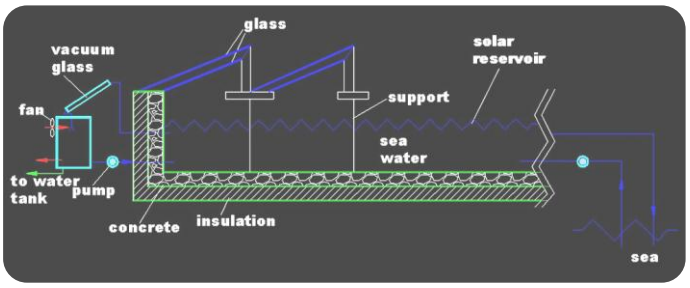

Figure 8-4: Proposed large scale application

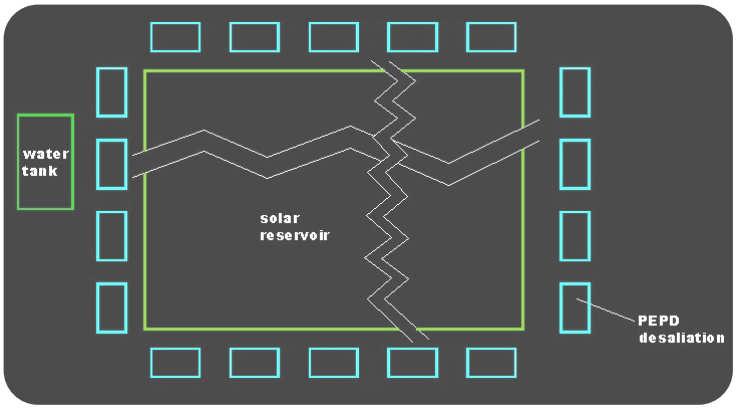

Figure 8-5: Overview of the proposed large scale application

Table 8-4: Cost of a proposed 1000m³/d system

Item		Qty	unit cost (£)	Total Cost (£)
Solar Reservoir 30000m² x 1m (depth)	concrete/brick (m³)	900	40	36000
	insulation (m³)	1000	250	250000
	vacuum glass (m²)	30000	10	300000
	steel support (T)	140	500	70000
	coating (m²)	35000	1.5	52500
				708500
Land	40000 (m²)			
Desalination Unit	20L/h	2075	350	726250
Water Tank	600 (m³)	1	10000	10000
Construction				100000
Miscellaneous				25000
				861250
Total				1569750

The cost breakdown for a 1000m³/d system is given in Table 8-4. It can be seen that the cost of the solar unit is significantly reduced to around 45% of the total cost of the system. And if a 1000m^3/d system driven by the VTC is considered (4 time village application equals 1000m^3/d), it can be seen the solar pond driven HDD unit is only 55% of the cost of the VTC driven system. However, in terms of land requirement, the VTC

system requires less than 20000m^2 which 50% less than the 40000^2 land required for the solar reservoir system. The cost of product water might be higher than that of the VTC system. Operational challenges in terms of out of the laboratory system performance in different climate conditions and actual costs can only be established through field trials.

8.2.2 Turbine Cogeneration

A proposed system based on the incorporation of a Rankine cycle power generation system and a humidification/dehumidification desalination system is illustrated in Figure 8-3. The solar collector produces hot water at a temperature of 120°C ~ 150°C. Hydrofluoroether HFE7100 which has the boiling point of 60°C may be used as the working fluid. Vaporisation of HFE7100 at 120°C will produce a vapour at 5.0bar and the higher pressure vapour then drives the turbine or expander to produce mechanical energy and hence electricity at the alternator. The discharge vapour may condense at 60°C at the condenser and the condensed liquid is pumped back to the boiler to complete the Rankine cycle. The heat rejected at 60°C could be used for heating or driving desalination.

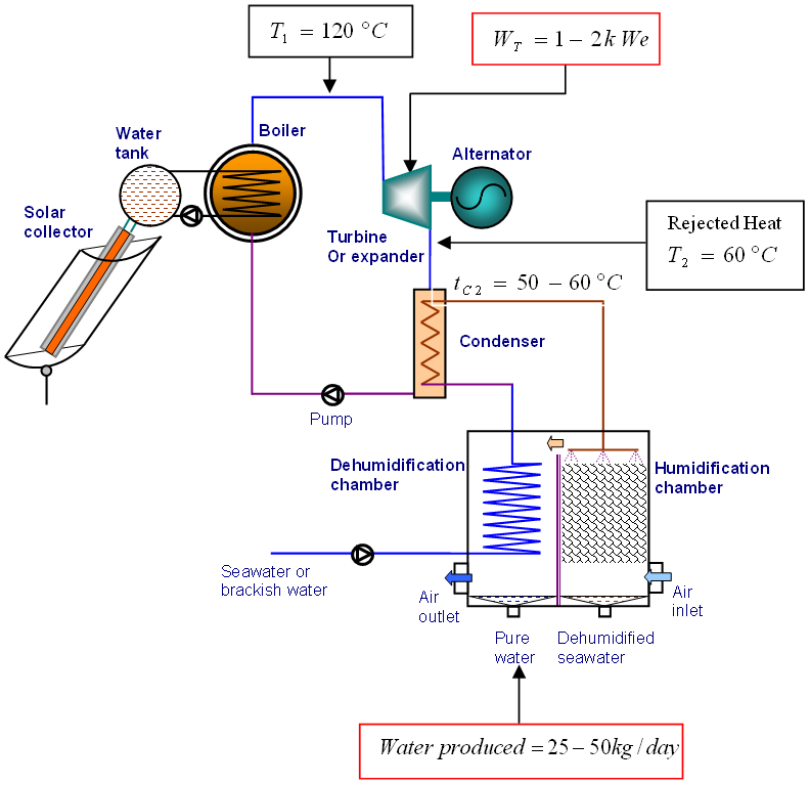

Figure 8-3: Proposed combined water and power system

References

[1] Aage Stangeland, Scenarios for Global CO2 Emissions. The Bellona Foundation, 2007.

[2] FAO, Review of World Water Resources by Country, Rome 2003.

[3] http://enviroscope.iges.or.jp/contents/eLearning/waterdemo/factsforall.htm <accessed 28/04/11>

[4] Niemczynowicz, J. (2000). Present challenges in water management. Water International. 25: 139-147.

[5] Abdul Khaleq Lalzad, 2005. Development of Novel Small-Scale Desalination, London South Bank University, PhD Thesis.

[6] Michael Krebs, 2009. Water shortage in Mexico City could echo the global water issue http://www.digitaljournal.com/article/279761 <accessed 05/01/2010>

[7] Tom Gardner-Outlaw and Robert Engelman, Sustaining Water, Easing Scarcity: A Second Update, Population Action International, 1997.

[8] http://aftermathblog.wordpress.com/2006/01/19/water-stress-map/ <accessed 20/12/2009>

[9] Shmuel Neumann, Solar Desalination Business Plan, Strategic Solutions Technology Group, 2008.

[10] Jenny Baxter, 2010. Water Industry, Market Report 2010, Keynote.

[11] ABB Group, Solutions for the water cycle Leakage management, ABB-Water Industrial Sector Initiative, 2009.

[12] Joachim Koschikowski, Water Desalination: When and Where Will it Make Sense?, Fraunhofer Institute for Solar Energy Systems ISE Freiburg, Germany, 2011

[13] Koussai Quteishat, Desalination 2008: Where Do We Stand? Developments in Technologies: Technical and Economic, Middle East Desalination Research Centre, ADIRA WORKSHOP, Marrakech, Morocco 26-27 April, 2008

[14] Amy K. Zander et al., Desalination: A National Perspective. The National Academy of Science, 2008.

[15] O.K. Buros, 2000. The ABCs of Desalinating. IDA.

[16] O. Souilah et al., Water reuse of an industrial effluent by means of electro-deionisation Desalination 167 (2004) 49-54.

[17] Brian P. Hernon et al., Electrodeionization in Power Plant Applications, Presented at the 8th Annual Ultrapure Water Expo '94, Philadelphia, Pennsylvania, May 9-11, 1994.

[18] L. Garcia-Rodreguez, 2003. Renewable energy applications in desalination: state of the art. Solar Energy 75 (2003) 381-393.

[19] Michael Papapetrou et al., 2010. Roadmap for the Development of Desalination Powered by Renewable Energy. Fraunhoper Verlag.

[20] El-Dessoukey, et al., 1998. Performance of compact parallel feed multiple effect evaporation. International workshop on desalination. University of Rome, Dec. 1998.

[21] S. Loupasis, 2002. Technical analysis of existing renewable energy sources desalination schemes. Commission of the European Communities Directorate-General for Energy and Transport.

[22] T. Pankratz, 2000. Large-scale desalination plants-A drought-proof water supply. International Desalination News, Issue 3-4 (2000) 3-6.

[23] Michael Schorr, 2011. Desalination, Trends and Technologies. Intech.

[24] IAE Statistics, CO_2 Emissions From fuel Combustion Highlights, 2010 Edition.

[25] Koussai Quteishat, Desalination 2008: Where Do We Stand? Developments in Technologies: Technical and Economic, Middle East Desalination Research Centre, Adira Workshop, Marrakech, Morocco 26-27 April, 2008

[26] Soteris A. Kalogirou, Solar thermal collectors and applications, Progress in Energy and Combustion Science 30 (2004) 231–295

[27] Enermodal, Cost Reduction Study for Solar Thermal Power Plants, Enermodal Engineering Limited, 650 Riverbend Drive, Kitchener, ON N2K 3S2, A Report Prepared for The World Bank, (1999).

[28] http://www.solarmillennium.de/Technology/Parabolic_Trough_Power_Plants/History/The_History_of_Parabolic_Trough_Power_Plants_,lang2,105.html (accessed 20/02/09)

[29] Wolfgang Eichhammer et al., Assessment of the World Bank/GEF Strategy for the Market Development of Concentrating Solar Thermal Power, Prepared for The World Bank (2005).

[30] http://www.solarmillennium.de/front_content.php?idcat=109> (accessed: 26/02/09)

[31] http://en.wikipedia.org/wiki/Solar_Two (accessed: 26/02/09)

[32] Robert F. Boehm, Concentrating Solar Power, SET2008 - 7th International Conference on Sustainable Energy Technologies; Seoul, Korea 24-27 August, 2008

[33] D. R. Mills and Graham L. Morrison, 1997. Advanced Fresnel Reflector Powerplants-Performance and Generating Costs. Proceedings of Solar '97, Australian and New Zealand Solar Energy Society, Paper 84.

[34] Eerik Wissenz (2008), The principles of solar concentration, http://www.solarfire.org/The-Principles-of-Solar.html (accessed: 19/02/09)

[35] E.E Delyannis and A. Delyannis, Economics of Solar Still, Desalination, 52 (1985) 167-176

[36] Abdul Khaleq Lalzad, 2005. Development of Novel Small-Scale Desalination, London South Bank University, PhD Thesis.

[37] J. Bednarski, M. Minamide, O.J. Morin, Test program to evaluate and enhance seawater distillation process for the metropolitan water district of southern California, Proceedings of the IDA World Congress on Desalination and Water Sciences, vol. I, Madrid, Spain, October 1997, pp. 227–241

[38] http://ec.europa.eu/environment/etap (accessed 03/03/11)

[39] Fulya Verdier, MENA Regional Water Outlook Part II Desalination Using Renewable Energy Task 1 – Desalination Potential, Fichtner, 2011

[40] K. Bouronni, M.T. Chaibi, L. Tadrist, Water desalination by humidification and dehumidification of air: State of the art. Desalination, 137(2001)167.

[41] H. Müller-Holst, M. Engelhardt, M. Herve, W. Schölkort. Small-scale thermal seawater desalination simulation and optimization of system design. Renewable Energy, 14(1998)311.

[42] H. Müller-Holst, M. Engelhardt, W. Schölkopf. In Proceedings of the Mediterranean Conference on Policies and Strategies for Desalination and Renewable Energies". Greece, 21-23 June 2000, p.285.

[43] M. Farid, A.W. Al-Hajaj. Solar desalination with a humidification-dehumidification cycle. Desalination, 106(1996)427.

[44] T. Baumgarthner et.al. In Proceedings 8 Internationales Sonnenforum, June 23 – July 2, Berlin, DGS (German Section of ISES), 1992, Munchen, p.432.

[45] M. S. Saadawy, A. Karameldin and E. R. Negeed. A Novel Super-Cooled Humidification-Dehumidification System Driven by Thermal Vapour Compression

Unit (HDDTVC) for Seawater Desalination. Twelfth International Water Technology Conference, IWTC12 2008, Alexandria, Egypt 169.

[46] G.P. Narayan, M.H. Sharqawy, E.K. Summers, J.H. Lienhard V, S.M. Zubair, and M.A. Antar, "The potential of solar-driven humidification-dehumidification desalination for small-scale decentralized water production," Renewable and Sustainable Energy Reviews, Vol. 14, No. 4, pp.1187-1201, May 2010.

[47] R.H. Xiong et al.Experimental investigation of a baffled shell and tube desalination column using the humidification-dehumidification process. Desalination 180 (2005) 253-261

[48] S. Yanniotis and K. Xerodemas, 2003. Air Humidification for Seawater Desalination. Desalination 158, pp. 313-319

[49] James R. Beckman et al. Brackish and seawater desalination using a 20 ft^2 dewvaporation tower. Desalination 140 (2001).

[50] E.W. Lemmon, R.T. Jacobsen, S.G. Penoncello and F. Daniel, Thermodynamic Properties of Air and Mixtures of Nitrogen, Argon, and Oxygen from 60 to 2000 K at Pressures to 2000 MPa, J. Physical and Chemical Reference Data, 29(3) (2000) 331.

[51] R.W. Hyland and A. Wexler, Formulations for the Thermodynamic Properties of the Saturated Phases of H2O from 173.15 K to 473.15 K. ASHRAE Transactions Part 2A, Paper 2793, 1983.

[52] D.J. Wessel, ASHRAE Fundamentals Handbook 2001 (SI Edition), American Society of Heating, Refrigerating, and Air- Conditioning Engineers, 2001.

[53] A. Prufi and W. Wagner, The IAPWS formulation 1995 for the thermodynamic properties of ordinary water substance for general and scientific use, J. Physical and Chemical Reference Data, 31(2) (1995) 387–535.

[54] Richter, John L., 1996. Optics of a two-trough solar concentrator. Solar Energy 56, 191–198.

[55] Price, H., Lupfert, E., Kearney, D., et al., 2002. Advances in parabolic trough solar power technology. Journal of Solar Energy Engineering 124 (5), 109–125.

[56] Schwarze et al. 2008. Characterisation and design methods of solar cookers. Solar Energy 82, 157–163.

[57] Zheng Hongfei, Tao Tao, He Kaiyan, Abdulkarim Mayere, A new trough solar concentrator and its performance analysis, Solar Energy, 85(1), 198-207 (2011)

[58] J.M Coulson and J. F. Richardson (1999). Coulson & Richardson's Chemical Engineering: Fluid Flow, Heat Transfer and Mass Transfer (Sixth Edition ed.). Butterworth Heinemann. ISBN 0750644443.

[59] A.S. Nafey et al. Solar desalination using humidification–dehumidification processes. Part II. An experimental investigation. Energy Conversion and Management 45 (2004) 1263–1277.

[60] K. Bourouni et al. Water desalination by humidification and dehumidification of air: state of the art. Desalination 137 (2001) 167-l 76.

[61] Brunold, S., Frey, R., Frei, Ulrich, 1994. Comparison of three different collectors for process heat applications. Proc. SPIE Vol. 2255, p. 107-118, Optical Materials Technology for Energy Efficiency and Solar Energy Conversion XIII.

[62] Duffie JA, Beckman WA. Solar engineering of thermal processes. 2nd ed. New York: John Wiley &Sons, 1991.

[63] Kreith F, Kreider JF. Principles of solar engineering. New York: McGraw±Hill, 1985.

[64] S. Kalogirou. Use of parabolic trough solar energy collectors for sea-water desalination. Applied Energy 60 (1998) 65±88.

[65] Renato Lazzarin and Luigi Nalini, 2004. Air humidification; Technical, health and energy aspects. Carel.

[66] Jorge L. Wolpert, 2003. Solar Powered Ejector Air Conditioning System for Mexican Climate. PhD Thesis, University of Nottingham.

[67] Sekulii-, D. P., R. K. Shah, and A. Pignotti, 1999, A review of solution methods for determining effectiveness-NTU relationships for heat exchangers with complex flow arrangements, Appl. Mech. Rev., Vol. 52, No. 3, pp. 97-117.

[68] T.S. Saitoh and A. Hoshi, Proposed solar Rankine cycle system with phase change steam accumulator and CPC solar collector. IECEC (2002), paper no. 20150.

[69] A.C. Oliveira, C. Afonso, J. Matos, S. Riffat, M. Nguyen and P. Doherty, A combined heat and power system for buildings driven by solar energy and gas, Applied Thermal Engineering 22 (2002) (6), pp. 587–593.

[70] S. B. Riffat, Hybrid-CHP – A Hybrid Combined Heat and Power System, Final Report of EU Research Contract n. ENK5-CT-2000-0080, European Commission, (2003).

[71] U. Drescher, D. Bruggemann, Fluid selection for the Organic Rankine Cycle (ORC) in biomass power and heat plants, Appl. Therm. Eng. 27 (2007) 223–228.

[72] Enermodal, Cost Reduction Study for Solar Thermal Power Plants, Enermodal Engineering Limited, 650 Riverbend Drive, Kitchener, ON N2K 3S2, A Report Prepared for The World Bank, (1999).

[73] Oliver, Jason Ryan, (2005), A micro-cooling, heating, and power *(*m-CHP*)* instructional module, Mississippi State University.

[74] A. Hammerschmid et al., Demonstration of an innovative small-scale biomass CHP module based on a 730kW_{el} screw-type steam engine, 2nd World Conference and Exhibition on Biomass for Energy, Industry and Climate Protection 10-14 May 2004, Rome, Italy.

[75] He kaiyan, Zheng hongfei, Liu Yixin, Chen ziqian. An imaging compounding parabolic concentrator. Proceeding of ISES Solar World Congress. 2007.2:589-592.

[76] A. Eslamimanesh, M.S. Hatamipour. Economical study of a small-scale direct contact Humidification-Dehumidification desalination plant. Desalination, Volume 250, Issue 1, 1 January 2010, Pages 203-207.

[77] International Desalination Association. Desalination for a better world, http://www.idadesal.org/t-homevideo.aspx. Accessed 19/12/09

[78] http://ga.water.usgs.gov/edu/waterdistribution.html, Accessed 10/05/2011

[79] Sandeep Parekh, M.M. Farid, J.R. Selman and Said Al-Hallaj , "Solar desalination with humidification-dehumidification technique - a comprehensive technical review", Desalination, 160 (2003) 167-186.

[80] http://people.bath.ac.uk/absmaw/Facade/sunlight_01.pdf , Accessed 11/10/11

Appendix A

World population (1950-2050) based on different projections and variants (UN, 2009).

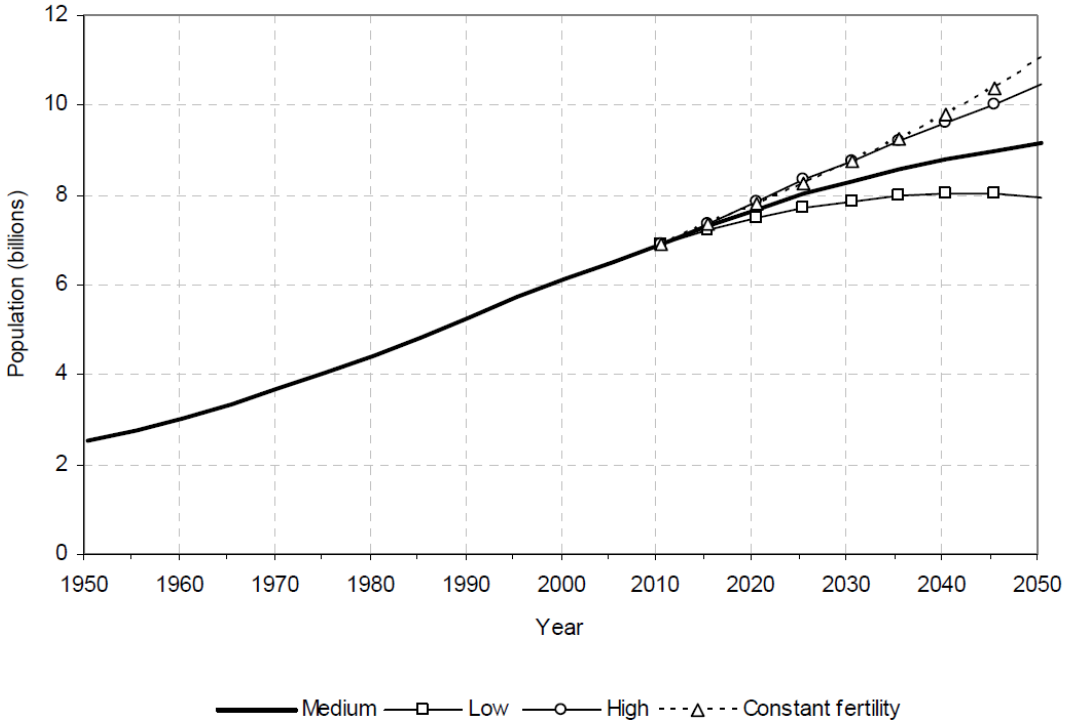

Appedix B

Population, Annual Renewable Freshwater Availability, 1950, 1995 and 2025 (PAI, 1997)

Country	Total Annual Renewable Freshwater Available (10^6 m^3)	1950		1995		2025	
		Population ($1x10^6$)	Per capita Water availability (m^3)	Population ($1x10^6$)	Per capita Water availability (m^3)	Population ($1x10^6$)	Per capita Water availability (m^3)
Afghanistan	50	8.9	5,582	19.7	2,543	45.3	1,105
Albania	21.3	1.2	17,317	3.4	6,296	4.3	4,959
Algeria	14.8	8.8	1,691	28.1	527	47.3	313
Angola	184	4.1	44,541	10.8	17,012	25.5	7,202
Argentina	994	17.2	57,959	34.8	28,590	47.2	21,077
Armenia	13.3	1.4	9,801	3.6	3,654	4.2	3,171
Australia	343	8.2	41,733	17.9	19,198	23.9	14,333
Austria	90.3	6.9	13,021	8	11,224	8.3	10,873
Azerbaijan	33	2.9	11,388	7.5	4,379	9.7	3,395
Bahrain	0.09	0.12	776	0.56	162	0.86	104
Bangladish	2,357	41.8	56,411	118.2	19,936	179.9	13,096
Barbados	0.05	0.21	237	0.26	192	0.29	169
Belarus	74	7.7	9,529	10.4	7,129	9.6	7,655
Belgium	12	8.6	1,447	10.1	1,234	10.3	1,217
Beliza	16	0.07	231,884	0.21	75,117	0.38	42,667
Benin	25.8	2	12,610	5.4	4,770	12.3	2,102
Bhutan	95	0.73	129,428	1.8	53,672	3.6	26,056
Bolivia	300	2.7	110,538	7.4	40,464	13.1	22,847
Botswana	14.7	0.39	37,789	1.5	10,138	2.6	5,707
Brazil	6,950	53.9	128,763	159	43,707	216.6	32,089
Bulgaria	205	7.3	28,272	8.5	24,092	7.5	27,506
Burkina Faso	28	3.6	7,663	10.5	2,672	23.5	1,194
Burundi	3.6	2.5	1,466	6.1	594	12.3	292
Cambodia	498	4.3	114,611	10	49,691	16.9	29,317
Cameroon	268	4.5	60,009	13.2	20,315	28.5	9,397
Canada	2,901	13.7	211,181	29.4	98,667	36.4	79,731
Cape verde	0.3	0.15	2,055	0.39	777	0.68	442
Cen. Africa	141	1.3	107,306	2.9	48,139	6	23,477
Chad	43	2.7	16,178	6.3	6,788	12.6	3,400
Chile	468	6.1	76,948	14.2	32,935	19.6	23,941
China	2,800	554.8	5,047	1,220	2,295	1,480	1,891
Colombia	1,070	11.9	89,570	35.8	29,877	52.7	20,316
Comoros	1.02	0.17	5,896	0.61	1,667	1.3	760
Congo	832	0.81	1,029,703	2.6	320,864	5.7	144,771
Costa Rica	95	0.86	110,209	3.4	27,745	5.6	16,940
Cote D'ivoire	77.7	2.8	27,990	13.7	5,674	24.4	3,185

Appendix B (continued)

Croatia	61.4	3.9	15,948	4.5	13,629	4.2	14,471
Cuba	34.5	5.9	5,897	10.9	3,147	11.8	2,924
Cyprus	0.9	0.49	1,822	0.75	1,208	0.95	947
Czech Rep	58.2	8.9	6,521	10.3	5,671	9.6	6,046
Denmark	13	4.3	3,044	5.2	2,489	5.3	2,442
Djibouti	2.3	0.06	37,097	0.6	3,827	1.1	2,028
Dominican	20	2.4	8,500	7.8	2,557	11.2	1,791
Ecuador	314	3.4	92,707	11.5	27,400	17.8	17,644
Egypt	58.1	21.8	2,661	62.1	936	95.8	607
El Salvador	18.95	1.9	9,713	5.7	3,347	9.2	2,055
Equat. Guinea	30	0.23	132,743	0.4	75,000	0.79	37,594
Eritrea	8.8	1.1	7,719	3.2	2,775	6.5	1,353
Estonia	17.6	1.1	15,985	1.5	11,828	1.3	14,013
Ethiopia	110	18.4	5,967	56.4	1,950	136.3	807
Fiji	28.6	0.29	98,789	0.78	36,416	1.2	24,402
Finland	113	4	28,187	5.1	22,126	5.3	21,345
France	198	41.8	4,734	58.1	3,408	60.4	3,279
Gabon	164	0.47	349,680	1	152,416	2.1	77,432
Gambia	8	0.29	27,211	1.1	7,201	1.9	4,032
Germany	171	68.4	2,501	81.6	2,096	80.9	2,114
Ghana	53.2	4.9	10,857	17.3	3,068	36.3	1,464
Greece	58.7	7.6	7,752	10.5	5,610	10.1	5,822
Guatemala	116	2.9	39,070	10.6	10,922	21.7	5,354
Guinea	226	2.6	88,627	7.3	30,752	15.3	14,785
Guinea-Bissau	27	0.5	53,465	1.1	25,257	1.9	14,055
Guyana	241	0.4	569,740	0.83	290,361	1.1	216,338
Haiti	11	3.3	3,373	7.1	1,544	12.5	879
Honduras	63.4	1.4	45,942	5.7	11,213	10.7	5,950
Hungary	120	9.3	12,851	10.1	11,874	8.7	13,846
Iceland	168	0.14	1,174,825	0.27	624,535	0.34	500,000
India	2,085	357.6	5,831	929	2,244	1,330	1,567
Indonesia	2,530	79.5	31,809	197.5	12,813	275	9,190
Iran	117.5	16.9	6,947	68.4	1,719	128.3	916
Iraq	109.2	5.2	21,171	20.1	5,434	41.6	2,625
Ireland	50	2.9	16,841	3.5	14,100	3.7	13,430
Israel	2.15	1.3	1,709	5.5	389	7.9	270
Italy	167	47.1	3,545	57.2	2,919	51.7	3,227
Jamaica	8.3	1.4	5,916	2.5	3,363	3.4	2,463
Japan	547	83.6	6,541	125.1	4,374	121.3	4,508
Jordan	1.71	1.2	1,382	5.4	318	11.9	144
Kazakhstan	169.4	6.7	25,272	16.8	10,073	20	8,450
Kenya	30.2	6.3	4,820	27.2	1,112	50.2	602

Appendix B (continued)

Kuwait	0.16	0.15	1,053	1.7	95	2.9	55
Kyrgyzstan	61.7	1.7	35,460	4.5	13,834	5.9	10,370
Laos	270	1.8	153,846	4.9	55,305	10.2	26,465
Latvia	34	1.9	17,445	2.5	13,407	2.1	16,129
Lebanon	5.58	1.4	3,867	3	1,854	4.4	1,261
Lesotho	5.2	0.73	7,084	2	2,565	4	1,290
Liberia	232	0.82	281,553	2.1	109,279	6.6	35,296
Libya	0.6	1	583	5.4	111	12.9	47
Lithuania	24.2	2.6	9,427	3.7	6,478	3.5	6,873
Luxembourg	5	0.29	16,892	0.41	12,285	0.47	10,730
Madagascar	337	4.2	79,688	14.9	22,657	34.5	9,775
Malawi	18.7	2.9	6,491	9.7	1,933	20.4	917
Malaysia	456	6.1	74,632	20.1	22,642	31.6	14,441
Mali	67	3.5	19,034	10.8	6,207	24.6	2,726
Malta	0.03	0.31	96	0.37	82	0.42	71
Mauritania	11.4	0.83	13,818	2.3	5,013	4.4	2,566
Mauritius	2.2	0.49	4,462	1.1	1,970	1.5	1,485
Mexico	357.4	27.7	12,885	91.1	3,921	130.2	2,745
Moldova	13.7	2.3	5,852	4.4	3,088	4.9	2,814
Mongolia	24.6	0.76	32,326	2.5	9,988	4.1	6,071
Morocco	30	8.9	3,351	26.5	1,131	39.9	751
Mozambique	208	6.2	33,559	17.3	12,051	35.4	5,868
Myanmar	1,082	17.8	60,677	45.1	23,988	67.6	15,996
Namibia	45.5	0.51	89,041	1.5	29,622	2.9	15,172
Nepal	170	7.9	21,623	21.5	7,923	40.6	4,192
Netherlands	90	10.1	8,899	15.5	5,813	16.1	5,576
New Zealand	327	1.9	171,384	3.6	91,828	4.9	67,036
Nicaragua	175	1.1	159,381	4.1	42,445	7.6	22,909
Niger	32.5	2.4	13,542	9.2	3,552	22.4	1,452
Nigeria	280	32.9	8,502	111.7	2,506	238.4	1,175
North Korea	67	9.5	7,062	22.1	3,032	30	2,230
Norway	392	3.3	120,061	4.3	90,489	4.7	84,084
Oman	1.93	0.46	4,232	2.2	874	6.5	295
Pakistan	468	39.5	11,844	136.3	3,435	268.9	1,740
Panama	144	0.86	167,442	2.6	54,732	3.8	38,105
Papua New Guinea	801	1.6	496,590	4.3	186,236	7.5	106,149
Paraguay	314	1.5	211,022	4.8	65,037	9.4	33,565
Peru	40	7.6	5,241	23.5	1,700	35.5	1,126
Phillippines	323	20.9	15,390	67.8	4,761	105.2	3,071
Poland	56.2	24.8	2,264	38.6	1,458	39.9	1,406
Portugal	69.6	8.4	8,281	9.8	7,091	9.4	7,374

Appendix B (continued)

Qatar	0.05	25	2,000	0.55	91	0.78	64
Romania	208	16.3	12,752	22.7	9,152	21.1	9,859
Russia	4,498	102.2	44,015	148.5	30,298	131.4	34,233
Rwanda	6.3	2.1	2,972	5.2	1,215	12.9	485
Saudi Arabia	4.55	3.2	1,421	18.3	249	42.4	107
Senegal	39.4	2.5	15,760	8.3	4,740	16.9	2,332
Sierra Leone	160	1.9	82,305	4.2	38,141	8.2	19,512
Singapore	0.06	1	587	3.3	180	4.2	142
Slovak	30.8	3.5	8,894	5.3	5,770	5.5	5,632
Solomon	44.7	0.1	496,667	0.38	118,254	0.84	52,962
Somalia	13.5	3.1	4,395	9.5	1,422	23.7	570
South Africa	50	13.7	3,654	41.5	1,206	71.6	698
South Korea	66.1	20.4	3,247	44.9	1,472	52.5	1,258
Spain	111.3	28	3,974	39.6	2,809	37.5	2,968
Sri Lanka	43.2	7.7	5,626	17.9	2,410	23.9	1,805
Sudan	154	9.2	16,757	26.7	5,766	46.9	3,287
Suriname	200	0.22	930,233	0.43	468,384	0.61	330,579
Swaziland	4.5	0.26	17,045	0.86	5,251	1.7	2,687
Sweden	180	7	25,663	8.8	20,482	9.5	18,925
Switzerland	50	4.7	10,652	7.2	6,977	7.6	6,595
Syria	53.69	3.5	15,362	14.2	3,780	26.3	2,041
Tajikistan	101.3	1.5	66,123	5.8	17,382	9.7	10,393
Tanzania	89	7.9	11,286	30	2,964	62.4	1,425
Thailand	179	20	8,946	58.2	3,073	69.1	2,591
Togo	12	1.3	9,029	4.1	2,938	8.8	1,370
Trinidad & Tobago	5.1	0.64	8,019	1.3	3,963	1.7	3,014
Tunisia	3.9	3.5	1,105	8.9	434	13.5	288
Turkey	193.1	20.8	9,280	60.8	3,174	85.5	2,251
Turkmenistan	72	1.2	59,455	4.1	17,669	6.5	11,128
Uganda	66	4.8	13,860	19.7	3,352	44.9	1,467
Ukraine	231	36.9	6,259	51.8	4,463	45.9	5,024
UAE	1.99	0.1	28,471	2.2	902	3.3	604
UK	71	50.6	1,403	58.1	1,222	59.5	1,193
USA	2,478	157.8	15,702	267.1	9,277	332.5	7,453
Uruguay	124	2.2	55,382	3.2	38,920	3.7	33,586
Uzbekistan	129.6	6.3	20,526	22.8	5,694	36.5	3,551
Venezuela	1,317	5.1	258,539	21.8	60,291	34.8	37,872
Viet Nam	376	29.9	12,553	73.8	5,095	110.1	3,415
Yemen	5.2	4.3	1,205	15	346	39.6	131
Zaire	1,019	12.2	83,634	45.5	22,419	105.9	9,620
Zambia	116	2.4	47,541	8.1	14,355	16.2	7,177
Zimbabwe	20	2.7	7,326	11.2	1,787	19.3	1,034

Appendix C

Installed desalination capacity by location as at 2004

Countries	Capacity (m^3/d)	Countries	Capacity (m^3/d)	Countries	Capacity (m^3/d)
Algeria	544,393	Germany	289,882	Pakistan	38,729
Angola	780	Gibraltar	30,140	Palau Pacific	180
Antarctica	754	Greece	76,673	Palestine	5,046
Antigue	39,072	Grenada	300	Paraguary	5,091
Antilles	13,899	Guinea	2,726	Peru	39,002
Antilles	288,233	Honduras	651	Philippines	38,032
Argentina	26,516	Hungary	815	Poland	30,212
Ascension	2,862	India	450,296	Polynesia	200
Australia	331,186	Indonesia	199,970	Portugal	13,500
Austria	26,153	Iran	643,711	Qatar	762,932
Azerbaijan	12,910	Iraq	397,753	Romania	120
Bahamas	71,971	Ireland	12,475	Russia	126,142
Bahrain	516,059	Israel	771,872	Saudi Arabia	6,569,172
Barbados	35,946	Italy	673,739	Senegal	132
Belarus	12,640	Jamaica	7,830	Singapore	328,726
Belgium	10,173	Japan	1,299,691	Slovenia	3,280
Belize	2,787	Jordan	328,507	Somalia	408
Bermuda	28,796	Kazakhstan	211,512	South Africa	102,524
Botswana	270	Kenya	400	Spain	2,418,974
Brazil	25,349	Kiribati	330	Sudan	21,876
Bulgaria	1,320	Korea	785,499	Sweden	4,592
Cambodia	240	Kuwait	2,181,026	Switzerland	13,393
Canada	70,906	Laos	9,600	Syria	8,183
Cape Verde	26,173	Lebanon	18,390	Taiwan	335,755
Cayman islands	26,957	Liechtenstein	151	Thailand	40,269
Chile	134,592	Libya	859,514	Trinidad	117,351
Columbia	12,800	Malaysia	37,318	Tunisia	81,209
Comoros	268	Maldives	15,332	Turkey	22,182
Congo	800	Malta	148,572	Turkmenistan	165,807
Costa Rica	1,363	Marshalls	2,650	Turks & Caicos	2,004
Cuba	25,117	Mauritania	4,654	UAE	5,532,777
Cyprus	106,850	Mexico	431,083	Ukraine	21,000
Czech	35,637	Morocco	56,856	UK	295,901
Denmark	26,052	Mozambique	189	USA	6,128,009
Djibouti	554	Myanmar	240	Uzbekistan	31,600
Dominican	2,294	Namibia	12,297	Venezuela	28,302
Ecuador	7,685	Nauru pacific	1,136	Vietnam	680
Egypt	303,915	Nethrelands	238,177	Virgin Islands	23,709

Appendix C (continued)

El Salvador	378	New Zealand	220	Yemen	77,948
Eritrea	1,000	Nicaragua	2,400	Yugoslawia	2,204
Fiji	1,020	Nigeria	9,570	Unknown	70,518
Finland	1,521	Norway	1,884		
France	219,257	Oman	334,879		

Appendix D

Analysis of CO2 emission

Tech	Use [%]	Capacity [m³/d]	Energy [kWh/m³]	Energy [kWh/d]	Energy [kWh/y]	Carbon Emission [kgCO2/y]
RO	60	39,000,000	3	117,000,000	42,705,000,000	23,060,700,000
MSF	26.8	17,420,000	13.5	235,170,000	85,837,050,000	46,352,007,000
MED	8	5,200,000	6.5	33,800,000	12,337,000,000	6,661,980,000
ED	3.6	2,340,000	1.5	3,510,000	1,281,150,000	691,821,000
Hybrid	0.8	520,000	1.5	780,000	284,700,000	153,738,000
EDI	0.3	195,000	1.5	292,500	106,762,500	57,651,750
Other	0.3	195,000	1.5	292,500	106,762,500	57,651,750
Total	99.8	64,870,000	29	390845000	1.42658E+11	77,035,549,500

2010 Global CO2 Emission = 29 billion tonnes
2010 Desalination (@ current capacity) CO2 Emission = 77 million tonnes
2010 Power & Heat (@ 41% of global emission) CO2 Emission = 11 billion tonnes

Supply by Desalination	Demand [m³/y]	Total Energy [kWh/m³]	Energy [kWh/y]	CO2 [kg/y]	CO2 [tonne/y]
10%	5.2E+11	29	1.508E+13	8.1432E+12	8143200000

2050 Global CO2 Emission = 58 billion tonnes
2050 Desalination (@ 10% of 2025 demand) CO2 Emission = 8 billion tonnes
2050 Power & Heat (@ 41% of global emission) CO2 Emission = 24 billion tonnes

Appendix E

- Desalting Plants Powered by Renewable Energy by Location, (Wangnick, 2004)

Countries	No of Units	Capacity (m^3/d)		
		Solar	Wind	Geothermal
Australia	6	16		
Bulgaria	1	2		
Canada	4	7	10	
Cape Verde	4	2	300	
Chile	2	17		
China	2	7		
Egypt	4		425	
France	2	60	12	
Germany	2	20	6	
Greece	17	51	968	1900
Grenada	1	2		
Haiti	1	2		
India	5	13		
Indonesia	1	12		
Italy	3	22		
Japan	6	73		
Jordan	1	5		
Kuwait	4	77		
Libya	3	1500	2000	
Mexico	5	62		
Oman	1	1		
Pakistan	2	24		
Qatar	2	44		
Russia	2	4		
Saudi Arabia	5	500		
Spain	3	74	50	
Tunisia	3	10		
UAE	2	580		
USA	7	123		

Appendix F

Calculation procedure of psychrometric properties using EES sofware

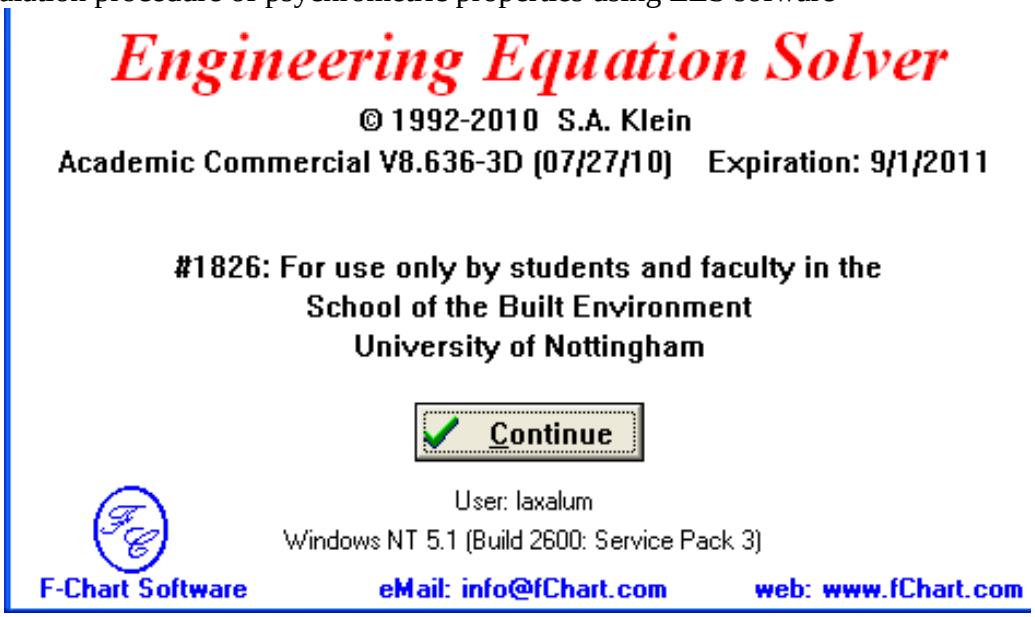

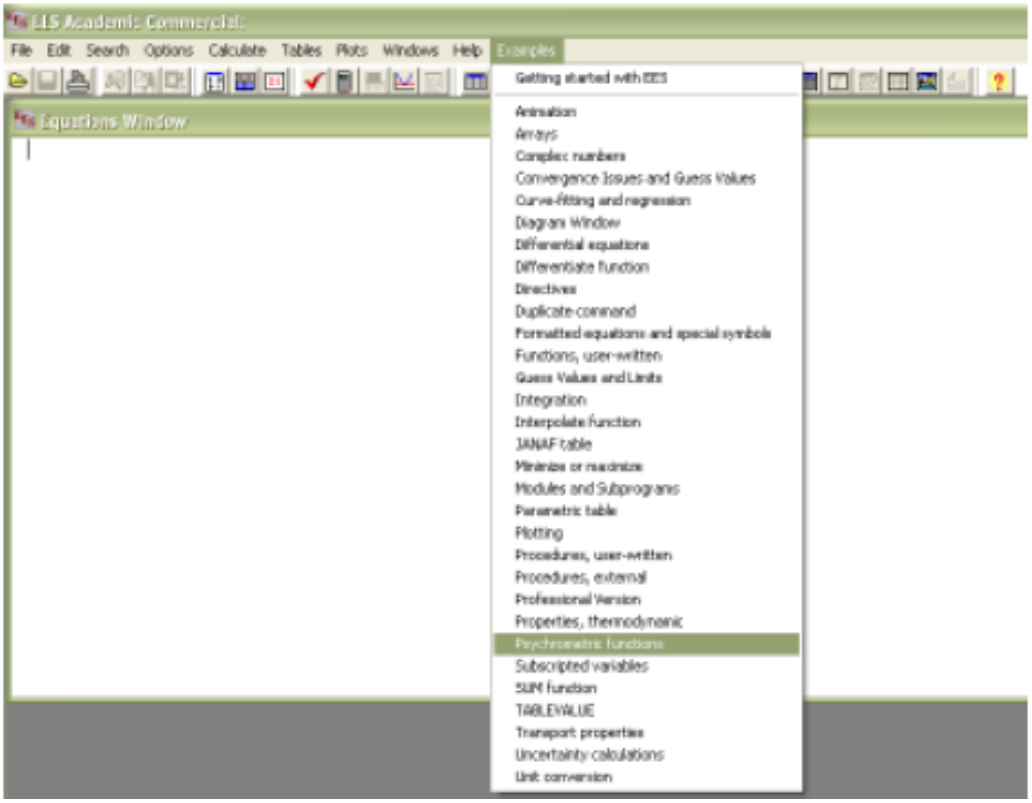

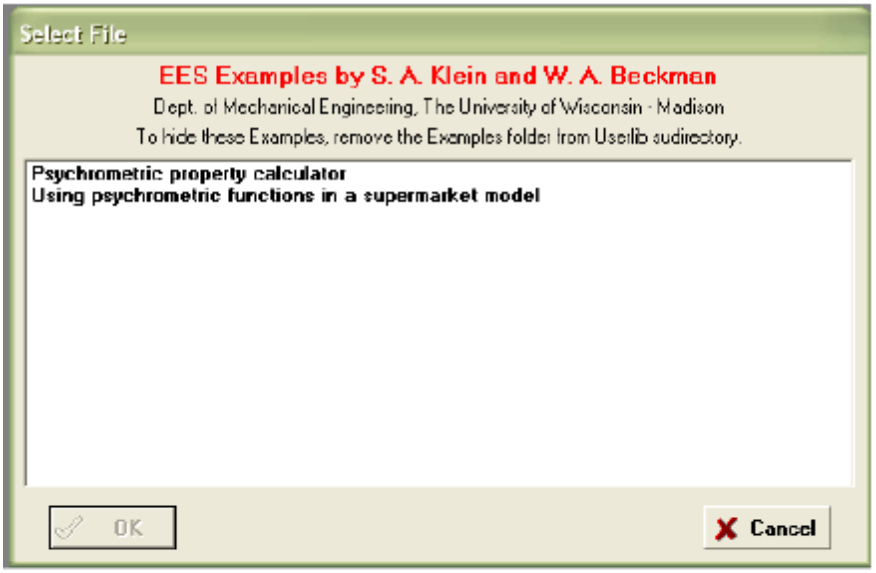
Select File
EES Examples by S. A. Klein and W. A. Beckman
Dept. of Mechanical Engineering, The University of Wisconsin - Madison
To hide these Examples, remove the Examples folder from Userlib subdirectory.
Psychrometric property calculator
Using psychrometric functions in a supermarket model
OK
Cancel

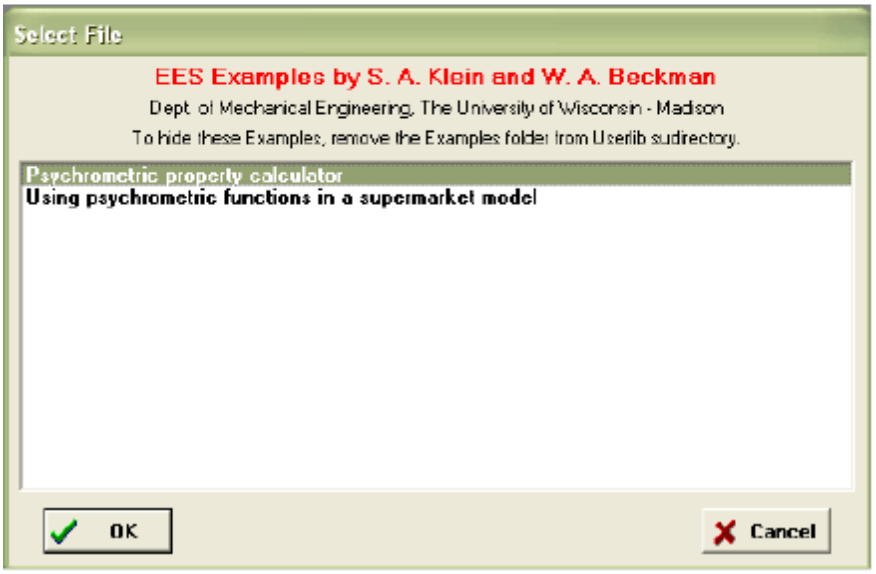
Select File
EES Examples by S. A. Klein and W. A. Beckman
Dept. of Mechanical Engineering, The University of Wisconsin - Madison
To hide these Examples, remove the Examples folder from Userlib subdirectory.
Psychrometric property calculator
Using psychrometric functions in a supermarket model
OK
Cancel

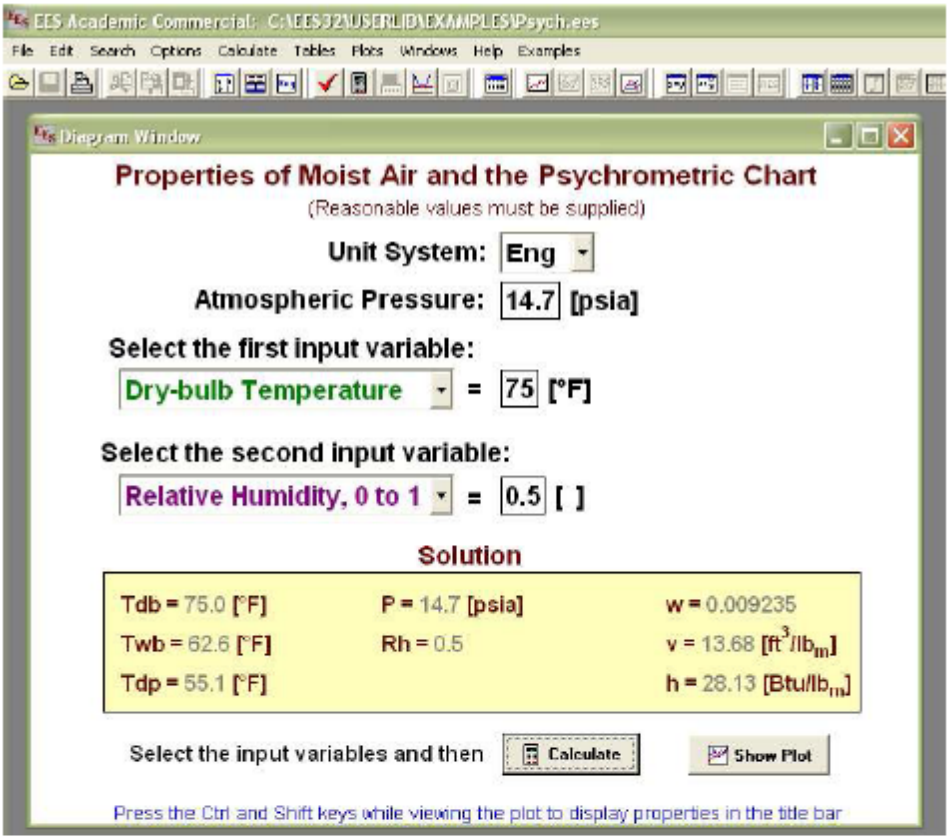
EES Academic Commercial: C:\EES32\USERLIB\EXAMPLES\Psych.ees
File Edit Search Options Calculate Tables Plots Windows Help Examples
Diagram Window
Properties of Moist Air and the Psychrometric Chart
(Reasonable values must be supplied)
Unit System: Eng
Atmospheric Pressure: 14.7 [psia]
Select the first input variable:
Dry-bulb Temperature = 75 [°F]
Select the second input variable:
Relative Humidity, 0 to 1 = 0.5 [ ]
Solution
Tdb = 75.0 [°F]
P = 14.7 [psia]
w = 0.009235
Twb = 62.6 [°F]
Rh = 0.5
v = 13.68 [ft3/lbm]
Tdp = 55.1 [°F]
h = 28.13 [Btu/lbm]
Select the input variables and then
Calculate
Show Plot
Press the Ctrl and Shift keys while viewing the plot to display properties in the title bar

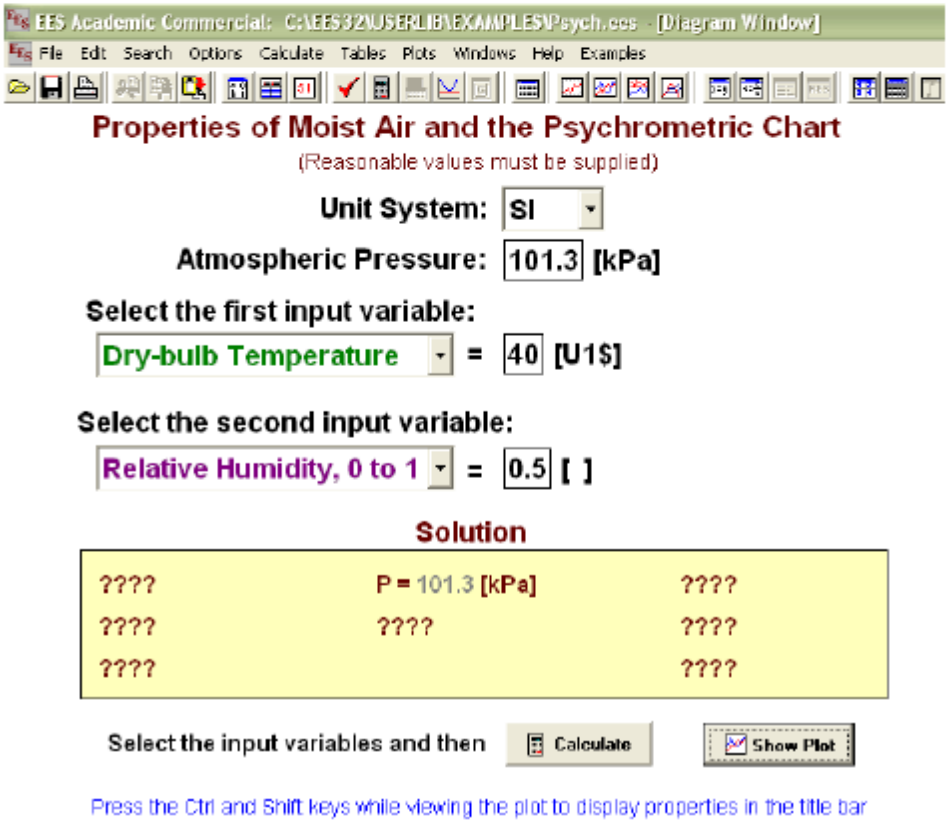
EES Academic Commercial: C:\EES32\USERLIB\EXAMPLES\Psych.ees - [Diagram Window]
File Edit Search Options Calculate Tables Plots Windows Help Examples
Properties of Moist Air and the Psychrometric Chart
(Reasonable values must be supplied)
Unit System: SI
Atmospheric Pressure: 101.3 [kPa]
Select the first input variable:
Dry-bulb Temperature = 40 [U1$]
Select the second input variable:
Relative Humidity, 0 to 1 = 0.5 [ ]
Solution
???? P = 101.3 [kPa] ????
???? ???? ????
???? ????
Select the input variables and then
Calculate
Show Plot
Press the Ctrl and Shift keys while viewing the plot to display properties in the title bar

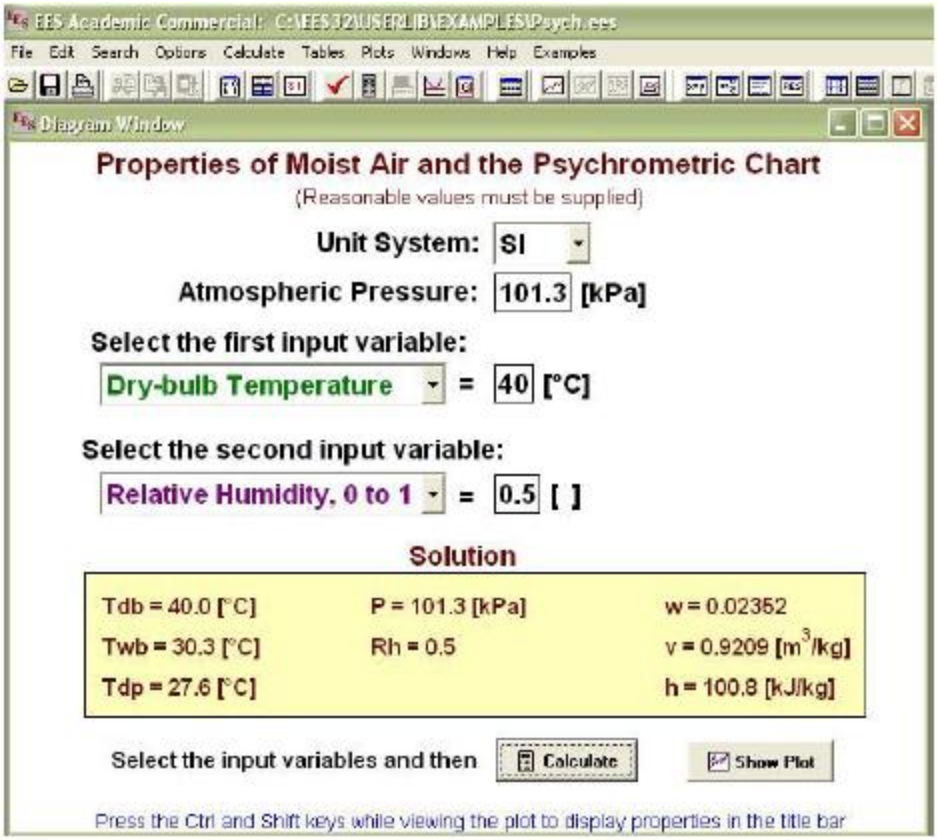
EES Academic Commercial: C:\EES32\USERLIB\EXAMPLES\Psych.ees
File Edit Search Options Calculate Tables Plots Windows Help Examples
Diagram Window
Properties of Moist Air and the Psychrometric Chart
(Reasonable values must be supplied)
Unit System: SI
Atmospheric Pressure: 101.3 [kPa]
Select the first input variable:
Dry-bulb Temperature = 40 [°C]
Select the second input variable:
Relative Humidity, 0 to 1 = 0.5 [ ]
Solution
Tdb = 40.0 [°C]
P = 101.3 [kPa]
w = 0.02352
Twb = 30.3 [°C]
Rh = 0.5
v = 0.9209 [m3/kg]
Tdp = 27.6 [°C]
h = 100.8 [kJ/kg]
Select the input variables and then
Calculate
Show Plot
Press the Ctrl and Shift keys while viewing the plot to display properties in the title bar

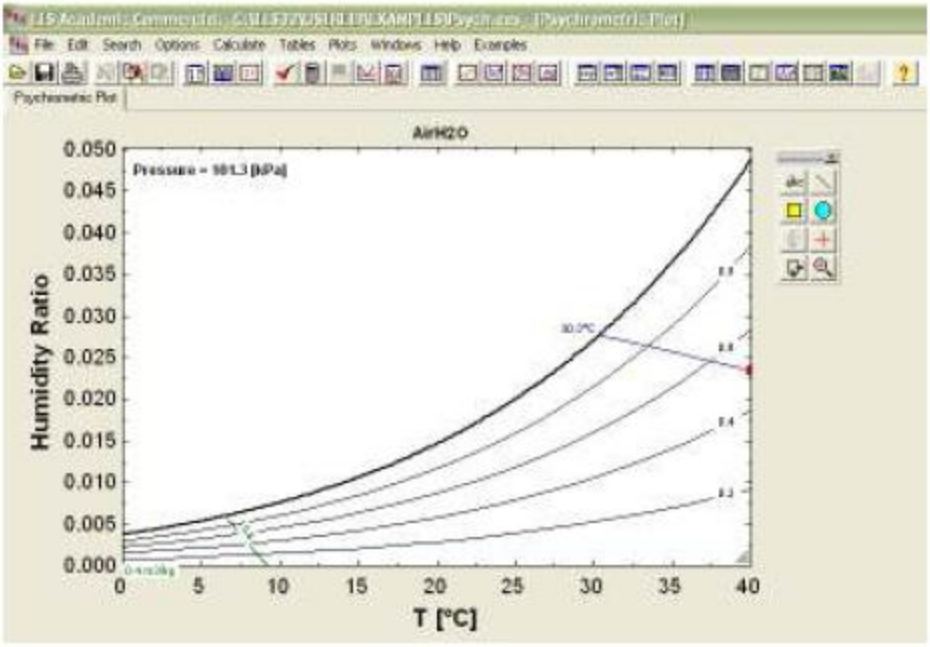
Psychrometric Plot
AirH2O
Pressure = 101.3 [kPa]
Humidity Ratio
0.050
0.045
0.040
0.035
0.030
0.025
0.020
0.015
0.010
0.005
0.000
0
5
10
15
20
25
30
35
40
T [°C]

Appendix G

The design method of the multiple curved-surfaces focusing light v-trough solar concentrator (VTC)

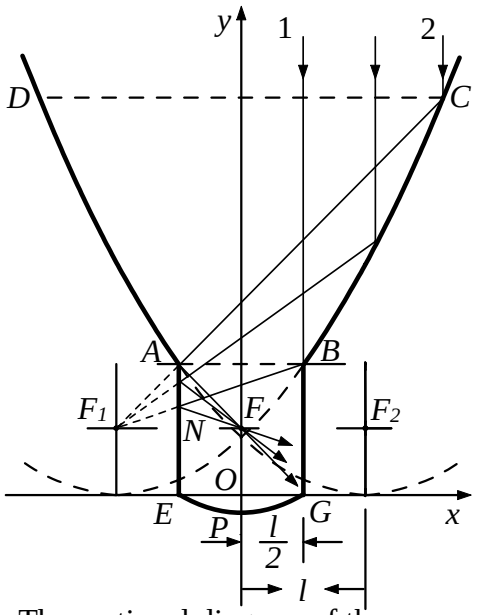

Figure H-1: The sectional diagram of the new concentrator

The $x-y$ coordinate system is established as shown in Figure H-1. Curve DA and CB respectively is the section of two parabolic curves with same size and aperture upturned. F_1 and F_2 respectively is two focus points of the parabolic curves. Equations of the parabolic curves can be given by

$$y=\frac{1}{2p}(x+l)^2 \qquad (H1)$$

$$y=\frac{1}{2p}(x-l)^2 \qquad (H2)$$

Where p is the focus parameter , l is the level distance between focus point F_1 and y axis. Make beeline *AB* parallel with *x* axis and cut the parabolic curves and order, $|AB|=\frac{|F_1F_2|}{2}=l$. Linear segment *AE* and *BG* is vertical with x axis, respectively. The reasonable length of *AE* and *BG* is the width of the secondary reflection plane mirror. In order to make the sun light directly radiating to linear segment *AB* to be reflected again to the receiver, another parabolic curve ***EPG*** is designed as lower trough paraboloid

concentrator. Its focus line also superposes with the center line of the high-temperature solar receiver. And then, all reflection surfaces are obtained together with parabolic curve segment *DA* and *CB,* linear segment *AE* and *BG,* and parabolic curve segment *ENG*.. This new multiple curved-surfaces focusing light trough solar concentrator is just their two dimensions level move.

- **The distance of two parabolic curve focus points**

It is noticeable that the light exit width *l* of the new compound paraboloid concentrator must satisfy a condition, namely bigger than a numerical value. The value can be determined as follows,

In Figure H-1, the Y coordinate of point *B* can be obtained by Eq. (H1)

$$y_B = \frac{1}{2p}(x_B + l)^2 = \frac{1}{2p}(\frac{l}{2} + l)^2 = \frac{9l^2}{8p} \qquad (H3)$$

The Y coordinate of point *B* should be over its focus point. It must be $y_B > \frac{P}{2}$. Therefore,

$$\frac{9l^2}{8p} > \frac{p}{2} \qquad (H4)$$

Namely $l > \frac{2}{3}p$, $0 < p < \infty$. Also, it requires the distance of two parabolic curve focus points $|F_1F_2| > \frac{4}{3}p$. Due to l、 p being positive, then $0 < \frac{p}{l} < \frac{3}{2}$.

- **The minimum height of the secondary reflection plane mirror**

It can be seen from Figure H-1 that light 1 is reflected by parabolic curve segment *CB* to point *N* on the plane mirror AE. Relative other reflective point, the point *N* is lowest. So, the minimum height of the secondary reflection plane mirror should be the length of AN. Position of point *N* can be determined by the point of intersection of beeline BF_1 and *AE*.

The equation of beeline BF_1 is

$$\frac{y - y_{F1}}{x - x_{F1}} = \frac{y_{F1} - y_B}{x_{F1} - x_B} \qquad (H5)$$

$$\frac{y-\frac{p}{2}}{x-l}=\frac{\frac{p}{2}-\frac{9l^2}{8p}}{l+\frac{l}{2}} \qquad (H6)$$

Coordinate the equation to get,

$$y=(\frac{3l}{4p}-\frac{p}{3l})x+\frac{3l^2}{4p}+\frac{p}{6} \qquad (H7)$$

Also, The equation of beeline *AE* is,

$$x=-\frac{l}{2}$$

And then, the intersection point coordinate of beeline BF_1 and *AE* is given by,

$$y_N=(\frac{3l}{4p}-\frac{p}{3l})(-\frac{l}{2})+\frac{3l^2}{4p}+\frac{p}{6}=\frac{3l^2}{8p}+\frac{p}{3} \qquad (H8)$$

Therefore, the minimum height of the secondary reflection plane mirror should be

$$|AE|>h=y_A-y_N=\frac{9l^2}{8p}-\frac{3l^2}{8p}-\frac{p}{3}=\frac{3l^2}{4p}-\frac{p}{3} \qquad (H9)$$

Under the conditions of focus parameter *p* certain, the minimum height *h* of the plane mirror AE changes with *l*. *h* increases rapidly with *l* regardless of the value of *p*. But when *p* is relative small, same *l* requires relatively bigger *h* value.

- **Determining the lower trough paraboloid concentrator**

It is known that the focus point of the lower trough paraboloid concentrator is also in mirror image point *F*. And then, its parabolic curve equation in $x-y$ axis system should have same focus parameter *p*. The equation for the lower concentrator is given as,

$$y=\frac{x^2}{2p}+\frac{2l^2}{8p}-\frac{p}{3} \qquad (H10)$$

- **Light inlet width selection**

The maximum light inlet width is DC. Any light which is incident out of DC cannot be reflected to AE. Light 2 is the farthest light which can be reflected to AE. So, the maximum light inlet width $DC=2x_C$ can be calculated as long as the coordinate of

the intersection point *C* between the beeline F_1A and parabolic curve segment *CB* can be determined.

The coordinate of point A is known:

$$x_A = -\frac{l}{2} \qquad (H11)$$

$$y_A = \frac{1}{2p}(x_A - l)^2 = \frac{1}{2p}(-\frac{l}{2} - l)^2 = \frac{9l^2}{8p} \qquad (H12)$$

The coordinate of point F_1 is known:

$$x_{F1} = -l$$

$$y_{F1} = \frac{p}{2}$$

Straight line equation through point *A* and F_1 is,

$$\frac{y - y_{F1}}{x - x_{F1}} = \frac{y_A - y_{F1}}{x_A - x_{F1}}$$

So,

$$\frac{y - \frac{p}{2}}{x + l} = \frac{\frac{9l^2}{8p} - \frac{p}{2}}{-\frac{l}{2} + l}$$

Adjust the equation to get,

$$y = (\frac{9l}{4p} - \frac{p}{l})x + \frac{9l^2}{4p} - \frac{p}{2} \qquad (H13)$$

The coordinates of intersection point *C* satisfy the equation group:

$$\begin{cases} y_C = (\frac{9l}{4p} - \frac{p}{l})x_C + \frac{9l^2}{4p} - \frac{p}{2} \\ y_C = \frac{1}{2p}(x_C + l)^2 \end{cases}$$

Solve above equation group, which it can be got,

$$x_C = \frac{5l}{4} - \frac{p^2}{l} + \sqrt{(\frac{9l}{4} - \frac{p^2}{l})^2 + p^2} \qquad (H14)$$

Therefore, the maximum inlet width is,

$$\Phi = 2x_C = 2l\left(\frac{5}{4} - \frac{p^2}{l^2} + \sqrt{(\frac{9}{4} - \frac{p^2}{l^2})^2 + \frac{p^2}{l^2}}\right) \qquad (\text{H15})$$

It can be found from Eq. (H15) that the maximum inlet width of the unit is determined by focus parameter *p* and outlet width *l*. It is necessary to select the value of *p* and *l* reasonably so as to gain the maximum inlet width. The maximum inlet width increases linearly along with the outlet width *l* when *p* is constant. At constant l, Φ decreases with increase in *p*.

- **The aspect ratio of the concentrator**

The aspect ratio of the collector is the ratio of the inlet aperture to the height of the concentrator. This is given by [75],

$$\alpha = \frac{a_1}{H} = \frac{5lp - \frac{4p^3}{l} + 4p\sqrt{(\frac{9l}{4} - \frac{p^2}{l})^2 + p^2}}{\left(\frac{9l}{4} - \frac{p^2}{l} + \sqrt{(\frac{9l}{4} - \frac{p^2}{l})^2 + p^2}\right)^2 - p^2} \qquad (\text{H16})$$

where *H* is the distance from the inlet aperture to connect line between point F_1 and point F_2. It is obvious that the ratio depend on the focal parameter p of the parabolic line and the distance l between two flat mirrors. If let $l = p$, then it can be obtained $\alpha = 1.04$. It means the height of the concentrator is roughly equal to its width of the inlet aperture, which is completely acceptable.

- **The concentration ratio of the concentrator**

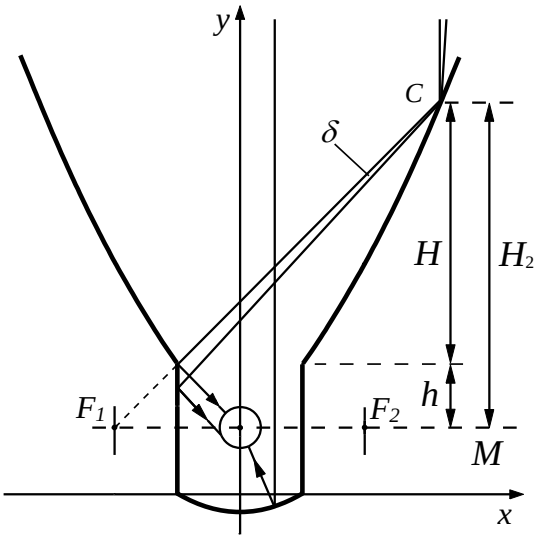

Assume again the distance from the point C to the point F_1 is S_1, the distance from point F_1 to point M is L, then it can be obtained from the figure.

$$S_1 = \frac{r}{\sin\delta} \text{ and } L = l + \frac{a_1}{2} \qquad \text{(H17)}$$

where r is the radius of the receiving tube. According to the geometrical relation, it can be found

$$S_1 = \sqrt{H^2 + L^2} \qquad \text{(H18)}$$

Then the concentration ration of the concentrator can be calculated as

$$C_1 = \frac{a_1}{2\pi r} = \frac{a_1}{2\pi S \sin\delta} = \frac{a_1}{2\pi \sin\delta \cdot \sqrt{H^2 + (l + \frac{a_1}{2})^2}} \qquad \text{(H19)}$$

According to the equation of the aspect ratio of the system, substitute it into the Eq. H19 to obtain,

$$C_1 = \frac{a_1}{2\pi \sin\delta \cdot \sqrt{\frac{a_1^2}{\alpha^2} + (l + \frac{a_1}{2})^2}} \qquad \text{(H20)}$$

In order to find the effect of the inlet aperture width on the maximal concentration ratio, order $\frac{dC_1}{da_1} = 0$, then we can get $a_1 = 2l$, therefore

$$C_{1\max} = \frac{\alpha}{2\pi \sin\delta \cdot \sqrt{\alpha^2 + 1}} \qquad \text{(H21)}$$

To proving the size of the $C_{1\max}$, let $p = l$ and $l = 350mm$, then $\alpha = 1.04$

$$C_{1\max} = \frac{1.04}{2\pi \sin\delta \sqrt{2.08}} \qquad \text{(H22)}$$

If the tracking accuracy is up to 0.5°, then $C_{1\max} = 13$, the minimal permissible diameter is 17.1mm. The higher the tracking accuracy of the device is, the better its operation effect is, and the smaller the receiver would be, and the more it would save the material. Meanwhile, with the aspect ratio of the system close to 1, high concentration ratio can be obtained without affecting the of the collector. Therefore this device can get a quite high concentration ratio which is normally up to more than 10.

Publications

A. Mayere, S. Riffat, Solar Driven Micro-CHP System: A State of the Art Review, 8th International Conference on Sustainable Energy Technologies Aachen, Germany, 2009

A. Mayere, S. Riffat, A Novel Solar Driven Micro-CHP System: A State of the Art Review, Journal of Energy and Power Engineering 4 (11) (2010) 30-35

A. Mayere, S. Riffat, Experimental Investigation of Small Scale Humidification Dehumidification Desalination Unit, 9th International Conference on Sustainable Energy Technologies Shanghai, China, 2010

Zheng Hongfei, Tao Tao, He Kaiyan, Abdulkarim Mayere, A new trough solar concentrator and its performance analysis, Solar Energy, 85(1), 198-207 (2011)

A. Mayere, S. Riffat, Y. Yuan, Design and Performance Analysis of Solar Humidification Dehumidification Desalination (HDD) System, 10th International Conference on Sustainable Energy Technologies Istanbul, Turkey, 2011

A. Mayere, S. Riffat, L. Begrambekov, Critical Analysis of Desalination Systems Using Humidification Dehumidification Techniques, 10th International Conference on Sustainable Energy Technologies Istanbul, Turkey, 2011

A. Mayere, S. Riffat, Guoquan Qiu, Barry West, Hao Liu, Hybrid Biomass/Solar Micro CHP system with ORC, 10th International Conference on Sustainable Energy Technologies Istanbul, Turkey, 2011

A. Mayere, S. Riffat, Psychrometric Energy Desalination Process: Design and Performance Analysis. Journal of Applied Energy. APEN-D-11-01108 (under review)

A. Mayere, S. Riffat, Performance of V-Trough Solar Concentrator for Water Desalination. Journal of Applied Thermal Engineering (under review)